Academy of Sciences of the Republic of Uzbekistan
Physical-Technical Institute of the Scientific Association “Physics–Sun”
National Academy of Sciences of Ukraine
V. Lashkaryov Institute of Semiconductor Physics

A.A. Akopyan, O.Yu. Borkovskaya, N.L. Dmitruk, A.V. Karimov, R.V. Konakova, V.V. Milenin, A.V. Sachenko, M.N. Tursunov, D.M. Yodgorova

PHOTOCONVERTERS WITH AlGaAs/GaAs HETEROJUNCTION ON TEXTURED GaAs SUBSTRATES

(Physico-technological aspects)

General editorship by
Prof. Dr. Phys.-Math. Sci. N.L. Dmitruk
and Prof. Dr. Techn. Sci. R.V. Konakova

Tashkent: FAN
2004

UDC 621. 382. 2

Photoconverters with AlGaAs/GaAs Heterojunction on Textured GaAs Substrates (Physico-technological aspects). A.A. Akopyan, O.Yu. Borkovskaya, N.L. Dmitruk, A.V. Karimov, R.V. Konakova, V.V. Milenin, A.V. Sachenko, M.N. Tursunov, D.M. Yodgorova. Tashkent: FAN.

The monograph presents the results of physico-technological studies of photoconverters made on the basis of AlGaAs/GaAs heterostructures LPE-grown on textured and flat growth surfaces of *n*-GaAs (100) (donor concentration $\geq 10^{18}$ cm^{-3}).

The authors widely use the results of their own investigations in the area. Particular attention is given to the features of optical, electric and photoelectric phenomena in heterostructures with textured interface of *p*-*n* junction that provide higher efficiency for photoconverters on the so-called soft substrates as compared with those on flat substrates, all other factors being equal. Some peculiarities of ohmic and barrier contacts formation on textured GaAs surfaces are also considered.

The monograph is intended for researchers and engineers engaged in semiconductor photoelectronics, as well as for postgraduates and undergraduates dealing with the above problems.

Reviewer – Prof. Dr. Phys.-Math. Sci. MARONCHUK Igor Evgenievich

NSBN 966-7700-03-8

© text
AKOPYAN Arsen Artashesovich
BORKOVSKAYA Olga Yurievna
DMITRUK Nikolai Leontievich
KARIMOV Abdulaziz Vakhitovich
KONAKOVA Raisa Vasilievna
MILENIN Viktor Vladimirovich
SACHENKO Anatolii Vasilievich
TURSUNOV Mukhammad Nishanovich
YODGOROVA Dilbar Mustafaevna

Contents

Foreword....... 6
Introduction....... 8
References....... 11
Chapter I....... 13
TECHNOLOGY FOR FORMATION OF MICRORELIEFS OF DIFFERENT TOPOLOGIES TO GROW ALGAAS/GAAS HETEROJUNCTIONS AND THE PROPERTIES OF TEXTURED SURFACES....... 13
1.1. TECHNOLOGY OF SURFACE MICRORELIEF FORMATION....... 13
1.2. OPTICAL PROPERTIES OF TEXTURED SURFACES....... 18
1.2.1. CALCULATIONS OF SPECTRAL CURVES FOR THE COEFFICIENT OF LIGHT REFLECTION FROM THE SURFACE OF SC ON THE BASIS OF ALGAAS–GAAS HETEROSTRUCTURE, WITH ALLOWANCE MADE FOR SURFACE RELIEF USING THE EFFECTIVE MEDIUM METHOD....... 18
1.3. STUDIES OF OPTICAL CHARACTERISTICS OF THE GAAS MICRORELIEF SURFACES....... 23
1.3.1. SPECULAR AND DIFFUSE REFLECTION OF LIGHT....... 24
1.3.2. MULTIANGLE ELLIPSOMETRY MEASUREMENTS....... 29
1.3.3. IR REFLECTION SPECTRA....... 30
1.4. INVESTIGATION OF PHOTOLUMINESCENCE SPECTRA....... 33
REFERENCES....... 38
Chapter II....... 39
SOME TECHNOLOGICAL ASPECTS OF FORMATION OF HETERO-PHOTOCONVERTERS MADE ON THE BASIS OF AlGaAs–GaAs HETEROJUNCTIONS....... 39
2.1. LIQUID-PHASE EPITAXY WITH AN INDUSTRIAL PLANT....... 40
2.2. DEVELOPMENT OF TECHNOLOGICAL PROCEDURES FOR GROWTH OF ALGAAS–GAAS HETEROEPITAXIAL JUNCTIONS....... 45
2.3. MONITORING OF THE GROWN EPITAXIAL LAYER COMPOSITION....... 47
2.4. LIQUID-PHASE EPITAXY (SHIFTING TECHNIQUE)....... 49
2.4.1. GROWTH OF EPITAXIAL LAYERS WITH *P-N* JUNCTIONS....... 49
2.4.2. EPITAXIAL GROWTH OF HETEROLAYERS ON THE BASIS OF ALGAAS....... 52
2.4.3. LIQUID-PHASE EPITAXY ONTO A TEXTURED SURFACE....... 53
2.4.4. THE PROBLEM OF ALTERNATIVE TECHNIQUES FOR FORMATION OF HETERO-PHOTOCONVERTERS WITH MICRORELIEF INTERFACES OF *P-N* JUNCTIONS....... 57
REFERENCES....... 58

Chapter III **.. 60**
MORPHOLOGY AND CHEMICAL COMPOSITION OF TEXTURED GaAs SURFACES. TECHNIQUE FOR FORMATION AND PROPERTIES OF OHMIC AND BARRIER CONTACTS TO TEXTURED GaAs AND Al(In)GaAs SURFACES. **.. 60**
3.1. APPLICATION OF AUGER ELECTRON SPECTROSCOPY FOR ANALYSIS OF CHEMICAL COMPOSITION OF SURFACES WITH NONUNIFORM TOPOGRAPHY 60
3.1.1. AUGER ANALYSIS OF FLAT AND ROUGH GAAS SURFACES 61
3.1.2. EFFECT OF GAAS SURFACE RELIEF ON ATOMIC COMPOSITION 63
3.1.3. THE EFFECT OF NONUNIFORM SURFACE TOPOGRAPHY OF GAAS SUBSTRATES ON CHEMICAL COMPOSITION OF $IN_XGA_{1-X}AS$ EPITAXIAL FILMS GROWN ON THEM 68
3.2. ELECTROPHYSICAL CHARACTERISTICS OF BARRIER STRUCTURES WITH FLAT AND MICRORELIEF SURFACES 70
3.2.1. INTERRELATION BETWEEN THE TOPOGRAPHIC, STRUCTURAL AND ELECTRICAL CHARACTERISTICS OF THE BARRIER CONTACTS ON THE BASIS OF GAAS, INGAAS AND P^+-ALGAAS–P-GAAS–N-GAAS–N^+-GAAS HETEROJUNCTIONS 70
3.2.2. THE GEOMETRIC STRUCTURE OF INGAAS SURFACE AND ELECTRICAL CHARACTERISTICS OF THE AU–*N*-INGAAS–N^+-GAAS SCHOTTKY BARRIERS 79
3.3. DEVELOPMENT OF TECHNOLOGY FOR FORMATION OF OHMIC AND BARRIER CONTACTS TO GAAS AND ALGAAS EPITAXIAL LAYERS 82
3.3.1. THE VACUUM SPUTTERING TECHNIQUE 82
3.3.2. ELECTROCHEMICAL DEPOSITION TECHNIQUE 85
3.4. PROPERTIES OF NONRECTIFYING CONTACTS FOR SOLAR PHOTOCONVERTERS ON THE BASIS OF III–V COMPOUNDS 87
3.5. EFFECT OF SURFACE ROUGHNESS ON THE PROPERTIES OF OHMIC CONTACTS TO GAAS 90
3.6. INVESTIGATIONS OF ELECTROPHYSICAL CHARACTERISTICS OF BARRIER STRUCTURES ON THE BASIS OF HETEROJUNCTIONS OBTAINED. DETERMINATION OF BARRIER PARAMETERS AND CURRENT FLOW MECHANISM 98
3.6.1. MANUFACTURING TECHNOLOGY FOR BARRIER CONTACTS 98
3.6.2. EFFECT OF SURFACE ROUGHNESS ON THE SCHOTTKY BARRIER CHARACTERISTICS 99
3.6.3. DEVELOPMENT OF CONTACTS OF THE REQUIRED CONFIGURATION TO PHOTOCONVERTERS USING EXPLOSIVE PHOTOLITHOGRAPHY 103
3.7. SIMULATION STUDIES OF DIFFUSION PROCESSES IN METAL–GAAS CONTACT 105
3.7.1. FORMULATION OF THE PROBLEM AND THEORETICAL BACKGROUND 106

REFERENCES 118
Chapter IV 120
THE FEATURES OF PHOTOCONVERSION IN SOLAR CELLS MADE ON THE BASIS OF TEXTURED THIN-FILM $Al_xGa_{1-x}As$–GaAs HETEROSTRUCTURE 120
4.1. OPTICAL LOSSES IN THE TEXTURED $AL_XGA_{1-X}AS$–GAAS HETEROSYSTEM 120
4.2. PHYSICAL MECHANISMS FOR PHOTOCURRENT FORMATION IN HETEROJUNCTIONS WITH RELIEF SURFACES 125
4.3. CALCULATION OF SHORT-CIRCUIT CURRENT IN $IN_XGA_{1-X}AS$-BASED *P-N* JUNCTIONS 133
4.4. PHOTOCONVERSION EFFICIENCY IN TEXTURED $AL_XGA_{1-X}AS$–P-GAAS–N-GAAS HETEROSYSTEM 135
4.5. THEORETICAL ANALYSIS OF PHOTORESPONSIVITY FOR THE HETEROJUNCTION PHOTOCONVERTERS WITH MICRORELIEF INTERFACES 138
REFERENCES 147
CHAPTER V 148
PHOTORESPONSIVITY OF THE PHOTOCONVERTERS 148
5.1. MEASUREMENTS AND MODELLING OF CHARACTERISTICS TO DETERMINE PHOTOCONVERSION PARAMETERS 149
5.2. PHOTORESPONSIVITY OF THE PHOTOCONVERTERS FABRICATED BY VARIOUS MODIFICATION OF THE LPE TECHNIQUE 151
5.3. PHOTORESPONSIVITY OF THE PHOTOCONVERTERS FABRICATED BY GPE 157
5.4. EFFECT OF GAMMA IRRADIATION ON PHOTOCONVERSION CHARACTERISTICS OF GALLIUM ARSENIDE BARRIER STRUCTURES WITH TEXTURED INTERFACE 160
REFERENCES 168
Conclusion 169

Foreword

This monograph reflects progressive trends in technology applied for formation of solar energy converters made on the basis of semiconductor (AlGaAs–GaAs) heterojunctions. Such photoconverters have been developed in recent years by the research teams from the V. Lashkaryov Institute of Semiconductor Physics of the National Academy of Sciences of Ukraine (Kiev) and the Physical-Technical Institute of the Scientific Association "Physics–Sun" of the Academy of Sciences of the Republic of Uzbekistan (Tashkent). The results of their investigations have been applied, in particular, when executing the joint Project UZB-56(J) supported by the Science and Technology Center in Ukraine.

The developments and solutions concerning photovoltaic conversion of solar energy that are summarized and generalized in this monograph are of particular importance for the Republic of Uzbekistan and southern regions of Ukraine where such source of electric energy seems the most promising as compared to the traditional ones.

Cooperation of Ukrainian and Uzbek researchers is one more step on the way leading to practical application of the scientific results. The feature of joint investigations is that heavily doped single-crystalline GaAs wafers with purposefully formed textured growth surfaces serve as substrates on which photoconverter active elements are formed.

For the first time hetero-photoconverters have been made and studied on microrelief GaAs surfaces prepared using anisotropic chemical etching and liquid-phase epitaxy (LPE). Along with this, the authors performed unique calculations and studies of a number of physical effects occurring on textured (microrelief) GaAs and AlGaAs surfaces, as well as in heterostructures grown on such surfaces and textured metal–semiconductor interfaces. One should note, in particular, simulation of diffusion processes in *p*-*n*

junctions and metal–semiconductor contacts formed on textured substrates, as well as simulation of photoconversion processes in such objects. These investigations make it possible to optimize the parameters of both technological process and photoconverters by computer simulation, thus saving much time and costs required for similar works that are made at technological and diagnostic plants.

The results of investigations presented in this monograph will be of use not only for technologists and those developing photoconverters but also for a wide range of specialists engaged in physics of semiconductor devices, as well as for postgraduates and undergraduates dealing with the above problems.

Vice-President
of the Academy of Sciences of the Republic of Uzbekistan
General Director
of the Physical-Technical Institute
of the Scientific Association "Physics–Sun"
of the Academy of Sciences of the Republic of Uzbekistan
Prof. Dr. Phys.-Math. Sci. S.L. LUTPULLAEV

Introduction

In recent years the continuing aggravation of the problem of energy carriers and rise in the cost of usual energy sources gave rise to searches for nontraditional ones. A significant place among them is occupied, for more than half a century, by semiconductor photoconverters of solar radiation. Many hopes are associated with the solid-state (semiconductor) solar power engineering whose main active elements are the above photoconverters.

The pioneer works aimed at conversion of solar radiation into electric energy with semiconductor solar cells started as long ago as the thirties of the last century. They have been initiated and directed by Academician A.F. Ioffe at the Leningrad Physico-Technical Institute. Later on these researches made an important strategic line of fundamental investigations of semiconductor materials and devices, as well as large-scale industrial developments which served, to a great extent, to successful realization of the Soviet space program. They made a great impact on the development of solar power engineering in the world [1-4].

For a rather short period solar power engineering has traveled the distance from the first silicon solar cells with *p*-*n* junction (whose efficiency did not exceed several percent) to highly efficient cascade solar cells with heterojunctions on the basis of III–V compounds (synthesized, for the first time, at the Ioffe Physico-Technical Institute by the team under direction of Zh.I. Alferov). The above pioneer works have found further development in activity of the specialists from NASA and NREL (USA), Fraunhofer Institute for Solar Energy Systems (Germany), Sharp (Japan), University of New South Wales (Australia) and other research teams [5-8], as well as at the Soviet universities and academic institutes in Russia Federation, Ukrainian, Uzbek and Turkmenian Soviet Republics.

A big practical experience in development of various semiconductor photoconverters and application of them in economy and for special purposes has been gained at the V. Lashkaryov Institute of Semiconductor Physics of the National Academy of Sciences of Ukraine and the Physical-Technical Institute of the Scientific Association “Physics–Sun” of the Academy of Sciences of the Republic of Uzbekistan. This experience has been generalized by the leading experts in a number of well-known monographs, reviews and numerous papers in scientific journals (see, e.g., *[**]*). Particular interest has been aroused by the works dealing with increase of photoconversion efficiency by application of various treatments of front semiconductor surfaces in actual photoconverter constructions. Such works were being performed for many years at the V. Lashkaryov Institute of Semiconductor Physics under direction of Academician S.V. Svechnikov, Corresponding Member V.G. Litovchenko, Prof. N.L. Dmitruk and Prof. A.P. Gorban. It was shown that one of the effective methods for reduction of optical losses and increase of photoconversion efficiency is (along with application of antireflecting coatings) formation of textured semiconductor surfaces [9-11].

In particular, Prof. N.L. Dmitruk and co-authors have advanced some effective techniques for texturing surfaces of III–V semiconductors using anisotropic chemical etching. This enabled to reduce the coefficient of visible light reflection from 40–60% down to 3–5% and concurrently improve the recombination parameters of the metal–semiconductor interfaces. At that photosensitivity of the Au (Ag)–GaAs (InP) surface-barrier structures grew by several times, both in IR and UV, as compared to that of the structures with flat surfaces [11-14].

In the same years in Uzbekistan a number of investigations of photoelectric phenomena have been carried out under direction of Academician S.A. Azizov, Academician M.S. Saidov, Academician E.I. Adirovich, Prof. P.M. Karageorgii-Alkalaev and Prof. A.Yu.

Leiderman [15-19], as well as various technological aspects of LPE-growing of heterojunctions on the basis of III–V compounds have been intensely developed [18-21]. The estimations demonstrated that use of the developed techniques for GaAs surface texturing in combination with the technology and experience of GaAs and AlGaAs growing and doping in the course of epitaxy may be promising in development of highly efficient photoconverters on new generation on the basis of GaAs–AlGaAs–GaAs heterojunctions.

The experience gained in the course of experimental examination of this idea has found its generalization in this monograph. Joint investigations made by the r4search teams from the V. Lashkaryov Institute of Semiconductor Physics of the National Academy of Sciences of Ukraine and the Physical-Technical Institute of the Scientific Association “Physics–Sun” of the Academy of Sciences of the Republic of Uzbekistan have become possible due to support by the Science and Technology Center in Ukraine (Project UZB-56(J)).

References

[1] Zh.I. Alferov, V.M. Andreev, V.D. Rumyantsev. Fiz. Tekhn. Poluprov. 2004. v. 38. p.937 (in Russian).

[2] A.F. Ioffe, A.V. Ioffe. Phys. Z. Sow. 1935. v. 7. p.343.

[3] N.A. Goryunova. Synopsis of the Thesis. Leningrad Univ.–Phys.-Techn. Inst. 1951 (in Russian).

[4] Zh.I. Alferov, V.M. Andreev, M.B. Kagan, I.I. Protasov, V.G. Trofim. Fiz. Tekhn. Poluprov. 1970. v. 4. p.12 (in Russian).

[5] R.P. Leon, S.G. Bailey, G.A. Mazaris, W.D. Williams. Appl. Phys. Lett. 1986. v. 49. p.945.

[6] P. Jenkins, G.A. Lendis, N.S. Fatemi, D. Scheiman, X. Li, S.G. Bailey. Sol. Energy Mater. Sol. Cells. 1994. v. 33. p.125.

[7] J. Knobloch, A. Noel, U. Schubert, F.J. Kamerewerd, S. Klubmann, W. Wetling. Proc. 23rd IEEE PVSC. Louisville. 1993. p. 271.

[8] J. Zhao, A. Wang, M.A. Green. Progress in Photovoltaics. 1994. v. 2. p.227.

[9] T.Ya. Gorbach, S.V. Svechnikov. Ukr. Fiz. Zh. 1987. v. 32. p.1110 (in Russian).

[10] T.Ya. Gorbach, E.V. Pidlisnyi, S.V. Svechnikov. Optoel. i Poluprov. Tekhn. 1988. No 13. p.34 (in Russian).

[11] O.Yu. Borkovskaya, T.Ya. Gorbach, N.L. Dmitruk, O.N. Mischuk. Fiz. Tekhn. Poluprov. 1989. v. 23. p.2113 (in Russian).

[12] O.Yu. Borkovskaya, N.L. Dmitruk, O.N. Mischuk. Fiz. Tekhn. Poluprov. 1991. v. 25. p.487 (in Russian).

[13] N.L. Dmitruk, E.V. Basiuk, G.Ya. Kolbasov, O.A. Yakubtsov, I.A. Molchanovskii, T.A. Taranets. Appl. Surf. Sci. 1995. v. 90. p.489.

[14] N.L. Dmitruk, O.Yu. Borkovskaya, I.N. Dmitruk, S.V. Mamykin, Sz. Horvath, I.B. Mamontova. Appl. Surf. Sci. 2002. v. 190. p.455.

[15] Semiconductor Arsenides and Phosphides of the Elements of III Group. Ed. Yu.V. Shmartsev. Tashkent: FAN, 1981 (in Russian).

[16] P.M. Karageorgii-Alkalaev, A.Yu. Leiderman. Photosensitivity of Semiconductor Structures with Deep Impurities. Tashkent: FAN, 1981 (in Russian).

[17] A.S. Saidov, M.S. Saidov, E.A. Koschanov. Liquid-phase Epitaxy of Compensated Layers of Gallium Arsenide and Solid Solutions on Its Basis. Ed. V.N. Tuchkevich. Tashkent: FAN, 1986 (in Russian).

[18] Photosensitive Structures and Solar Cells on the Basis of Gallium Arsenide. Ed. M.S. Saidov. Tashkent: FAN, 1986 (in Russian).

[19] Photoelectric Phenomena in Semiconductors and Optoelectronics. Ed. E.I. Adirovich. Tashkent: FAN, 1972 (in Russian).

[20] A.V. Karimov. Multifunctional; Gallium-arsenide Thin-junction Structures. Tashkent: FAN, 1992 (in Russian).

[21] M. Mirzabaev, K. Rasulov, A. Komilov. Heliotekhnika. 1995. No 6. p.23 (in Russian)

Chapter I

TECHNOLOGY FOR FORMATION OF MICRORELIEFS OF DIFFERENT TOPOLOGIES TO GROW ALGAAS/GAAS HETEROJUNCTIONS AND THE PROPERTIES OF TEXTURED SURFACES

For development and optimization of the technological procedure used for surface microrelief formation in the basic semiconductor (n^+-GaAs) and epitaxial films (GaAs and AlGaAs), the research team from the V. Lashkaryov Institute of Semiconductor Physics of the National Academy of Sciences of Ukraine (Kiev) used anisotropic etching (to obtain random microreliefs of different morphologies) and holographic photochemical and photoresistive chemical etching (to form appointed periodic microreliefs). The etching conditions were stabilized and checked. Control over microrelief morphology and its statistical-geometric parameters was exerted using optical and atomic force microscopies. Structure perfection of the starting *n*-GaAs substrates, heterojunctions and microtextured wafers was studied with x-ray diffraction and x-ray topography, while the quantitative atomic composition of the near-surface layers was estimated with Auger electron spectroscopy.

The optical characteristics of the textured surfaces of n-GaAs single crystals, epitaxial films and heteroepitaxial layers grown on them were studied by measuring spectra of specular and diffuse light reflection.

1.1. TECHNOLOGY OF SURFACE MICRORELIEF FORMATION

To develop and optimize technological conditions for microrelief formation at surfaces and active interfaces in

AlGaAs/GaAs (100) heterojunctions, we studied the features of selective etching of single-crystalline n^+-GaAs material and n-GaAs, p-$Al_xGa_{1-x}As$ and $In_xGa_{1-x}As/n^+$-GaAs epitaxial layers. Dendrite-like microrelief was formed in concentrated HNO_3 (65%) that served as universal etchant for all the above compounds. The etching process was proceeding according to the redox mechanism.

Microrelief formation goes through several stages as etching time increases. At the first stage one can observe single etching polyhedrons at the surface. These are predominantly octahedrons whose lateral faces are single-crystalline natural (111) faces. Along with them, some other dissolution patterns are observed. They are confined with cube and rhombic dodecahedron (110) faces. At further dissolution microrelief passes through a number of unstable morphologic forms, up to formation of developed dendrites with branches of the first and subsequent orders.

One can also exert control over microrelief formation by varying the etchant temperature and nitric acid concentration. In particular, one can slow down the process and increase microrelief size by diluting nitric acid with water or decreasing the etchant temperature. A rather thick (up to ~10 nm [1]) oxide layer is formed at the dendrite-like microrelief surface. This is predominantly As_2O_3, which is evidenced by characteristic bands in the reflection spectrum in the λ = 2−20 μm wavelength range (see Fig. 1.1). When Ga (In) atoms go into solution, they produce vacancies in the GaAs lattice sites, since Ga and In oxides (Ga_2O_3 and In_2O_3) rather well dissolve in the strong acid media. After oxide is etched away in KOH (or HCl solutions), GaAs microrelief surface becomes more enriched in As than flat one [1]. If one assumes that flat surface is enriched in gallium [2], then microrelief surface seems to become of higher stoichiometry. For ternary compounds dendrite formation passes through the same stages. However, since their etching rate is higher, the etching mode should be softer.

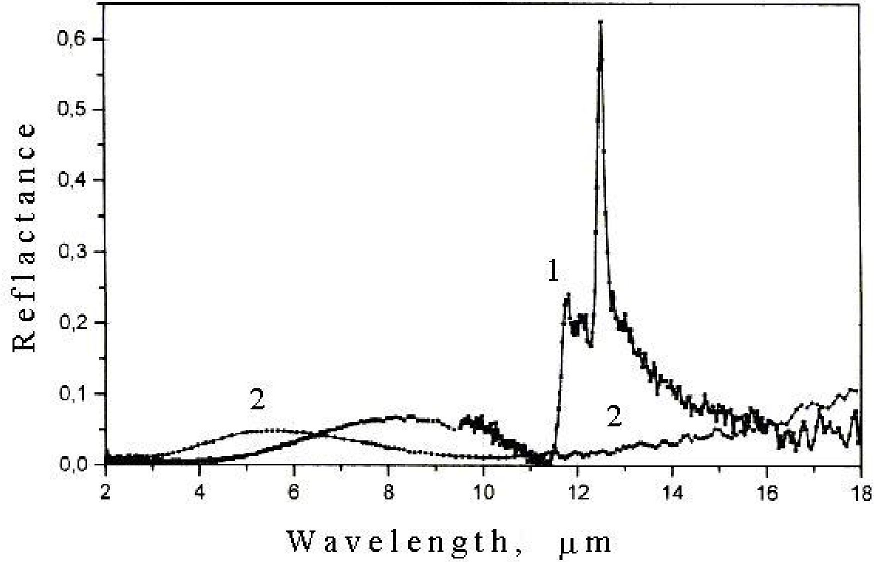

Fig. 1.1. Spectra of light reflection from n-GaAs surface with microrelief of dendrite like before (1) and after (2) the etching out of oxide

We determined the optimal etching modes in concentrated HNO_3 for n^+-GaAs wafers with chemo-mechanically polished surface. These are as follows: T = 17–20 °C, t ≈ 45 s, while those for n-GaAs epitaxial films and p-$Al_{0.85}Ga_{0.15}As$–n^+-GaAs structures are T = 22 °C, t ≈ 15 s and T = 20 °C, t ≈ 5 s, respectively.

At the same time, one should note that microrelief lateral uniformity is immediately determined by the material uniformity and perfection. The n^+-GaAs wafers (with the dopant concentration $N_d \approx 2\cdot10^{17}$ cm^{-3}) demonstrated nonuniformly distributed growth defects, judging from the results of x-ray studies. That is why their relief had areas with different development degrees and, consequently, bigger statistical spread of their optical and electrical parameters. Contrary to this, rather uniform reliefs were obtained for n-GaAs epitaxial films and more uniform n^+-GaAs substrates with $N_d \sim 2\cdot10^{18}$ cm^{-3}.

To obtain quasi-grating-like microrelief at the GaAs (100) surface as a set of oriented along [110] V-grooves whose period varies along the surface over some range, we used a

multicomponent selective etchant on the basis of HF, H_2SO_4 and H_2O_2. The degree of etching selectivity depends, first of all, on the ratio between the contents of oxidant (H_2O_2) and complexing agents (HF and H_2SO_4). Relief formation begins from shallow pits that gradually form "etching channels" whose length and period depend on both etchant content and conditions. At opposite wafer sides (with (100) orientation) the grooves are positioned at perpendicular directions and are confined with crystallographic planes for which etching rate is minimal. These may be {111}A or {111}B planes, angle of intersection with the upper surface is to be 54°44′ (the actual value is less, ~40–44°), or {hhl} planes close to them.

The results of our studies enabled us to select those etchants and conditions that made it possible to obtain rather developed quasi-gratings. For n^+-GaAs these are the following mixtures: $1H_2SO_4$:1HF:$0.5H_2O_2$, with etching temperature from 24 up to 29–30 °C and etching duration from 3 down to 1 min.; for p-AlGaAs compound the corresponding values are $1H_2SO_4$:2HF:$1.5H_2O_2$ with etching temperature of 24–26 °C and etching duration from 5 up to 15 s.

One can see the AFM patterns for microreliefs obtained in Fig. 1.2.

In addition to the above, to obtain strictly periodic relief, we developed a holographic photochemical etching technology (using H_2SO_4:H_2O_2:H_2O = 1:1:100 etchant and Ar laser, with wavelength of 488 nm, that enabled us to obtain interference pattern at the semiconductor surface), as well as technology for chemical photoresist etching. In the latter case to provide the required resistive properties of the compounds chalcogenide vitreous semiconductor (CVS) used for masks, we varied (i) chemical pretreatment of GaAs wafers (to reduce the oxide layer thickness),

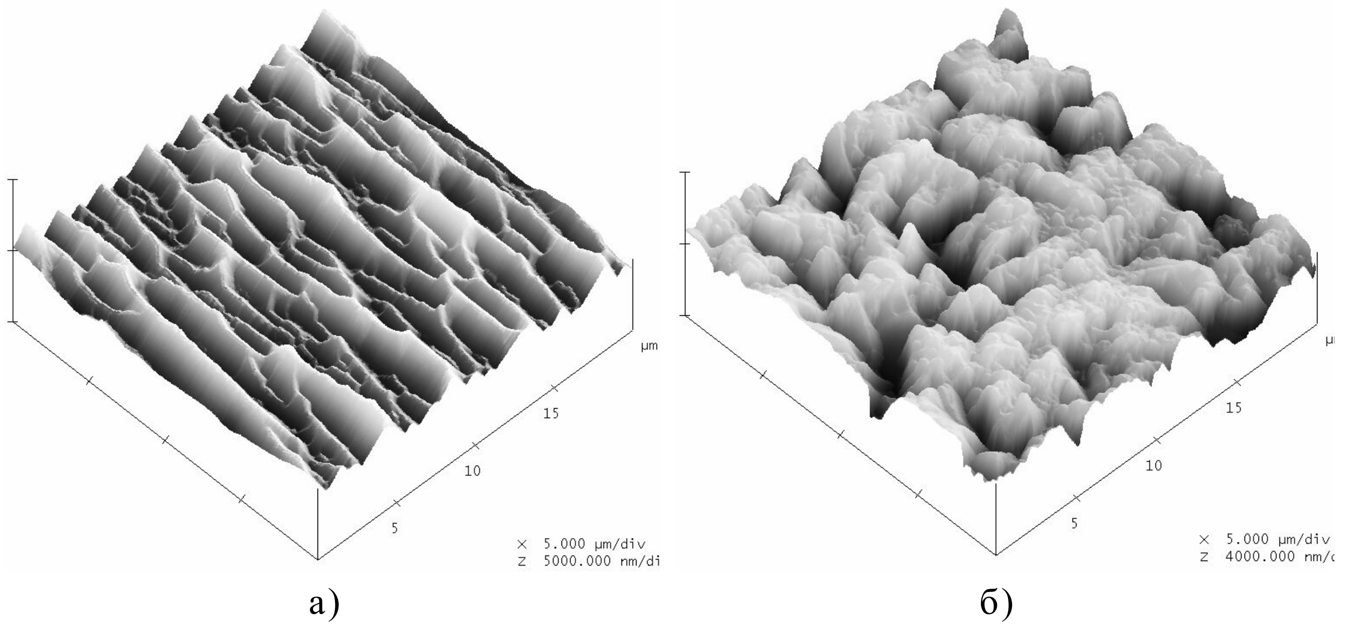

Fig. 1.2. AFM patterns of anisotropically etched AlGaAs film surfaces with quasi-grating-like (a) and dendrite-like (b) microreliefs

Fig. 1.3. AFM patterns of GaAs surface bi-grating-like microreliefs of different development degrees

(ii) thickness of Cr layer (that provided CVS adhesion), and (iii) the CVS composition. As_2Se_3 has been chosen as optimal when using $H_2SO_4:H_2O:H_2O_2$ = 1:1:100 for etching GaAs. The diffraction gratings on them were obtained with holographic technique. In these ways we obtained diffraction gratings with periods $d = \lambda/2\sin\theta$ (where θ is the light incidence angle), varying from 1 up to 5 μm, as well as bigratings (a set of two gratings oriented at perpendicular directions) (Fig. 1.3). Such surfaces can be used for amplification of light absorption and development of specifically selective (angle, polarization) solar cells (SCs).

1.2. OPTICAL PROPERTIES OF TEXTURED SURFACES

1.2.1. Calculations of spectral curves for the coefficient of light reflection from the surface of SC on the basis of AlGaAs−GaAs heterostructure, with allowance made for surface relief using the effective medium method

It is known that the surface of SC made on the basis of AlGaAs−GaAs heterostructures reflects more than 30% incident light in the 0.3–1.2 μm wavelength range (see Fig. 1.4). This is due to high values of refraction (n) and absorption (k) coefficients. To reduce the reflection coefficient R, one should use interference antireflecting coatings with optimal optical parameters. The upper AlGaAs layer of the heterostructure has optical parameters that differ from those of the GaAs substrate: the AlGaAs refraction coefficient n_2 is substantially less than that of GaAs (n_3,) while $k_2 \ll n_2$. This fact makes it possible to reduce the coefficient R of light reflection from the SC surface by optimizing the upper AlGaAs layer thickness (thus corresponding to one-layer antireflection).

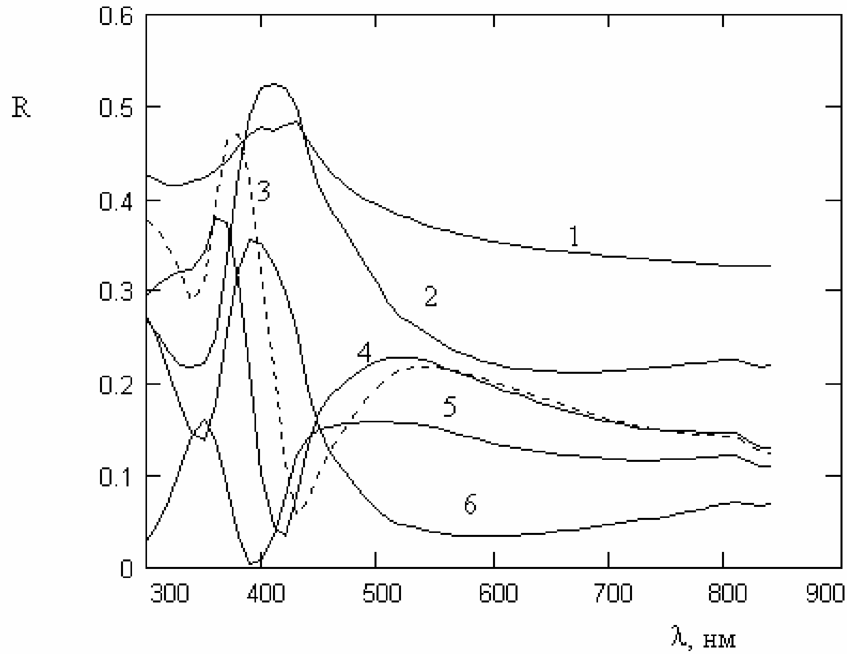

Fig. 1.4. Theoretical spectral curves for the coefficient of light reflection from the GaAs surface (1), AlGaAs–GaAs (2) and SiO_2–AlGaAs relief layer–AlGaAs–GaAs systems (3–6) as function of the SiO_2 and AlGaAs relief layer thicknesses. The optical constants of the AlGaAs upper relief layer are used within the effective medium approximation (Bruggeman model) at the ratio between AlGaAs and air of 0.7. The geometric thicknesses of the SiO_2 and AlGaAs relief layers are 0 and 40 (3), 20 and 30 (4), 50 and 20 (5), 90 and 0 nm (6), respectively

Further reduction of optical reflection losses can be obtained by relief formation on the photodetector surface. When characteristic dimensions of surface relief are greater the incident light wavelength, one can simulate the relief effect within the effective medium approximation (see, e.g., [3]). In the opposite case (when characteristic dimensions of surface relief are below the incident light wavelength) one should consider the relief effect using the ray optics approximation. And, finally, one can reduce optical losses by depositing an additional antireflecting coating.

We made a theoretical analysis of spectral dependencies of light reflection coefficient for the above cases of reflection from GaAs surface, as well as from AlGaAs–GaAs and SiO_2–relief AlGaAs layer–AlGaAs–GaAs systems, as function of the AlGaAs, SiO_2 and relief AlGaAs layer thicknesses. The numerical

calculations were performed for the 300–850 nm wavelength range using the recurrence relations for complex amplitude reflection coefficient [4]. We considered normal incidence of light.

According to [4], the expression for the amplitude coefficient r_{j-1} of light reflection from the (j-1)-th interface can be presented as

$$r_{j-1} = \frac{f_{j-1} + r_j \exp(-2i\Phi_j)}{1 + f_{j-1} r_j \exp(-2i\Phi_j)}. \qquad (1)$$

Here $f_{j-1} = \frac{N_{j-1} - N_j}{N_{j-1} + N_j}$ are the classical Fresnel reflection coefficients relating to the (j-1)-th interface; $\Phi_j = \frac{2\pi}{\lambda} d_j$, $d_j = N_j l_j$ and l_j are the phase, optical and geometric thicknesses, respectively; $N_j = n - ik$ is the complex refractive index for the j-th layer. When performing calculations, we made allowance for dispersion of refractive (n) and absorption (k) indices of GaAs substrate, AlGaAs layer and relief AlGaAs layer. Presence of relief was taken into account within the effective medium approximation using the Bruggeman approach:

$$x \frac{\varepsilon^{(2)} - \varepsilon}{\varepsilon^{(2)} + 2\varepsilon} + (1 - x) \frac{\varepsilon^{(0)} - \varepsilon}{\varepsilon^{(0)} + 2\varepsilon} = 0. \qquad (2)$$

Here ε is the effective dielectric function of the medium; $\varepsilon^{(2)}$ is the AlGaAs dielectric function; $\varepsilon^{(0)}$ is that of the surrounding medium (air); x is the ratio between AlGaAs and air (it is determined by relief character and depth). The following x values were used in our calculations: x = 0.3, 0.5, 0.7 and 0.9.

The refractive and absorption indices of the effective medium layer, n and k, were calculated from the obtained ε values using the following expressions:

$$n = \sqrt{\frac{\sqrt{\varepsilon_1^2 + \varepsilon_2^2} + \varepsilon_1}{2}}, \qquad k = \sqrt{\frac{\sqrt{\varepsilon_1^2 + \varepsilon_2^2} - \varepsilon_1}{2}}$$

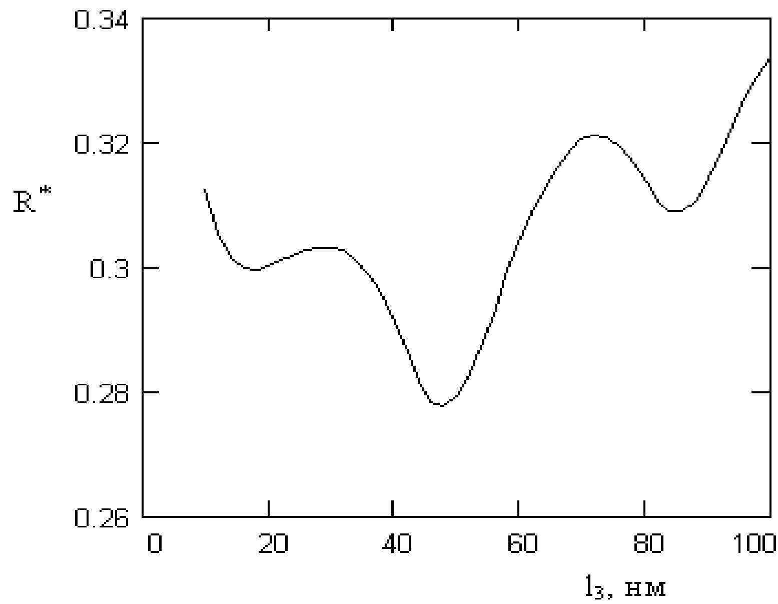

Fig. 1.5. Theoretical curve for the averaged over solar spectrum coefficient of light reflection R^* from the AlGaAs–GaAs system as function of the geometric thickness l_3 of the AlGaAs layer. The averaged over solar spectrum coefficient of light reflection from the GaAs surface $R^*_{GaAs} = 0.38$

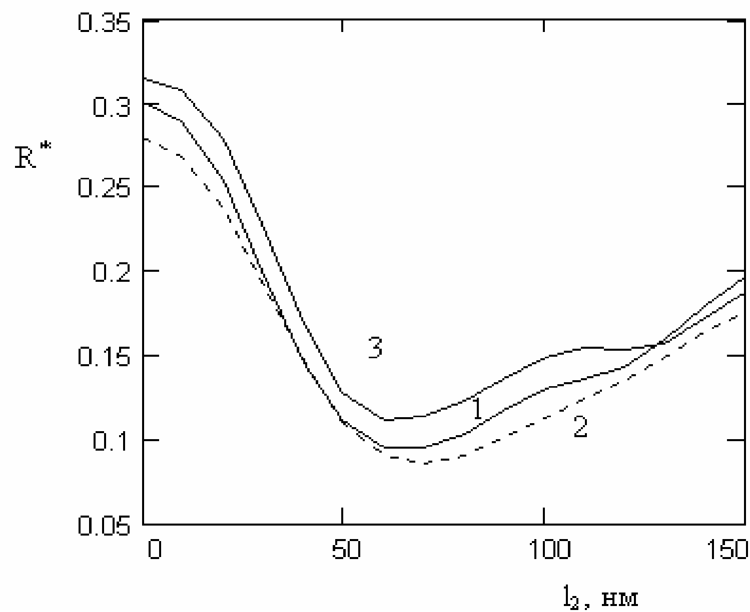

Fig. 1.6. Theoretical curves for the averaged over solar spectrum coefficient of light reflection R^* from the AlGaAs relief layer–AlGaAs–GaAs system as function of the geometric thickness l_3 of the AlGaAs relief layer (the AlGaAs layer thickness being 35(1), 45(2) and 65 (3) nm, respectively). The optical constants of the AlGaAs upper relief layer are used within the effective medium approximation (Bruggeman model) at the ratio between AlGaAs and air of 0.4

where $\varepsilon_{1,2}$ are the real and imaginary parts of the dielectric function of the effective medium ε, respectively. The results obtained are presented in Figs. 1.4−1.8.

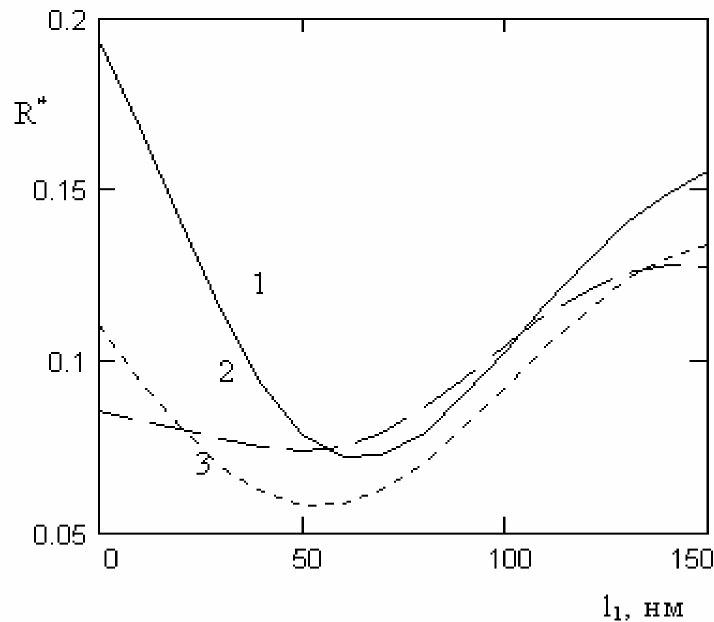

Fig. 1.7. Theoretical curves for the averaged over solar spectrum coefficient of light reflection R^* from the SiO_2−AlGaAs relief layer−AlGaAs−GaAs system as function of the geometric thickness of the SiO_2 film (the AlGaAs relief layer thickness being 30 (1), 50 (2) and 70 nm (3), respectively). The geometric thickness of the AlGaAs layer is 45 nm in all cases. The optical constants of the AlGaAs upper relief layer are used within the effective medium approximation (Bruggeman model) at the ratio between AlGaAs and air of 0.4

Several conclusions can be made from these results:

– Optimization of the AlGaAs layer thickness enables one to reduce the coefficient R of reflection from SC surface by one half (to the value $R \approx 0.2$).

– A relief whose optical thickness is up to 15 nm practically does not affect the reflection coefficient; substantial effect begins from thicknesses ≥ 35 nm. Reflection becomes minimal at geometrical thicknesses of the relief layer of 70−110 nm.

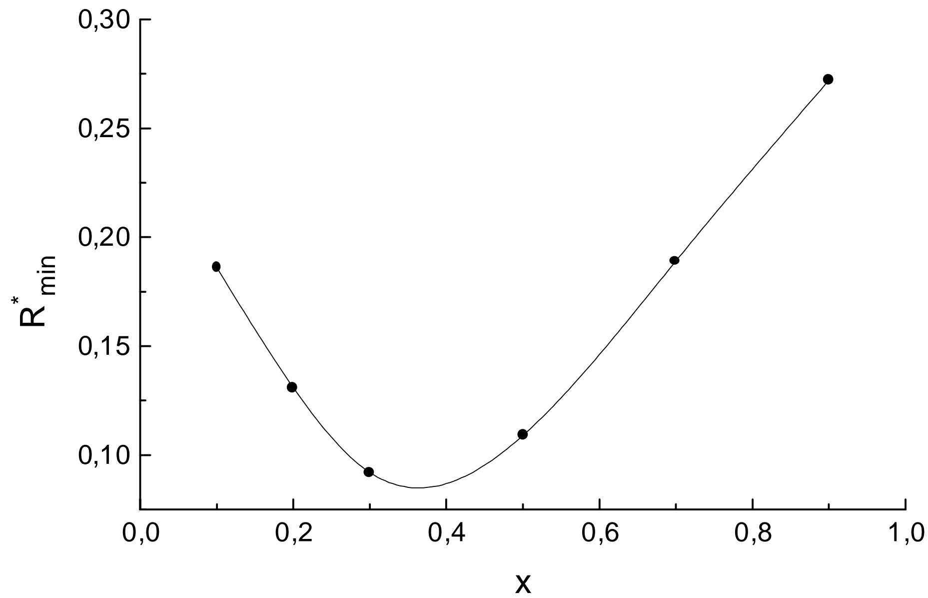

Fig. 1.8. Theoretical curves for the minimal value of the averaged over solar spectrum coefficient of light reflection R^* from the AlGaAs relief layer–AlGaAs–GaAs system as function of the ratio x between AlGaAs and air within the effective medium approximation (Bruggeman model)

– Deposition of a SiO_2 antireflecting coating enables one to efficiently reduce optical reflection losses down to (2–3) % in the 500–850 nm wavelength range.

– Combination of a SiO_2 antireflective coating with relief formation on the photodetector surface may be efficient.

1.3. STUDIES OF OPTICAL CHARACTERISTICS OF THE GaAs MICRORELIEF SURFACES

Optical characteristics of microtextured surfaces (serving as substrates for further epitaxy) determine ability of such surfaces for reduction of optical losses in SCs. These characteristics were one of the main factors taken into account when choosing microtexturing conditions.

When studying the optical properties of microrelief and flat (for comparison) surfaces of GaAs and its solid solutions on which PECs are based, we measured:

- spectra of specular, diffuse and total reflection of light in the λ = 0.4–1.0 μm wavelength range that is of importance for PEC operation;
- spectra of specular reflection in IR (λ = 2–18 μm) - to characterize material doping level (from the plasma edge), to determine the random-mean-square (*rms*) height of microrelief δ and to check presence of oxide layer on the surface (from the characteristic absorption bands);
- photoluminescence spectra in the λ = 0.47–1.0 μm wavelength range – to determine presence of solid solutions and estimate their composition (x) from the edge radiation, as well as to determine structure perfection of the substrate and epitaxial layers;
- Raman spectra in the ν = 30–600 cm^{-1} wave number range – to estimate material structure perfection in the near-surface region;
- Angle dependencies of the ellipsometric angles ψ and Δ at laser monochromatic excitation with λ = 632.8 nm – to determine thicknesses and refractive indices of dielectric layers on the surfaces of GaAs and its solid solutions that are used as antireflecting or protective coatings.

1.3.1. Specular and diffuse reflection of light

To determine total light reflection in the fundamental photosensitivity region of GaAlAs/GaAs SC (0.4–0.9 μm), we measure the specular reflection spectra (using a spectrometer ІКС-12 equipped with an attachment for specular reflection) and diffuse reflection spectra (using a spectrophotometer СФ-4 with an integrating sphere) at normal light incidence onto the sample.

From these spectra we calculated the spectra of total (diffuse + specular) reflection of light in the wavelength range which is of importance for PEC operation, as well as the spectra of the so-called haze parameter:

$$H_R = R_{dif} / \left(R_{spec} + R_{dif} \right). \tag{3}$$

If R_0 is the reflection coefficient of a flat sample, then we have for relief surface:

$$R_{spec.} = R_0 \exp\left[-\left(\frac{4\pi\sigma_{rms} n}{\lambda} \right)^2 \right],$$
$$R_{dif} = R_0 - R_{spec.}, \tag{4}$$

and one may use the following expression for theoretical estimation of the haze parameter:

$$H_R = 1 - \exp\left[-\left(\frac{4\pi\sigma_{rms} n}{\lambda} \right)^2 \right], \tag{5}$$

where n is the refractive index of the ambience and σ_{rms} is the *rms* deviation of the surface from flat one.

Shown in Fig. 1.9 are typical spectra of specular (a), diffuse (b) and total (c) reflection coefficients for polished (chemically and mechano-chemically) and textured (with dendrite-like and quasi-grating-like microreliefs) *n*-GaAs surfaces. One can see that the specular reflection coefficient can be reduced down to 1–2% by choosing the proper chemical texturing conditions, while the diffuse reflection coefficient in this case can be reduced down to a value < 15% only (Fig. 1.10). The corresponding curves for GaAs surface with a deterministic (not random) diffraction bigrating-type relief are presented in Fig. 1.11.

From the results obtained we calculated the effective reflection coefficients averaged over the AM0 solar spectrum for the spectral range studied ($\overline{R}$). It was found that specular $\overline{R}$ decreases from 37.8% (for chemically polished n-GaAs surface) down to 0.4–0.6% (for microtextured surface). The total reflection coefficient $\overline{R}_\Sigma$ decreased from 40.4% (for polished surface) down to 14.8% (for surface with dendrite-like microrelief) and to ~13% (for the optimized quasi-grating-like microrelief). For GaAs

surface with the bigrating-type relief (period of ~4.8 μm) $\overline{R}_{\Sigma}$ was 24.7–28.4%, depending on the grating depth and form. Thus this periodic relief still was not optimal for practical application in photoelectric converters (PECs).

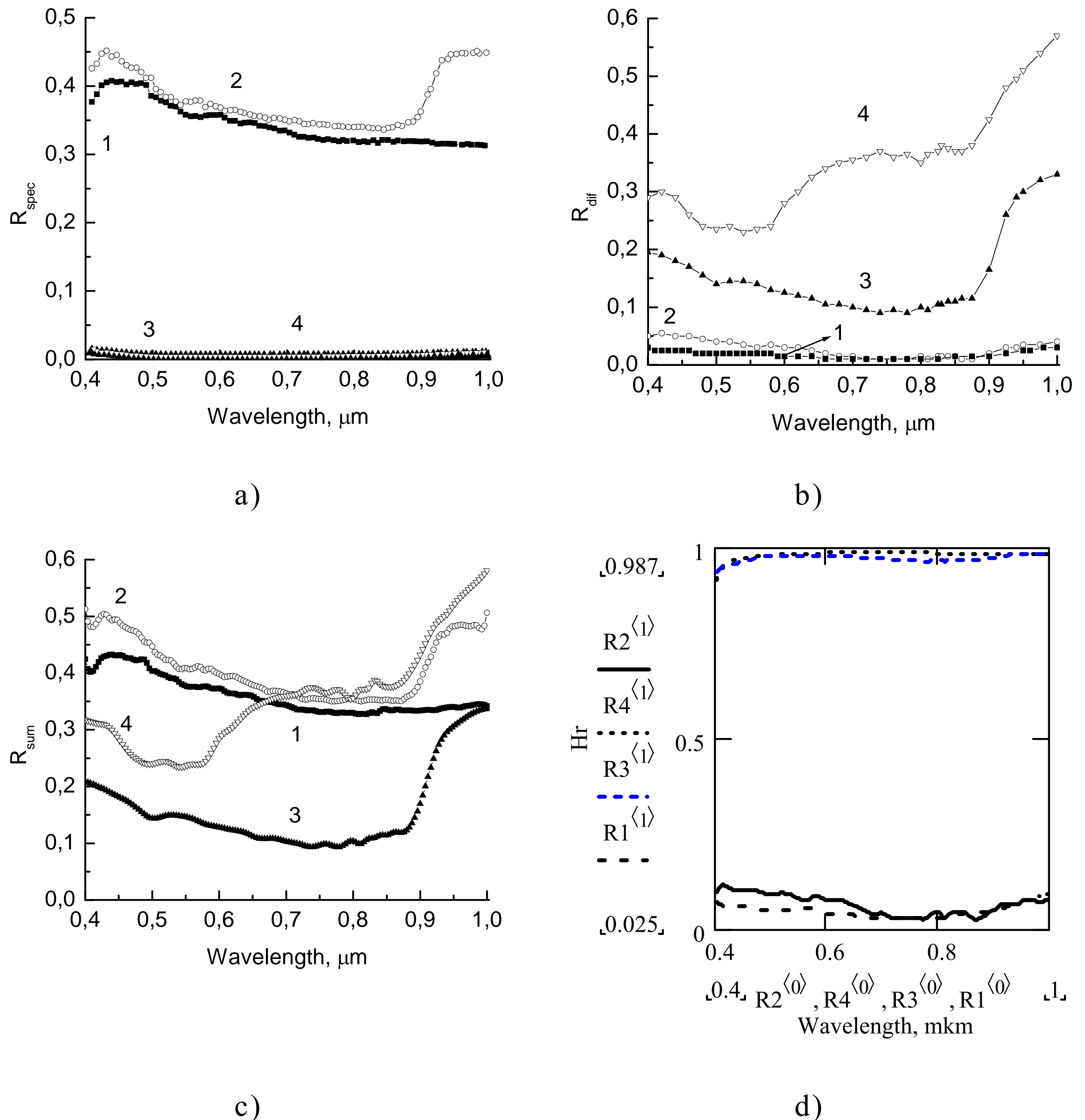

Fig. 1.9. Spectra of specular (a), diffuse (b) and total (c) reflectance and haze parameter (d) for n-GaAs surfaces: (1) – chemically-mechanically polished, (2) – etched in polishing etchant, (3) - with surface microrelief of dendritic type, (4) – with microrelief of quasi-grating type

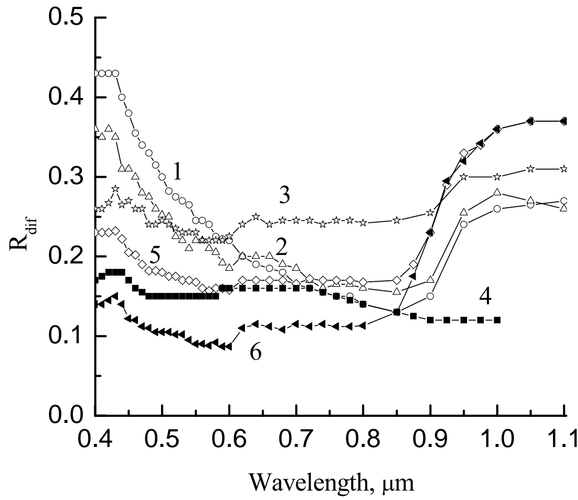

Fig. 1.10. Diffuse reflectance for n-GaAs surface with microrelief of quasi-grating (1-4) and dendritic (5, 6) type obtained at various technological conditions. The etchant composition is given in text, temperature and duration are: 22 °C, 1 min (1), 24 °C, 1 min (2), 30 °C, 1 min (3), 24 °C, 3 min (4), 24 °C, 30 s (5), 24 °C, 45 s (6)

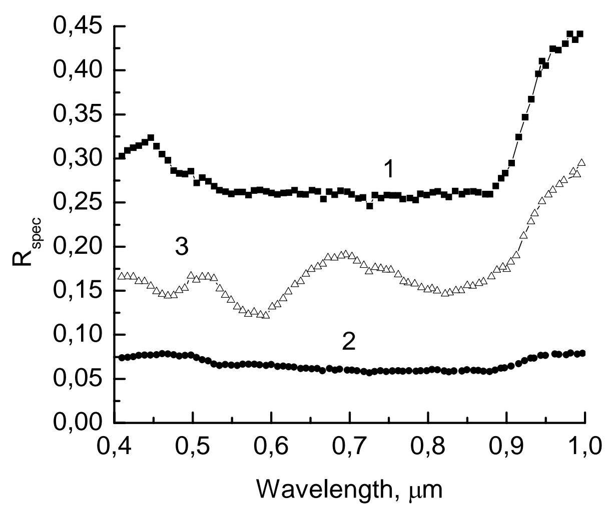

a)

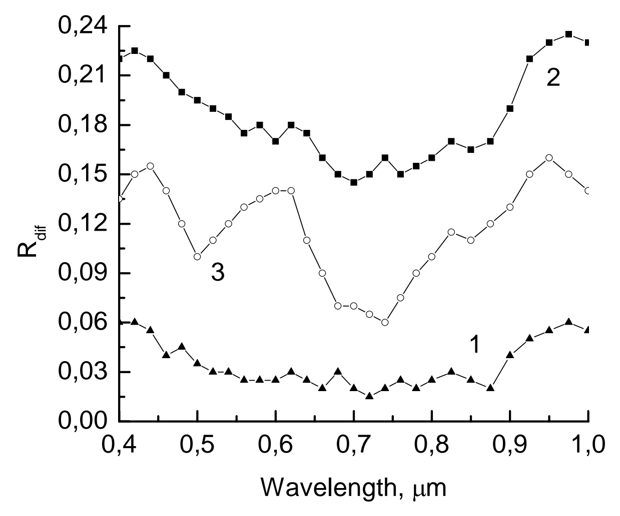

b)

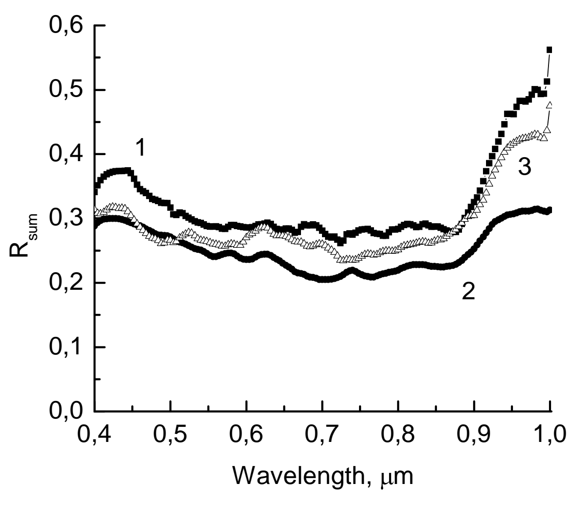

c)

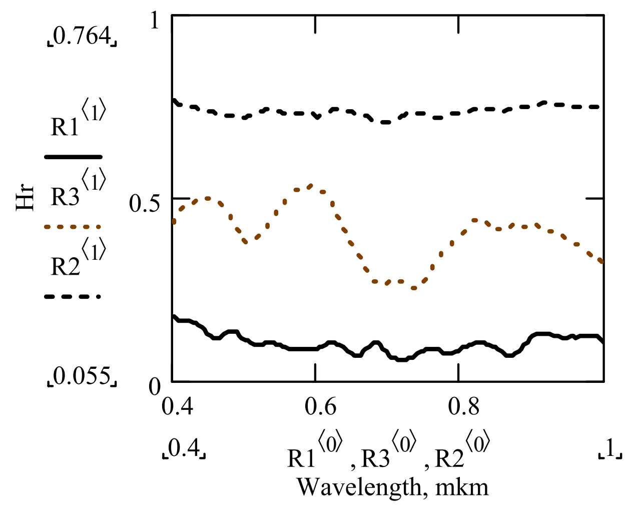

d)

Fig. 1.11. Spectra of specular (a), diffuse (b) and total (c) reflectance and haze parameter (d) for n^+-GaAs surfaces: chemically polished (1) and with surface microrelief of diffraction bigrating type (2, 3), where (3) – for deeper bigrating

We also studied the reflection spectra for *n*-InGaAs–*n*-GaAs heteroepitaxial structures grown on flat and microtextured (quasi-grating-like relief) *n*-GaAs substrates. Depending on variations of intrinsic surface microrelief of epitaxially-grown InGaAs layers, $\overline{R}_{\Sigma}$ varied from 33.3% to 40.8%. At the same time, among the epitaxial structures grown on a textured substrate there were such ones for which $\overline{R}_{\Sigma} \cong 14.3\%$. This fact evidences that the advanced

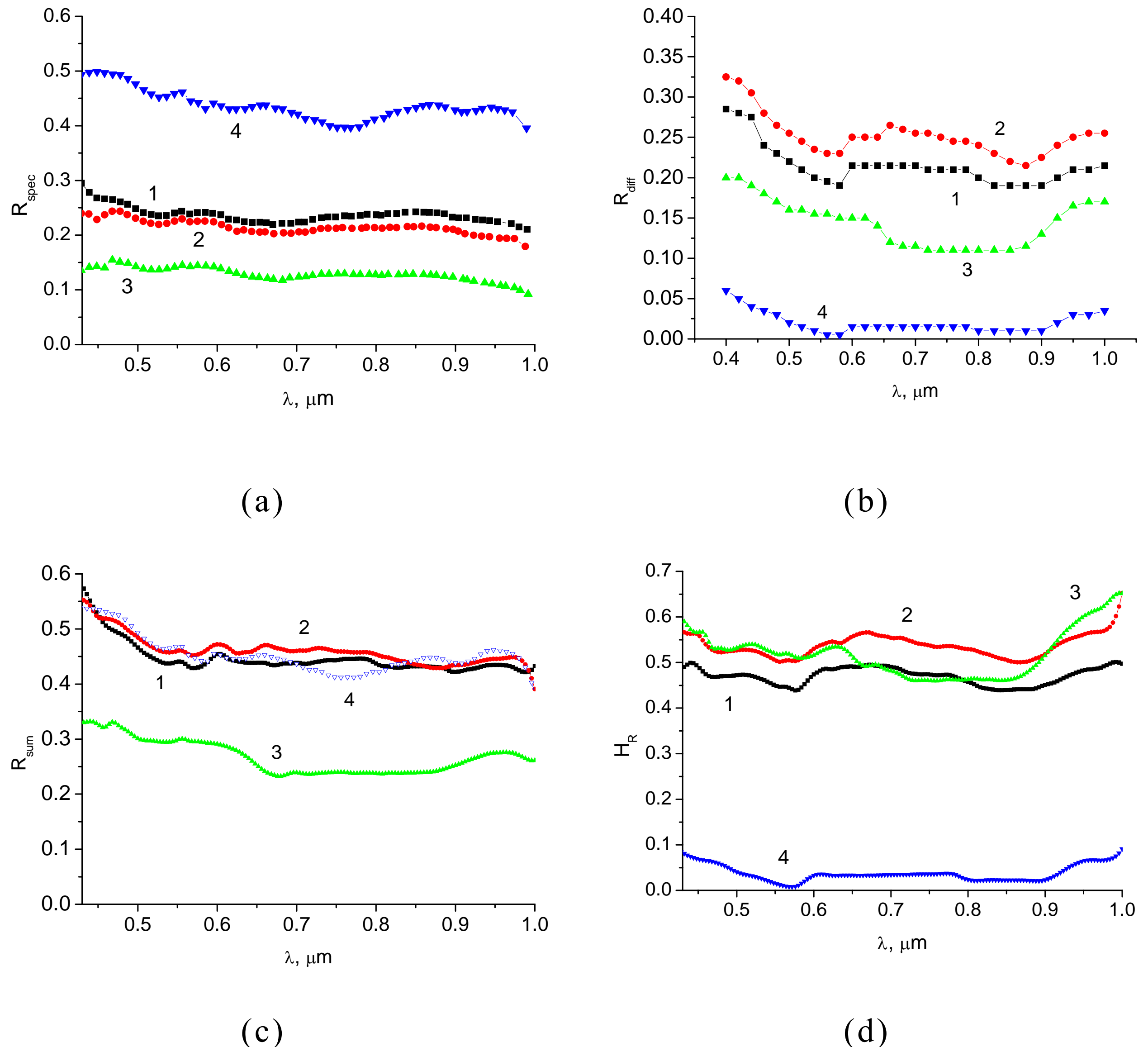

Fig. 1.12. The spectra of specular (a) and diffuse (b) reflection from the n^{+}-GaAs (substrate) /*n-p*-GaAs /p^{+}-$Al_xGa_{1-x}As$/ p^{+}-GaAs structures with substrate microreliefs: 1 – quasi-grating-like (28 °C, 30 s) (MO-1); 2 – quasi-grating-like (24 °C, 30 s) (MO-2); 3 – dendrite-like (22 °C, 45 s) (MO-3); 4 - flat (x ≈ 0.6) (MO-4). The calculated from them spectra of total reflection (c) and haze parameter (d)

technique for epitaxial growth of heterojunctions on substrates with microtextured surfaces is promising for reduction of optical losses in heterophotoconverters.

Shown in Fig. 1.12 are the spectra of specular, diffuse, total reflection and haze parameter of light at almost normal incidence onto the samples of the p^+-GaAs/p^+-$Al_xGa_{1-x}As$/n-p-n^+-GaAs heterojunction structure with “cap”-layer (p^+-GaAs) thickness of ~0.3 μm and various substrate microrelief.

Optimal for PECs are the spectra with minimal total reflection and the haze parameter close to 1. From the value of this parameter one can estimate σ_{rms} and compare it to the AFM results.

1.3.2. Multiangle ellipsometry measurements

Shown in Fig. 1.13 are the results of multiangle monochromatic ellipsometry measurements. Their particular features (minimum of $\psi(\varphi)$, limiting values of $\Delta(\varphi)$) and the total set of the data for 15–25 angles of incidence enable one to determine with sufficient accuracy n, k and d for thin dielectric layers (in our case, SiO_x) on the reference samples with flat surfaces. To this end, we applied the computer software that has been developed for solution of the inverse problem of ellipsometry.

The results obtained (along with the value of the achieved minimum of the fitting objective function) are presented in Tables 1.1 and 1.2.

Table 1.1. Оптические параметры и толщина слоев многослойной структур № 1-3

sample #	n_{SiO2}	k_{SiO2}	d_{SiO2}, nm	n_{ox}	k_{ox}	d_{ox}, nm	n_{sputt}	k_{sputt}	d_{sputt}, nm	n_{GaAs}-substr	k_{GaAs}-substr	F
1	–	–	–	2.052	0.067	15.00	3.251	0.005	50.00	3.861	0.196	3.503
2	1.479	0.076	67.13	–	–	–	–	–	–	3.854	0.219	0.333
3	1.495	0.042	68.64	–	–	–	3.341	0.015	89.99	3.864	0.207	0.074

1 – oxide/$Al_xGa_{1-x}As$/GaAs (КН-20); 2 – SiO_x/GaAs; 3 – SiO_2/p^+-$Al_xGa_{1-x}As$/GaAs (SEM-1).

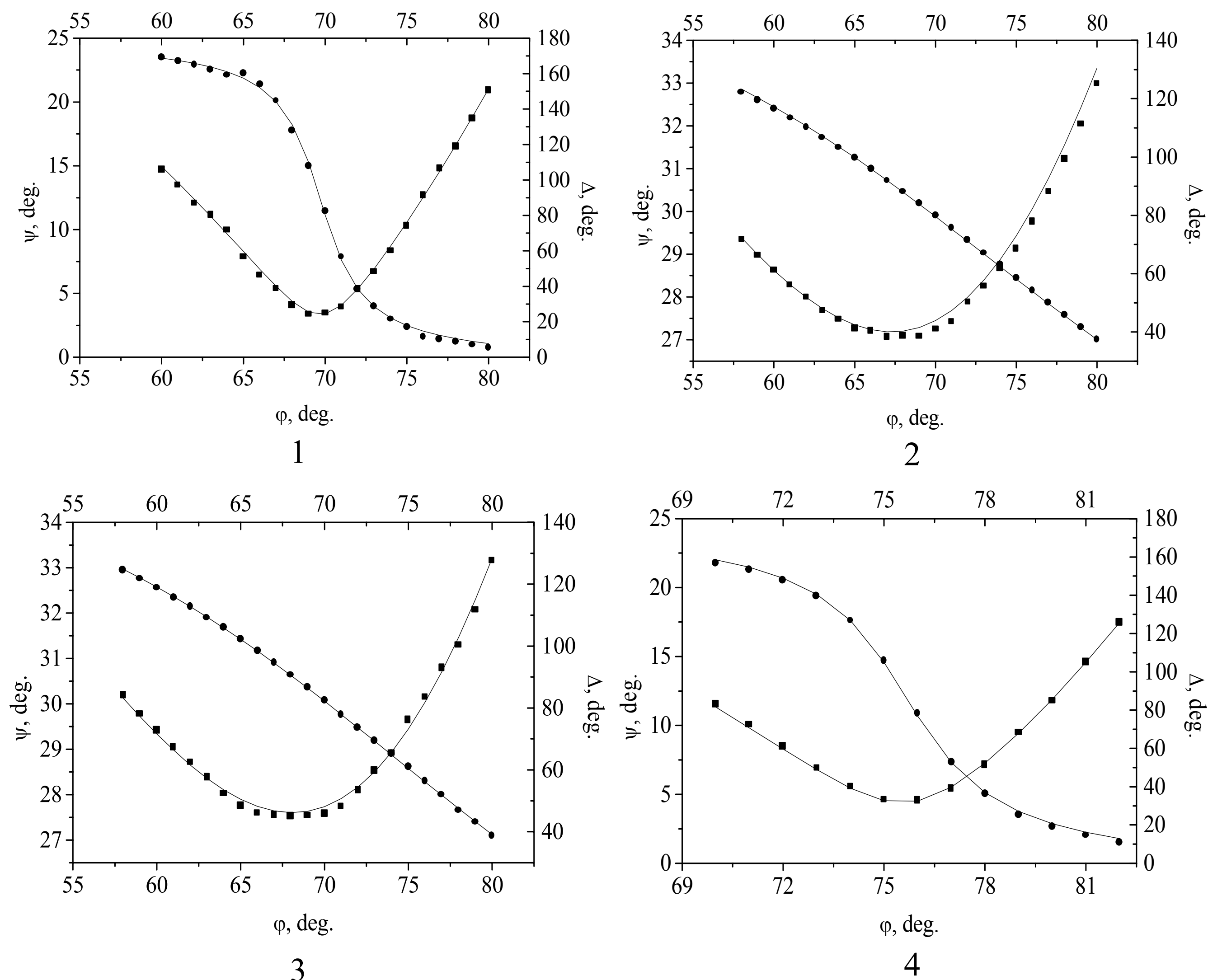

Fig. 1.13. The experimental (marks) and calculated (curves) angular dependencies $\psi(\varphi)$ and $\Delta(\varphi)$ for the structures 1, 2, 3, 4 (see Tables 1.1 and 1.2)

Table 1.2. Оптические параметры и толщина слоев многослойной структуры № 4

sample #	n_{ox}	k_{ox}	d_{ox}, nm	n_{layer2}	k_{layer2}	d_{layer2}, nm	n_{layer1}	k_{layer1}	d_{layer1}, nm	n_{GaAs}-substr	k_{GaAs}-substr	F
4	2.219	0.070	2.160	3.841	0.215	318.16	3.239	0.041	637.10	3.866	0.187	1.039

4 – oxide/p^+-GaAs (layer 2)/p^+-$Al_xGa_{1-x}As$ (layer 1)/p-n-GaAs/n^+-GaAs (100) (MO-4).

1.3.3. IR reflection spectra

We studied IR reflection spectra in the 2–18 μm wavelength range for the GaAs samples with formed surface relief.

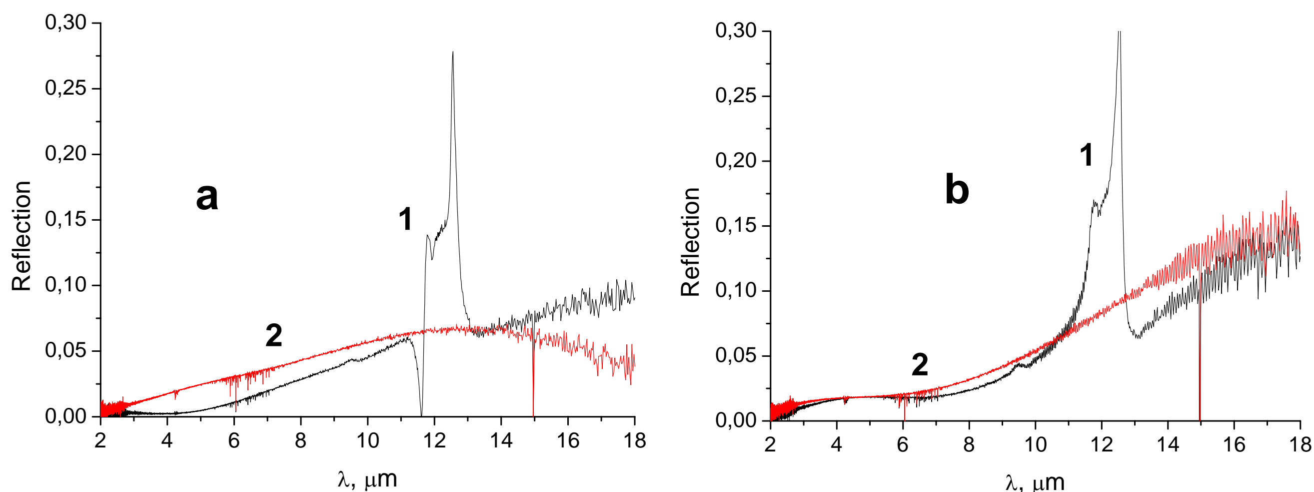

Fig. 1.14. The reflection spectra of the n-GaAs (100) samples (dopant concentration of $(2\div5)\cdot10^{16}$ cm^{-3}) with dendrite-like surface microrelief (a) and porous surface (b), taken before (curve 1) and after oxide etching-off (curve 2)

Figures 1.14a,b present the reflection spectra of the samples n-GaAs (100) (impurity concentration of $(2\div5)\cdot10^{16}$ cm^{-3}) with dendrite-like surface relief (a) and porous surface (b), both before etching (curve 1) and after etching-off oxide in 0.75% HCl during 5 min. (curve 2). The sharp peaks in the reflection spectra 1 indicate

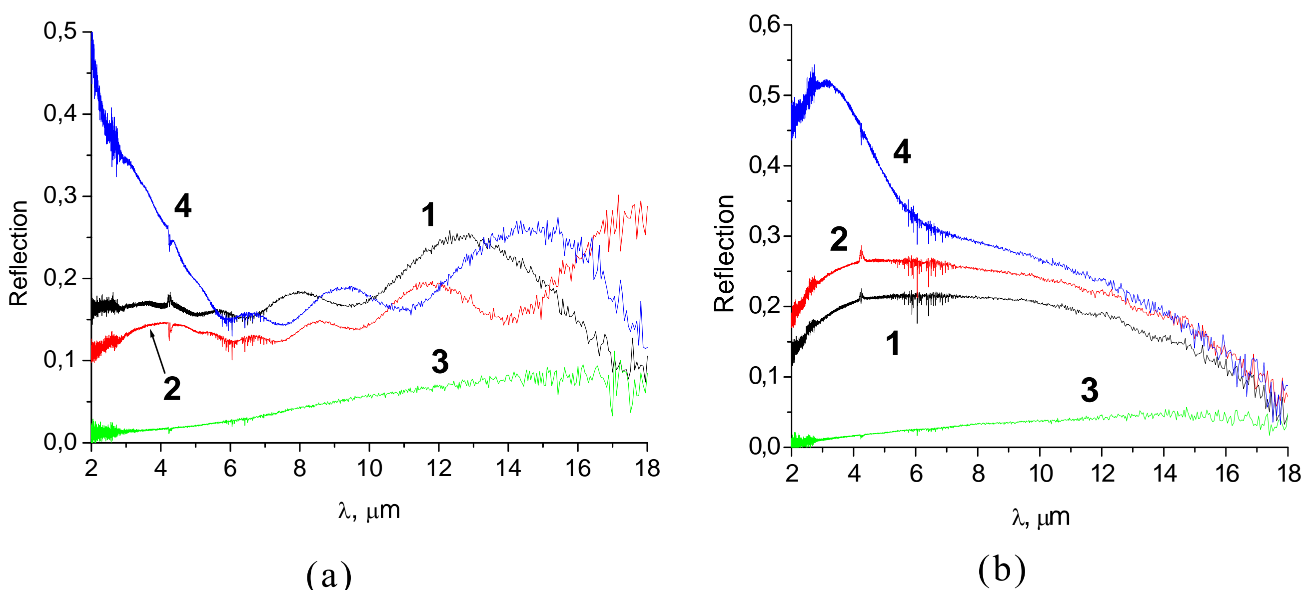

Fig. 1.15. The reflection spectra of p^+-GaAs/p^+-$Al_xGa_{1-x}As$/p-n-n^+-GaAs heterojunction structures taken before (a) and after (b) of p^+-GaAs layer etching-off: 1 - M0-1, 2 - M0-2, 3 - M0-3, 4 - M0-4

at presence of oxide layer on the surface. This layer was formed during microtexturing. After double etching the surface is completely free from the oxide layer (which, according to [1], was a micro-island layer of As_2O_3).

Shown in Fig. 1.15a are the reflection spectra for the samples M0-1–M0-4, These samples are the p^+-GaAs/p^+-$Al_xGa_{1-x}As$/p-n-n^+-GaAs heterojunction structures VPE-grown on the (100) n^+-GaAs substrates with flat (MO-4) and microtextured surfaces (MO-1 and MO-2 – with quasi-grating-like microrelief, MO-3 – with dendrite-like microrelief).

Figure 1.15b presents the reflection spectra for the above structures after etching-off the p^+-GaAs layer in the etchant citric acid:H_2O_2. One can see that etching results in disappearing of the interference structure of the spectra related to the p^+-GaAs layer (in the case of the flat sample MO-4) or to quasi-periodical grating on the surfaces of the samples MO-1, 2.

The results of our studies of IR reflection spectra for the (100) microtextured n^+-GaAs substrates (impurity concentration of ~10^{18} cm^{-3}) are presented in Fig. 1.16 (1 – dendrite-like microrelief, 2 and 3 – quasi-grating-like microrelief).

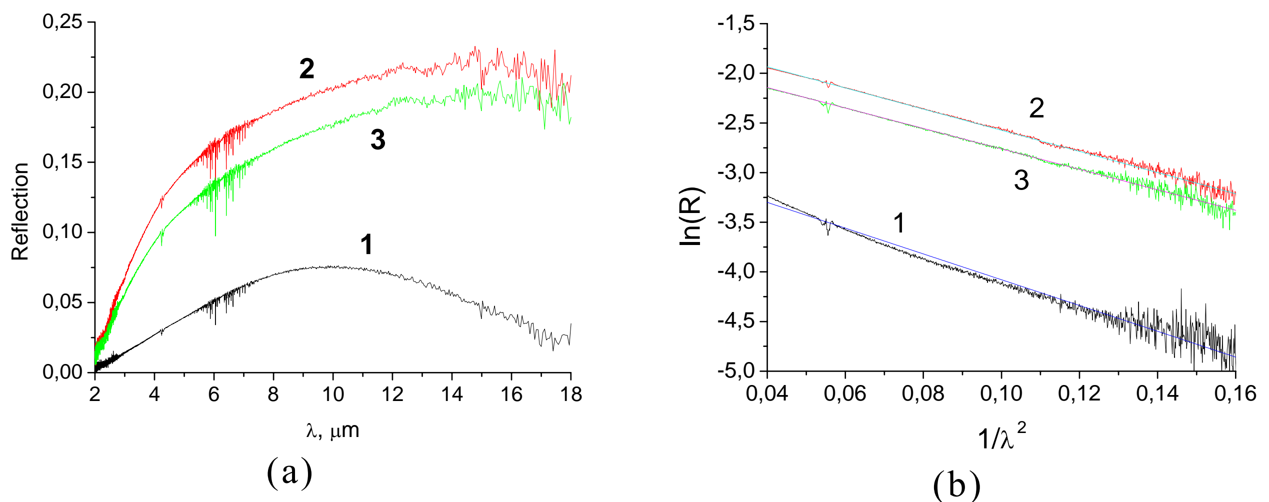

Fig. 1.16. The reflection spectra of (a) microtextured n^+-GaAs (100) substrates (impurity concentration of ~10^{18} cm^{-3}): 1 – dendrite-like microrelief, 2, 3 – quasi-grating-like microrelief; (b) – high-energy portions of the reflection spectra in the $\ln R-1/\lambda^2$ coordinates

From analysis of spectral curve 1 falling off in the low-energy region we estimated doping degree for the corresponding sample: $N_d - N_a \approx 1.8 \cdot 10^{18}$ cm^{-3}.

Figure 1.16b shows the high-energy portion of spectra for the microtextured (100) n^+-GaAs substrates with microreliefs of dendrite-like and quasi-grating-like type in the $\ln R - 1/\lambda^2$ coordinates. Assuming scattering at surface microrelief to be isotropic (according to the scalar theory of light scattering) and approximating the reflection spectrum by the expression $R = R_0 \exp\left[-(4\pi\sigma/\lambda)^2\right]$ (where R_0 is the coefficient of light reflection from flat surface, σ is the root-mean-square (*rms*) deviation of surface from flat one, λ is the light wavelength), we determined from Fig. 1.16 the mean size of nonuniformities: 1 - $\sigma_1 \approx 0.29$ μm, 2 - $\sigma_2 \approx 0.26$ μm, 3 - $\sigma_3 \approx 0.26$ μm. These results are in good agreement with the AFM data.

1.4. INVESTIGATION OF PHOTOLUMINESCENCE SPECTRA

We investigated photoluminescence (PL) spectra, as well as Raman spectra, of multilayer heterostructures, finished SCs and microtextured n^+-GaAs substrates at room temperature. These studies, along with the results of XRD and photoelectric investigations, enable one to determine more accurately their composition and perfection degree.

The spectra were measured with a monochromator МДР-3. The lines 476.5, 496.5, 488 and 514.5 nm of argon lasers ЛГН-404 and ЛГН-503 served as excitation source when recording PL spectra. Signal registration was made with photomultiplier tubes (PMTs) „ФЭУ-100" (in the UV and visible ranges) and „ФЭУ-62" (in near IR). PMTs were supplied from a high-voltage source that provided 1.77 kV for „ФЭУ-100" and 1.5 kV for „ФЭУ-62". A signal from the PMT output comes to the dc amplifier input. After amplification it goes to a circuit which forms from it a signal of variable amplitude. Further this signal is brought to the linear input

of a soundmap of PC where it is processed with the program mdr3.exe. This program controls (i) a synchronous motor that turns a diffraction grating of the monochromator МДР-3 and (ii) its gearset, and takes the signal from the linear input of the soundmap or a double-bit counter.

The registration system can operate in two modes: as a dc amplifier with following analog-to-digital conversion or photon counter. The required operation mode is chosen depending on the excitation source used, PMT, intensity of the spectrum measured and requirements for accuracy and speed of measurements.

At room temperature the main PL band is that stemming from interband recombination, so the composition x of direct-gap compositions was determined from the position of the PL peak:

$$E_g^{\Gamma} = 1.424 + 1.266x + 0.266x^2, \quad (6)$$

while at higher (> 0.45) x it was determined from the energy of indirect-gap transitions:

$$E_g^{X} = 1.900 + 0.125x + 0.143x^2. \quad (7)$$

In the latter case the PL peak may be weak and smeared out. Therefore, when interpreting the PL spectra, we also took into account the results obtained with other methods, in particular, x-ray diffraction (XRD).

Figure 1.17 presents spectra of several heteroepitaxial structures (M3, M4, SE#44, SEM-1). One can see a clear peak that makes it possible to determine composition of the $Al_xGa_{1-x}As$ layer.

If at T = 300 K there is no PL band related to a heavily doped $Al_xGa_{1-x}As$ layer, then one can obtain the required information from the Raman spectra.

Figure 1.18 shows such dependencies for the structure EM-304. On one of its sides an $Al_xGa_{1-x}As$ layer was VPE-grown. Of several low-intensity lines in the 260–400 cm^{-1} region, three are pronounced clearly. Two of them (at 264 cm^{-1} and 290 cm^{-1}) correspond to TO and LO phonons of GaAs, while the line at

400 cm^{-1} corresponds to the LO mode of $Al_xGa_{1-x}As$ with x = 0.82 according to the following equation [7]:

$$E(mV) = 44.634 + 8.78x + 3.32x^2. \qquad (8)$$

This value of x agrees also with that given by the technologists (x = 0.8÷0.85).

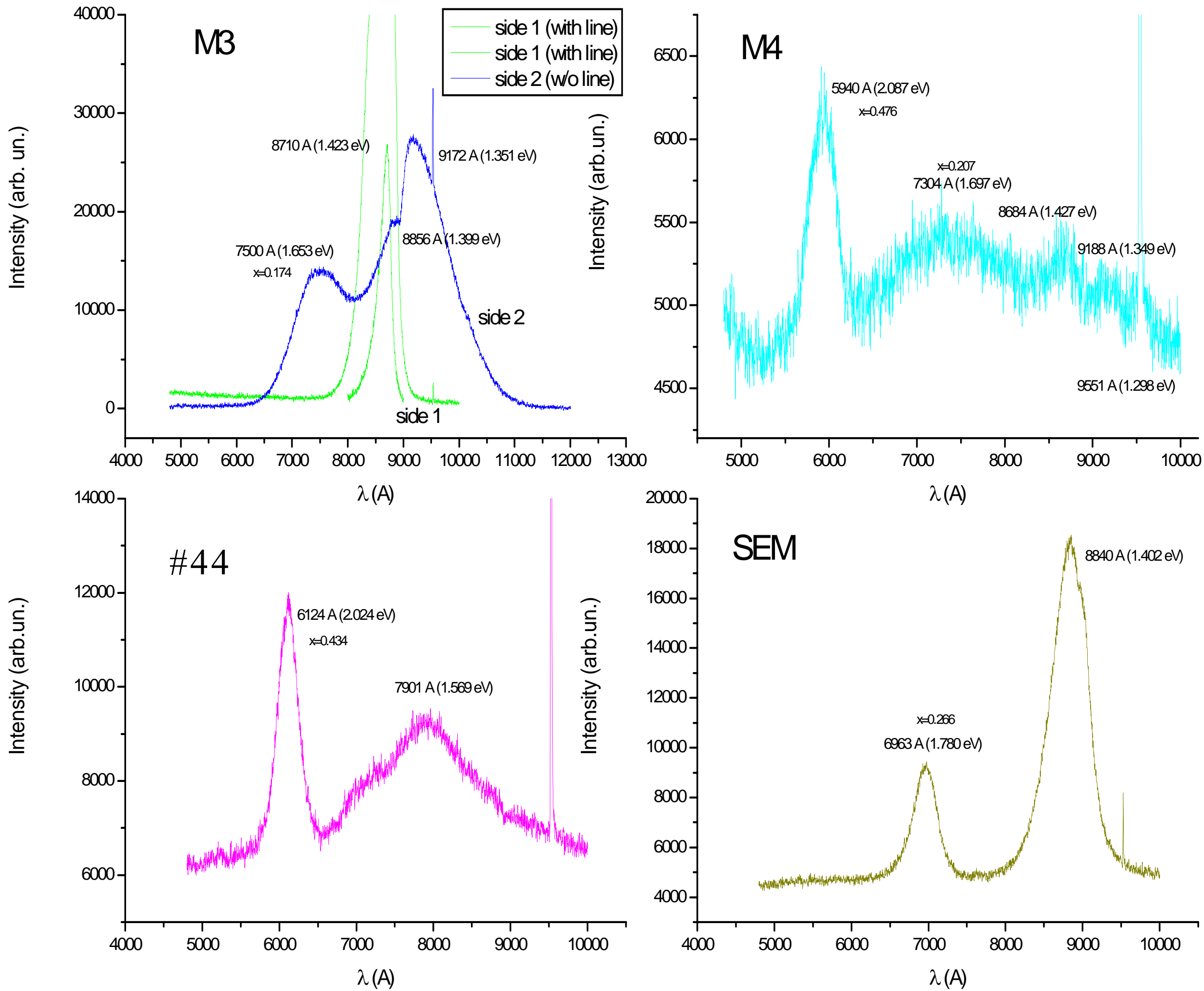

Fig. 1.17. PL spectra of the p^+-$Al_xGa_{1-x}As/p^+$-n-GaAs structures obtained with different LPE techniques (M3, M4, #44) and VPE (SEM)

Our objective was to characterize their composition depending on the manufacturing technology and substrate microrelief. A typical batch of heterostructure was those AK 143–150 with different $Al_xGa_{1-x}As$ layer thicknesses. They have been LPE-grown in a horizontal shifting container on flat and textured n-n^+-GaAs substrates.

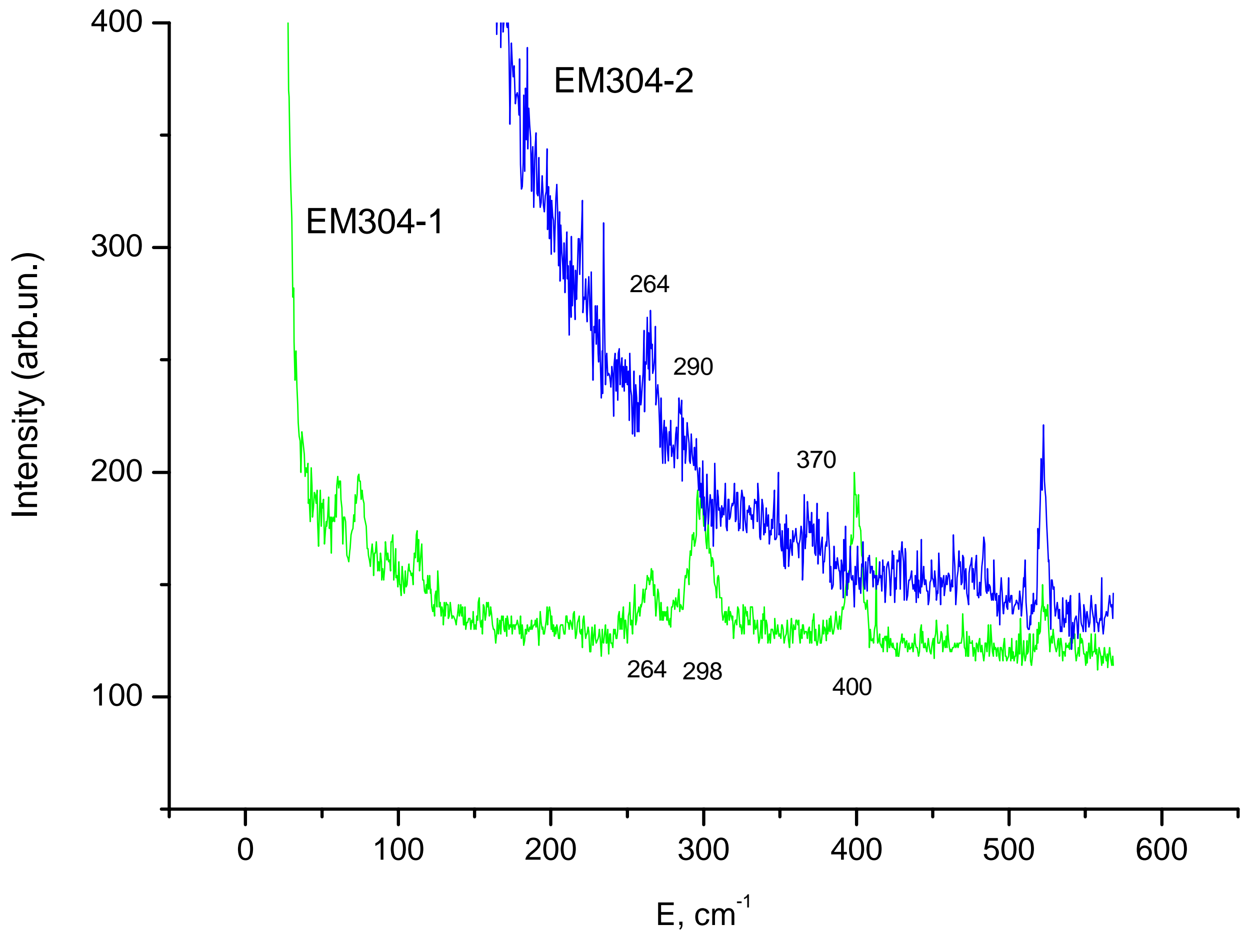

Fig. 1.18. Raman spectra of the p^+-$Al_xGa_{1-x}As$/p^+-n-n^+-GaAs structure VPE-grown on microtextured (porous) n^+-GaAs surface (EM-304-1 – on the p^+-$Al_xGa_{1-x}As$ side, EM-304-2 – on the n^+-GaAs side)

According to the data supplied by the technologists, for heterostructures with a thin (~2 μm) $Al_xGa_{1-x}As$ layer (sample # 150 – a flat buffer layer, sample # 149 – a textured buffer layer with a quasi-grating-like relief) a clearly pronounced PL peak was observed at an energy E = 1.79 eV (# 149) and 1.77 eV (# 150). This corresponded to the compositions x = 0.27 and 0.26, respectively. The peak of interband recombination in the GaAs substrate was more pronounced for the flat sample # 150 than for the textured sample # 149. This fact may indicate at a thicker layer of $Al_xGa_{1-x}As$ solid solution in the case of textured substrate. This conclusion was supported by the XRD results.

For thicker $Al_xGa_{1-x}As$ layers rather broad peaks were observed too. They corresponded to the composition x = 0.16, 0.20 and 0.41 (for different samples). This may indicate at formation of a graded-gap (or layered) structure during heteroepitaxial growth. A difference between x values for the flat and textured structures was insufficient (x = 0.19 for the textured sample # 143 and x = 0.20 for the flat sample # 144). At the same time, a rather weak and smeared out PL peak at $\lambda \approx 600$ nm was observed for the structures # 143, 144 and 146. According to Eq. (8), this corresponds to x = 0.73÷0.75. This result is in agreement also with those obtained by XRD.

References

[1] Gorbach T.Ya., Pidlisnyi Ye.V., Svechnikov S.V. // Optoelektron. i Poluprovodn. Tekhn. 1988. No.13. p.34.

[2] Nemoshkalenko V.V., Aleshin V.G., Gassanov L.G. Poverkhnost'. 1983. No.2. p.88.

[3] Rowlands S.F., Livingstone J., Lund C.P. Proc. 17th EPVSEC. Munich. Germany. 2001. p. 3011.

[4] Berning P.H. In: Physics of Thin Films. G. Hass (Ed.) vol. 1. Academic Press. New York. 1963. p.69.

[5] Dmitruk N.L., Kotova N.V., Pidlisnyi E.V., Barlas T.R. Resonant excitation of vibrational modes on a microrelief surface of GaAs. Phys. Solid State. 1993. vol.35(1). p.8.

[6] http://web.nps.navy.mil/~jppowers/

[7] Pavesi L., Guzzi M. // J. Appl. Phys. 1994. vol.75(10). p.4779.

Chapter II

SOME TECHNOLOGICAL ASPECTS OF FORMATION OF HETERO-PHOTOCONVERTERS MADE ON THE BASIS OF AlGaAs–GaAs HETEROJUNCTIONS

Single-crystalline layers and *p*-*n* junctions in semiconductor compounds are obtained mainly by the following three techniques of epitaxial growth: (i) vacuum evaporation and condensation, (ii) gas-transport chemical reactions, and (iii) liquid-phase epitaxy (LPE).

The vacuum evaporation and condensation technique makes it possible to obtain single-crystalline layers of elemental semiconductors and some semiconductor compounds. However, this technique cannot be applied to solid solutions of III–V semiconductor compounds, since most of them decompose at temperatures below those of melting, so the layers may be non-stoichiometric and with nonuniform electrophysical parameters [1].

In the gas-transport chemical reactions technique the required product is formed either in a chemical reaction or due its recrystallization via a gas phase with the corresponding reagent-carrier. At that one cannot exclude completely presence of water vapors that may lead to inversion of the type of conductivity of the layers grown [2].

If one deals with III–V semiconductor compounds, then LPE has a number of advantages over the vapor-phase epitaxy (VPE) and other techniques. In particular, LPE enables one to obtain more perfect layers with lower dislocation density. It is almost the only technique for production of heavily doped layers of III–V semiconductor compounds. Besides, LPE can be used to obtain abrupt *p*-*n* junctions [3].

When III–V compounds are crystallized from solution-melts, both temperature and pressure considerably decrease in the course of growing; in addition, the installation used is considerably simpler. Taking the above factors into account, we took the technique of gallium arsenide crystallization from solution-melts as the basic one when developing technology for production of films for photoconverter (PC) structures.

2.1. LIQUID-PHASE EPITAXY WITH AN INDUSTRIAL PLANT

Industrial development of production of solar cells (SCs) on the basis of gallium arsenide has some peculiarities due to specificity of binary and ternary compounds of III–V semiconductors. Manufacturing is based mainly on application of LPE techniques which enable one to reduce the temperature of epitaxial layer growth by more than 300 °C as compared to the temperature of single-crystal synthesis. The main technique used at that is non-isothermal LPE from gallium solutions, with aluminum additions according to the solubility diagrams for arsenic in gallium (with and without aluminum) at a certain temperature [4].

Contrary to the use of the ovens for diffusion annealing (when the emphasis is on uniformity of temperature distribution in the quartz reactor volume), in the above case one has to provide possibility to purposely increase or decrease the oven temperature by a fraction of a degree. When many wafers are used, then the solution becomes depleted with components as the SC structure layer are epitaxially grown, so it is necessary to add these components. At that the requirements for purity of the reagents, gases and accessories used become stricter. The technological process of SC structure formation with LPE occurs in the purified hydrogen atmosphere. The recommended purification efficiency corresponds to the hydrogen dew-point temperature no less than −(50−60) °C.

Let us consider some characteristics of the industrial plants for growth of SCs on the basis of gallium arsenide. Over two decades ago the LPE technique using GaAs wafers of big area in a three-chamber vertical system has been considered in [5]. The feature of this technique was vertical loading of 200 wafers (area of 20×20 mm) in a single epitaxial process. The plant had an automatic system for temperature mode regulation, pure gases feed change-over and control over graphite boat loading into the oven. The wafers were loaded into the graphite boat in the dry nitrogen atmosphere to exclude melt oxidation. In the course of epitaxial growing the junction depth and uniformity over the wafer area were monitored. The mean junction depth value was determined from the results for 40–50 samples.

The results of studies of commercial GaAs-based SCs (20×40 mm size - yearly output of 20 million, 20×60 mm size - yearly output of 50 million) are given in [6]. LPE is performed in the hydrogen atmosphere; the cooling rate is 0.2 °C/min. Contacts to the front (back) faces are made by concurrent sputtering of Au and Zn (Au and Te). TiO_2–Al_2O_3 is used for antireflecting coatings.

When analyzing the advances in industrial manufacturing of SCs on the basis of GaAs, one can state that the most often used structure is *p*-AlGaAs–*p*-GaAs–*n*-GaAs–n^+-GaAs (substrate). The parameters of its constituents are as follows:

p-AlGaAs - thickness of 0.1–0.3 μm, dopants Be and Zn, charge carrier concentration of $3\cdot10^{18}$ cm^{-3};

p-GaAs - thickness of 0.1–0.4 μm, dopant Be; *n*-GaAs - thickness of 10–15 μm, dopant Sn, charge carrier concentration of $3\cdot10^{17}$ cm^{-3}; n^+-GaAs (substrate) - charge carrier concentration of $2\cdot10^{18}$ cm^{-3}. The main improvements involved (i) changes in the construction of the cassette that makes it possible to add melt in the course of epitaxial growth without interrupting the manufacturing process, and (ii) technology of front contact deposition.

The n-GaAs layer thickness is determined by the following two factors: 1) the thickness of a “junction layer” formed between the low-resistance n^+-GaAs substrate and growing epitaxial layer; 2) the depth of complete absorption of solar radiation in gallium arsenide (about 5 μm) [7]. Thus the n-GaAs layer thickness at LPE is chosen depending on the “junction layer” thickness. Usually the latter is estimated to be 2–5 μm, so the n-GaAs layer is grown up to a thickness of no less than 10 μm.

Before deposition of the front contact and after deposition of the back contact, the SC surface is covered with an antireflecting coating. The contact is deposited onto the p-GaAs layer using photolithography and etching of the p-AlGaAs layer.

The pilot factory of the Physical-Technical Institute (FTI) of the Scientific Association “Physics–Sun” of the Academy of Sciences of Republic of Uzbekistan is engaged in production of SCs on the basis of gallium arsenide. The existing technological equipment makes it possible to produce annually up to 10 000 SCs (with area of 0.3 cm^2) on the basis of GaAs wafers (size of 2.6×2.6 cm^2) [8]. Each wafer provides 20 SCs. The layout of the front contact grid of SC makes it possible to apply concentrated (up to 40 kW/m^2) radiation under outer space conditions.

The schematic of the plant for LPE growth of SCs is presented in Fig. 2.1. This plant was developed on the basis of a standard furnace СДО-80/4. The improvements involved mainly the construction of the graphite plunger-type cassette (with vertical arrangement of a package of GaAs substrates) and equipment. As a result, the SC efficiency and product yield increased.

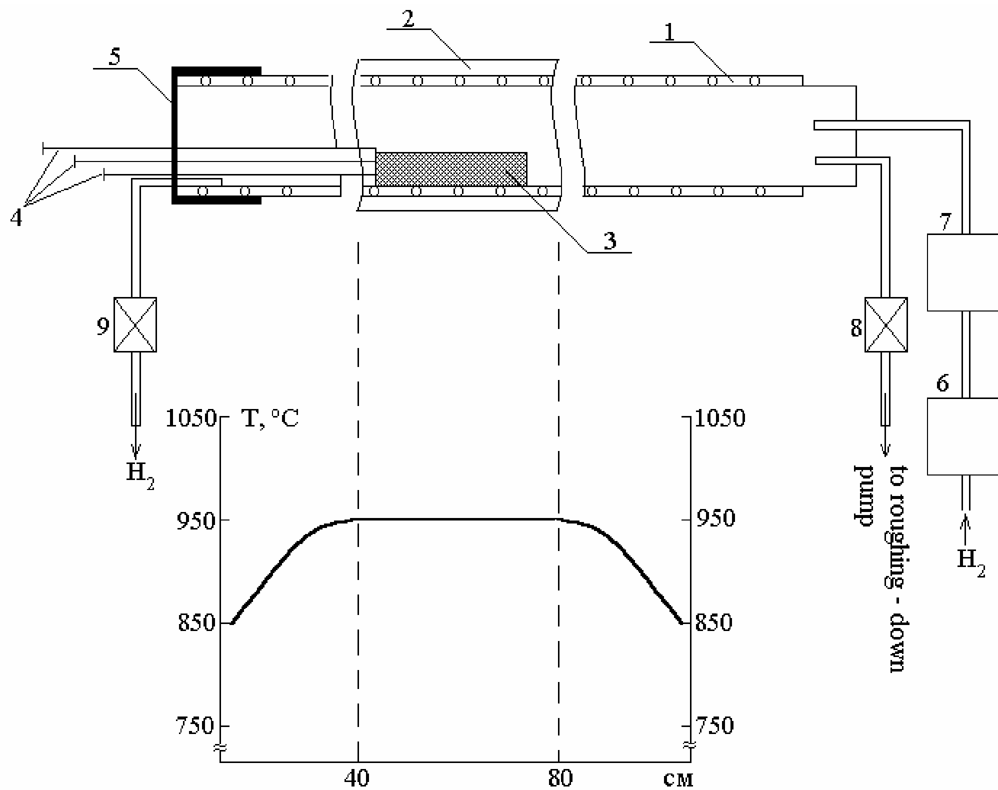

Fig. 2.1. A schematic diagram of the plant for LPE-growth of epitaxial layers: 1 – heater; 2 – LPE zone; 3 – graphite container; 4 – control rods; 5 – vacuum seal; 6 – palladium purification; 7 – gallium purification of hydrogen; 8 – vacuum valve; 9 – bubbler.

To eliminate low-temperature film crystallization, the graphite cassette construction provides complete removal of solution at epitaxial layer growth temperatures. Such a cassette enables one to grow (in a single technological process, if necessary) epitaxial structures whose area exceeds 50 cm^2. Epitaxial layers were closed-space grown from a solution whose volume was confined with two parallel GaAs substrates (area of 23×23 mm^2) making a gap whose width varied in the 400–1000 μm range.

The process of SC structure formation involves the following three stages. At the first stage an epitaxial n-GaAs "buffer" layer (isotype with substrate) is formed. The temperature at the beginning of epitaxy was 840 °C, while that at the end of growth was 810 °C. This layer serves as SC base; its thickness is about 10 μm. The charge carrier concentration in it is $(1–3)\cdot10^{17}$ cm^{-3} It was measured with Hall technique, as well as was determined from C–V

curves for p-n structures. Our studies showed that at the beginning of “buffer layer” growth (when its thickness is 2–3 μm) one can observe the growth faults that are characteristic for the crystallographic orientation (100). Further growth of the “buffer layer” (up to thickness of 10 μm) results in improvement of its structure perfection due to fault density reduction by an order of magnitude. In GaAs total absorption of solar radiation occurs at a depth of about 5 μm. So the “buffer layer” thickness of about 10 μm is quite enough for obtaining SC of highest efficiency.

We studied zinc diffusion into the n-GaAs “buffer” layer from the Ga+Al+As+Zn solution in hydrogen atmosphere at temperatures of 720–800 °C. This diffusion occurs at the second stage of SC structure formation. The required values of charge carrier concentration and depth of p-GaAs “diffusion layer” occurrence were provided by variation of temperature and duration of diffusion at the chosen optimal temperature.

At the third stage the front p-$Ga_{1-x}Al_xAs$ heterojunction (window) with $x \geq 0.7–0.75$ is formed at a temperature of 700–720 °C, along with formation of the p-GaAs “diffusion layer”. When choosing Al content in the p-$Ga_{1-x}Al_xAs$ layer, we tried to reconcile the following conflicting requirements: 1) the window bandgap should be as much as possible ($x \to 1$); 2) layer composition should provide obtaining collectors with good contact and adhesion properties; 3) layer composition should provide temporal stability of layer parameters; 4) growth of solid solution with composition $x \geq 0.7–0.75$ provides practically invariant Al content in the epitaxial layer depth at the chosen growth temperatures (700–720 °C), because Al segregation coefficient is close to unity.

The p-$Ga_{1-x}Al_xAs$ layer thickness was 1–2 μm. It was found that reduction of this layer formation temperature down to 700 °C makes it possible to obtain (along with reduction of the gap between the substrates) layers with thicknesses below 1 μm. This value is close to the predicted optimal thickness.

The front contacts are formed immediately at the surface of p-GaAs after selective etching off the optical window in the p-$Al_xGa_{1-x}As$ layer. This provides increase of the filling factor for I–V curve and improves reproducibility of SC characteristics. Such contacts demonstrate increased strength, so the SCs are more resistant against damage in the course of soldering at assembling.

The SCs were characterized by a solar radiation simulator with a xenon lamp (irradiance of 850 W/m^2) at a temperature of 25 °C. Shown in Fig. 2.2 is histogram of SC product percent depending on SC efficiency. According to the histogram (obtained for 250 SCs), the average SC efficiency at single solar irradiation is 17.6%.

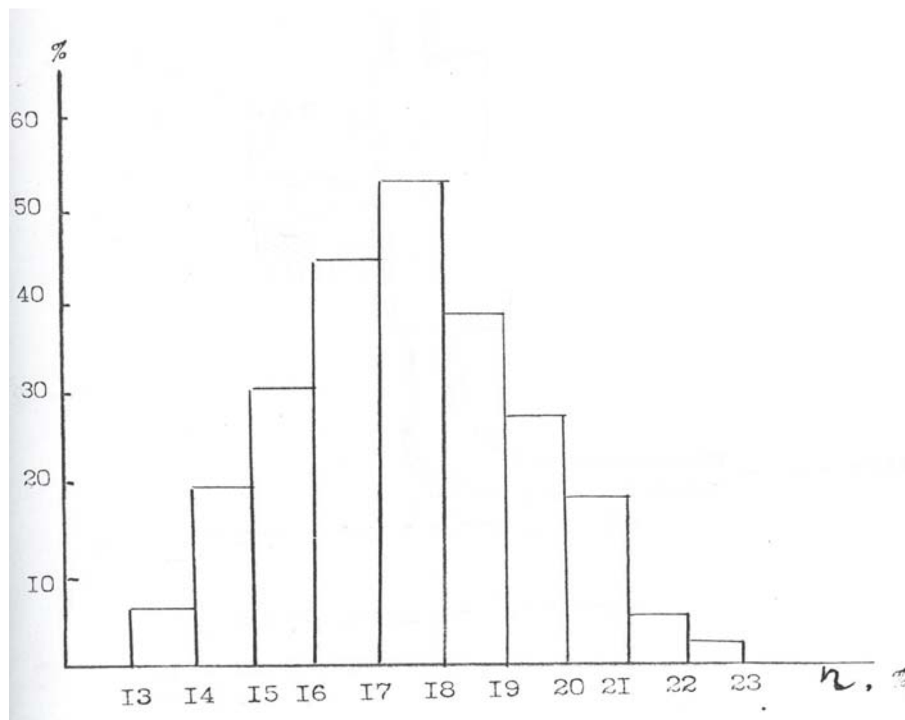

Fig. 2.2. Histogram of SC product percent as function of SC efficiency.

2.2. DEVELOPMENT OF TECHNOLOGICAL PROCEDURES FOR GROWTH OF AlGaAs–GaAs HETEROEPITAXIAL JUNCTIONS

Production of efficient hetero-photoconverters on the basis of AlGaAs–GaAs system is determined, to a great extent, by technological possibilities to obtain high-quality GaAs and AlGaAs layers. Investigation of comparative contributions from the *p-n* junction diffusion and base regions into the total collection

coefficient Q made for Si and GaAs photoelectric converters have shown that the base region contribution for the GaAs photoelectric converters usually does not exceed 10%, while that for the Si photoelectric converters is up to 95%. Therefore the main factors which determine possibility for further increase of efficiency for the p-$Ga_{1-x}Al_xAs$–p-GaAs–n-GaAs hetero-photoconverters are as follows: optimization of the Al depth profile, of the p-GaAs layer thickness and of the surface composition, as well as use of microrelief surface that increases absorption of incident radiation.

To grow GaAs and AlGaAs epitaxial layers, we used a graphite two-section cassette with sliding rulers and container. This cassette made it possible to realize both zinc diffusion from gas phase and growth of AlGaAs solid solution in a single technological cycle. The cassette had two work volumes. In one of them a movable graphite container with cells for vertical GaAs wafer positioning was located, while another volume was intended for (Al+Ga+As+Zn) solution-melt. The cassette was equipped with a sliding graphite ruler-bolt to make a closed work volume and move a sliding container to provide contact between the solution-melt and substrates. In this cassette the substrates were vertically positioned into a special container at certain spacing, and the solution-melt was fed from below. In this case a closed-space growth occurs from solution-melt placed in a narrow gap between the two substrates. This made it possible to monitor thickness of the epitaxial layers during their growth.

After cutting into required configuration and corresponding pretreating the GaAs substrates (area S of about $20\times\cdot 20$ mm^2, orientation <100>, dopant concentration n^+ of about 10^{18} cm^{-3}) were placed (with spacing of 500 μm) into containers then were put into a graphite cassette with solution-melt and loaded into an open-type reactor. The cassette enabled one to concurrently grow epitaxial layers on six substrates. The GaAs buffer layers (thickness of 10 μm, dopant concentration $n = (1\div 2)\cdot 10^{17}$ cm^{-3})

were LPE-grown. The samples with a buffer layer obtained in the above way were placed (with spacing *l* of 300 μm) into another container to obtain *p*-AlGaAs. An $Al_xGa_{1-x}As$ layer was grown from solution-melt located in the 300 μm gap, in the 600–800 °C temperature range, using forced cooling.

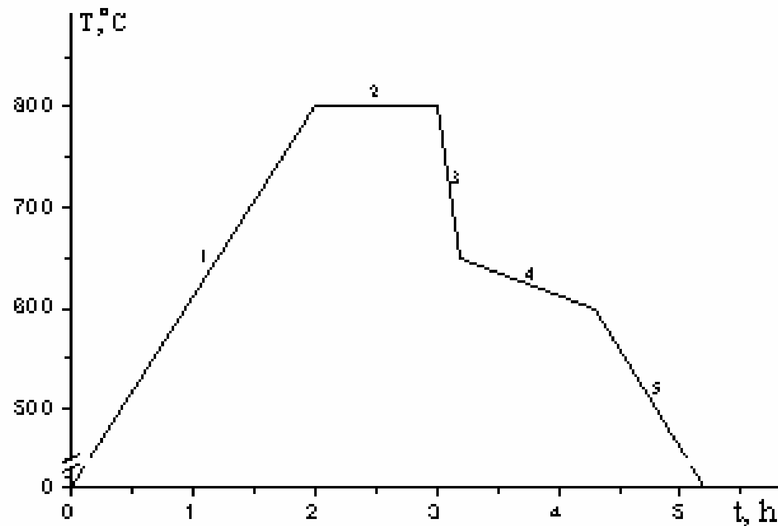

Fig. 2.3. Temperature-time diagram of the technological process.

Shown in Fig. 2.3 is the temperature–time diagram of the technological process. Due to high coefficient of Al segregation in the solution-melt, at forced cooling of the system Al is intensively captured by solid solution at the first moment. After Al depletion in the solution-melt, growth of the AlGaAs layer practically stops. Thus the thickness of the grown AlGaAs layer is determined by Al content in the confined narrow gap of the solution-melt volume located between two plates.

2.3. MONITORING OF THE GROWN EPITAXIAL LAYER COMPOSITION

AlGaAs is the basic material for the heterojunctions studied by us. Table 2.1 presents the experimentally selected (at preset temperatures) ratios between the concentrations of Al and Ga components and added GaAs source. These materials form a solution-melt with appointed value *x* for the substituting element.

Table 2.1. Experimentally selected (at preset temperatures) ratios between the concentrations of Al and Ga components and added GaAs source

T, °C	Al	Ga	GaAs	x_{Al}
700	4.9	4289	82.8	0.35
800	9.1	15355	296	
900	16.7	45797	884	

To illustrate, we consider obtaining of solution-melt for $Al_{0.35}Ga_{0.65}As$ epitaxial layer growth. Let A_x, B_x and C_x be the first, second and third component, respectively, and the required solution-melt mass be M (in g). One can determine the unknown N_x value for the preset melt mass. This is the Al portion (x). For any temperature one can preset the same melt mass:

$$\frac{A_x + B_x + C_x}{N_x} = M_{\text{const}}$$

Our studies of epitaxial layer growth showed that the optimal initial growth temperature was about 800 °C. Starting from this temperature, we obtained the required values for epitaxial layers of solid solutions with different compositions of substituting element (see Table 2.2).

Table 2.2.

T, °C	Al	Ga	GaAs	x_{Al}
800	11.3	14174	273	0.4
	17	11812	228	0.5
	25.6	9449	182	0.6
	40	7087	136.8	0.7
	69	4725	91.2	0.8
	159	2362	45.6	0.9

One can see from Table 2.2 that, at preset temperature (in our case this is 800 °C), Ga content changes as Al content grows. At any value of the ratio between the component contents the total weight of the melt is reduced to the same value (say, 2 g). (The

actual composition of the epitaxial layers obtained on the basis of this table may differ from the preset one by up to 10%.)

2.4. LIQUID-PHASE EPITAXY (SHIFTING TECHNIQUE)

2.4.1. Growth of epitaxial layers with *p-n* junctions

It is known that LPE-growth of various structures made on the basis of III–V semiconductor compounds occurs from solution-melt. The plant advanced for the first time by Nelson was a rotation oven [3]. However, the rotation and vertical versions of LPE technique did not provided complete removal of oxide layers formed on the melt surface [10]. To remove this layer, the facilities with shifting container having several baths are used [11]. However, if the container construction is not optimal, then solution-melt may flow from one bath to another.

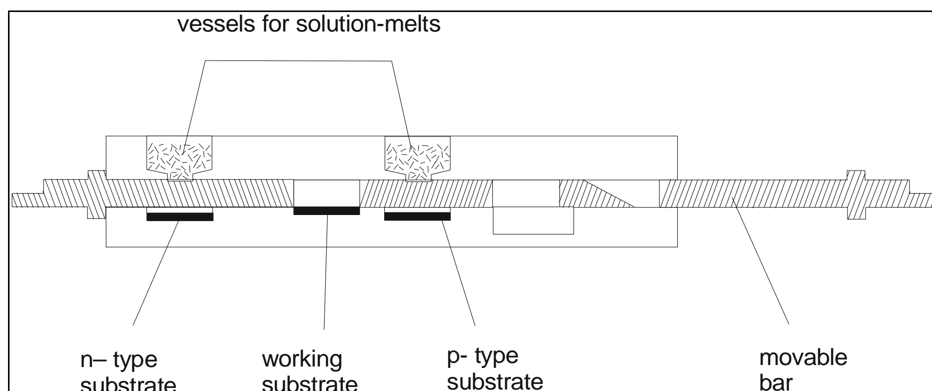

Fig. 2.4. Sectional view of a facility for epitaxial layers growing with the “shifting technique”.

To prevent solution-melt flow from one bath to another and remove oxide layer, a special facility has been advanced in [12] (see Fig. 2.4). It differs from the known analogs in that the cut-off part of solution-melt is shifted with a movable bar and goes to the substrate. Such technique for epitaxial layers growing is named “shifting technique”.

In this technique the solution-melt and substrate are placed in a graphite container and heated in a horizontal quartz chamber by a

blowing-through flow of purified hydrogen up to the initial crystallization temperature. Then they are put into contact; after this programmed cooling begins. During cooling the epitaxial layer is precipitated onto the substrate surface. The saturated solution-melt (dissolver + source) is obtained by its keeping at crystallization temperature T_{cr} immediately at the source. The layers grown from the saturated solution-melt have a plane film–substrate interface.

The solution-melt becomes incompletely saturated when it is disconnected from the source below the crystallization temperature (at $T_{cr} - \Delta T$) or is heated up to $T_{cr} + \Delta T$ before its contacting with the substrate. At that the surface is etched at the moment of melt contact with the substrate, and then, as the system is being cooled, an epitaxial layer is growing. Its surface practically does not follow the substrate surface morphology.

The solution-melt may also be oversaturated due to its cooling (by ΔT) when it has no contact with the source (i.e., before its contact with the substrate). The layers grown from oversaturated solution-melt may follow, up to a point, the substrate surface morphology.

When multicomponent solid solutions are grown with the shifting technique, the melt surface tension may be nonuniform, and the layer grows unevenly. To obtain relatively even surface in such cases, one should press the solution-melt layer with a load or plug. This practice is used also to restrict the solution-melt thickness (in such case this technique becomes similar to the “capillary” one). Thus the shifting technique has wide potentialities in epitaxial layers growing.

We used *n*- and *p*-GaAs as sources for melt saturation. The melt was obtained by heating a mechanical Ga+GaAs mixture containing dopants (say, Zn, Te, Si, Sn). GaAs was etched in a hot etchant $3HNO_3$+HCl+$2H_2O$ for 1–3 min. before mixing. Before and after etching, GaAs was treated in boiling CCl_4 and distilled water

and then was dried. To reduce uncontrolled dopants content and make the solution-melt homogeneous, it was kept for 2–3 hours in a hydrogen flow at a temperature of 850 °C.

Particular attention is given to purity and choice of parameters of the materials and components used. To provide (at a preset optimal electron concentration of (3–5)×10^{17} cm^{-3}) photon absorption in the space-charge region of *p*-*n* junction, the *p*-layer thickness should be less than 1 μm, and acceptor concentration in it should be N_a = 10^{19} cm^{-3} (to increase abruptness of the *p*-*n* junction). At that the decisive role belongs to the temperature mode of epitaxial layer growing (Fig. 2.5). The thicknesses of epitaxial layers are set by choosing the melt volumes and duration of epitaxial growing.

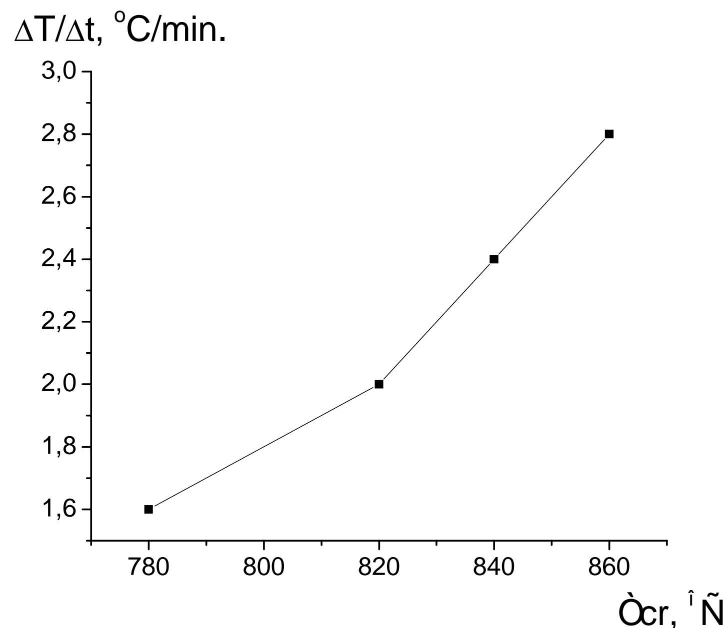

Fig. 2.5. The temperature mode of epitaxial layers growing.

Application of the epitaxial growth technique advanced in [12] provides the following advantages:

• melt contacting with the initial substrate removes supersaturation of solution and prevents dissolving of the work substrate and its contamination with uncontrolled impurities;

- removal of oxide layer from the contacting melt surface provides complete wetting of the substrate;
- system cooling according to the mode advanced in [4] makes it possible to obtain good morphology of layer surface and structure perfection.

The epitaxial layers grown with the above technique have (i) defect density that is by an order below that in the substrate, (ii) flat (mirror) surface, and (iii) even interface of *p*-*n* junction (see Fig. 2.6).

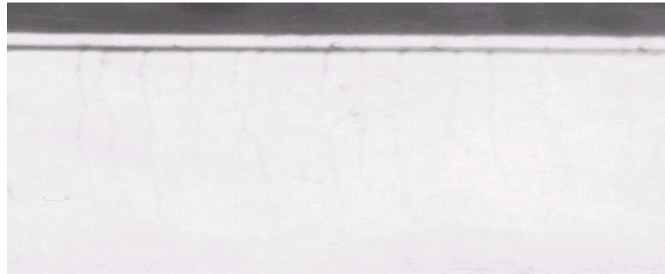

Fig. 2.6. The interface of the *p*-GaAs/*n*-GaAs *p*-*n* junction.

2.4.2. Epitaxial growth of heterolayers on the basis of AlGaAs

Heterolayers on the basis of III–V compounds can be formed by application of the LPE facility developed by us [13] in combination with the technique for epitaxial growing layers of III–V compounds [14]. Figure 2.7 gives schematically the working part of the cassette used for epitaxial layer growing. It enables one to obtain epitaxial layers of III–V semiconductor compounds using either the isothermal epitaxy-mixing (at a constant temperature) of two solution-melts or forced cooling.

The cassette involves the base (1) with grooves (2 and 4) to cut off a part of solution-melts; the substrate (3) is placed at the center. There is a movable rod (5) with two holes (6 and 7) to feed solution-melts to the substrate. A stationary part has a hole for solution-melt (9), those of other type (11) and feeding solution-melt (10) of another composition (13) using a plunger (15). The melt of another composition (13) is fed through the hole (16) that is closed with a plug (17).

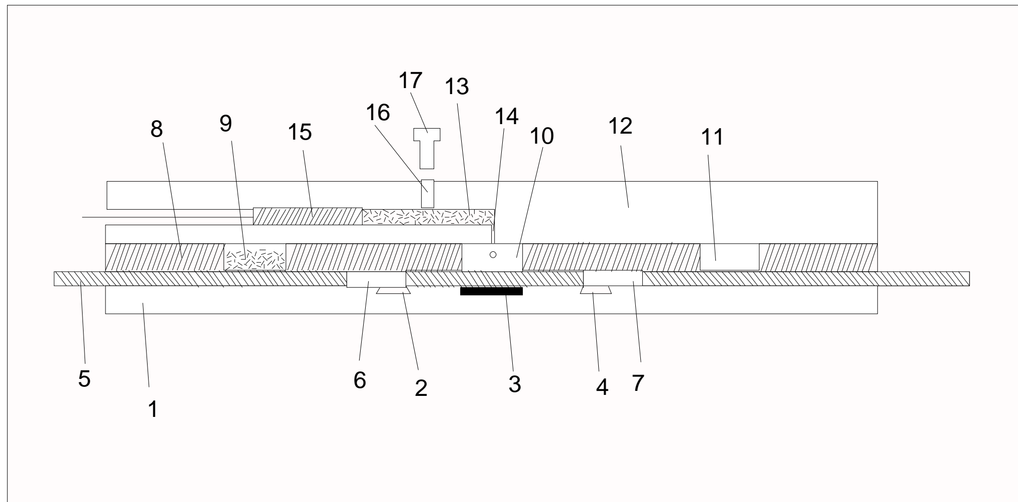

Fig. 2.7. Sectional view of the working part of the combined (shifting + plunging) LPE facility.

It should be noted that choice of the initial condition of boundary layer is of particular importance when growing epitaxial layers. Whatever the technique used (isothermal or forced cooling), the growing layer "follows" the composition of solution-melt formed at the crystallization front. Layer perfection depends on the degree of melt supersaturation.

2.4.3. Liquid-phase epitaxy onto a textured surface

The PEC parameters depend essentially on the properties of *p*-*n* junction and illuminated surface. The quality of *p*-*n* determines junction practically the filling factor of the load characteristic. In the case of continuous *p*-*n* junction the structure series resistance increases, and the filling factor may drop down to 50%. Besides, in structures with high (over 2) ideality factors *n* recombination processes are enhanced. At that development of contact grids of low series resistance is of importance.

Along with optimization of contacts and the structure itself, the possibilities for increase of PEC efficiency may be broadened by efficient use of solar radiation, minimization of the "dead layer" and reduction of surface recombination. Even in the case of an ideal *p*-*n* junction, up to 30% incident light is reflected from a flat

surface. This means that in actual practice the requirements for high absorptivity and small coefficient of solar radiation reflection are not met.

To reduce the reflection coefficient, various antireflecting coatings (made of different oxides) are usually applied. Texturing of illuminated surface also gives good results [15-17]. In [18] it was noted that formation of certain microrelief at the surface or *p-n* junction interface should increase photoconversion efficiency as compared to the case of plane geometry. So we considered the problem of obtaining photoconverters on microrelief and flat surfaces of the growth surface of GaAs substrates.

To solve the above problem, it was necessary to develop technology for fabrication (under the same conditions) of photoconverters with microrelief and flat surfaces. At first glance the problem seems very easy. However, up to now there are no data in the literature concerning epitaxial layers growing on microrelief surfaces, except for porous ones [19-22]. Obviously wetting of surface implies removal of the upper atomic surface layer; so growing of epitaxial layers on microrelief surfaces has to be done from a saturated solution-melt. To this end, the solution-melt has to contact with an additional source before starting the epitaxy process.

When growing each epitaxial layer from GaAs in single process, it was found that for the samples with microrelief surfaces the surface wetting temperatures were somewhat over those for the samples with flat surfaces. As a result, at temperatures optimal for flat structures, the GaAs surface of quasi-grating-like type often were wet nonuniformly, and layer growth on them was not continuous. At the same time the layers of AlGaAs solid solutions grown on quasi-grating-like surfaces of GaAs had satisfactory properties.

The above fact enables one to conclude that, when Ga+GaAs+Al solution-melt contacts with GaAs surface, a eutectic

solution is formed at their interface. It gets equilibrium after partial etching-off the surface (oxide) of GaAs crystal. Thus surface wetting occurs and a layer of solid solution grows. In the case of Ga+GaAs melt, contrary to the above, it is saturated and is in equilibrium with the contacting GaAs crystal, so substrate surface wetting may be incomplete. To remove this factor, the solution-melt should be in a quasi-equilibrium state, so that one could exert control over it by varying temperature, as well as its feed to the substrate surface.

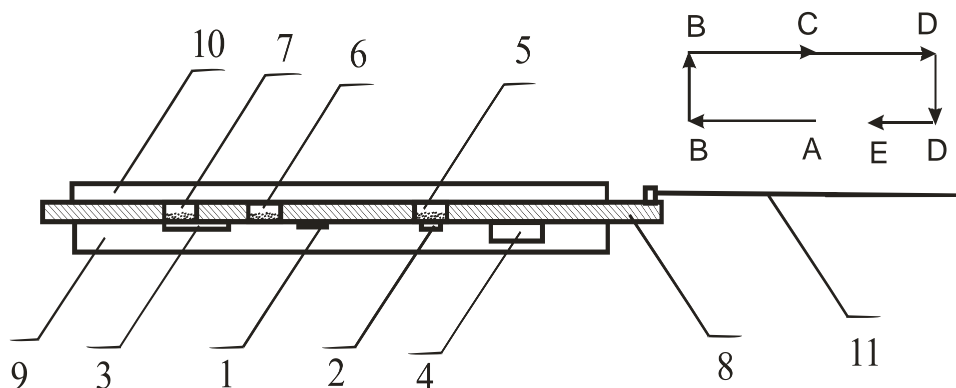

Fig. 2.8. Sectional view of the working part of the facility for LPE-growing of photoconversion structures.

When going to fabrication of photoconverters, it should be noted that all the layers forming the structure (including heterojunctions) should be grown in a single technological process. This is of particular importance if aluminum-containing layers are applied as illuminated surface. The reason is that aluminum melts, being oxidized, prevent wetting of the surface at which heterolayer has to be grown. Taking all the above considerations into account, the Physical-Technical Institute of the Scientific Association "Physics–Sun" of the Academy of Sciences of Republic of Uzbekistan developed a facility with three cells for solution-melts (see Fig. 2.8).

The facility involves the base (9) with grooves for the substrate (1) and sources of the first (2) and second (3) type and a

pit (4) for dumping the first solution-melt. Over the base there is a movable rod (8) with three holes for the three solution-melts: the first one – for buffer layer growing from the first solution-melt (5), the second one – for formation of a *p-n* junction from the second solution-melt (6), and the third one – for growing of the upper layer from the solution-melt (7). There is a cap (10) in the upper part; a stick (11) is attached to the movable rod; this stick realizes motion of solution-melts through the positions A–E in the course of the process.

The above facility makes it possible to grow (in a single cycle and without interrupting the process) all the layers of a photoconversion structure, with either flat or microrelief surface. The peculiarity of this facility is that, in the course of picking up temperature required for epitaxy, the first and third solution-melts (initial position A) are being saturated, while the second solution-melt is depleted by the difference between the temperature of intermediate layer epitaxy and the initial temperature of the buffer layer growth. In the next stage, when the first solution-melt (saturated) is moved to the substrates (position B), the second solution-melt is partially dissolving the source (3) and becomes saturated. At this moment the third solution-melt (having no contact with the source) is being supersaturated as the system is being cooled. Then the saturated second solution-melt is shifted (and the first solution-melt is put into the pit (4)) on the surface of the grown buffer layer; an interlayer will be grown at cooling. At that the third solution-melt, being in contact with the source (3), goes from supersaturation to saturation. And, at last, the third saturated solution-melt is shifted onto the surface of the grown interlayer from which (at system cooling) the upper layer with aluminum will be grown.

Just this technique enables to reach the single temperature mode for flat and microrelief surfaces. By varying the temperature interval ΔT of one layer, one can exert control over the condition of another solution-melt and parameters of the growing layer. The

temperature mode of epitaxy process chosen experimentally for three sequential layers of *n*-*p*-*p*-types (whatever the combination of paired substrates) is presented in Fig. 2.9.

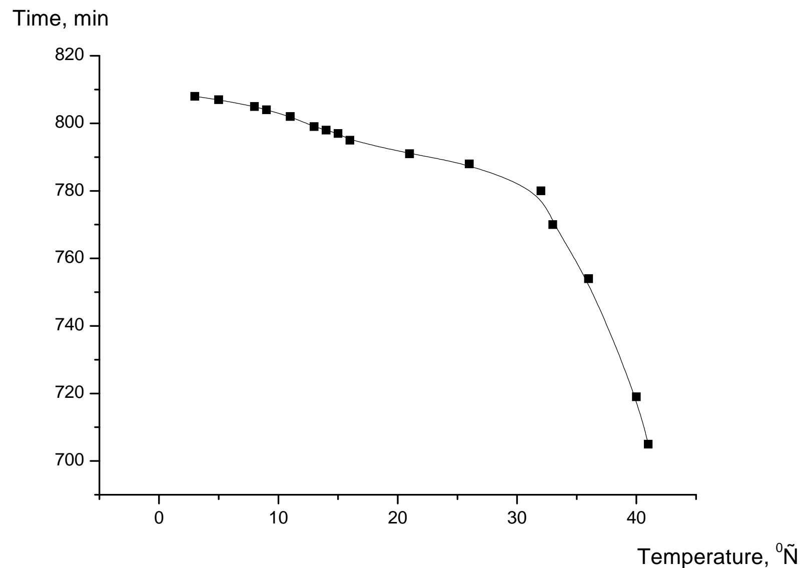

Fig. 2.9. The temperature mode of epitaxy process for three sequential layers of *n*-*p*-*p*-types.

2.4.4. The problem of alternative techniques for formation of hetero-photoconverters with microrelief interfaces of *p*-*n* junctions

The textured surface formation technology is based mainly on isotropic chemical etching of crystal surfaces. The etching process depends on crystal orientation and structure perfection. In bulky crystals-substrates control over the etched-off layer is not mandatory. But when it is required to form microrelief on an epitaxial layer, complete removal of the active layer may be a problem. In particular, the buffer layer thickness in SCs must be 3−7 μm. It becomes difficult to control the process of film etching, so it seems expedient to search for some alternative ways for obtaining photoconversion structures with microrelief components. In particular, a microrelief may be formed at an interface or illuminated surface. In both cases photoconversion efficiency may increase. However, application of additional technological operations in the process of SC fabrication may affect the photoconversion parameters.

References

[22] Andreev V.M., Dolginov. L.M., Tretyakov. D.N. Liquid-phase Epitaxy in Semiconductor Device Technology. Moskow: Sov. Radio. 1975 (in Russian).

[23] Weiner M.E.// J. Electrochem. Soc. 1973. v. 119. p. 496.

[24] Nelson. H.// RCA Rev. 1963. v. 24. No 4. p. 603.

[25] Hansen M., Anderko K. Constitution of Binary Alloys. v. 1, 2. New York et al. 1958.

[26] Ioshida S., Mitsui K. et al.// In: Proc. 17th IEEE Photovolt. Spec. Conf. (Kissimmee, 1-4 May 1984). New York. 1984. p. 42.

[27] Mardesich N. et al.// In: Proc. 18th Photovolt. Spec. Conf (Las Vegas, 21-25 Oct. 1985). New York. 1985. p. 105.

[28] Ukhanov Yu.I. Optics of Semiconductors. Moscow: Nauka, 1977 (in Russian).

[29] Muminov R.A., Tursunov M.N.// Heliotekhnika 1991. No 6. p. 48 (in Russian).

[30] Bustanov Kh.Kh., Mirzabaev M., Potaenko K.D., Tursunov M.N.// Author's Certificate USSR No 1173799. 15 April 1985 (in Russian).

[31] Dawson L.R., Whelan J.M.// Bull. Amer. Phys. Soc. 1968. v. 13. Ser. 2. p. 375.

[32] Panish M.B., Sumski S., Hayashi I.// Met. Trans. 1971. v. 2. p. 795.

[33] Karimov A.V., Mirzabaev M.// Author's Certificate USSR No 762253. 16 May 1980 (in Russian).

[34] Karimov A.V., Mirzabaev M., Mirtursunov Sh.Z., Mukhitdinova N.F. Author's Certificate USSR No 913759. 16 November 1981 (in Russian).

[35] Karimov A.V., Mirtursunov Sh.Z.// Author's Certificate USSR No 1037795. 22 April 1983 (in Russian).

[36] Zhao Jianhua, Wang Aihua, Green M.A., Ferrazza F.// Appl. Phys. Lett. 1998. v. 73, No 14. p. 1991.

[37] Brown A.S., Green M.A.// J. Appl. Phys. 2003. v. 94. No 9. p. 6150.

[38] Dmitruk N.L., Borkovskaya O.Yu., Konakova R.V., Mamontova I.B., Mamykin S.V., Voitsikhovskyi D.I.// Zh. Tekhn. Fiz. 2002. v. 72. No 6. p. 44 (in Russian).

[39] Dmitruk N.L., Borkovskaya O.Yu., Maeva O.I., Mamontova I.B.// Sensors & Actuators A 1999. v. 75. p. 151.

[40] Mamutin V.V., Ulin V.P., Tretyakov V.V., Ivanov S.V., Konnikov S.G., Kop’ev P.S.// Pis’ma v ZhTF 1999. v. 25. No 1. p. 3 (in Russian).

[41] Soldatenkov F.Yu., Ulin V.P., Yakovenko A.A., Fedorova O.M., Konnikov S.G., Korolkov V.I.// Pis’ma v ZhTF 1999. v. 25. No 21. p. 15 (in Russian).

[42] Kidalov V.V., Sukach G.A., Revenko A.S., Potapenko B.P.// Fiz. Tekhn. Poluprov. 2003. v. 37. No 11. p. 1303 (in Russian).

[43] Arsentyev I.N., Baidakova M.V., Bobyl A.V., Vavilova L.S., Konnikov S.G., Ulin V.P., Boltovets N.S., Konakova R.V., Milenin V.V., Voitsikhovskyi D.I.// Pis’ma v ZhTF 2002. v. 28. No 17. p. 57 (in Russian).

[44] Karimov A.V., Yodgorova D.M.// In: Proc. Conf. “Photoelectric Phenomena in Semiconductors 2004”. 20-21 April 2004. Tashkent. Uzbekistan. p. 37.

[45] Dmitruk N.L., Borkovskaya O.Yu., Karimov A.V., Kostylyov V.P., Mamontova I.B., Kotova N.V. In: Proc. Conf. “Photoelectric Phenomena in Semiconductors 2004”. 20-21 April 2004. Tashkent. Uzbekistan. p. 143.

Chapter III

MORPHOLOGY AND CHEMICAL COMPOSITION OF TEXTURED GaAs SURFACES. TECHNIQUE FOR FORMATION AND PROPERTIES OF OHMIC AND BARRIER CONTACTS TO TEXTURED GaAs AND Al(In)GaAs SURFACES.

Application of textured surfaces in photoelectric converters (PEC) and the features of formation of semiconductor, insulator and metal layers on such surfaces, are usually considered from the viewpoint of improving the PEC optical and electron properties. At that essential factors for growth of semiconductor or metal (in the case of contact formation) layers are morphology and chemical composition of textured surfaces. The effect of these factors on the properties of contacts to PEC simulated for test structures with microrelief semiconductor surfaces of various types are considered below.

3.1. APPLICATION OF AUGER ELECTRON SPECTROSCOPY FOR ANALYSIS OF CHEMICAL COMPOSITION OF SURFACES WITH NONUNIFORM TOPOGRAPHY

For electrons with energies of 100−1000 eV (that are analyzed in Auger spectra) mean free paths lie in the 1−3 nm range. Just this important feature, that determines surface sensitivity of the Auger electron spectroscopy (AES) technique when analyzing ideally flat surfaces, leads to variation of intensities of Auger electron emission in the case of surfaces with micro-roughness. A distinction between these intensities for rough and ideally flat surfaces may be interpreted as variation of electron concentration. Thus the features of surface topography may result in loss of

secondary emission electrons due to their interaction with surface irregularities.

In addition, when considering excitation of Auger electrons in a solid with nonuniform surface topography, one should take into account also scattering of primary electrons which results in appearance of a great number of secondary electrons (accompanied with corresponding increase of the intensity of Auger peaks. It was shown in [1] that growth of surface roughness may lead to change of Auger line intensity up to 40%.

For quantitative analysis of the GaAs and InxGa1-xAs film composition we measured intensities of Ga, As, In, o and c Auger lines (Auger transition energies Eк of 1070, 1228, 404, 510 and 272 eV, respectively). The primary electron energy was Ep = 3 keV. The element concentration depth profiles in the near-surface regions were obtained at Ar+ ion etching (energy of 1 keV). They are presented in Figs. 3.1–3.4, while morphology of flat (uniform topology) and rough GaAs surfaces are shown in Figs. 3.5 and 3.6, respectively.

3.1.1. Auger analysis of flat and rough GaAs surfaces

According to [2], the Auger electron current of the i-th element of the material matrix M may be written as

$$I_{wxy,i} = GI_p n_i k A_w \lambda_m^i \left(1 + r_m^i\right) R \,. \quad (1)$$

Here the factor G takes account of the efficiency of electron collection by the measuring equipment; I_p is the primary electron current density; n_i is the concentration of i-th atoms in the material matrix M; the coefficient k takes account of the angular dependence of Auger electron emission; A_w is the Auger electron escape coefficient; λ_m^i is the mean escape depth for Auger electrons of a given energy; r_m^i is the backscattering factor (it takes account of additional vacancy production in the level W by the backscattered electrons with energies over the level W_i ionization threshold); the coefficient R takes account of sample roughness.

Expression (1) enables one to calculate n_i from the measured Auger electron current if one knows the values of the parameters entering that expression. However, determination of these parameters often makes a complicated problem even for homogeneous samples, to say nothing of the subjects with nonuniform rough surfaces.

The parameter R in (1) characterizes variation of the Auger electron emission current for rough surface as compared to the case of ideally flat one (for which $R = 1$). Depending on the surface topography, the R values may be over, as well as below, unity [3]. One should take into account, however, that electron emission from rough surface is less probable than from flat one. The reason for this is as follows. Those electrons which leave flat surface never come back, while in the case of rough surface the emitted electrons may be captured by it again. It is impossible to get a general expression for R that would describe rough surface. One can, however, note some empirical regularity [4]:

- the intensity of Auger electrons escape from a surface with a sinusoidal relief with amplitude A and period B will be the same as that for a surface with a sinusoidal relief with amplitude A′ and period B′, if $A'/B' = A/B$;
- if a surface relief has characteristic amplitude A and period B, then the intensity of Auger electrons escape from a surface will be less at higher ratios A/B;
- the intensity of Auger electrons escape from a surface is maximal at glazing incidence of primary electrons.

Loss of Auger electrons at their path to an analyzer (due to their interaction with surface relief) affects also the value of the factor G. This factor depends on the solid angle from which the electrons are collected to the electron-optical system of the analyzer. When scanning a rough surface, the value of the measured signal has to be corrected with allowance made not only for the analyzer geometry but for probe position as well (azimuth

of the point where electrons leave surface and its distance from the pit center) So taking into account signal variation due to the factor G is a rather complicated problem even for flat surfaces, to say nothing of those with microprofiles.

Summing up the above, one may note that those methods of quantitative analysis are most suitable for studying rough surfaces which allow to exclude the parameters R and G with some standard procedure. For instance, this may be determination of the corresponding concentration from the ratio between the Auger electron peaks for the elements which are present in the sample studied. In this case the network concentrations (n_i) are calculated from the segment intensities I_i using the expression [6]

$$c_i = \frac{I_i / S_i}{\sum_i I_i / S_i}, \quad (2)$$

where S_i is the sensitivity factor for the i-th pure element.

3.1.2. Effect of GaAs surface relief on atomic composition

Using Eq. (2), we calculated the Ga and As Auger concentration depth profiles in GaAs samples with flat and relief surfaces (see Figs. 3.1 and 3.2). The surface topography of the samples studied was obtained with atomic force microscopy (AFM); it is presented in Figs. 3.5 and 3.6. The results of quantitative analysis of chemical composition of these samples are close, despite considerable distinctions in both amplitudes and periods of their surface reliefs (Figs. 3.1 and 3.2). This may be due to reduction of Auger peak heights resulting from presence of a contamination layer on the surface.

It is well known that the actual surfaces have adsorbed contaminations (oxides and carbides). To correct the sought amounts $n_{\mathrm{Ga}} / n_{\mathrm{As}}$ for presence of surface oxides and other compounds, one should take into account decay of the Auger electron flow when passing through such contamination layer.

Strict calculation of the contamination layer effect can be realized by introduction into expression (3) of a factor [6]

$$F = \frac{\exp(-xE_{\mathrm{Ga}}^{m} / \cos\theta)}{\exp\left(-xE_{\mathrm{As}}^{-m} / \cos\theta\right)} \qquad (3)$$

(that takes into account reduction of the relative intensities of Ga and As lines). Here $x = \frac{d}{\lambda_e}$ is the reduced thickness of the surface contamination layer (whose thickness is d), λ_e is the electron free path in a hydrocarbon film; m is the index of power at electron kinetic energy $E_{\mathrm{Ga,As}}$ (it takes account of λ_e dependence on $E_{\mathrm{Ga,As}}$); θ is the angle of Auger electron escape from the sample relative to the surface normal. Such an approach, however, is of little acceptability, since it requires accurate determination of the contamination layer thickness. On the other hand, surface layer removal with ion etching is not always acceptable because sputtering rates and thus surface concentration changes due to ion etching are different for atoms of different semiconductor compound components.

One could qualitatively take into account presence of surface contamination layer through introduction of a "universal" factor $\exp(-14.3 \cdot E^{-0.5})$ (with E measured in eV) [7], assuming that this layer thickness is the same for all the samples studied. Such an assumption, however, obviously comes into conflict with the results on Auger profiling presented in Figs. 3.1 and 3.2.

The attenuation of a signal from the i-th element (distributed homogeneously in the layer from z_1 to z_2) may be allowed for by the following coefficient [6]:

$$Q = \left(e^{-z_1 / \lambda_i \cos\theta} - e^{-z_2 / \lambda_i \cos\theta}\right), \qquad (4)$$

where λ is the Auger electron free path.

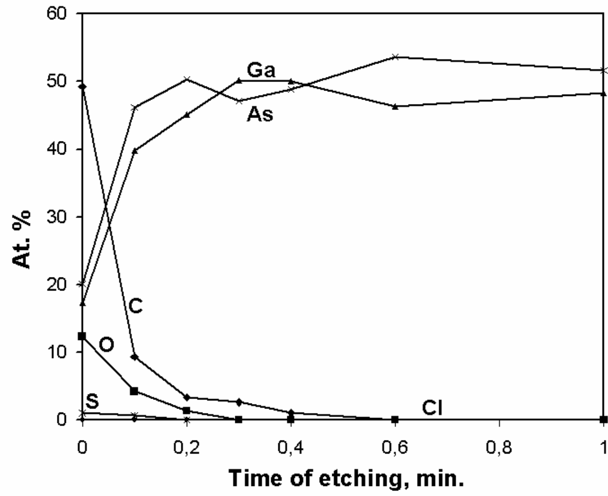

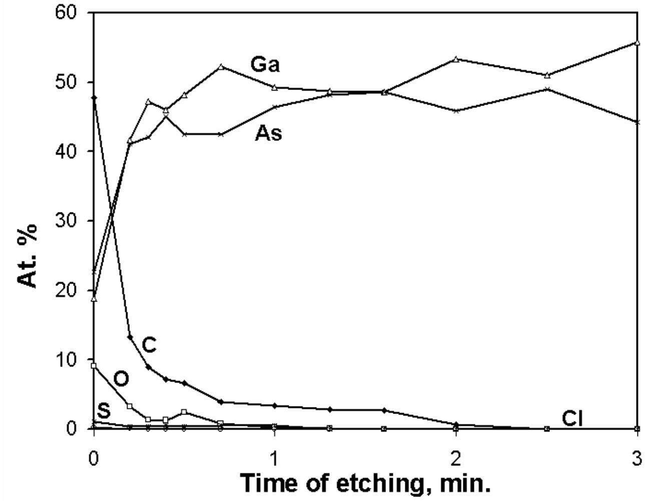

Fig. 3.1. Chemical composition of the GaAs near-surface layer with uniform surface topography.

Fig. 3.2. Chemical composition of the GaAs near-surface layer with rough surface.

Leaning upon the results of studies (Figs. 3.1 and 3.2), let us consider that a homogeneous GaAs sample is covered with a homogeneous film (with carbon and oxygen concentrations n_C and n_O, respectively). Let us calculate arsenic (n_{As}) and gallium (n_{Ga}) concentrations, as well as contamination layer thickness d.

To obtain expression for signals from As and Ga, one should allow for attenuation (by a factor of $e^{-z/\lambda' \cos\alpha_p}$) of the primary electron beam in the O and C layer whose thickness is d. Here λ' is the effective path of primary electrons and α_p is the angle of their incidence. Taking into account that $z_1 = d$ and $z_2 = \infty$, one has:

$$I_{Ga} = n_{Ga} e^{-1.33d/\lambda_{Ga}} e^{-d/\lambda \cdot \cos\alpha_p} S_{Ga} I_0 \qquad (5)$$

$$I_{As} = (1 - n_{Ga}) e^{-1.33d/\lambda_{As}} e^{-d/\lambda \cos\alpha_p} S_{As} I_0, \qquad (6)$$

where I_0 is a signal from the element taken as a scale when determining the factors $S_i = I_i/I_0$. For carbon and oxygen Auger signals

$$I_C = n_C \left(1 - e^{-1.33d/\lambda_1}\right) S_C I_0, \qquad (7)$$

$$I_O = (1 - n_C)\left(1 - e^{1.33d/\lambda_0}\right) S_O I_0, \qquad (8)$$

where S is the element sensitivity factor.

Expressions (5)−(8) form a set of equations in four unknowns: n_c, n_{Ga}, d and I_0. This set can be solved numerically. Table 3.1 presents the results of calculation of the contamination layer thicknesses and atomic concentrations of Ga and As in the near-surface region for flat and rough GaAs surfaces. We used the experimental data presented in Figs. 3.1 and 3.2.

Table 3.1. Calculated contamination layer thicknesses and atomic concentrations of Ga and As for flat and rough GaAs surfaces

Type of surface	d, Å	n_{Ga}, at. %	n_{As}, at. %
Flat	12.6	43.2	56.8
rough	20.3	37.8	62.2

The particular attention is attracted by the fact of higher (as compared to flat surface) content of excess arsenic at rough surfaces. This may be due to some features of chemical reactions that are proceeding during selective etching of GaAs. Maybe the chemical process forming quasi-grating-like relief is accompanied by appearance of thicker As oxide layer, while at the starting flat surface Ga oxides predominated. Considerable oxygen content at the same surfaces (Figs. 3.1 and 3.2) can serve as an argument supporting the above assumptions.

Knowing the sputtering rate, one can estimate thickness of the contamination layer on the surfaces studied. The etching mode used provided sputtering rate of 4 nm/min. (at ion energy of 1 keV). Assuming that the time needed to remove the layer corresponds to the pinch-off point on the time axis at which a signal from oxygen atoms disappears (see Figs. 3.1 and 3.2), one obtains the following thickness values: d = 12.3 Å for the flat surface and d = 13.8 Å for the rough surface.

The obtained values for the flat surface are in good agreement with the data presented in Table 3.1. A discrepancy with the thickness value for the rough surface seems to be related to the features of interaction between the ion beam and this surface. This might lead to change of the sputtering coefficient and character of sample atoms intermixing, affect primary beam energy scattering and change surface topography and character of selective etching [14]. These mechanisms have not been adequately studied yet (even for flat surfaces). Taking them into account makes a big problem when layer-by-layer analyzing subjects with rough surfaces [8, 9].

Let us assume that selective etching is the most essential effect related to excitation with an ion beam. Indeed, for GaAs deviation by ≈10% from the standard sputtering mode is achieved when only 1.4 atomic monolayers are removed by sputtering [10]. The processes of GaAs selective etching were studied rather comprehensively in [11]; for GaAs the ratio between the Ga and As sputtering coefficients k_p is 0.78.

For the equilibrium state of a binary alloy one can write down the following simple interrelation between the component concentrations at the surface ($n^S_{\mathrm{Ga}}, n^S_{\mathrm{As}}$), in the bulk ($n_{\mathrm{Ga}}, n_{\mathrm{As}}$) and sputtering coefficients k_p^{Ga} and k_p^{As} [6]:

$$m = \frac{n^S_{\mathrm{Ga}}}{n^S_{\mathrm{As}}} = \frac{n_{\mathrm{Ga}}}{n_{\mathrm{As}}} \frac{k_p^{\mathrm{As}}}{k_p^{\mathrm{Ga}}} . \qquad (9)$$

It enables us to determine the ratio between the Ga and As concentrations at the surface from the experimental data (Figs. 3.1 and 3.2). The calculated m values differ considerably from each other even at comparison with the data for the flat surface (m = 1.2, while m_{Table} = 0.8) and much more for the rough surface (m = 1.3, while m_{Table} = 0.6). One may assume that these discrepancies are related to neglect of disturbances caused by ion beam. This assumption is confirmed by the fact of bigger discrepancies in m obtained at different approaches for rough surfaces.

3.1.3. The effect of nonuniform surface topography of GaAs substrates on chemical composition of $In_xGa_{1-x}As$ epitaxial films grown on them

Shown in Figs. 3.3 and 3.4 are component contents in the near-surface layers of the $In_xGa_{1-x}As$ ($x \approx 0.0045$) epitaxial films grown on GaAs with flat and rough surfaces, respectively.

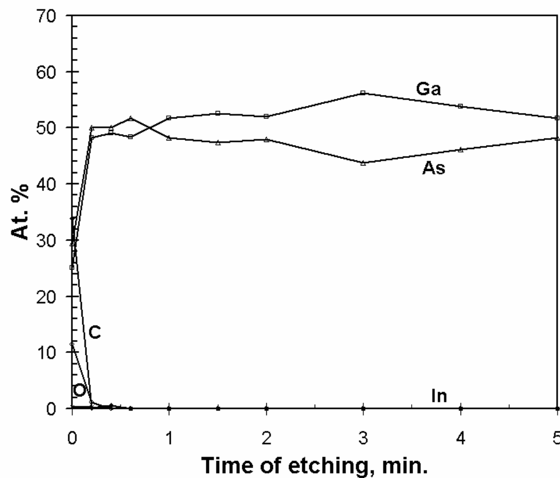

Fig. 3.3. Chemical composition of the $In_xGa_{1-x}As$ near-surface layer grown on the flat GaAs surface.

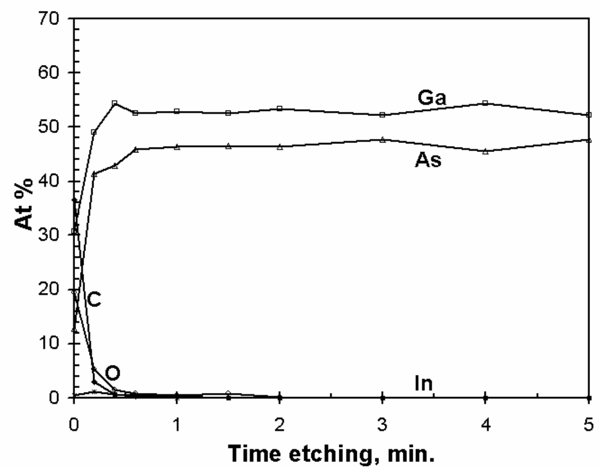

Fig. 3.4. Chemical composition of the $In_xGa_{1-x}As$ near-surface layer grown on the rough (quasi-grating-like) GaAs surface.

These data indicate at distinction in chemical composition of the near-surface layers of the subjects studied. Taking into account that the film thickness ($d \approx 3$ μm) is much over the substrate relief height (≤ 1 μm), it is unlikely that the distinctions observed in the thickness dependencies of concentrations in the near-surface layers were related to those in substrate morphologies. They seem to result from some technological factors. This consideration is confirmed by the fact that the grown layers are characterized by inhomogeneous In content distribution with thickness: absence of In atoms at film depth and segregation in the near-surface layer.

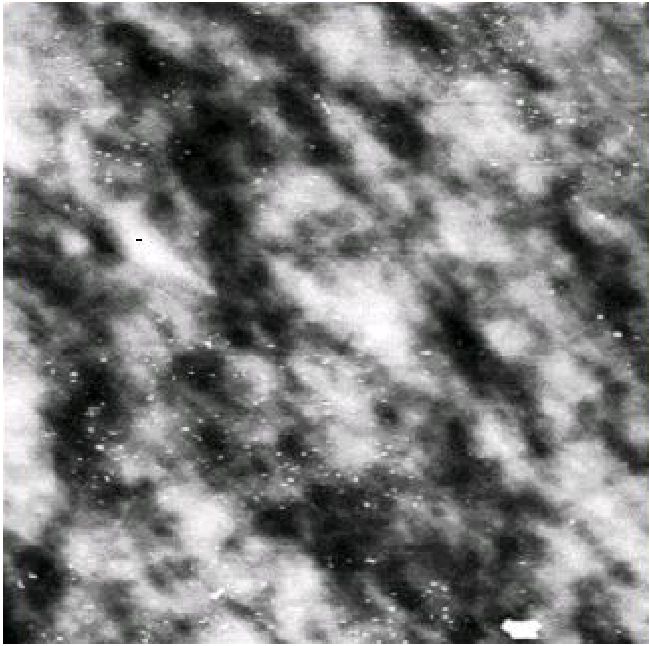

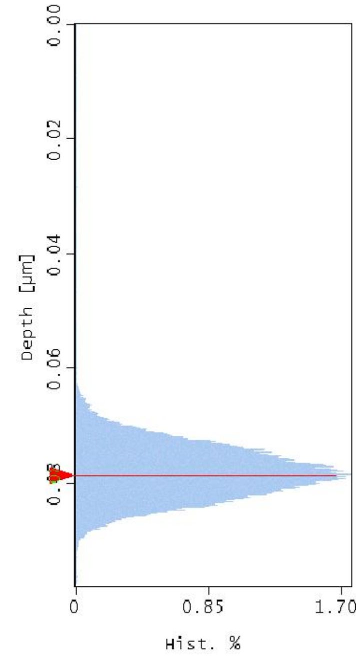

Fig. 3.5. Morphology of the flat GaAs surface.

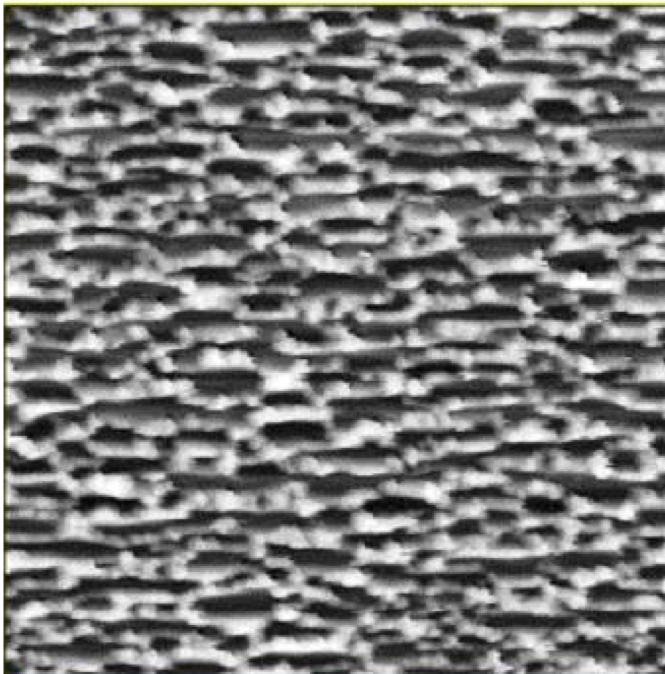

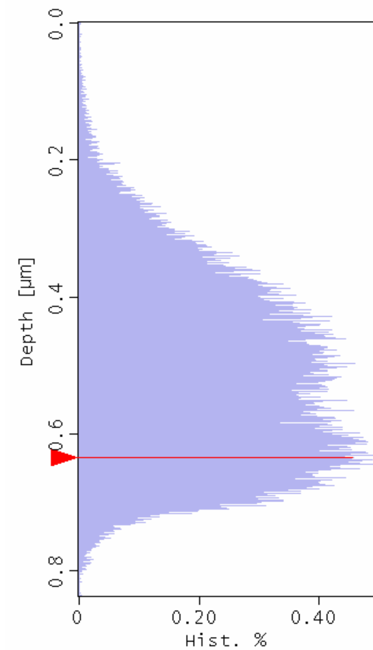

Fig. 3.6. Morphology of the rough GaAs surface.

The above data indicate at a distinction in chemical composition of the near-surface layers for the objects studied. These data, however, are not related to the epitaxial preparation of the substrates. Indeed, the film thickness d (about 3 mm) is much over the height of substrate relief (≤ 1 μm). This fact obviously levels (due to spreading and wetting) the effect of substrate relief on film formation. It seems that the observed distinction is due to

some technological factors. Such assumption is supported by the fact that the grown layers are characterized by inhomogeneous distribution of In atoms in depth (they are segregated in the near-surface layer and are absent in the film depth).

So, the peak heights of the Auger electrons emitted from a relief surface depend on the geometry and size of microscopic nonuniformities. This may result in pseudo-variation of surface concentrations of the atoms analyzed. Using the method of relative intensities of the Auger lines of those elements that are present in the subjects studied, one can avoid the effect from this artifact if the roughness characteristic sizes are not comparable to the mean free path of excited particles. In that case correct determination of stoichiometric composition of the surface substances analyzed depends on the applied model for the contamination layer which affects (attenuates) Auger signal from sample atoms. The presented concentrations of Ga and As atoms at flat and rough surfaces were obtained under the assumption that there was a homogeneous film (containing carbon and oxygen atoms) that covered the samples studied.

3.2. ELECTROPHYSICAL CHARACTERISTICS OF BARRIER STRUCTURES WITH FLAT AND MICRORELIEF SURFACES

3.2.1. Interrelation between the topographic, structural and electrical characteristics of the barrier contacts on the basis of GaAs, InGaAs and p^+-AlGaAs–p-GaAs–n-GaAs–n^+-GaAs heterojunctions

Surface morphology and quantitative description of the structures studied were obtained with atomic force microscopy (AFM) using a Nanoscope Dimension 3000 (Digital Instruments, USA). Shown in Figs. 3.7 and 3.8 are the AFM patterns of the flat and microrelief GaAs surfaces with deposited Ti and Au layers, each 20 and 30 nm thick. These patterns were obtained in the

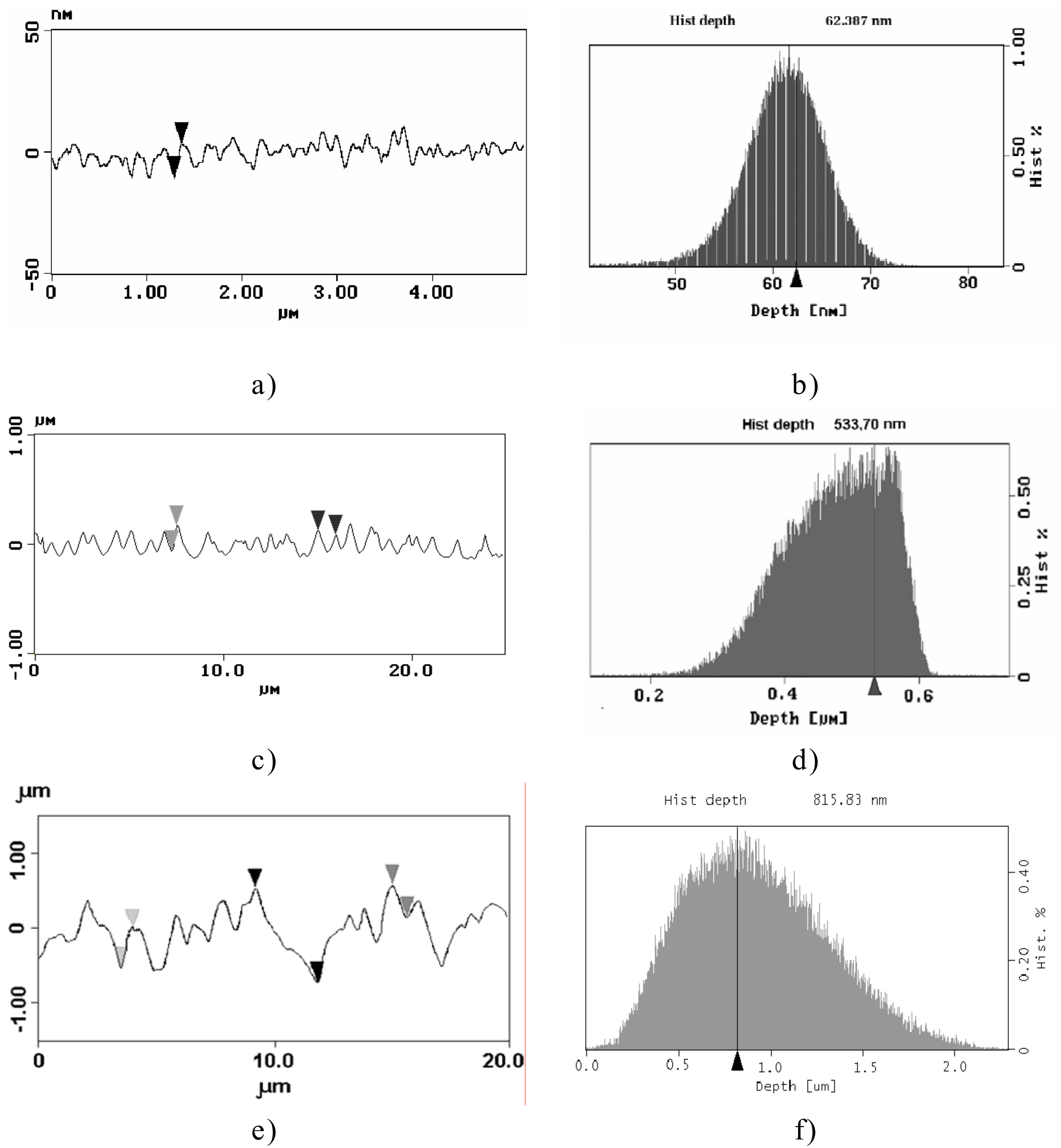

Fig. 3.7. Microrelief profiles (a, c, e), roughness height histograms (b, d, f) for flat (a, b) and microrelief of quasigrasting (c, d) and dendrite (e, f) surfaces of the Au–Ti–n-GaAs(100) structure.

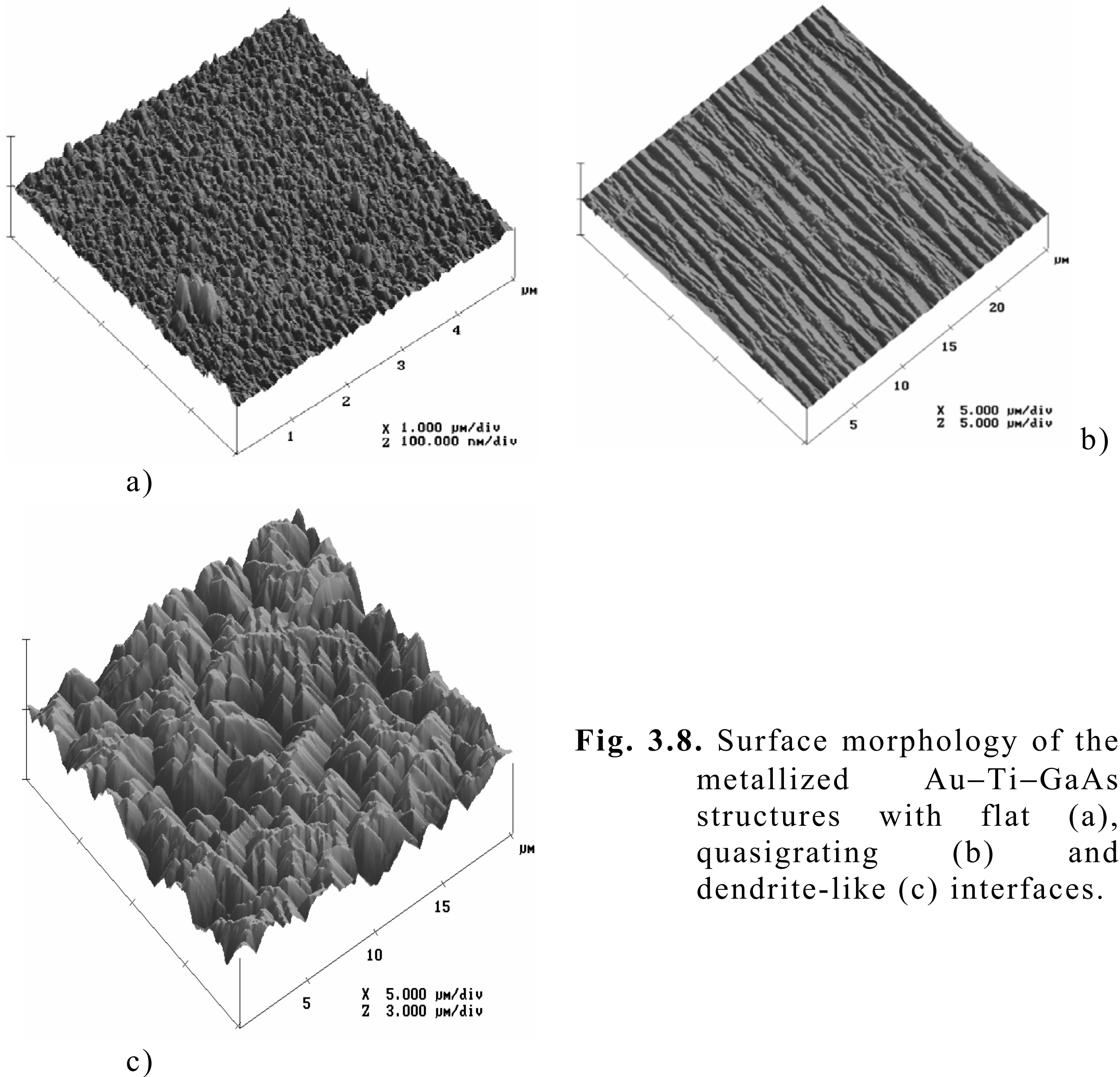

Fig. 3.8. Surface morphology of the metallized Au–Ti–GaAs structures with flat (a), quasigrating (b) and dendrite-like (c) interfaces.

scanning mode, with roughness height determination from the modulated current through a console with silicon nitride tip. The same figures give also the microrelief profiles and roughness height histograms for the analyzed surface areas (5×5 μm^2) - flat surface, 25×25 and 20×20 μm^2 – microrelief surface with a set of [110]-oriented V-grooves and dendrites, respectively. One can see that microscopic roughness distribution for the flat surface is Gaussian; the mean roughness height is ~ 0.01 μm. For the microrelief surface the microscopic roughness distribution is close to Gaussian, while their height is ~ 0.2 μm.

An analysis of the AFM patterns enabled us to determine the surface area excess over that of the projected surface. This excess is ~ 0.6% for the flat surface and ~ 30–50% (in different regions) for the microrelief one. Comparison between the roughness heights (d ~ 0.3 μm) and width W (≈ 0.06–0.07 μm) of the near-surface space-charge region (SCR) at a given dopant concentration in semiconductor ($N_d \approx 2 \div 3 \cdot 10^{17}$ cm^{-3}) shows that d > W, so SCR follows the surface relief (which is continuous).

The interactions in contact depend substantially on the surface roughness. So actual contacts formed under such conditions always realizes in a number of points and small areas. The area of factual current flow is only a portion of the total area. This feature of contact structures may be characterized with fractal dimensionality that is decisive for I–V curves.

Our investigations of microreliefs of the metallized flat and quasi-grating-like surfaces of the base material (GaAs) showed that both surfaces could be characterized by the corresponding fractal dimensionalities. The flat surface (see Fig. 3.9) has fractal dimensionality ~ 2.43. The microrelief surface of the quasi-grating-type (see Fig. 7.3c, d) has fractal dimensionality ~ 2.52, that agrees with the results of [12].

More complicated microrelief is demonstrated by the samples with dendrite-like surfaces obtained with anisotropic etching (Fig. 3.7e, f and Fig. 3.8c). At that some microplanes (located at angles of 40–65° in the microrelief formed) are observed. As was shown by us earlier [13], the microplanes located at angles > 60° set conditions for increase of the thermal-field current component in barrier structures. This effect manifests itself as an apparent decrease of the Schottky barrier (SB) height φ_B; it should be taken into account when developing solar cells.

The microrelief quality correlated with the form of I–V and C–V curves of the SB diode structures formed on the samples with flat and microrelief surfaces. Comparison of the difference N_d - N_a

≈ $(2\div4)\cdot10^{17}$ cm^{-3} (calculated from C−V curves of the flat structures) with its apparent value (calculated for the samples with textured surface) enabled us to estimate the coefficient of surface area increase resulting from its texturing (K_s). For the structures studied $K_s \approx 1.65$. This value is in good agreement with the above results of microrelief analysis with AFM.

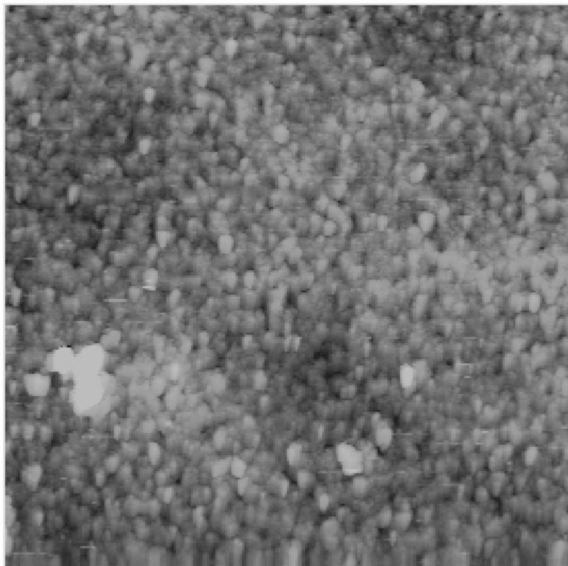

a)

D=2,429

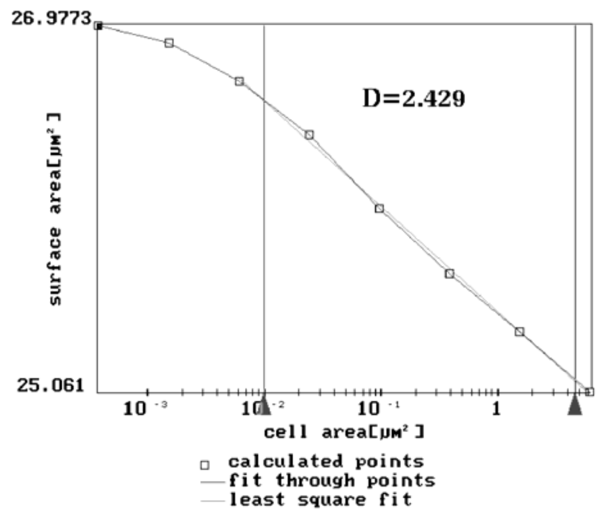

b)

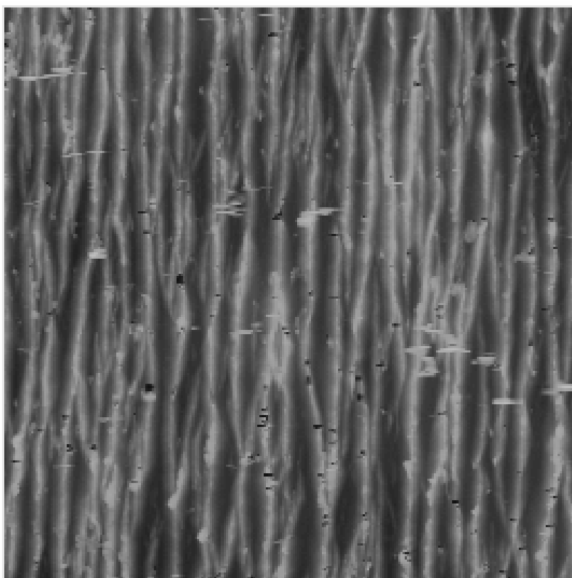

c)

D=2,517

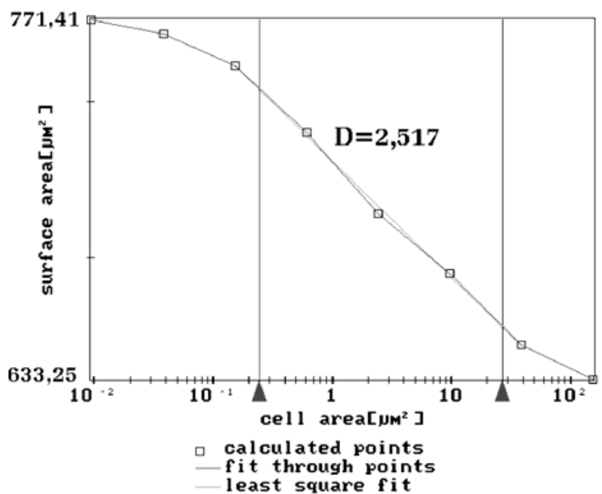

d)

Fig. 3.9. Surface morphology (a, c) and surface area dependence on the microrelief unit cell area (b, d) for the flat Au−Ti−GaAs (a, b) and microrelief Au−Ti−GaAs (c, d) structures.

As was noted earlier, presence of microplanes located at big angles (predominantly in the case of dendrite-like microrelief) contributes to the thermal-field current through SB. This follows from the form and analysis of the forward branches of I–V curves (Fig. 3.10) of the structures with different types of interface texturing, as well as with flat interface. One can see that the samples with dendrite-like microrelief have an excess current component at the initial portion of the forward branch of I–V curve (at voltages of 0.05÷0.2 V). This excess current component appears due to electric field increase in some microrelief regions. It is proportional to the area of such regions and results in some decrease of the SB height (by ~ 0.04÷0.08 eV). The same excess component of the forward current is observed at the initial portion of I–V curves of diode structures with deep quasi-grating-like relief at the metal–GaAs interface.

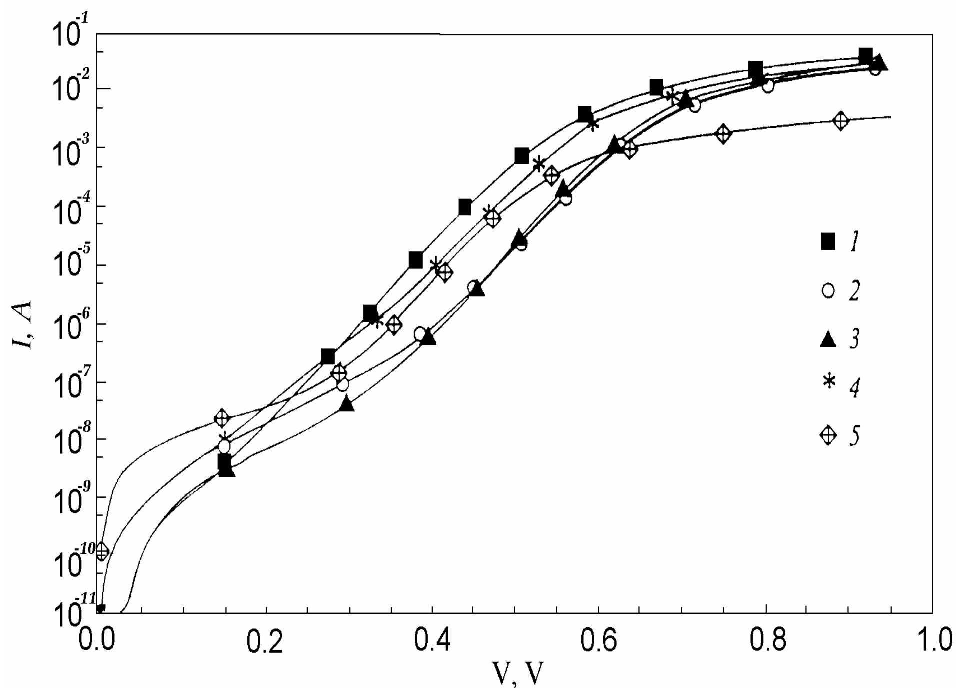

Fig. 3.10. Forward branches of I–V curves of the Au–Ti–n-GaAs Schottky-barrier diode structures with flat (1) and textured (2-5) interfaces. 2, 3 – quasi-grating-like microrelief, 4, 5 – dendrite-like microrelief.

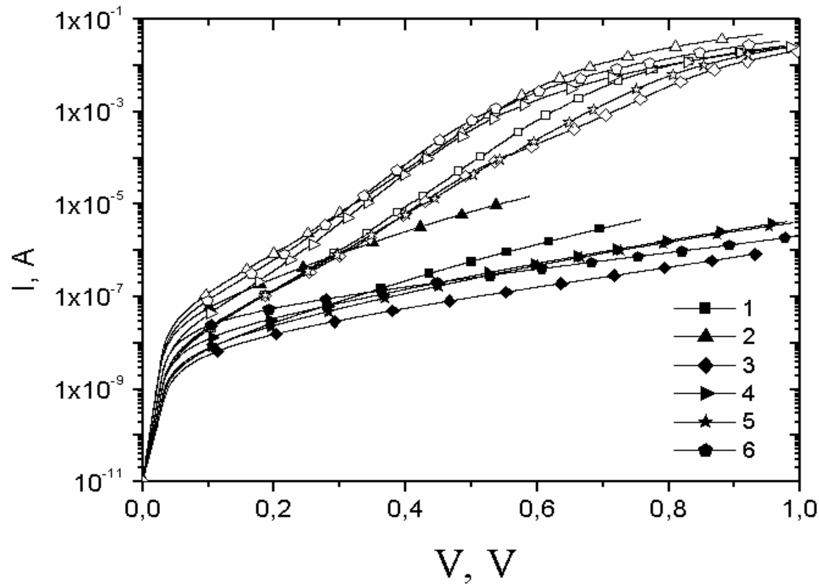

Fig. 3.11. I–V curves of the Au–n^+-GaAs diode structures; open (full) marks show the forward (reverse) branch of I–V curve.

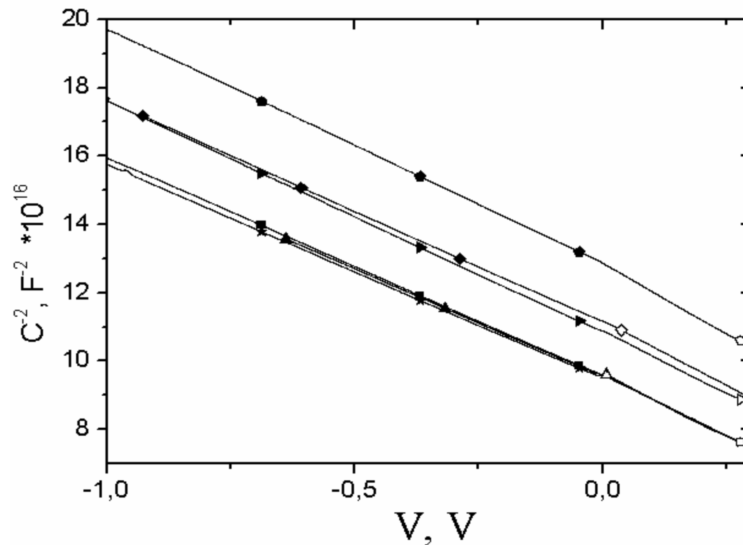

Fig. 3.12. $1/C^2$ = f(V) curve for the Au–n^+-GaAs diode structures. Diode markings are the same as in Fig. 3.11.

Both I–V and C–V curves of the diode structures were taken also for the Au–n^+-GaAs barrier contacts with complicated microrelief surface (bi-grating-like). The sets of I–V and $1/C^2 = f(V)$ curves for such barrier structures are presented in Figs. 3.11 and 3.12, respectively.

Table 3.2 gives the basic parameters of these barrier structures calculated from I–V and C–V curves. One can see that the pinch-off voltage obtained from C–V curve is about twice as big as SB

height, and the ideality factor n considerably excesses unity and approaches 2. This fact (in our case) indicates at presence of an interlayer at the interface between the metal and microrelief GaAs surface.

Table 3.2. Parameters of the Au–GaAs Schottky barriers formed on the microrelief (bigrating-like) GaAs surface.

Diode #	SB parameters calculated from the forward branch of I–V curve			SB parameters calculated from C–V curve	
	φ_B, V	n	I, 10^{-7} A	$V_{pinch\text{-}off}$, V	N, 10^{18} cm^{-3}
1	0.8235	1.7710	1.040	1.53	1.29
2	0.7712	1.8055	7.871	1.51	1.31
3	0.8178	1.8891	1.294	1.71	1.27
4	0.8053	1.6012	2.107	1.59	1.22
5	0.8035	2.0376	2.251	1.50	1.32

One can see from the above results that the forward branch of I–V curve of SB diodes can be approximated (for the samples of both types – with flat and textured interfaces) by a sum of currents - thermionic current I_T, recombination current in SCR I_R, and leakage current:

$$I = I_T \exp[q(V - IR_S)/nkT] + I_R \exp[q(V - IR_S)/2nkT] + \frac{V - IR_S}{R_{sh}} \qquad (10)$$

Here $I_T = A^*T^2\exp(-\varphi_B/kT)$; $I_R = qn_i/2\tau_p$; $A^* = 8.2$ A·cm^{-2}K^{-2}; φ_B is the SB height averaged over the barrier area (with allowance made for its thermal-field decrease); T is the absolute temperature; q is the elementary charge; k is Boltzmann constant; R_{sh} (R_S) is the shunt (series) resistance; n_i is the electron concentration in the intrinsic semiconductor; τ_p is the minority charge carrier lifetime.

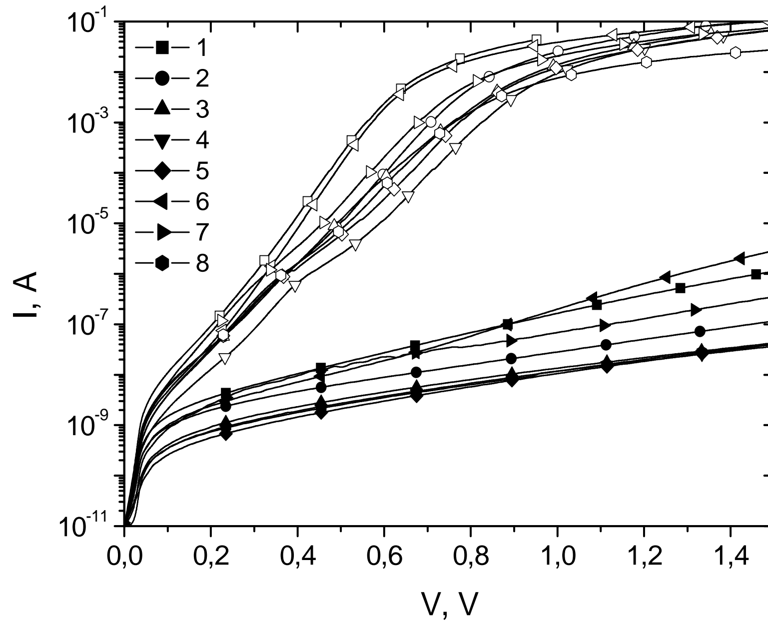

Fig. 3.13. As in Fig. 3.11, but for the Au–n-n$^+$-GaAs Schottky-barrier diodes fabricated on the basis of the LPE-grown n-n$^+$-GaAs structures.

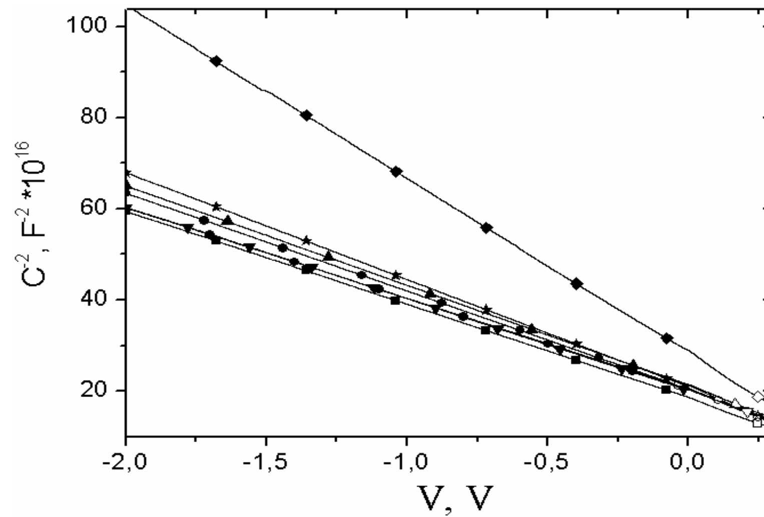

Fig. 3.14. As in Fig. 3.12, but for the Au–n-n$^+$-GaAs Schottky-barrier diodes. Diode markings are the same as in Fig. 3.13.

Computer simulation of the above dependence enabled us to determine parameters $I_{T,}$ n, I_R, R_S и R_{sh} by fitting it to the experimental curve, and thus to calculate φ_B and τ_p. It was found that the calculated τ_p value is $(1.5–2.2)\cdot 10^{-10}$ s and agrees with the ambipolar diffusion length of charge carriers determined from the photoelectric measurements.

Similar results were obtained for the Au–n-n$^+$-GaAs SB diode structures formed on the n-n$^+$-GaAs structures where the n-layer

was LPE-grown at FTI of SA "Physics-Sun. The typical I–V and C–V curves of such structures are shown in Figs. 3.13 and 3.14.

3.2.2. The geometric structure of InGaAs surface and electrical characteristics of the Au–*n*-InGaAs–n^+-GaAs Schottky barriers

We studied morphology of flat and textured surfaces of $In_xGa_{1-x}As$ with low In content using AFM and optical microscopy. The InGaAs surface microrelief was formed from the GaAs growth surface GaAs and by special selective etching of InGaAs grown on the standard flat surface of GaAs substrate. The typical microphotographs of flat InGaAs surface are presented in Fig. 3.15a, b (optical microscopy) and Fig. 3.16 (AFM). From these microphotographs one can see that, during InGaAs film growth on the flat GaAs surface, an InGaAs epitaxial layer is formed either as a banded (Figs. 3.15a, 3.16) or cellular structure, depending on the epitaxial growth mode.

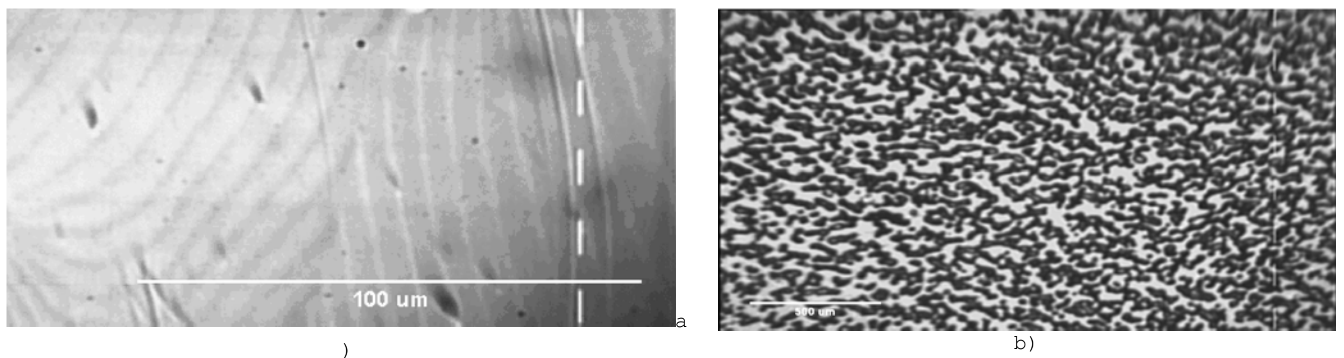

Fig. 3.15. Banded (a) and cellular (b) surface morphologies of the $In_xGa_{1-x}As$ film grown on the flat GaAs surface: a – $In_xGa_{1-x}As$ ($x \approx 0.01$); b – $In_xGa_{1-x}As$ ($x \approx 0.008$).

Shown in Fig. 3.17 are morphology of the dendrite-like InGaAs surface (Fig. 3.17a) obtained by etching of the n-InGaAs epitaxial layer and that of InGaAs surface obtained due to epitaxial plane growth on the textured (quasi-grating-like) GaAs surface (Fig. 3.17b). An analysis of the geometric structure of InGaAs

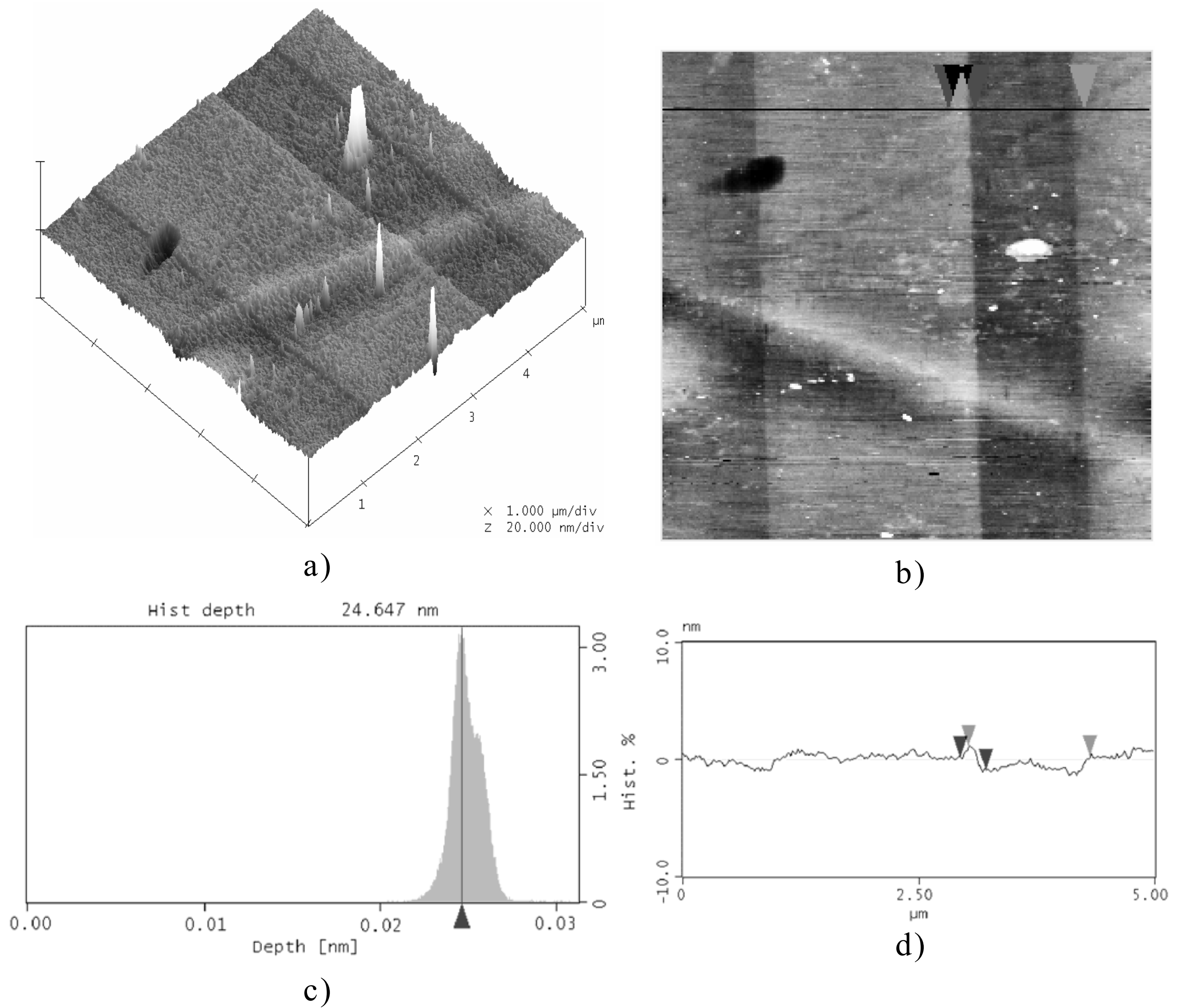

Fig. 3.16. Surface morphology (a, b), roughness height histograms (c) and microrelief profile (d) of the banded $In_xGa_{1-x}As$ film grown on the flat GaAs surface.

surface shows that microreliefs on both flat and textured surfaces, whatever the ways of their formation, are nonuniform.

However, the substrate nonuniformity seems to become smooth (averaged) on the textured InGaAs surface. This is confirmed by the measurements of I–V and C–V curves of Schottky barriers (SBs) and C–V curves of isotype n-InGaAs–n^+-GaAs heterojunctions (Table 3.3), as well as by the contact resistance calculations from I–V curves.

The measurements of I–V curves of the n-InGaAs–n+-GaAs isotype heterojunctions (40 μm in diameter) showed that in the

heterojunctions studied with x ≤ 1% the band offset at the heterojunction interface is minimal, and I–V curve is symmetric in heterojunctions grown on both flat and textured GaAs surfaces.

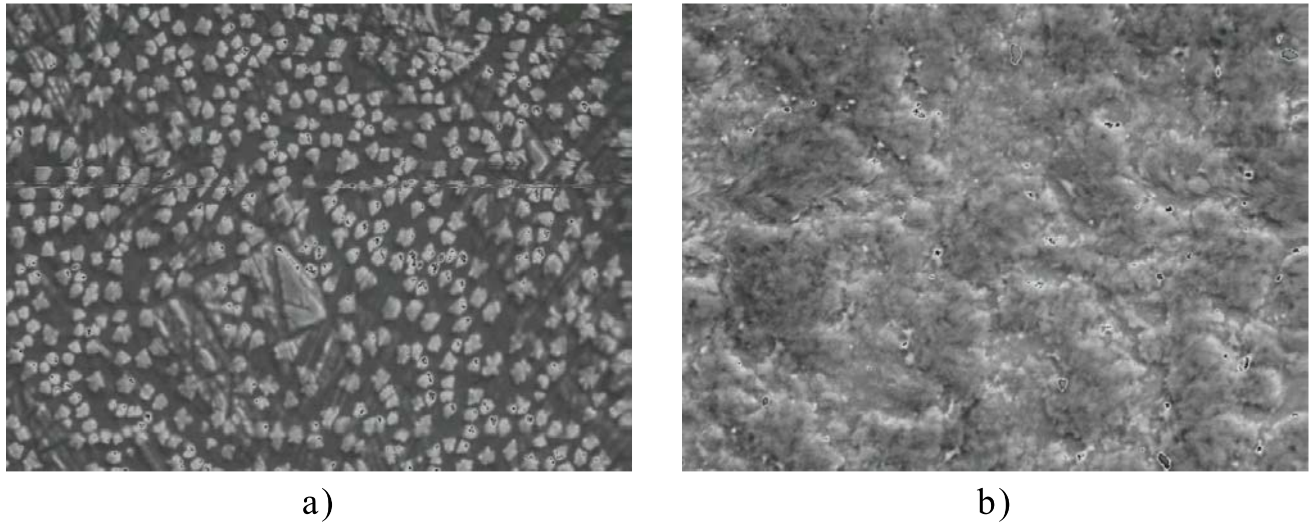

a) b)

Fig. 3.17. Dendrite-like surface morphology of the n-$In_xGa_{1-x}As$ film after selective etching of $In_xGa_{1-x}As$ (a) and surface morphology of the n-InGaAs film after n-InGaAs epitaxy on the quasi-grating-like GaAs surface (b): a - $In_xGa_{1-x}As$ (x ≈ 0.0092), b - $In_xGa_{1-x}As$ (x ≈ 0.0045). (magnified ×640)

Table 3.3. Schottky barrier parameters of the Au–n-InGaAs–n^+-GaAs and isotype n-InGaAs–n^+-GaAs heterojunctions depending on the type of n^+-GaAs surface microrelief.

Type of structure	In content, %	φ_B, V	n	φ_B, V	N_d, 10^{17} cm^{-3}	R_c,Ω
Au–n-InGaAs–n^+-GaAs; flat	≤1%	0.8–0.88	1.3–2.8	1.04–1.19	1.8–2	
Au–n-InGaAs–n^+-GaAs; n^+-GaAs– quasi-grating-like	≤1%	0.82–0.88	1.3–2.2	1.04–1.1	4–5	
In–n-InGaAs–n^+-GaAs–In; flat	≤1%					3÷1
In–n-InGaAs–n^+-GaAs–In; n^+-GaAs– quasi-grating-like	≤1%					5–8

3.3. DEVELOPMENT OF TECHNOLOGY FOR FORMATION OF OHMIC AND BARRIER CONTACTS TO GaAs AND AlGaAs EPITAXIAL LAYERS

Formation of nonrectifying contacts is one of the most important problems when developing semiconductor photoconverters on the basis of heterojunctions (HJs) made by III−V compounds. Generally lead contacts to solar elements on the basis of GaAs and AlGaAs/GaAs HJs are fabricated using the following two techniques: (i) vacuum sputtering of metals and alloys and (ii) electrochemical deposition of the corresponding metal coatings.

3.3.1. The vacuum sputtering technique

The eutectic alloy of gold with germanium (plus a nickel layer) is widely used as material for contacts to gallium arsenide. This alloy makes it possible to form nonrectifying contacts to *n*-GaAs with charge carrier concentrations over 10^{13} cm^{-3}.

Gold−germanium eutectic alloying with GaAs wafer surface occurs at temperatures over 440 °C (the temperature of the ternary gold−gallium arsenide eutectic). The alloy of gold with germanium transforms into a liquid state at a temperature of 356 °C. It forms drops of arbitrary size due to weak wetting of GaAs. Alloying occurs from arbitrary-shaped drops that alloy to different depths. A nickel layer at the surface of the eutectic alloy of gold with germanium somewhat increases wetting of GaAs; this, however, does not solve the problem of contact uniformity.

The phase and structural studies of the gold−germanium−nickel contacts showed that nickel, when dissolving in the eutectic, interacts intensely with gold, germanium and gallium arsenide. As a result, various compounds are formed which are metastable and, as time goes by, change their properties. Nickel diffusion through the layer of gold with germanium to gallium arsenide is observed even at 300 °C.

Nickel penetrates easily into the *n*-layer during alloying. There it produces acceptor levels and compensates partially (or

overcompensates completely) the semiconductor near-contact layer (depending on the charge carrier concentration value in gallium arsenide). During device production the upper nickel layer continuousness is broken and gold atoms diffuse from the technological layer into the near-contact region. Arsenic and gallium atoms diffuse to the contact surface from the other side.

The mechanism of impurity atoms diffusion in the GaAs lattice is predominantly dissociative. The ionized impurity atoms diffuse quickly through interstitials if the front vacancies are filled. At that diffusion of neutral impurity atoms through lattice sites is low. Unrestricted diffusion of impurity atoms into the contact region from either technological layers or a thick contact layer (made by gold with germanium) results in continuous increase of the doped region thickness. This occurs in the case of the contact between the gold−germanium eutectic and nickel, and seems to be one of the reasons for degradation of its electrical parameters.

Application of “chemical” isolation of the gold−germanium eutectic layer from the upper technological layers and minimization of its thickness is one of the ways to stop degradation of contacts and for decrease their resistivity. For this one should replace the nickel layer that coats the gold−germanium eutectic alloy by a material which is chemically inert to gold, germanium and GaAs. In that case the whole deposited layer gold−germanium can be transferred to the GaAs lattice during contact alloying. Thickness of the recrystallized region which is formed during contact alloying is determined by that of the deposited gold−germanium film only, because, due to the lack of diffusing impurity atoms, further diffusion will be determined mainly by the vacancy mechanism whose rate at the set temperatures is inessential.

Titanium boride was chosen as “chemically” stable antidiffusion layer. Since the charge carrier concentration in *p*-layer of semiconductor is $\sim 10^{20}$ cm^{-3}, Ta or Ti are usually chosen as contacts; they may be coated also with a TiB_x antidiffusion layer.

We used an updated plant УВН-75P to form metal layers on the GaAs, AlGaAs and InGaAs surfaces. Four magnetrons were placed in the sputtering chamber to sputter the required material. There was also an apparatus for photon cleaning of the surfaces of semiconductor wafers which were mounted on a disc. The disc could be rotated about its axis; one could fix consecutively the tables either opposite to the magnetron evaporators or over the apparatus for photon cleaning, without chamber seal failure. One could fix a semiconductor wafer (40 mm in diameter) on the table and provide uniform distribution of sputtered material over the wafer area (with spread no more than 5%). Thus it was possible to make photon cleaning of wafer surface and sputter, layer-by-layer, four different materials in a single technological cycle without chamber seal failure.

When depositing the contact layers, the chamber was evacuated to a pressure below $5 \cdot 10^{-5}$ Pa; then photon cleaning of the GaAs wafer surface was performed. After this we filled the chamber with argon up to a pressure of about $5 \cdot 10^{-1}$ Pa. Contacts were alloyed at hydrogen delivery into the ovens at temperatures of 480–500 ºC.

We formed and studied (i) AuGe–TiB_x–Au ohmic contacts (Au(180 nm)–Ge(30 nm)–TiB_x(100 nm)–Au(200 nm) to the *n*-GaAs wafers 350 μm thick with charge carrier concentration of $(1\div2)\cdot10^{17}$ cm^{-3} and (ii) Ta–TiB_x–Au contacts (thicknesses were 100 nm–100 nm–200 nm, respectively) to *p*-AlGaAs/*p*-GaAs/*n*-GaAs films with charge carrier concentration of 10^{20} cm^{-3} in *p*-AlGaAs. Test structures of two types were prepared for studies of contact resistivity:

- *n*-GaAs–AuGe–TiB_x–Au contact – to perform measurements using the current spreading technique;
- *p*-AlGaAs–AuGe–TiB_x–Au contact - to perform measurements using the transmission line technique.

To measure contact resistance with the current spreading technique, we formed round contacts (diameter d_c = 20, 40, 60, 80, 100, 120, 140, 160 and 180 μm) on one side of a semiconductor wafer. On another side an entire contact was formed.

To measure contact resistance with the rectangular transmission line technique, we deposited an ohmic Ta−TiB_x−Au contact onto the semiconductor film surface' test structures were fabricated using photolithography and contact etching. This procedure was used to measure contact resistance on the *p*-AlGaAs film.

Ohmic contacts to flat and microrelief surfaces of *n*- and *p*-type semiconductors (GaAs, AlGaAs and InGaAs) were formed according to the above technological procedures. The electrophysical parameters of the contacts formed are considered below.

3.3.2. Electrochemical deposition technique

When realizing electrochemical deposition to make ohmic contacts, we used a) silver and b) palladium.

a) Silver was electrochemically deposited onto the front *p*-GaAs layer and n^+-GaAs back surface. This technique was chosen due to its accessibility, reproducibility and rather high efficiency; besides, it is relatively inexpensive.

To improve both contact resistance and adhesion of the deposited material, we have etched (before deposition of the front ohmic contact) strip-like valleys in the AlGaAs layer (to the *p*-GaAs layer). Silver deposition was made on the surface of selectively-etched areas (without any activators) immediately after photolithography. Silver layers with the best adhesion were obtained using the alkaline solution of the following composition:

- silver nitrate – 30−40 g/l;
- ferricyanic potassium – 75−100 g/l;
- soda ash – 38-50 g/l;

- potassium thiocyanate – 100-150 g/l.

Silver was deposited at a temperature of 18−25 ºC and current density of 0.28−0.32 A/cm^2; the deposition rate was 0.2 μm/min. After silver deposition we made thermal annealing of the structure in hydrogen at a temperature of 570−620 ºC for 2−3 min. Then we performed second silver or nickel deposition to increase contact cross section area. After this contact tinning was made by dipping into solder ПОС-40.

Resistivity of the contact obtained was determined using the traditional four-probe technique. It was from 10^4 up to $6\cdot10^{-4}$ $\Omega\cdot cm^2$, depending on the thermal annealing conditions and hole concentration in the *p*-GaAs layer. It is known from literature that such resistivity values make it possible to obtain filling coefficient of SE *I*−*V* curve over 0.8.

b) Pd layers on GaAs−AlGaAs surface were obtained using chemical deposition from the $PdCl_2$ + KCl + H_2O solution at a temperature of 50 ºC. Hydrofluoric acid was used to activate chemical reaction of metal deposition onto GaAs−AlGaAs surface.

To estimate quality of the contacts obtained, we took *I*−*V* curves of the metal−semiconductor junction. The contact properties were studied both before and after thermal annealing. One can see from Fig.3.18 that palladium makes ohmic contact to *p*-GaAs without additional thermal annealing. However, such annealing reduces contact resistance by a factor of about 5.

Further decrease of junction resistance and improvement of ohmic properties is obtained by deposition (over Pd layer) a nickel layer using electrolytic deposition followed by contact tinning in a tin or indium solder. In this case we found experimentally that metal−semiconductor junction resistance drops abruptly, and contact resistance decreases by an order of magnitude as compared with an annealed sample.

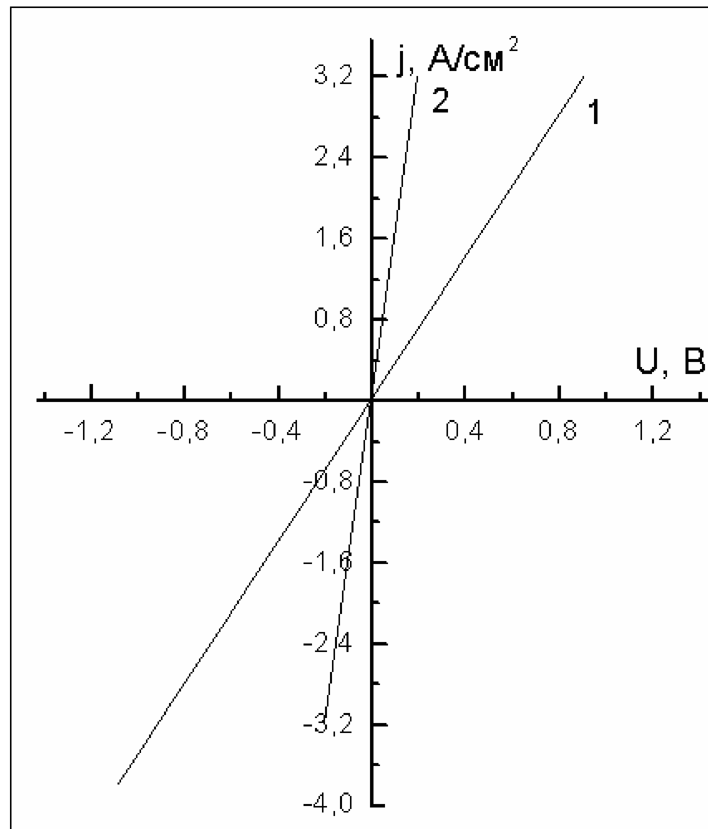

Fig. 3.18. *I–V* curves of Pd-based contact to *p*-GaAs taken before (1) and after (2) thermal annealing.

3.4. PROPERTIES OF NONRECTIFYING CONTACTS FOR SOLAR PHOTOCONVERTERS ON THE BASIS OF III–V COMPOUNDS

Thus far several techniques to form ohmic contacts to GaAs and GaAs-based solid solutions have been proposed. (For corresponding technologies and promising lines of their advancement see, e.g., [14-16].) It follows from [14-16] that the most widely used technique for obtaining nonrectifying contacts to III–V compounds is formation of a layer with high dopant concentration in a semiconductor near-surface region. This increases free charge carrier concentration up to the degeneration level and provides small width of depletion region in semiconductor.

Before metal deposition, such layer can be formed using solid-state diffusion, ion implantation or epitaxy. If these technological procedures are not available, then one should apply eutectic melt recrystallization to obtain a layer with high charge carrier concentration after metal layer deposition. A common feature of

the above approaches is a necessity to perform a high-temperature treatment of contact structures. Heating results in widening of the metal–semiconductor interfacial region due to mass transfer of the contact pair components, as well as in formation of solid solutions and intermetallic compounds. The contact junction region becomes structurally nonuniform. It involves grains whose size, density and chemical composition depend on the thermal treatment conditions. Presence of a distinct correlation between the structural-phase variations in contacts and contact resistance value poses an urgent problem of reduction of thermal treatment both effects and duration.

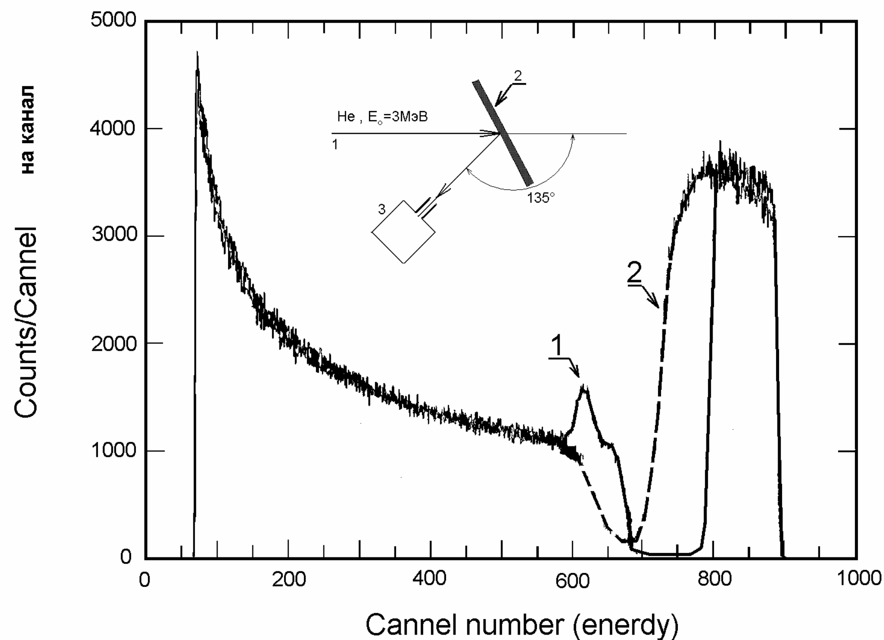

Fig. 3.19. Energy spectrum (measured after thermal annealing in hydrogen at T = 300 °C for 30 min.) of He^+ ions elastically scattered from AuGe films of different thicknesses (1 - ~100 nm, 2 - ~200 nm) deposited onto GaAs. Inset: 1 – probing ion beam; 2 – sample; 3 – receiver.

Contacts to n-GaAs were prepared using the above technique of alloying of an AuGe film of eutectic composition into semiconductor surface (previously cleaned in HCl and washed in deionized water). An Au layer 0.27 μm thick served as technological layer. All procedures were performed at a pressure of $\approx 5\cdot10^{-5}$ Pa.

The measurement of contact resistivity ρ_c was made using the long line technique [14]; the contact components distribution was analyzed using elastic backscattering of ions whose energy was 3 MeV [17]. (For geometry of the experiment see inset in Fig. 3.19.)

Shown in Fig. 3.19 are the energy spectra of elastically scattered ions He^+. These spectra characterize atomic composition and its variation over depth in the Au–AuGe–GaAs contact structures thermally annealed at T = 300 °C for 30 min. It was found that there is a peak in the ion backscattering spectra for the samples with metallization whose thickness was ≤ 100 nm (curve 1). This peak was identified as resulting from backscattering from Ga atoms on the Au surface. So one may assume that in these structures diffusion effects are pronounced rather well, even at relatively "soft" thermal treatments. The experimental evidences for Ga atoms migration (resulting from heating) from GaAs into the Au film were obtained in [18, 19]. At the same time the spectral features were related to the effects of multiple ion scattering in structures with disordered semiconductor surface layers [20].

Absence of the above peak for structures with thicker Au film (curve 2), as well as the results of [21, 22], enable one to assume that the features observed in the He^+ scattering spectra is determined by the local erosion effects at nonuniform temperature distribution in a semiconductor material. This mechanism seems to be rather convincing, taking into account that the temperatures of eutectic melting for the row Au/Ga/As–Au/Ga–Au/Ge [16] do not differ considerably from the annealing temperature used by us.

Solid-state reactions between Au and GaAs may also occur. They may result in arsenic sublimation and formation of gold gallides. This is related to the fact that the initial condition of GaAs surface and initial microstructure of gold do not change the character of gold interaction with gallium arsenide; they affect the arsenic sublimation and quantitative interrelations between the gallide phases only.

In our further investigations we used the structures for which ion backscattering spectra looked like curve 2 in Fig. 3.19. The contacts formed under the above conditions had considerable resistivities ρ_c; so we used more “severe” annealing conditions to obtain nonrectifying contacts.

Table 3.4 gives the results of our measurements of contact resistivity for a set of samples of that type which were annealed in hydrogen at 430 ºC for 30 s, i.e., under such conditions when interaction between the alloy film and GaAs is strongly increased due to melt formation.

Table 3.4. Contact resistivity at melting together Au–AuGe–GaAs.

Sample #	Charge carrier concentration n, cm^{-3}	Contact resistivity ρ_c, $\Omega \cdot cm^2$
1	$1.25 \cdot 10^{18}$	$1.5 \cdot 10^{-6}$
2	$1.28 \cdot 10^{18}$	$8.6 \cdot 10^{-6}$
3	$3.4 \cdot 10^{18}$	$8.98 \cdot 10^{-6}$
4	$1.8 \cdot 10^{18}$	$1.1 \cdot 10^{-6}$

After melting and solidification of the eutectic melts (resulting in formation in GaAs of a heavily doped layer neighboring to the metal–GaAs interface) we obtained ρ_c values which were below the previous ones by 2÷3 orders of magnitude and approached the theoretical ones for the corresponding dopant concentrations in the active GaAs layers [14, 23].

3.5. EFFECT OF SURFACE ROUGHNESS ON THE PROPERTIES OF OHMIC CONTACTS TO GaAs

The actual metal-semiconductor contacts are practically always nonuniform to an extent. Generally these nonuniformities are related to interface imperfection, presence of oxide layers on etched surfaces, structure of a metallized layer or reactions in metal-semiconductor contacts. The above sources of

nonuniformities result from drawbacks of technological processes used in production of contact structures. These drawbacks lead to uncontrolled spread of the electrophysical parameters of contact structures. In this connection investigation of the properties of metal-semiconductor junctions at purposeful formation of nonuniformities at their interfaces becomes of special importance. Many of such nonuniformities may be exemplified by a purposefully formed microrelief on a semiconductor surface.

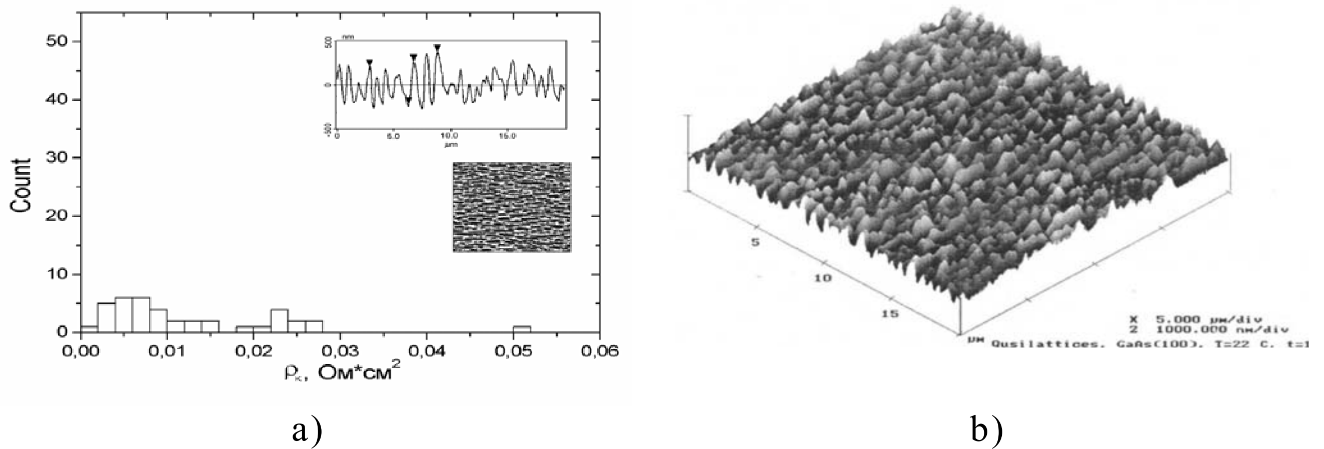

a) b)

Fig. 3.20. The results of studies of contact resistivity ρ_c of GaAs–Au (180 nm)–Ge (30 nm)–TiB_x (100 nm)–Au (200 nm) ohmic transitions on quasi-grating-like semiconductor surface (a) and AFM surface pattern (b).

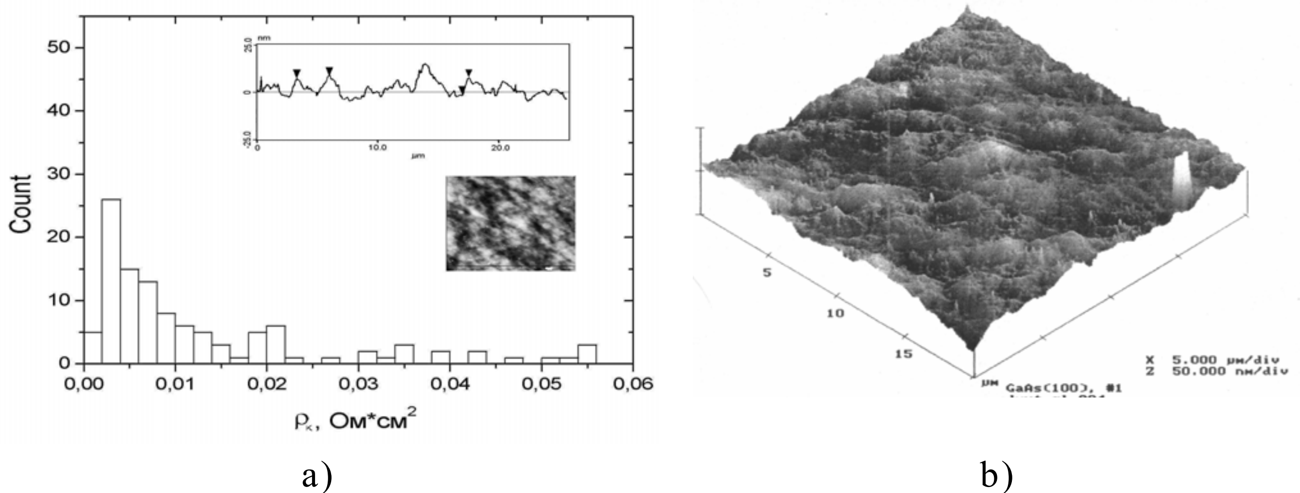

a) b)

Fig. 3.21. As in Fig.3.20 but for flat semiconductor surface.

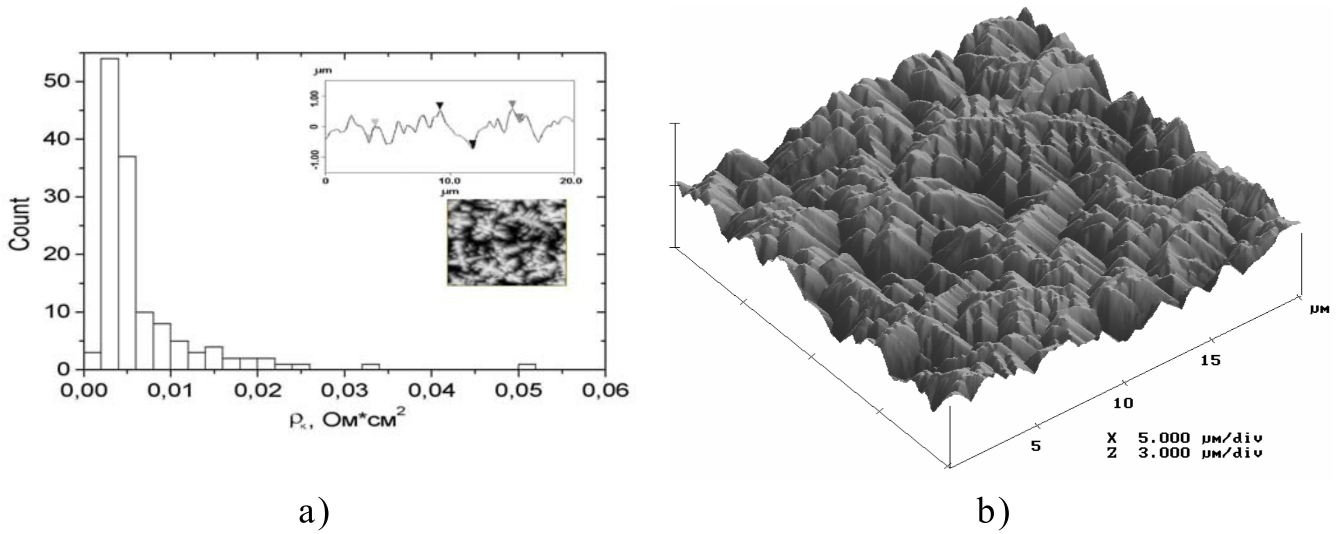

a) b)

Fig. 3.22. As in Fig.3.20 but for dendrite-like semiconductor surface.

Figures 2.5.3–2.5.5 present the results of our studies of contact resistivity ρ_c of the GaAs–Au (180 nm)–Ge (30 nm)–TiB_x (100 nm)–Au (200 nm) ohmic junctions. They were prepared on the semiconductor surfaces of different morphologies; the contact diameter was d_c = 400 µm. Formation of nonrectifying contacts was performed using thermal annealing in hydrogen at 500 °C for 1 min.

Contact resistivity ρ_c was defined as $\rho_c = \left(\frac{\partial J}{\partial V}\right)^{-1}_{V=0}$ where J is the current density. Being determined in such a way, this quantity should not depend on the contact area; this conclusion is in contradiction with the results presented in Fig 2.5.6.

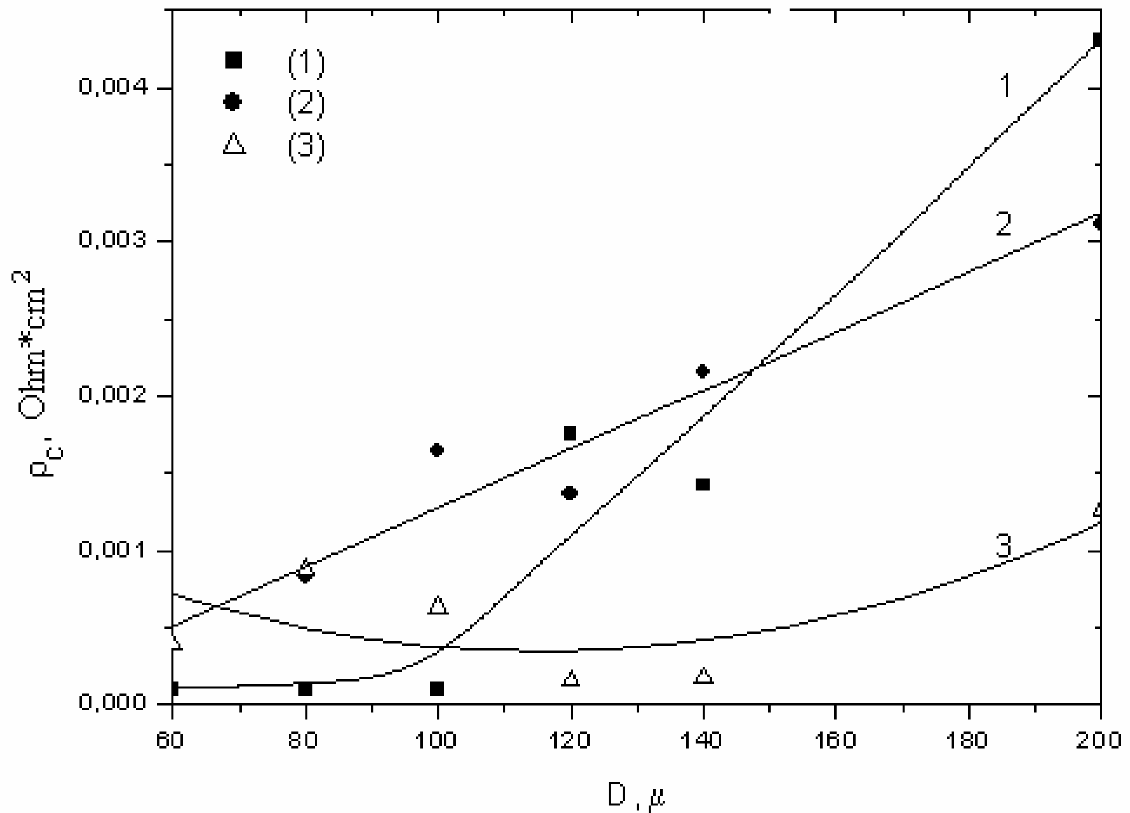

Fig. 3.23. Contact resistivity ρc as function of contact diameter dc : 1 – dendrite-like; 2 – flat; 3 – quasigrating surface GaAs

Thus the results shown in Figs. 3.20–3.23 indicate at an essential nonuniformity of ρ_c distribution over the wafer area, at both the initial and microrelief surfaces. This spread of ρ_c values depends on the contact area, and for diameter d_c it may be presented in the following sequence: quasi-grating-like surface–flat surface–dendrite-like surface. Whatever the current flow mechanism (thermionic, thermal-field, field), the resistivity ρ_c is proportional to $\exp(q\varphi_b)$ (where φ_b is the effective barrier height), and the Fermi level is pinned due to high density of surface states. Therefore the only way to affect contact resistivity is variation of the doping level in the semiconductor substrate with uniform planar distribution of impurities over the whole area of the contacting layer.

However the structural-phase distinctions at different semiconductor surface areas result in the fact that the actual contact area (disordered sections or those with Ge atoms that have

diffused here) differs essentially from the geometrical one. Indeed, it is well known that the eutectic melt AuGe wets poorly the actual GaAs surface. In this case contact formation will depend on composition and thickness of an oxide layer at the metals–semiconductor interface, possibility of its dissolving in the melt, and variation of the wetting angle of the melt due to absorption of Ga (As) atoms and loss of Ge atoms.

From this one can conclude that the geometrical sizes of regions and predominant current flow mechanisms differ essentially for different wafer sections. This leads to the observed spread of ρ_c values. Thus nonuniform oxide layer distribution of at an actual GaAs surface is the reason for nonuniform interdiffusion during thermal treatment and, as a result, for electrical nonuniformity of the interface.

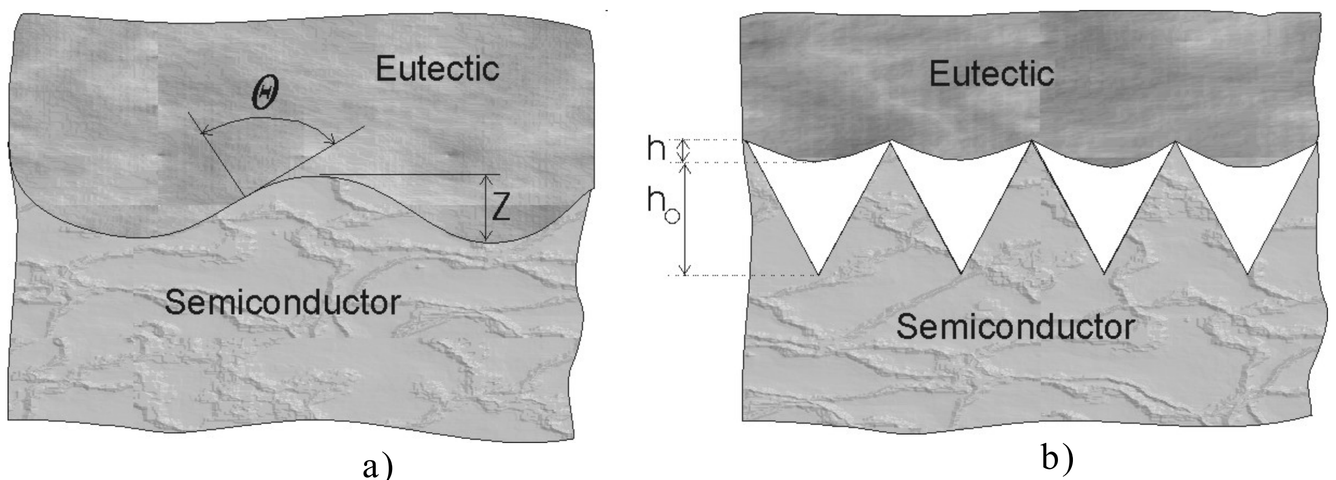

Fig.3.24. Wetting of surface with melts: a – the melt fills completely the valleys of a rough surface; b – the case of minimal wetting.

The above model for formation of electrical contact nonuniformities may be applied for analysis of the roughness effect on the properties of nonrectifying contacts. It is known that surface roughness affects wetting of surface by melts. Two limiting cases presented in Fig. 3.24 may occur, depending on the geometrical parameters of relief (ridge height, width and depth of valleys, as

well as wetting angles for surface areas where a relief has been formed).

Figure 3.24a corresponds to the case when a melt fills completely the valleys of a rough surface. At that, as was shown in [24], the actual contact area $S_a = kS_d$, where S_d is the area of a droplet on a flat surface and the coefficient

$$k = \int_0^{r_d} \frac{2\pi\alpha\left[(1+\frac{\partial z}{\partial x})^2\right]^{\frac{1}{2}} dx}{\pi r_d^2} \quad (11)$$

Here r_d is the radius of a droplet on a flat surface, α is some coefficient, z and x are the variable coordinates which characterize height of ridges and spacing between them.

In an actual situation no complete wetting of valleys occurs, so a case is realized that is intermediate between those presented in Fig. 3.24. One can show that, as θ grows, h decreases. This fact characterizes eutectic penetration into the valleys of a rough surface (see Fig. 3.24a).

There exists also another effect affecting S_a. It is due to roughness effect on melt spreading (kinetic factor). Since duration of contact between the melt and semiconductor is finite, presence of ridges serves as a peculiar barrier for spreading; at the same time longitudinal valleys are favorable for melt spreading. Thus the surface morphology features, as well as inhomogeneity of surface composition, affect the character of interactions between phases in metal–semiconductor contacts, i.e., on the electrophysical properties of HJs.

The above qualitative model for nonuniformity formation when fabricating ohmic contacts on rough surfaces makes it possible (i) to explain experimentally observed spread of electrical parameters, and (ii) to show the reasons for their instability (the main of which is appearance of intrinsic stresses). It was shown in [24] that intrinsic stress value in such structures is determined by

the roughness parameters and metal film thickness. Depending on the interrelation between the ridge height and metal film thickness, different situations may be realized, when intrinsic stresses are over, equal or below those in contacts formed on flat surfaces.

In what follows, we present the results of our studies of ohmic contacts to p^+-GaAs formed on substrates with textured surfaces of different types (quasi-grating- or dendrite-like, flat) at different fusion modes. We studied the following contacts:

1. Au–TiB_x–Ti–p-GaAs; the metallization components were formed using magnetron sputtering;

2. InZn–p-GaAs; thermal evaporation of alloy in the vacuum.

In the first case magnetron sputtering of metals was made onto a substrate heated up to 300 °C. Some samples were annealed in the hydrogen atmosphere at T = 500 °C or 600 °C for 1 min. The thicknesses of the sputtered metal layers were such: Au – 300 nm, TiB_x – 100 nm, Ti – 100 nm. In the second case alloy InZn was sputtered onto a “cold” p-GaAs substrate. Then thermal annealing of contacts was made in the vacuum at T = 300 °C for 15 min. The thickness of the deposited InZn layer was ≈300 nm.

Shown in Fig.3.25 are the contact resistance ρ vs the contact diameter curves for the Au–TiB_x–Ti–p-GaAs structures. Similarly to such curves for ohmic contacts to n-GaAs, a considerable spread of ρ values is observed for the samples of the same diameter, as well as considerable ρ dependence on contact diameter. This indicates at nonuniformity of the substrate material. Averaging of ρ values obtained for different contact diameters showed that in the diameter range of 40–120 μm ρ practically does not depend on the contact area for those samples which have been made on flat or dendrite-like p-GaAs surfaces. Considerable dependence of ρ on contact diameter is observed for the contacts made on quasi-grating-like surfaces. As diameter grows to 400÷600 μm, the spread of ρ values increases for all the sample types.

The ρ vs contact diameter curves for the InZn–p-GaAs structures is presented in Figs.3.25, d. Despite the lower ρ values, the dependence of ρ on contact diameter is observed in this case too. This dependence is pronounced clearly for all the three surface types.

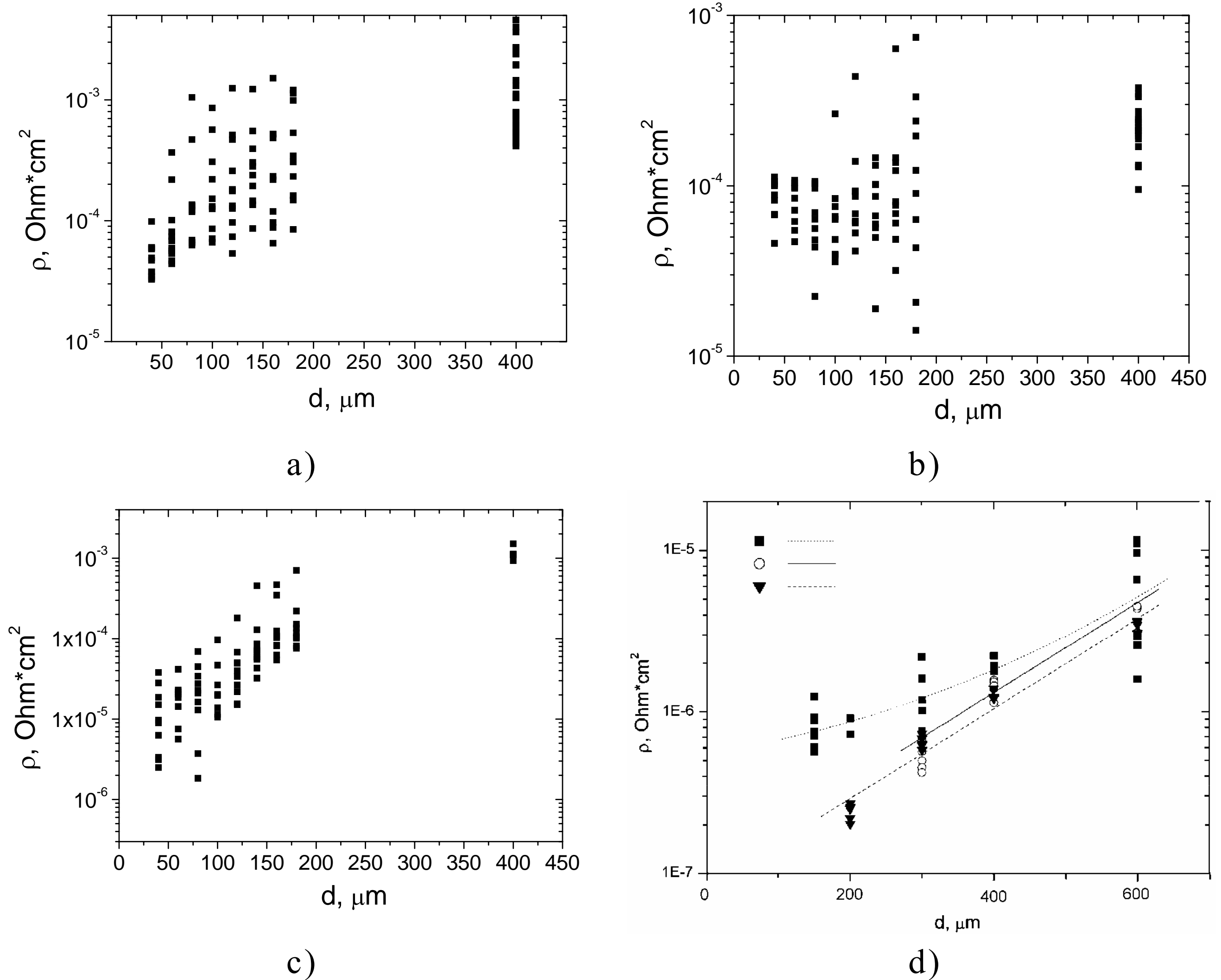

Fig. 3.25. Contact resistance of the Au–TiB$_x$–Ti–p-GaAs structures as function of the contact diameter: a – flat GaAs surface; b – dendrite-like GaAs surface; c – quasi-grating-like GaAs surface; d – same for the InZn–p-GaAs structures: ■ – flat GaAs surface; ▼ – dendrite-like GaAs surface; ○ – quasi-grating-like GaAs surface.

Note that decrease of ρ by a factor of 5–10 after thermal annealing at 500 °C for 1 min. in the hydrogen atmosphere was observed for all types of samples with the Au–TiB$_x$–Ti–p-GaAs

contacts. Thermal annealing at 600 °C (the rest of conditions being the same as above) resulted in growth of ρ for all the types of structure.

The results concerning ρ value are reproducible for both types of contacts to p-GaAs formed on flat, as well as textured, surfaces.

3.6. INVESTIGATIONS OF ELECTROPHYSICAL CHARACTERISTICS OF BARRIER STRUCTURES ON THE BASIS OF HETEROJUNCTIONS OBTAINED. DETERMINATION OF BARRIER PARAMETERS AND CURRENT FLOW MECHANISM

3.6.1. Manufacturing technology for barrier contacts

The barrier contacts to GaAs and GaAs-based solid solutions were used for studies of the quality of metal–semiconductor interfaces when a semiconductor had flat or textured surfaces. To this end it was necessary to develop technological procedures for barrier contact formation. We applied, first of all, the traditional technique of vacuum sputtering of polycrystalline metal layers onto semiconductor surface.

In addition, the barrier layers had to provide minimal mass transfer (both from the outer side of the contact system and that of semiconductor structure components to the outer elements) during service life. This can be achieved by formation of a barrier layer of amorphous or quasi-amorphous structure that would remain stable during the technological cycle of diode fabrication and long-term operation.

From the viewpoint of providing temperature stability and long-term operation of heterostructures, the near-surface regions and barrier layers are of key importance. So we concentrated our investigations mainly on the barrier layers at the metal–semiconductor interfaces with flat or microrelief surfaces of GaAs, AlGaAs and InGaAs. We studied different versions of technology for layer formation using magnetron sputtering of targets made of stoichiometric components – titanium borides and

thermal reactive magnetron sputtering of (Ti, Ta) targets in a mixture of nitrogen and argon.

For TiB_x magnetron sputtering we used continuous targets made of stoichiometric powder materials prepared with the powder metallurgy techniques. The magnetron construction enabled us also to use the coarse-grained targets.

The reactor chamber with magnetrons was evacuated by a turbomolecular pump with a nitrogen freezing-out system down to a residual pressure of $5\cdot10^{-5}$ Pa. Precise letting-to-argon and nitrogen was made using an original two-chamber system. Sputtering was performed at a pressure of 10^{-1} Pa in the chamber. The study of the technological processes was performed for the magnetron breakdown current range 0.2÷1.4 A. The layer formation rate was varied from 0.2 up to 2 nm/s.

The titanium and gold layers up to 100 nm thick were formed also with the traditional thermal sputtering technique using electron-beam heating. The processes were carried out in an oil-free vacuum; the residual pressure was $5\cdot10^{-4}$ Pa.

Taking into account that the contact systems to be investigated and optimized were complex and multiple-choice, we started from studies of barrier layers and barrier layer–semiconductor interfaces; then the near-surface regions were studied. After a preliminary analysis we chose the contact systems for comprehensive investigations.

3.6.2. Effect of surface roughness on the Schottky barrier characteristics

In subsection 3.4 an analysis was given of the properties of nonrectifying contacts formed on rough surfaces that are wet with eutectic melts. Here we shall present the results of our investigations of the metal–semiconductor contact structures fabricated by vacuum evaporation of metal onto rough surfaces. It was noted in [25, 26] that the properties of surface-barrier structures depend on interface nonplanarity whose contribution to

the current flow through the interface is related to increase of the effective contact area and improvement of perfection of the microrelief surface structure.

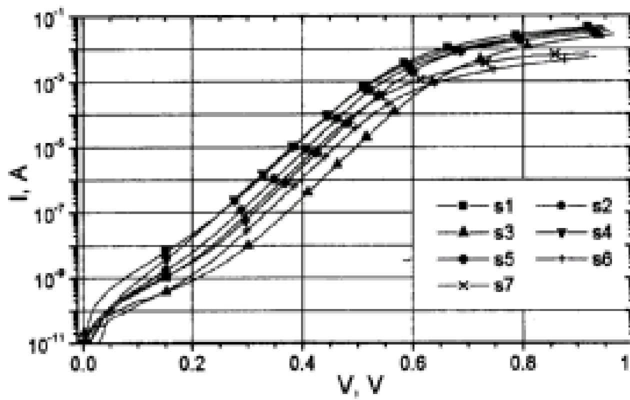

Fig.3.26. Forward branch of *I–V* curves for contacts formed on flat GaAs surface.

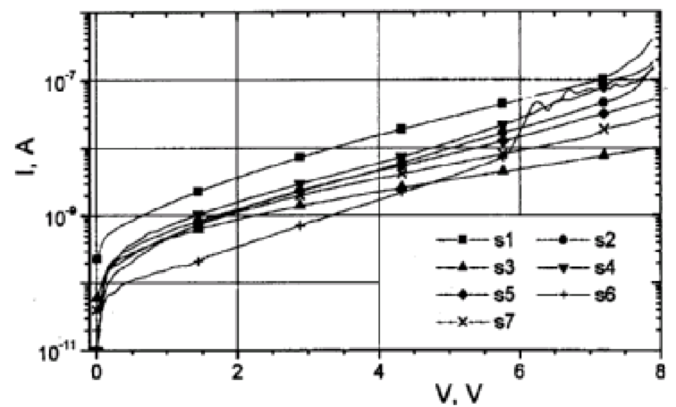

Fig.3.27. Reverse branch of *I–V* curves for contacts formed on flat GaAs surface.

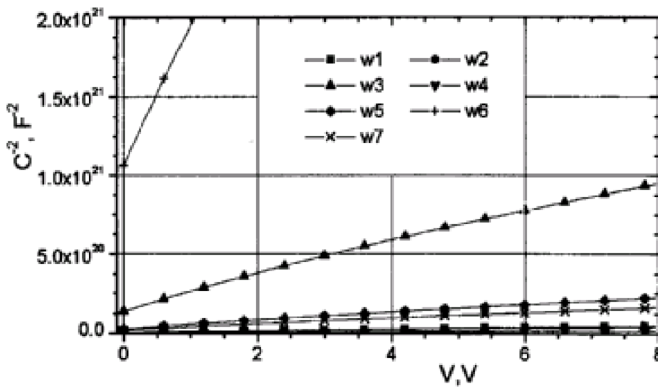

Fig.3.28. *C–V* curves for contacts formed on flat GaAs surface.

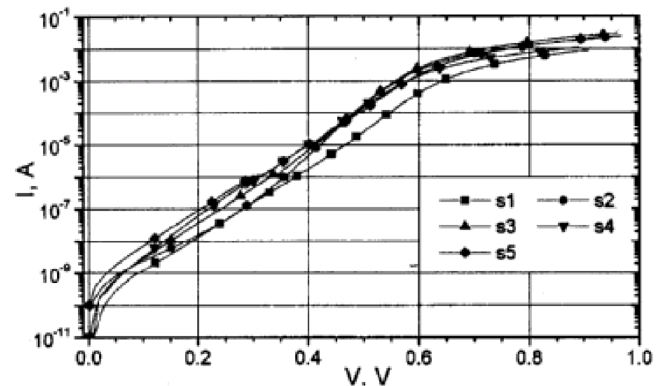

Fig.3.29. As in Fig. 3.26 but for dendrite-like GaAs surface.

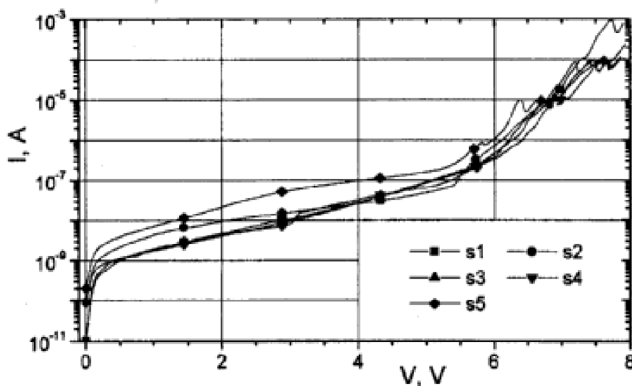

Fig.3.30. As in Fig. 3.27 but for dendrite-like GaAs surface.

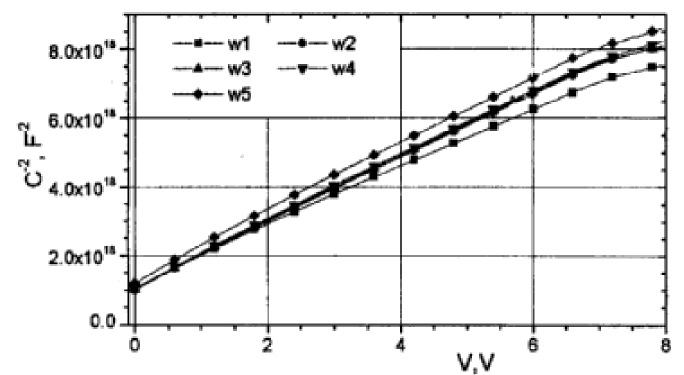

Fig.3.31. *C–V* curves for contacts formed on dendrite-like GaAs surface.

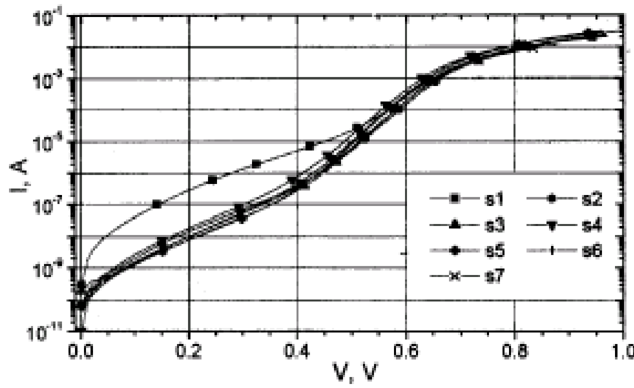

Fig.3.32. As in Fig. 3.26 but for quasi-grating-like GaAs surface.

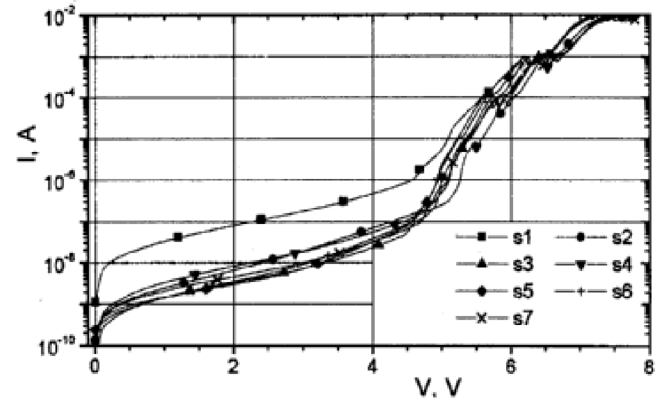

Fig.3.33. As in Fig. 3.27 but for quasi-grating-like GaAs surface.

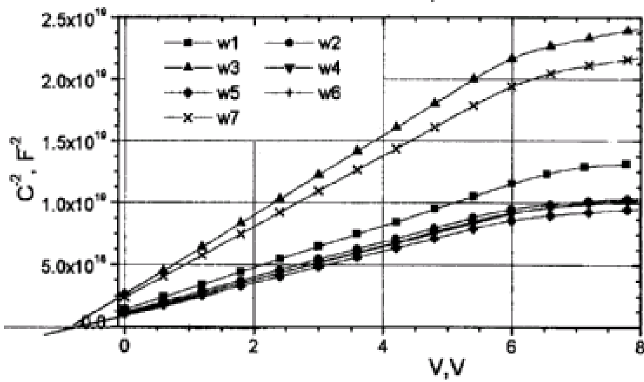

Fig.3.34. *C–V* curves for contacts formed on quasi-grating-like GaAs surface.

I–V and C–V curves of the barrier contacts formed by Au sputtering onto these surfaces are presented in Figs. 3.26–3.34. On can see that roughness of the initial surface is favorable to interface homogenization (decrease of spread of I–V and C–V curves). The typical values of the parameters of barrier structures obtained at such contact junctions are presented in Table 3.5.

Table 3.5. Barrier height φ_b and ideality factor n of Au–n-GaAs Schottky barriers formed on n-GaAs with different surface morphologies (the contact area is about $1.32 \cdot 10^{-2}$ cm^2; $N_d = (2 \div 3) \cdot 10^{16}$ cm^{-3}).

Surface type	Parameters		
	φ_b (*I–V* curves), V	φ_b (*C–V* curves), V	Ideality factor *n*
Flat	0.88	0.87	1.1
Quasi-grating-like	0.95	0.76	1.2
dendrite-like	0.88	0.94	1.2

One can see from Table 3.5 that there is no clearly pronounced correlation between the Schottky barrier parameters and topographic characteristics of semiconductor surfaces where these barriers were prepared. This conclusion is supported also by the results of studies of the Au–Ti–GaAs structures whose typical parameter values are given in Table 3.4 (note that change of the contact area by a factor of 4 did not affect the barrier parameter values). It was found that additional etching of the samples with quasi-grating-like surfaces is favorable to smaller spread of the contact parameter values for such structures, i.e., contact junction uniformity is improved.

Table 3.6. Barrier height φ_b and ideality factor n of Au–Ti–n-GaAs Schottky barriers formed on n-GaAs with different surface morphologies ($N_d = (2\div3)\cdot10^{16}$ cm^{-3}).

Surface type	Contact diameter d_c, μm	Parameters		
		φ_b (I–V curves), V	φ_b (C–V curves), V	Ideality factor n
Flat	250	0.79	0.92	1.06
	500	0.79	0.95	1.05
Quasi-grating-like	250	0.78	0.79	1.1
	500	0.81	0.82	1.05

An essential distinction between the samples with rough and flat surfaces was observed for reverse I–V curves only (Figs. 3.27,3.30, 3.33). This fact may be related to appearance of sections with higher field strength at nonuniformities. As a result, the contribution from the tunnel current component to the total current density grows abruptly

3.6.3. Development of contacts of the required configuration to photoconverters using explosive photolithography

We used the p^+-GaAs/p^+-$Al_xGa_{1-x}As$/p-GaAs–n-GaAs/n^+-GaAs and p^+-$Al_xGa_{1-x}As$–p-GaAs–n-GaAs–n^+-GaAs epitaxial heterostructures as material for PEC fabrication. Contacts of the required configuration (Fig.3.35) were made using explosive photolithography on flat and textured *p-n* junctions. A typical heterostructure had the following parameters:

- p^+-GaAs – thickness of 0.3 μm, hole concentration of 10^{19} cm^{-3};
- p^+-$Al_xGa_{1-x}As$ - thickness of 0.7 μm, hole concentration of 10^{19} cm^{-3}, $x = 0.6$;
- p-GaAs – thickness of 0.8 μm, hole concentration of 10^{19} cm^{-3};
- n-GaAs – thickness of 2.2 μm, electron concentration of $3 \cdot 10^{17}$ cm^{-3};
- n^+-GaAs – thickness of 350 μm, electron concentration of $2 \cdot 10^{18}$ cm^{-3}.

We studied also contacts formed with thermal evaporation of InZn alloy onto p-GaAs through a mask (the contact layout is presented in Fig.3.3.6).

To make contacts of the required configuration, the following sequence of procedures has been developed:

1) preparation of p^+-GaAs surface for ohmic contact deposition;

2) deposition of ohmic Ti–Au contact;

3) electrolytic deposition of Au coating (about 1 μm thick);

4) formation of the required layout using photolithography;

5) etching of the contact at the areas not protected with photoresist;

6) etching of p^+-GaAs down to $Al_xGa_{1-x}As$ at the areas not protected with photoresist and contact;

7) deposition of photoresist for explosive etching of AlN and development;

8) deposition of AlN;

9) removal of AlN photoresist deposited;

10) check of the presence of contacts between the gold areas.

To prepare p^+-GaAs for sputtering, the samples were etched in the solution $NH_4OH:H_2O_2:H_2O$ (1:1:200) during 30 s, then were washed in deionized water and methanol. The etching rate was about 0.1 μm/min.

Contact deposition was performed by magnetron sputtering of metals in the argon atmosphere, layer-by-layer, first Ti layer 100 nm thick, then Au layer 200 nm thick, in a single technological cycle without vacuum failure. During deposition the sample temperature did not exceed 300 °C. The upper contact metallization layer was formed with electrolytic deposition of a gold layer 1 μm thick; the required layout was made with photolithography. After this the Ti–Au contact was etched in the PEC windows in the solution $NH_4OH:H_2O_2:H_2O$ (1:1:200) during 2 min.

The aluminum nitride windows were made in the following way. After opening of windows, a photoresist layer was deposited onto the sample surface; the centrifuge speed of rotation was about 600 rpm. Then the sample was dried at a temperature of about 60 °C, aligned and developed. After washing (to remove developer) the sample was dried on the centrifuge. An AlN layer 100 nm thick was deposited using magnetron sputtering of Al in the nitrogen atmosphere. Removal of AlN from the areas coated with the photoresist was made by boiling in dimethylformamide followed with mechanical removal of swollen photoresist.

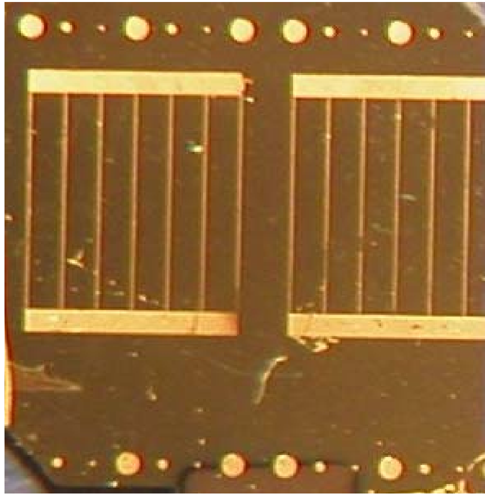

Fig. 3.35. The layout of the upper contact to PEC made on the basis of the p^+-GaAs/p^+-$Al_xGa_{1-x}As$/p-n-GaAs–GaAs/n^+-GaAs heterostructure. The contact grid was made using explosive photolithography. Circles designate test contacts for measurement of resistivity. (magnified ×33).

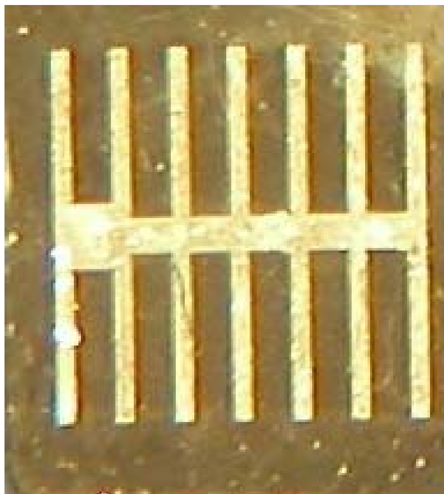

Fig. 3.36. As in Fig.3.35 but the contact grid was made using (In + Zn) sputtering through a mask. (magnified ×33).

The photographs of actual PEC prototypes with contact layout formed by explosive photolithography (sputtering through a mask) are shown in Fig.3.35 (3.36).

3.7. Simulation studies of diffusion processes in metal–GaAs contact

The main requirement for contacts in all types of semiconductor devices is abruptness of the metal–semiconductor interface [27, 28]. This means minimization or complete absence of transition layer. Wide metal concentration depth profile in a semiconductor results in degradation of electrophysical characteristics of both the Schottky-barrier (SB) devices and ohmic contacts.

The main reason for „smearing out” of a transition layer (its finite width) is penetration of metal atoms into a semiconductor and vice versa, i.e., mass transfer occurring at the

metal–semiconductor interface. This effect appears during contact formation and then is developing due to further technological procedures and device operation. Mass transfer can be affected by relaxation of intrinsic stresses (ISs), electric fields, radiation and other external actions [29, 30]. It should be noted that considerable width of a transition layer becomes especially essential when one deals with contacts to those devices (SB photoconverters, microwave devices, etc.) whose active area is in immediate neighborhood of metal–semiconductor interface. That is why mass transfer in metal–semiconductor contacts has been studied actively at all stages of the development of semiconductor devices technology, starting from the fifties of the last century. These studies were stimulated by the development of theory of diffusion, as well as application of advanced research techniques (Auger electron spectroscopy, secondary ion mass spectrometry, x-ray photoelectron spectroscopy, etc.) of high information ability.

3.7.1. Formulation of the problem and theoretical background

The stage of formation of metal–semiconductor interface with "pure" semiconductor neighboring on a solid solution where metal concentration is of the order (or somewhat over) of n_0 (here n_0 is the limiting concentration value for metal dissolved in semiconductor) can be studied mathematically using the theory of diffusion.

We studied diffusion of neutral metal atoms only in a semiconductor. Thus we did not consider the role of the space at the metal–semiconductor interface. We took into account, however, that, when metal atoms penetrate into a semiconductor, ISs appear in that region. They are due to mismatch of the metal and semiconductor lattices. As a rule, metal atoms are bigger than those of semiconductor. This results in their "pushing-off" out of semiconductor (rather than "drawing-in"). It is just this effect that determined the limiting solubility of a metal in a semiconductor.

An equation describing diffusion of metal atoms (whose concentration is n) in a semiconductor is of the following form:

$$\operatorname{div}\vec{j} = -\frac{\partial n}{\partial t}. \qquad (12)$$

The metal atom flow $\vec{j}_s$ in a semiconductor may be written as:

$$\vec{j}_s = -D_s\left(1 + \frac{K\Omega\beta}{kT}n\right)\vec{\Delta} n. \qquad (13)$$

Here D_s is the coefficient of metal diffusion in a semiconductor; K is the semiconductor compression modulus; β is the linear expansion coefficient of semiconductor lattice; Ω is the difference of atomic volumes of impurity and matrix (it may be positive or negative); k is the Boltzmann constant; T is the temperature during the diffusion process.

Inside the layer of the substance covering a semiconductor, the diffusion process is assumed to obey Eq. (12), with $\vec{j}_m$ set by the following equation:

$$\vec{j}_m = -D_m\vec{\nabla} n, \qquad (14)$$

where D_m is the coefficient of metal diffusion in a composition from which atom metals diffuse into a semiconductor.

Equations (12) and (13) determine a strongly nonlinear diffusion process. In the one-dimensional (1D) case they may be written as

$$\frac{\partial}{\partial x}\left[(1 \pm U)\frac{\partial U}{\partial x}\right] = \frac{\partial U}{\partial t}, \qquad (15)$$

where $U = n/n_a$ and $n_a = \dfrac{kT}{K|\Omega\beta|}$. The sign in parentheses is "minus" if $\beta\Omega<0$ and "plus" if $\beta\Omega>0$. For instance, diffusion of Pt and Cr in GaAs is described by Eq. (16) with "minus" sign in parentheses.

In Eq. (15) t and x are the dimensionless time and coordinate, respectively. To obtain plots in dimensional units for a concrete

case, one should multiply the dimensionless time t (coordinate x) by a dimensional scale factor θ ($\sqrt{D_s\theta}$).

The 1D Eq. (15) determines the diffusion process in a semiconductor with flat surface coated with a composition containing a metal. To elucidate the features of the nonlinearity effect on diffusion process, let us determine the solution of Eq. (15) in the following three cases:

$$\frac{\partial^2 U}{\partial x^2} = \frac{\partial U}{\partial t}; \tag{16}$$

$$\frac{\partial}{\partial x}\left[(1-U)\frac{\partial U}{\partial x}\right] = \frac{\partial U}{\partial t} \tag{16a}$$

("pushing-off"),

$$\frac{\partial}{\partial x}\left[(1+U)\frac{\partial U}{\partial x}\right] = \frac{\partial U}{\partial t} \tag{16b}$$

("drawing-in").

It should be noted that the case (16a) ("pushing-off" of metal atoms out of semiconductor) is the most interesting, but, at the same time, the most difficult one when solving Eq. 16. The reason is that, if the concentration U becomes over unity at some point, then the factor (1 - U) at $\frac{\partial U}{\partial x}$ may become zero and reverse its sign. As a result, the numerical solution of Eq. (16a) becomes unstable. We tried to avoid such cases in our study and restricted ourselves by considering the situations with $U < 1$ only. This somewhat restricted applicability of the results obtained. However, the effect of "uphill" diffusion still can be demonstrated.

To study the "pushing-off" effect at $U > 1$, one should apply some additional physical mechanisms (that are actual for $U \geq 1$ in the case (16a)) and take them into account in the diffusion equation.

The solutions of 1D Eqs. (15) and $\frac{\partial}{\partial x}\frac{\partial U}{\partial x}=\frac{\partial U}{\partial t}$ are shown in Figs. 3.38 and 3.39 at different time intervals t after starting the diffusion process. The initial condition for solutions presented in Fig. 3.38 a, b, c is such that metal concentration in the $-10 < x < 0$ region is $U_0 = 0$, while in the $0 < x < 2$ region $U_0 = 0.98$. At the boundary points $x = -10$ and $x = 2$ the metal atoms flow is set zero. At the point $x = 0$ the metal atoms flow remains continuous.

Figure 3.38 a, b, c demonstrates that this process (described by Eqs. (16b) and $\frac{\partial}{\partial x}\frac{\partial U}{\partial x}=\frac{\partial U}{\partial t}$) occurs somewhat differently. One can see in Fig. 3.38b a “hindered” diffusion process in the case of “pushing-off” (16a) and “enhanced” diffusion process in the case of “drawing-in”. The same effect is shown more clearly in Fig. 3.39 a, b where solutions for three cases are given at the same moments ($t = 1$ and $t = 3$). As time grows, the distinctions between the solutions for three cases become more pronounced.

Figure 3.40 a, b demonstrates the “uphill” diffusion effect described by Eqs. (16a) and $\frac{\partial}{\partial x}\frac{\partial U}{\partial x}=\frac{\partial U}{\partial t}$. One can see from Fig. 3.40a that the initial (at $t = 0$) model concentration profile is $U = 0.98e^x$ for $-10 < x < 0$ and $U = 0.98$ for $0 < x \leq 2$. The diffusion process begins at $t = 0$, One can seen easily from Fig. 3.39b that the metal concentration decreases with t in the range from $x = 0$ to $x \approx$-1. At $x < -1$ the metal concentration increases with time, as would be expected.

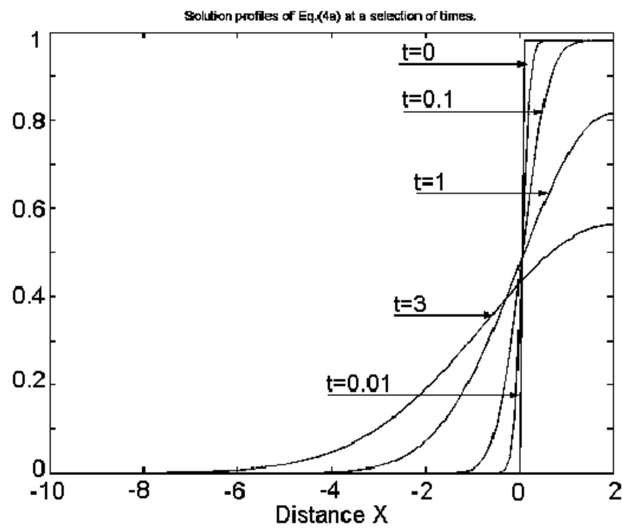

a)

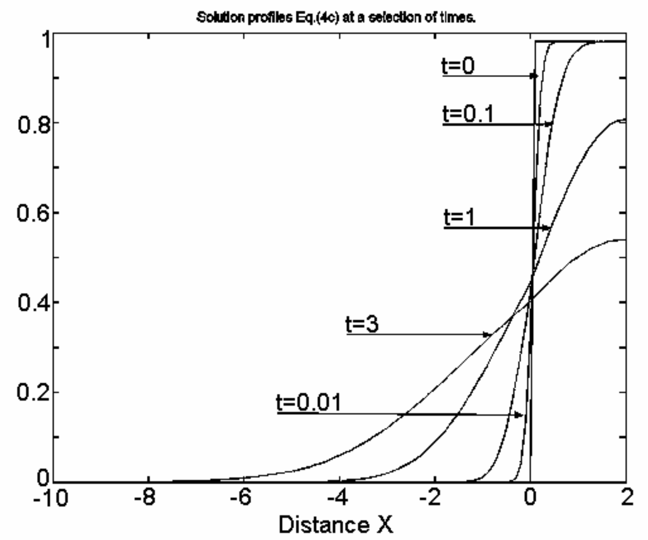

b)

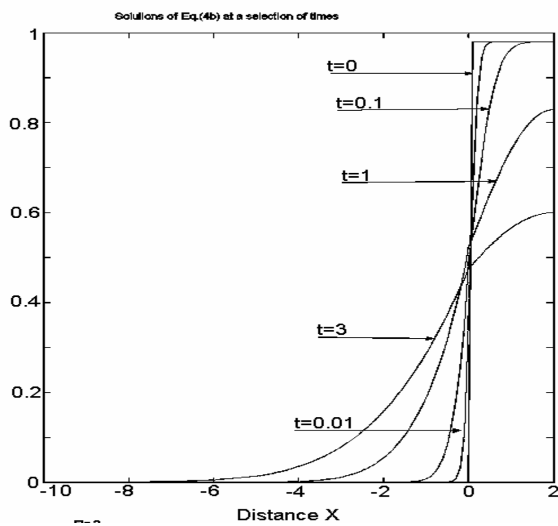

c)

Fig. 3.38. Evolution with time of the metal concentration depth profiles during diffusion from a metal layer into an "empty" semiconductor when diffusion obeys to Eq. 16 – a; 16a – b; 16b – c.

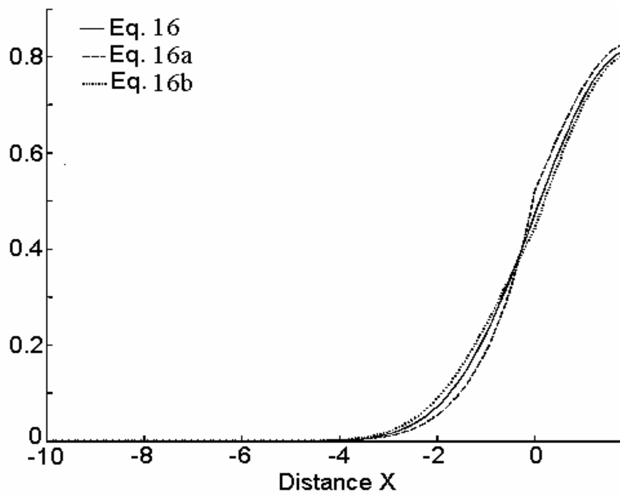

a)

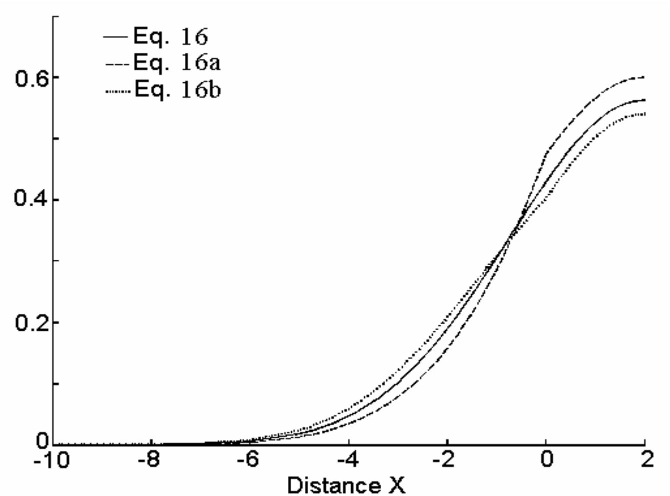

b)

Fig. 3.39. Spatial patterns of solutions of Eqs. (16)–(16b) at two points of time.

The same effect can be seen in Fig. 3.40b giving the solution of Eq. (16a) with a fixed boundary concentration $U_{x=0} = 0.98$ (this corresponds to a semiconductor contacting with the semi-infinite space $x > 0$ of a metal. In this case we assume (as earlier) that the initial metal concentration profile in a semiconductor at $x < 0$ is $U = 0.98e^x$.

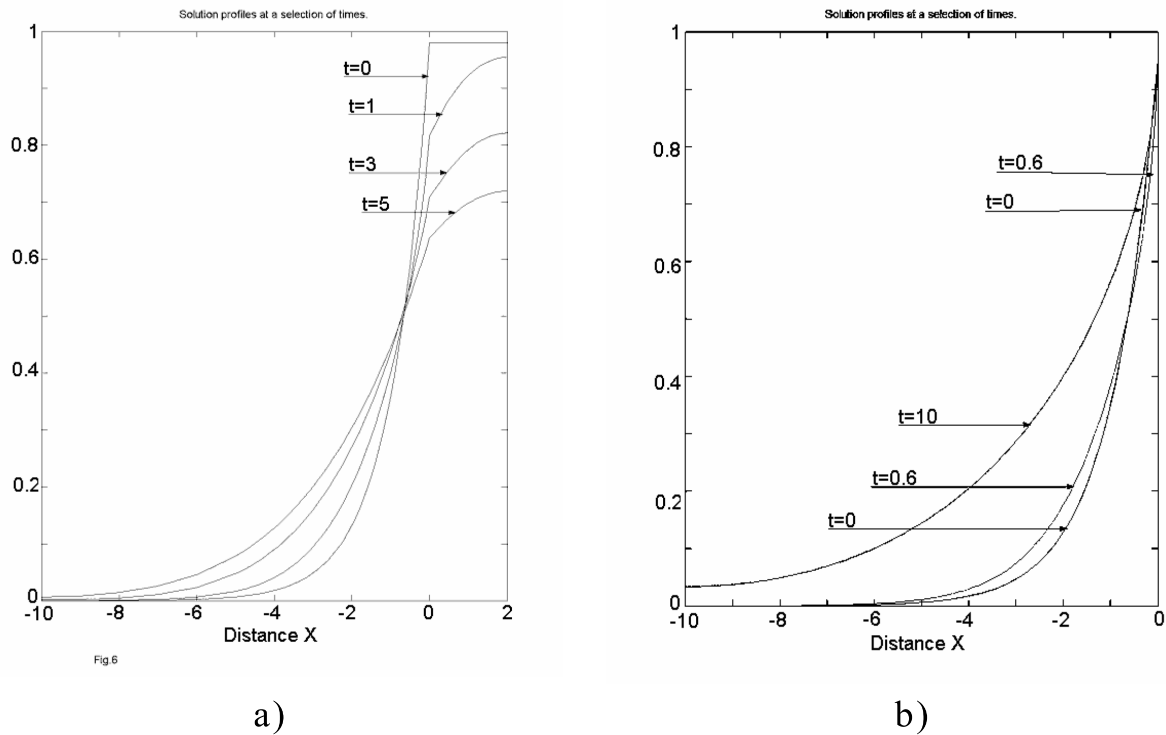

a) b)

Fig. 3.40. "Uphill" diffusion patterns for two different boundary conditions at semiconductor surface.

The actual metal–semiconductor interfaces are not flat; they have a relief formed by ridges and valleys. To get an impression of how metal is diffusing in a semiconductor in this case, it is insufficiently to solve 1D Eq. (12). An actual relief may be presented as a set of ridges of various shapes and heights (see Fig. 3.41 a, b).

To solve the problem in this case, let us assume that a semiconductor is in the shaded area; before diffusion starts, the metal concentration in a semiconductor is zero ($U = 0$). We assume that the metal–semiconductor interface is sawtooth, and the metal

atoms flow vanishes at the boundaries 1, 2 and 3 (Fig. 3.41a), i.e., the area considered is a section of an infinite sample.

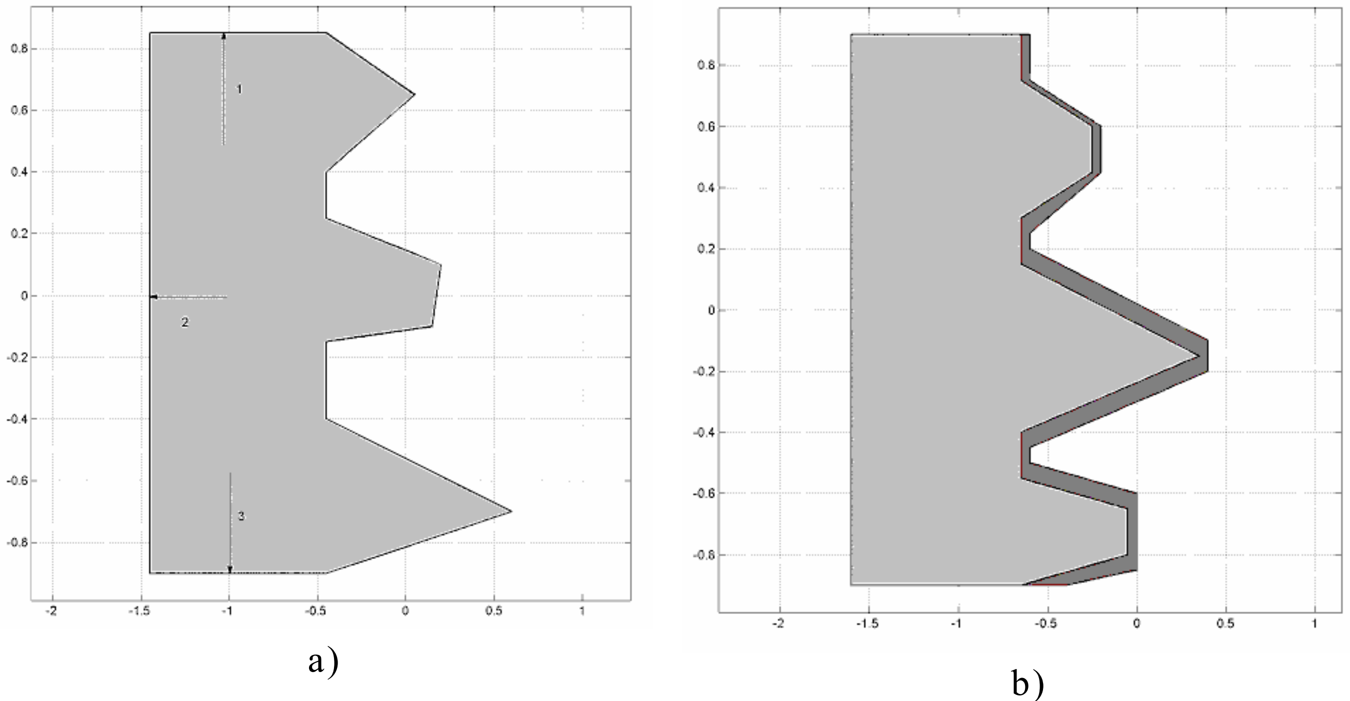

a) b)

Fig. 3.41. The semiconductor surface models considered by us when studying metal diffusion into a semiconductor with relief surface.

For the case presented in Fig. 3.41a we assume that the metal concentration at the sawtooth semiconductor surface remains constant (U = 0); this corresponds to the case of a semiconductor neighboring with semi-infinite space of metal. For the case presented in Fig. 3.41b we assume that a metal (the initial concentration U = 1) is in the dark region. For a semiconductor (light region) we assume that U = 0 at t = 0, and the metal atoms flow is zero at all the semiconductor boundaries.

At the first stage of our investigation we took into account neither the “draw-in” nor “pushing-off” effects and solved the linear problem. Shown in Figs. 3.42a, b is temporal dependence of diffusion for the case presented in Fig. 3.41a. One can see that at the first stage (small time values: t = 0.002; 0.005) the

equiconcentration profiles for metal somewhat resemble the semiconductor surface (Fig. 3.42).

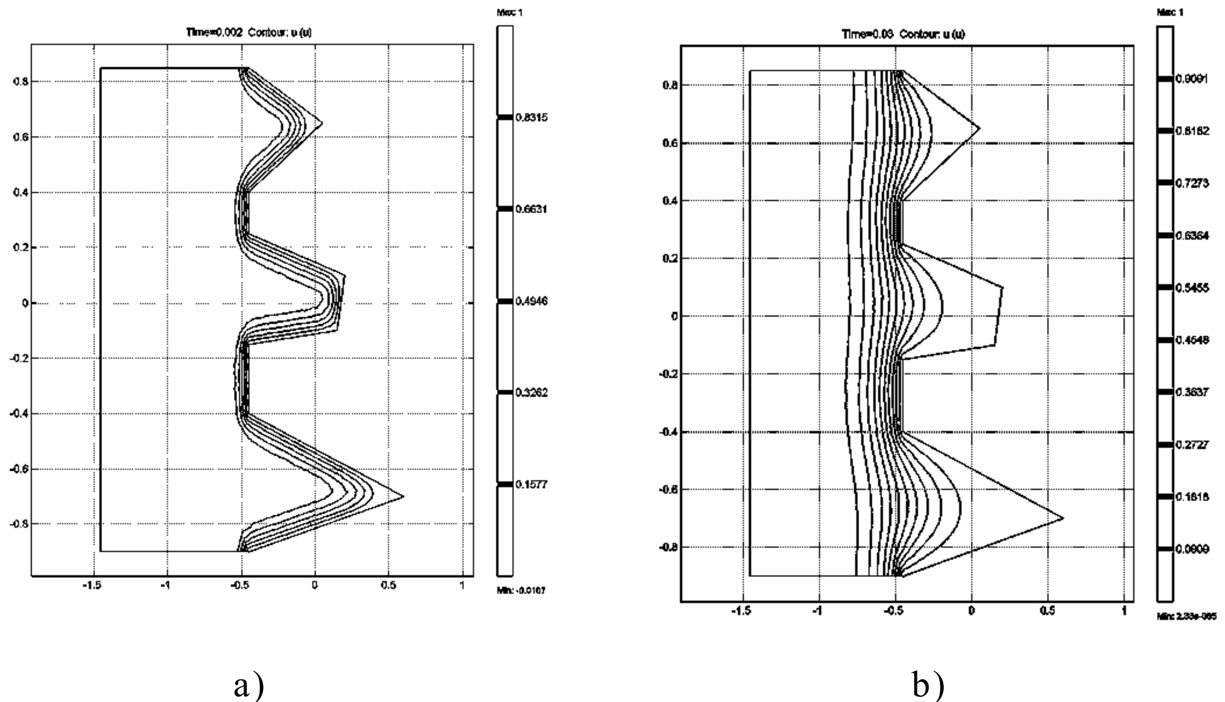

a) b)

Fig. 3.42. Time dependence of the contour curves for metal concentration in a semiconductor during diffusion (the metal concentration at the semiconductor boundary $U = 1$).

As time increases, the valleys of the semiconductor surface are filling with metal and the equiconcentration lines for metal become more smooth (see Fig. 3.42b for $t = 0.03$).

Figure 3.43a, b presents the process of metal diffusion into a semiconductor from a melt layer of finite volume deposited onto semiconductor. One can see that at small times (when the melt layer has not exhausted yet) the equiconcentration lines for metal follow, up to a point, the semiconductor surface form (Fig. 3.43). At big time values these lines become rather smooth and break. The valleys of different shapes and sizes are filled with metal in different ways (Fig. 3.43b).

Thus our investigation shows that, if the sample volume is doped (say, with acceptors whose concentration is n_a), then diffusion of donors from a melt to the semiconductor surface may result in appearance of *p-n* junctions of various shapes and areas,

depending on n_a, metal concentration in melt and duration of the diffusion process which depends strongly on the coefficient of metal diffusion in a semiconductor.

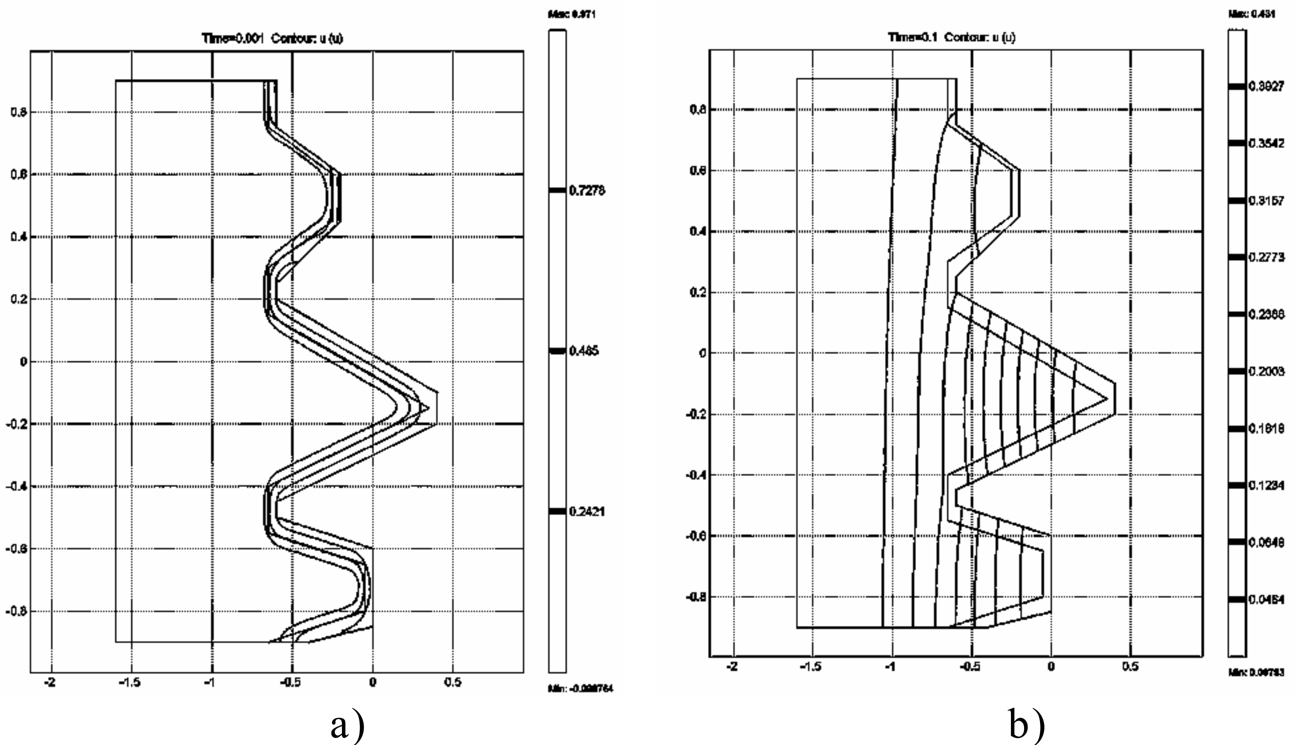

a) b)

Fig.3.43. As in Fig. 3.41 but for diffusion from a finite volume of a melt deposited on the semiconductor boundary (in a narrow layer of melt the metal concentration $U = 1$).

Figures 3.44a, b present temporal diffusion process for Zn in GaAs. The process was simulated taking the diffusion coefficient $D_s \approx 6 \cdot 10^{-12}$ cm^2/s (this value corresponds to a temperature of 800 ºC – see [31]). The unit of length in these figures is taken to be 10 μm. One can see that at $t \approx 28$ min. The metal concentration profiles follow rather well that of the surface (it will be recalled that $U = 1$ at the boundary). At $t \approx 140$ min. almost all the structure valleys are filled with metal (its concentration there is close to 1).

Figures 3.44c and 3.44d demonstrate the same situation but for $D_s = 6 \cdot 10^{-15}$ cm^2/s (this is closer to our experimental conditions).

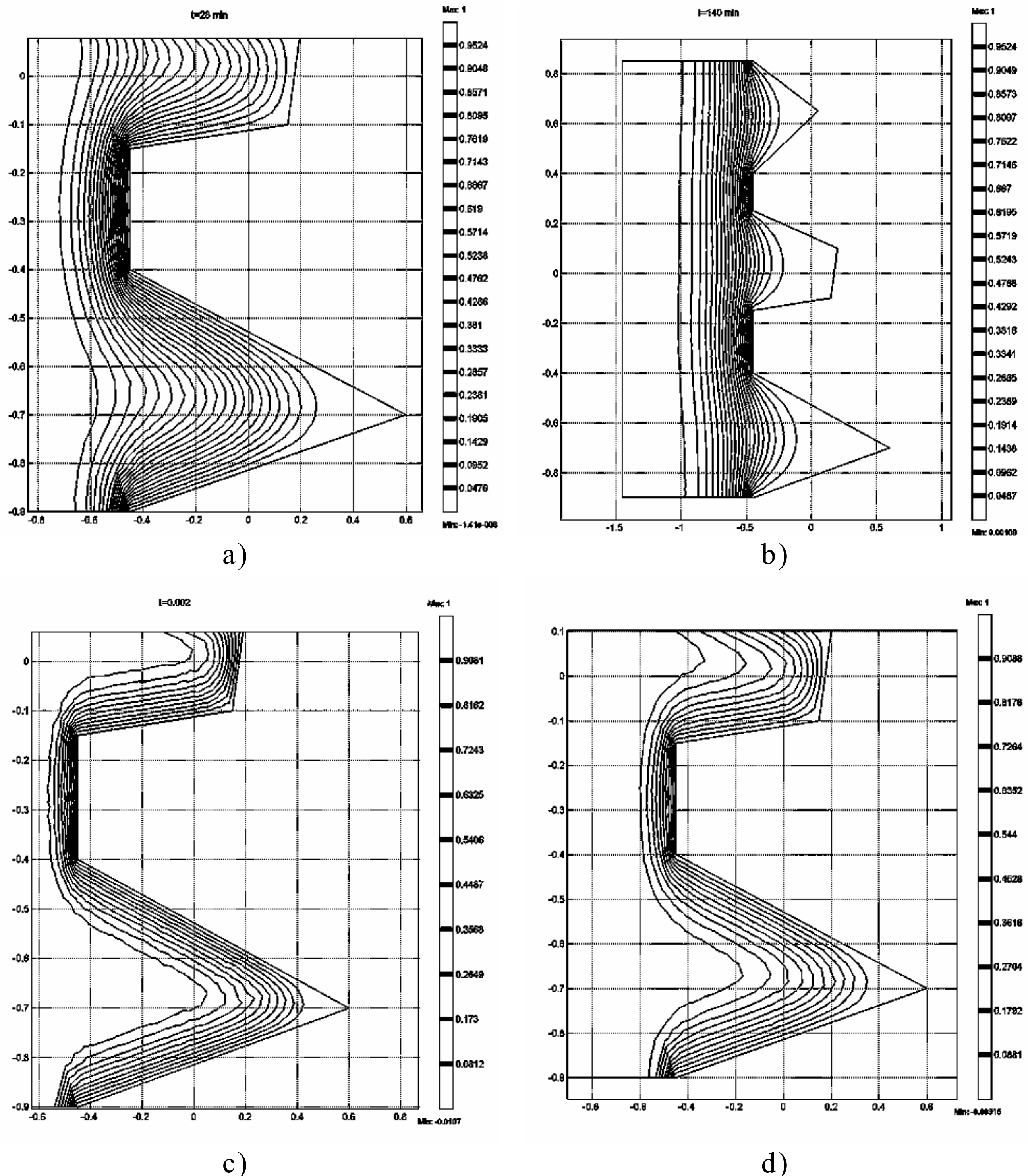

Fig. 3.44. As in Fig. 3.42 but for specified diffusion coefficients. a, b (unit of length is 10 μm) - D_s = $6 \cdot 10^{-12}$ cm/s. (this corresponds to Zn diffusion in GaAs at 800 °C); time of diffusion: a - 28 min., b - 240 min. c, d (unit of length is 1 μm) - D_s = $6 \cdot 10^{-15}$ cm^2/s; time of diffusion: c – about 1 h, d – about 2 h.

Figures 3.44c and 3.44d demonstrate the same situation but for D_s = $6 \cdot 10^{-15}$ cm^2/s (this is closer to our experimental conditions). (The unit of length, however, is 1 μm now.). Figure 3.44c

corresponds to process duration of about 1 hour, while Fig. 3.44d of about 2 hours. It is obvious that, since the diffusion coefficient is low, the diffusion process proceeds much slower. Therefore one may expect formation of a *p-n* junction whose form follows the semiconductor surface nonuniformities.

* *
*

The investigations described in this Chapter showed that:

- Textured GaAs surfaces are enriched with As. The enriched layer thickness is the smallest in the samples with dendrite-like surface morphology and the biggest in those with a quasi-grating. The results of local measurements of stoichiometry degree indicate that As atoms are located at microrelief ridges with higher probability than Ga atoms, while the latter are located mostly in the valleys. This fact determines local nonuniformity of the concentration of recombination centers.
- The resistivity of ohmic contacts obtained with sputtering in a vacuum is nonuniform over the wafer surface. The degree of this nonuniformity grows in the sequence "quasi-grating-like surface−flat surface−dendrite-like surface". This fact seems to result from nonuniform thickness of an oxide layer over the GaAs surface. The surface morphology features affect also the resistivity dependence on the contact area. This fact results from the effect of morphology on solder spreading due to distinctions in contact angles and spreading rates (the kinetic factor).
- The barrier characteristics of the Schottky diodes depend on surface morphology. This is especially true for reverse branches of I−V curves, due to increased both field strength and tunnel component of current. Besides, the tunnel-recombination, as well as the traditional generation-recombination, current components are observed in the case of relief metal−GaAs interfaces.

- Allowance for intrinsic stresses at simulation of diffusion processes in contacts results in diffusion enhancement or retardation, depending on the nature and sign of these stresses.

The above factors should be taken into account when designing PECs on textured semiconductor surfaces.

References

1. Wu O.R.T, Butler E.M. // J. Vac. Sci. Technol. 1982. v20. p.453.
2. Palmberg P.W.. Quantitative Auger analysis of solid surfaces by Auger electron spectroscopy. Ann. Chem. 1973. v.45, p.549A
3. Zaporozhchenko V.I. // Elektronnaya Promyshlennost’ 1978. N11-12. p.36 (in Russian).
4. Lifshits V.G. Electron Spectroscopy and Atomic Processes at Silicon Surface. Nauka, Moscow, 1985. (in Russian).
5. Il'in A.M. // Zurn. Tekhn. Fiz. 1994. v.64. N10. p.188.
6. Briggs P., Seah M.P. Practical Surface Analysis by Auger and X-ray Photoelectron Spectroscopy. Wiley, Chichester 1983. p.600.
7. Gorelich V.A. // Elektronnaya Promyshlennost'. 1978. N11(71)-12(72), p.47
8. Evans S., Pritchard R.G, Thomas J.M. // J.Phys. C. 1977. v.10, p.2433.
9. Sotnikov V.M. // Poverkhnost’ 1987. N 11. p.30 (in Russian).
10. Sotnikov V.M. // Poverkhnost’ 1989. N 8. p.45 (in Russian).
11. Kosiha R., Eoke G., Breza J., Liday J. / In: Proc. ASDAM-2002. Smolenice Castle. Slovakia. 14-16 Oct. 2002. p.203.
12. Moss T.S., Burrell G.J., Ellis B. Semiconductor Opto-Electronics, Butterworth & Co. (Publishers) Ltd, 1973.
13. Ivanova V.S., Balankin A.S., Bunin I.G., Oksogoev A.A. Synergetics and Fractals in Materials Science. Nauka: Moscow. 1994 (in Russian).
14. Rideut V.L. Solid State Electron. 1975. v.18. p.541.
15. Strikha V.I., Buzaneva E.V. // Poluprov. Tekhnika i Mikroelektronika. 1975. N.20. p.20 (in Russian).
16. Rhoderick E.H. Metal−semiconductor Contacts. Clarendon Press. Oxford. 1978.
17. Feldman C., Mayer J.W. Fundamentals of Surface and Thin Film Analysis. North-Holland. New York−Amsterdam−London. 1986.

18. Thin Films. Interdiffusion and Reactions. Eds. J.M. Poate, K.N. Tu, W. Mayer. Wiley. 1978.

19. Kwork S.P. // J. Vac. Sci. Technol. 1986. v.B4. p.1383.

20. Cheuag N.W., Grunthaner P.J., Grunthaner F.J., Mayer J.W., Ulrich B.M. // J. Vac. Sci. Technol. 1981. v.B4. N18. p.917.

21. Gyulai J., Mager J.W., Rodriguez V., Yu A. Y.C., Gopen H.J. // J. Appl. Phys. 1971. v.42. p.3278.

22. Khuan T.S. Batson P.E., Jackson T.N., Ruprecht H., Wilkie E.L. // J. Appl. Phys. 1983. v.54. p.6952.

23. Gol'dberg Yu.A. // Fiz. Tekhn. Poluprov. 1994. v.28. p.1681 (in Russian).

24. Zimon A.D. Adhesion of Films and Coatings. Sov. Radio: Moscow. 1977 (in Russian).

25. Borkovskaya O.Yu., Gorbach T.Ya., Dmitruk N.L. // Fiz. Tekhn. Poluprov. 1989. v.23. N12. p.2113 (in Russian).

26. Borkovskaya O.Yu., Gorbach T.Ya., Dmitruk N.L. // Pis'ma v ZhTF. 1981. v.17. N23. p.18 (in Russian).

27. Strikha V.I. Contact Effects in Semiconductors. Vyscha Shkola: Kiev. 1982 (in Russian).

28. Vyatkin A.P. The formation mechanism, structure and properties of gallium arsenide contacts with metals. / In: Gallium Arsenide. Tomsk Univ. Publ: Tomsk. 1969. p.169. (in Russian).

29. Venger E.F., Konakova R.V., Korotchenkov G.S., Milenin V.V., Russu E.V., Prokopenko I.V. Interactions between Phases and Degradation Mechanisms in Metal–InP and Metal–GaAs Structures. Information-Editing Dept. of the Inst. of Semiconductor Physics of the Natl. Acad. of Sci. of Ukraine: Kiev. 1999 (in Russian).

30. Venger E.F., Grendel M., Daniska V., Konakova R.V., Prokopenko I.V., Tkhorik Yu.A., Khazan L.S. Structural Relaxation in Semiconductor Crystals and Device Structures. Phoenix: Kiev. 1994 (in Russian).

Chapter IV

THE FEATURES OF PHOTOCONVERSION IN SOLAR CELLS MADE ON THE BASIS OF TEXTURED THIN-FILM $Al_xGa_{1-x}As$–GaAs HETEROSTRUCTURE

It is known that increase of photoconversion efficiency in semiconductor solar cells (SCs) is achieved, to a great extent, by reduction of optical losses related to light reflection and incomplete absorption in SCs made on the basis of indirect-gap semiconductors. Thus far the problem of minimization of these losses has been radically solved for silicon SCs by formation of a regular or irregular relief at their surfaces. Due to multiple light reflections, solar radiation is practically completely collected and absorbed in the SC base.

Another situation exists in gallium arsenide direct-gap SCs. Due to high absorption coefficient and small charge carrier diffusion length, photocurrent and photovoltage are formed at distances of several microns. To optimize technological procedures in this case, one has to clearly understand physics of these processes in textured GaAs-based structures. This concerns calculation of the features of optical losses reduction due to surface microrelief, as well as some photoconversion peculiarities resulting from an actual mechanism for current flow in wide-window heterostructures.

Following are the results of our investigations dealt with the above problems.

4.1. OPTICAL LOSSES IN THE TEXTURED $Al_xGa_{1-x}As$–GaAs HETEROSYSTEM

We calculated the optical losses due to light reflection in the $Al_xGa_{1-x}As$–GaAs heterosystem with surface relief. At that we

optimized the $Al_xGa_{1-x}As$ film thickness, taking into account an antireflection SiO_2 layer on this film. A combination of microrelief with an antireflection coating is known to result in bigger reduction of light reflection than that provided by a three- or four-layer antireflection coating [1].

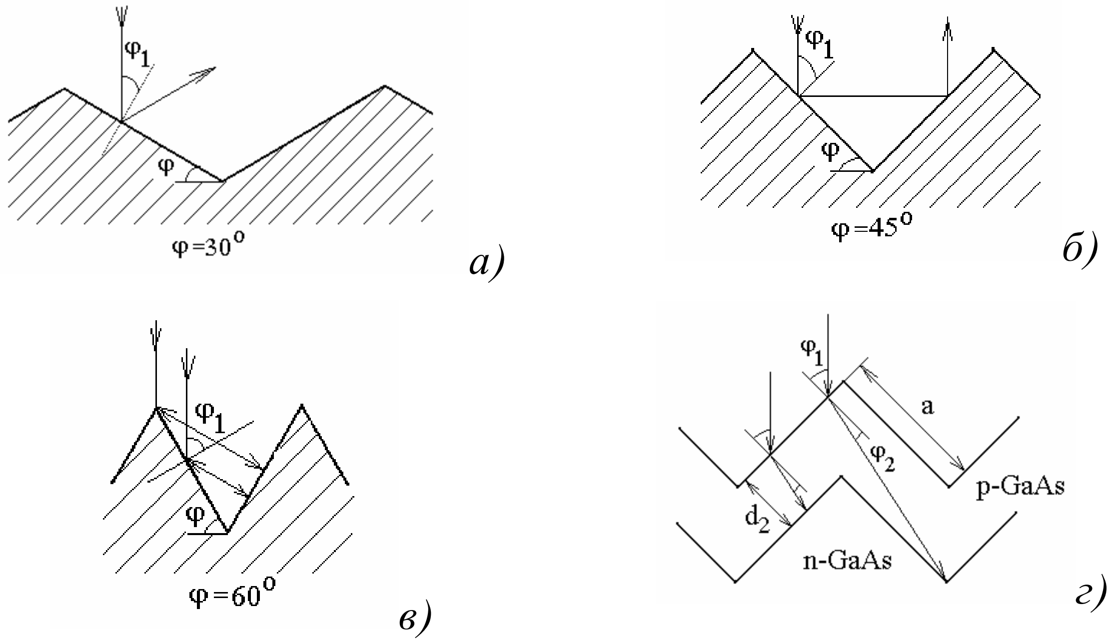

Fig. 4.1. Some versions of surface relief and geometry of the $Al_xGa_{1-x}As$–p-GaAs–n-GaAs heterostructures (a, b, c) and light beam path in p-GaAs (d).

According to [2], one can write down the short-circuit current density for the $Al_xGa_{1-x}As$–GaAs heterosystem as

$$J_{SC} = \frac{1}{A}\sum_{i=1}^{k} J_{SCi}(\lambda)\cdot A_i, \tag{1}$$

where $A = \sum_{i=1}^{k} A_i$ is the total heterosystem area, λ is the light wavelength and J_{SCi} is the short-circuit current density for microrelief regions of different slopes:

$$J_{SCi} = \frac{q}{hc}\int_0^{hc/E_g} f(\lambda)[1 - R_i(\lambda)]E_\lambda(\lambda)\lambda d\lambda. \tag{2}$$

Here E_g is the GaAs gap; $f(\lambda)$ is the coefficient of charge carrier collection from the $Al_xGa_{1-x}As$ layer and p- and n-GaAs

layers; $E_\lambda(\lambda)$ is the spectral density of photon flux in the AM0 solar spectrum; $R(\lambda)$ is the spectral dependence of reflection coefficient (that takes into account presence of relief and antireflection layers).

Our model for a regular microrelief was a set of V-like grooves with a changeable base angle φ. The reflection coefficient was calculated using the ray optics approximation ($\lambda << \delta$, where δ is a characteristic period of the relief). It should be noted that if the base angle is ≤ 30°, then only single reflection is possible; at 30°≤φ≤45° some light beams experience single reflection, while other experience double reflection; and when 45°≤φ≤60°, then some light beams experience double reflection, while other are reflected three times. Some geometry versions for the $Al_xGa_{1-x}As$–GaAs heterostructure with a regular relief are shown in Fig. 4.1.

Spectral coefficients $R_s(\lambda,\varphi_1)$ and $R_p(\lambda,\varphi_1)$ of single reflection for s- and p-polarized light (φ_1 is the angle of beam incidence onto the interface) for the $Al_xGa_{1-x}As$–GaAs heterostructure were calculated using Berning's approach [3]. The thickness of $Al_xGa_{1-x}As$ film was d_1, while that of antireflection SiO_2 film was d_0.

Shown in Figs. 4.2 and 4.3 is $R(\lambda,\varphi_1) = ½[R_s(\lambda,\varphi_1)+R_p(\lambda,\varphi_1)]$ as function of the $Al_xGa_{1-x}As$ film thickness d_1 (see inset in Fig. 4.2) and of wavelength λ (Figs. 4.2 and 4.3). One can see from the inset in Fig. 4.2 that the $R(\lambda,\pi/4)$ curves oscillate as d_1 grows. The curve minima approximately correspond to the odd d_1 values, (2n + 1)×0.05 μm (here n is an integer: n = 0, 1, 2...). Shown in Fig. 4.2 are the above spectral dependencies of reflection coefficients at various values of d_0 and d_1. One can see that these curves have three minima and two peaks in the spectral range considered.

By varying d_0 and d_1 values, one can vary both positions and values of the above extrema. And, as can be seen from Fig. 4.3, at big values (≥ 50°) of the angle of incidence φ_1 the spectral

reflection coefficients begin to substantially grow with the angle φ_1.

Our calculations have shown that optimal thickness values were ≈0.11 μm for the SiO_2 film and ≈0.030 μm for the $Al_xGa_{1-x}As$ film with x = 0.7.

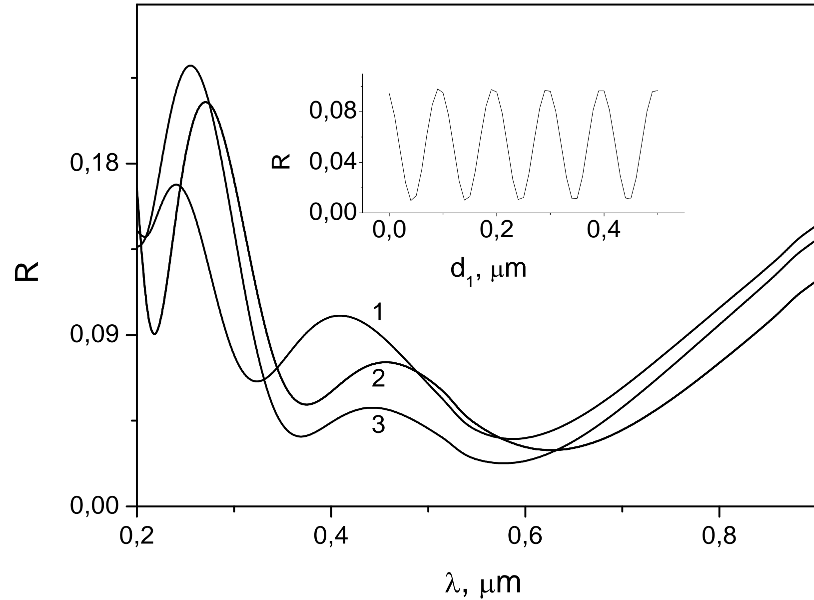

Fig. 4.2. Spectral dependencies of the reflection coefficient R for the $Al_xGa_{1-x}As$–p-GaAs–n-GaAs heterostructure with an antireflection SiO_2 coating at various thicknesses d_1 and d_2. d_0, d_1, μm: 1 - 0.11, 0.025; 2 – 0.12, 0.03; 3 - 0.11, 0.03.

For a regular relief formed by V-like grooves with base angle of 45° light beams experience double reflection. All relief areas contribute equally into the short-circuit current, and the resulting coefficient of specular reflection from heterosystem (averaged over the AM0 solar radiation spectrum) can be presented as:

$$\overline{R} = \frac{1}{2}\int_0^{hc/E_g} \frac{(R_s^2(\lambda,\pi/4)+R_p^2(\lambda,\pi/4))d\lambda}{\lambda^4\left[\exp\left(\frac{2.482}{\lambda}\right)-1\right]} \Big/ \int_0^{hc/E_g} \frac{d\lambda}{\lambda^4\left[\exp\left(\frac{2.482}{\lambda}\right)-1\right]}, \qquad (3)$$

where $R_s(\lambda,\pi/4)$ and $R_p(\lambda,\pi/4)$ are the spectral coefficients of single reflection for s- and p-polarization, respectively, when light beam are incident onto microfaces at an angle of 45°. Expression (3) is written down in the approximation when the solar radiation

spectrum is approximated by that of a blackbody whose temperature is 5800 K; λ is measured in μm.

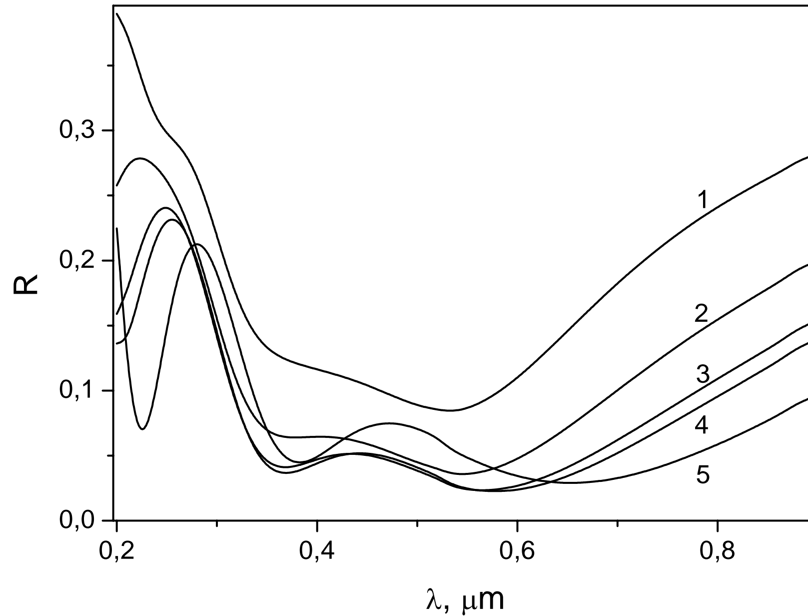

Fig. 4.3. As in Fig. 4.2, but at various angles of light incidence. d_0 = 0.11, d_1 = 0.03 μm: φ, º: 1 – 70, 2 – 60, 3 – 50, 4 – 45, 5 – 2.

Our calculations have shown that $\overline{R}\approx$0.6% if light absorption in GaAs is taken into account. From this result one can see that combination of relief with an antireflection SiO_2 layer really makes it possible to essentially reduce $\overline{R}$ down to those values which (in the case of a flat interface between silicon structures) could be achieved only by using five-layer antireflection coatings [1].

For a regular relief formed by V-like grooves with base angle of 60º we have triple reflection: the reflection angles are 60º (twice), and once the reflected beam is normal to the relief. The resulting coefficient of light reflection from the heterosystem (averaged over the AM0 solar radiation spectrum) may be written down, in the ray optics approximation, as:

$$\overline{R}=\frac{1}{2}\int_{0}^{hc/E_g}\frac{(R_s^2(\lambda,\pi/3)R_s(\lambda,0)+R_p^2(\lambda,\pi/3)R_p(\lambda,0))d\lambda}{\lambda^4\left[\exp\left(\frac{2.482}{\lambda}\right)-1\right]}$$

$$\left(\int_0^{hc/E_g} \frac{d\lambda}{\lambda^4 \left[\exp\left(\frac{2.482}{\lambda} \right) - 1 \right]} \right)^{-1} \quad (4)$$

Here $R_s(\lambda,\pi/3)$ and $R_s(\lambda,0)$ ($R_p(\lambda,\pi/3)$ and $R_p(\lambda,0)$) are the spectral coefficients of single reflection for s- (p-) polarization when light beam is incident onto the $Al_xGa_{1-x}As$–GaAs surface relief at an angle of 60º. In this case the optimized thickness d_1 is ≈0.030 μm; $\overline{R}$ is about 0.1% with allowance made for light absorption in GaAs. Other reflection minima occur at d_1≈0.090 μm ($\overline{R}$≈0.4%) and d_1≈0.17 μm ($\overline{R}$≈0.25%). One can see from the above results that at triple reflection (occurring at φ_1 = 60º) and with an antireflection coating the problem of integral reflection coefficient minimization for the $Al_xGa_{1-x}As$–GaAs system can be radically solved, even at several values of the $Al_xGa_{1-x}As$ film thickness.

4.2. PHYSICAL MECHANISMS FOR PHOTOCURRENT FORMATION IN HETEROJUNCTIONS WITH RELIEF SURFACES

We have performed a theoretical analysis of the effect of surface relief in $Al_xGa_{1-x}As$–GaAs heterosystem on the coefficient of light reflection and photocurrent under AM0 conditions. Two limiting cases of relief period were considered. In one case calculations were made in the ray optics approximation, i.e., the smallest geometrical size in the problem was light wavelength λ. In another case the reverse inequality was taken to be valid, and calculations were performed in the effective-medium approximation (Bruggeman model). In addition, we took into account presence of an antireflecting SiO_2 film and antireflecting action of a wide-gap $Al_xGa_{1-x}As$ “window”, as well as dispersion of the optical parameters of GaAs and $Al_xGa_{1-x}As$.

According to our previous results [2], quasi-periodic relief is most promising for solar cells (SCs). Therefore we considered, in the first case, a regular relief formed by V-grooves with the base

angle φ = 45°. With allowance made for antireflecting action of SiO_2 and $Al_xGa_{1-x}As$ films, the averaged coefficient of light reflection becomes less than 1%. The spectral reflection coefficient $R(\lambda)$ in this case is $\frac{1}{2}\left[R_s^2(\lambda,\pi/4)+R_p^2(\lambda,\pi/4)\right]$. $Al_xGa_{1-x}As$ film serves as a wide-gap "window" that can be used for abrupt decrease of the surface recombination effect. In addition, this film can serve as an antireflection coating.

We calculated short-circuit current for the geometry of $Al_xGa_{1-x}As$–p-GaAs–n-GaAs heterosystem shown in Fig. 4.1. One can see that in this case light beams propagate at an angle, and in an actual situation (when relief length and height, as well as p-GaAs layer thickness, are comparable to each other) some beams hit "neighboring" relief. As a result, those beams in p-GaAs layer (whose thickness is d_2) that hit their "own" relief travel a distance $d_2/\cos\varphi_2(\lambda)$ ($\varphi_2(\lambda)$ is the refraction angle in GaAs), while other beams travel a distance $(a + d_2)/\cos\varphi_2(\lambda)$ (a is the relief side length). The ratio between the areas for beams of the first and second kind is $[a - d_2(1 - \tan\varphi_2(\lambda))]/d_2[1 - \tan\varphi_2(\lambda)]$.

To take into account corresponding travel distance increase for light beams in a structure with relief, one may introduce the effective light absorption coefficients

$$\alpha_1(\lambda)=\alpha(\lambda)/\cos\varphi_2(\lambda)\,;\;\; \alpha_2(\lambda)=\alpha(\lambda)(a+d_2)/d_2\cos\varphi_2(\lambda)\,. \qquad (5)$$

for beams of the "first" and "second" type, respectively.

When calculating short-circuit current under AM0 conditions, we applied the Howell's approach (see [4]). Taking into account the above considerations and approximating solar radiation with that of a blackbody whose temperature is 5800 K, one can obtain the following expression for the short-circuit current density (measured in A/cm^2) in $Al_xGa_{1-x}As$–p-GaAs–n-GaAs structure:

$$J_{SC} = 0.9973\cdot(1-m)\left\{1-\frac{d_2}{a}\left[1-\tan\varphi_2(\lambda)\right]\right\}\int_0^1 \frac{\left[1-R(\lambda)\right]f(\alpha_1,\beta_1)}{z^4\left[\exp\left(\frac{2.863}{z}\right)-1\right]}dz +$$

$$0.9973\cdot(1-m)\frac{d_2}{a}\left[1-\tan\varphi_2(\lambda)\right]\int_0^1 \frac{\left[1-R(\lambda)\right]f(\alpha_2,\beta_1)}{z^4\left[\exp\left(\frac{2.863}{z}\right)-1\right]}dz\,, \quad (6)$$

Here m is the relative area shaded by contacts at the illuminated surface; $z=\lambda/\lambda_m$, $\lambda_m=$ 0.867 μm is the intrinsic photoeffect threshold for GaAs; $f(\alpha,\beta)$ is the coefficient of charge carriers collection from $Al_xGa_{1-x}As$ layer, p- and n-GaAs layers and space-charge region (SCR); β is the absorption coefficient for $Al_xGa_{1-x}As$ layer, $\beta_1=\beta/\cos(13.6^o)$ is the averaged effective coefficient of light absorption in $Al_xGa_{1-x}As$ layer with allowance made for relief.

According to the above, the collection coefficient is

$$f(\alpha,\beta)= f_n(\alpha,\beta) + f_{sc}(\alpha,\beta) + f_p(\alpha,\beta)\,, \quad (7)$$

where $f_n(\alpha,\beta)$ is the coefficient of charge carrier collection from p-GaAs and $Al_xGa_{1-x}As$ layers; $f_{sc}(\alpha,\beta)$ is that from SCR; $f_p(\alpha,\beta)$ is the coefficient of holes collection from n-GaAs layer. Following are the expressions for these coefficients when the n-GaAs layer thickness is much over the hole diffusion length L_p:

$$\begin{aligned} f_n(\alpha,\beta_1) = {} & \frac{\exp(-\beta_1 d_1)\alpha L_n}{(\alpha L_n)^2-1}(\alpha L_n + S_n\frac{\tau_n}{L_n}(1-\exp(-\alpha d_2)\cosh\frac{d_2}{L_n}) - \exp(-\alpha d_2)\times \\ & \sinh\frac{d_2}{L_n} - \exp(-\alpha d_2)(S_n\frac{\tau_n}{L_n}\sinh\frac{d_2}{L_n}+\cosh\frac{d_2}{L_n}))((S_n\frac{\tau_n}{L_n}\sinh\frac{d_2}{L_n}+\cosh\frac{d_2}{L_n})^{-1} + \\ & \frac{\beta_1 L_a}{(\beta_1 L_a)^2-1}(\beta_1 L_a + S_a\frac{\tau_a}{L_a}(1-\exp(-\beta_1 d_1)\cosh\frac{d_1}{L_a}) - \exp(-\beta_1 d_1)\sinh\frac{d_1}{L_a} - \\ & \beta L_a\exp(-\beta_1 d_1)\left(S_a\frac{\tau_a}{L_a}\sinh\frac{d_1}{L_a}+\cosh\frac{d_1}{L_a}\right))(S_n\frac{\tau_n}{L_n}\sinh\frac{d_2}{L_n}+\cosh\frac{d_2}{L_n})^{-1}\times \\ & (S_a\frac{\tau_a}{L_a}\sinh\frac{d_1}{L_a}+\cosh\frac{d_1}{L_a})^{-1}, \end{aligned} \quad (8)$$

$$f_{sc}(\alpha,\beta_1) = \exp(-\beta_1 d_1)\exp(-\alpha d_2)\left[1-\exp(-\alpha w)\right], \qquad (9)$$

$$f_p(\alpha,\beta_1) = \exp(-\beta_1 d_1)\exp(-\alpha(d_2+w))\frac{\alpha L_p}{1+\alpha L_p}. \qquad (10)$$

Here L_n and L_a (τ_n and τ_a) are the Shockley-Read-Hall diffusion lengths (lifetimes) of minority charge carriers in p-GaAs and $Al_xGa_{1-x}As$ layers, respectively; d_1(w) is the $Al_xGa_{1-x}As$ layer (SCR) thickness; S_n and S_a are the surface recombination velocities at the $Al_xGa_{1-x}As$–p-GaAs interface and $Al_xGa_{1-x}As$ surface, respectively. The quantity α in expressions (8)–(11) takes the values α_1 and α_2 determined by expression (5).

When performing numerical calculations, we used the following expressions for L_n and L_p (that take into account also radiative and Auger recombination in GaAs) [5]:

$$L_n = \sqrt{D_n\left(\frac{1}{\tau_n} + A_i p_p + C_p p_p^2\right)^{-1}}, \qquad L_p = \sqrt{D_p\left(\frac{1}{\tau_p} + A_i n_n + C_n n_n^2\right)^{-1}} \qquad (11)$$

Here D_n (D_p) is the electron (hole) diffusion coefficient for p- (n-) GaAs layer; p_p and n_n are the majority charge carrier concentrations in these layers; $A_i = 2\cdot10^{-10}$ cm^3 s^{-1} is the constant of interband radiative recombination in GaAs; $C_n = 1.6\cdot10^{-29}$ cm$^6\cdot$s^{-1} ($C_p = 4.6\cdot10^{-31}$ cm$^6\cdot$s^{-1}) is the electron (hole) interband Auger recombination in GaAs [5].

To apply expressions (6)–(10) in the case of a flat $Al_xGa_{1-x}As$–p-GaAs–n-GaAs interface, one should take into account that now the spectral reflection coefficient $R^*(\lambda)$ is $1/2\left[R_s(\lambda,0)+R_p(\lambda,0)\right]$, $\alpha_1 = \alpha_2 = \alpha$, $\beta_1 = \beta$, $\cos\varphi_1(\lambda)=1$, and $\tan\varphi_1(\lambda)=0$.

Shown in Figs. 4.4 and 4.5 are the short-circuit current density J_{SC} in $Al_xGa_{1-x}As$–p-GaAs–n-GaAs structure versus p-GaAs layer thickness d_2 and ratio between d_2 and relief side a curves. A comparison is made between the J_{SC} values with and without relief.

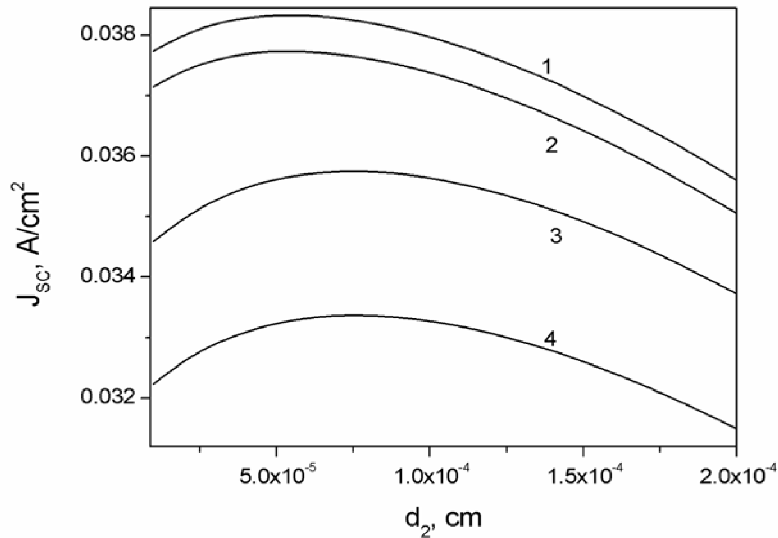

Fig. 4.4. Short-circuit current density in $Al_xGa_{1-x}As$–p-GaAs–n-GaAs heterostructure as function of the p-GaAs layer thickness d_2. d_1 (μm): 1 -$3\cdot10^{-2}$, b =1; 2 - $3\cdot10^{-2}$, b = 0; 3 - 10^{-1}, b = 1; 4 -$\cdot10^{-1}$, b = 0.

One can see that the short-circuit current density in the presence of a relief is always over that without it. The J_{SC} versus the p-GaAs layer thickness d_2 curve is non-monotone. It peaks at $d_2 \approx 0.5$ μm when there is a relief, and at $d_2 \approx 0.7$ μm without it. One can see from Fig.4.5 that the short-circuit current density increases with ratio $b = d_2/a$. This is due to growth of the photon path in p-GaAs layer. If $d_2 = 0.5$ μm and b = 1, this growth is as big as 2.7%. And the total increase of the short-circuit current in structures with relief surfaces is about 7% as compared to that in structures with flat surfaces. This is related to the total growth of the short-circuit current in structures with relief, due to both the above factor and decrease of the spectral reflection coefficient (with allowance made for double reflection of light).

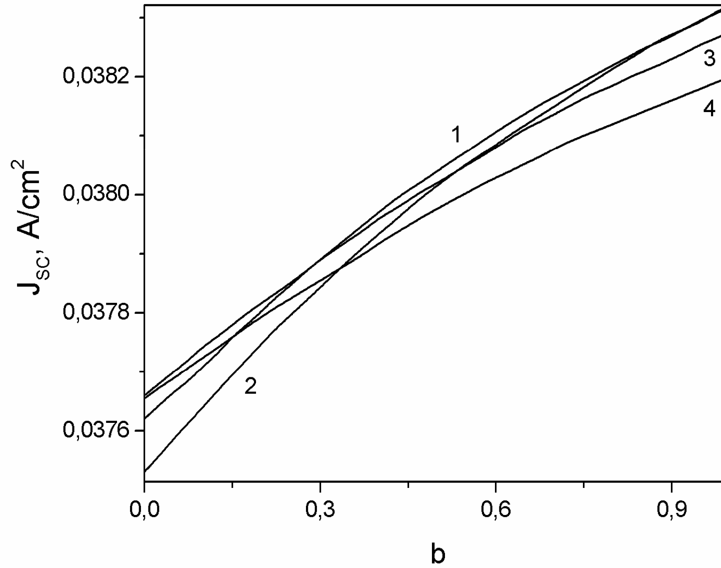

Fig. 4.5. Short-circuit current density in $Al_xGa_{1-x}As$–p-GaAs–n-GaAs heterostructure as function of the ratio b = d_2/a. d_2, μm: 1 - $5\cdot10^{-5}$, 2 - $6\cdot10^{-5}$, 3 - $7\cdot10^{-5}$, 4 - $8\cdot10^{-5}$.

In our calculations we used the following parameter values (taken from [5-10]): $\tau_n = 10^{-8}$ s, $\tau_p = 2\cdot10^{-8}$ s, $\tau_a = 10^{-9}$ s, $L_a = 10^{-4}$ cm, $D_n = 64.5$ cm^2 s^{-1}, $D_p = 6.45$ cm^2 s^{-1}, $S_n = 10^3$ cm/s, and $S_a = 5\cdot10^4$ cm/s. All calculations were made for x = 0.7. It should be noted that at the above parameter values the contributions into the total short-circuit current from $Al_xGa_{1-x}As$ film, p-GaAs layer, SCR and n-GaAs layer are 3.6; 79; 3.4 and 14%, respectively.

Using the results obtained in [11], we also calculated the short-circuit current in $Al_xGa_{1-x}As$–p-GaAs–n-GaAs system as function of the mean-square nanorelief size δ of $Al_xGa_{1-x}As$ surface. It was shown, in particular, that at δ = 10 nm the short-circuit current is over that in the structure without nanorelief by about 2%.

We performed computer simulation of photocurrent also for the widespread case when only part of a surface has relief. The dependence of short-circuit current density on the fraction of relief surface is presented in Fig. 4.6. It should be noted that this is just the case when agreement with the experimental data is achieved.

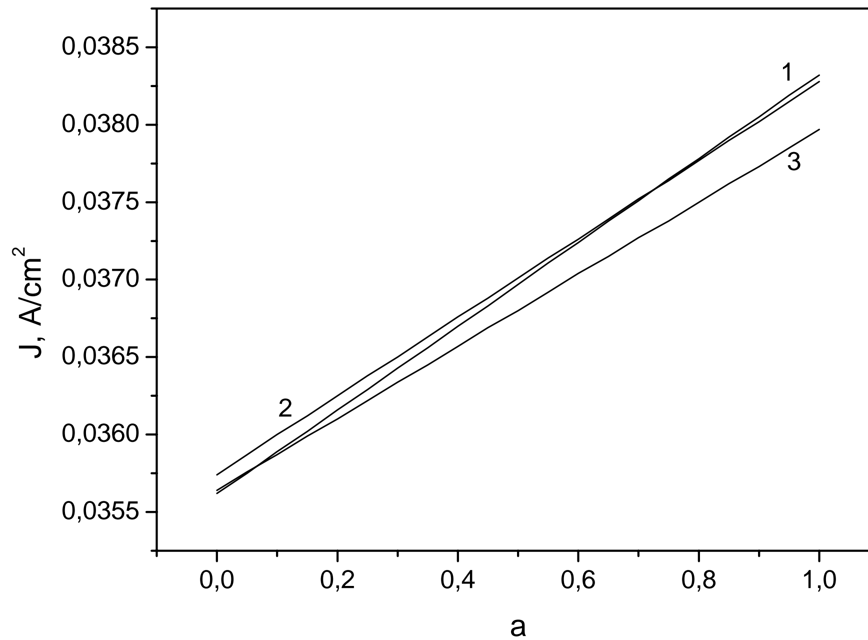

Fig.4.6. Short-circuit current density in SiO_2–$Al_xGa_{1-x}As$–p-GaAs–n-GaAs-based SC as function of the relief surface fraction at variation of the p-GaAs layer thickness: $d_2 = 5\cdot10^{-5}$ (1), $7\cdot10^{-5}$ (2) and 10^{-4} cm (3).

In another limiting case (the period of relief on $Al_xGa_{1-x}As$ surface is much less than the wavelength of incident light) a relief or porous layer formed on the illuminated $Al_xGa_{1-x}As$ surface may serve as antireflecting layer. Indeed, if the characteristic sizes of a relief are less than the wavelength of the incident light, then the relief effect can be simulated within the effective-medium approximation, as was done, say, in [12]. In our case such medium involves two components (phases): $Al_xGa_{1-x}As$ (relief ridges) and surrounding – air (relief valleys). Now the effective optical constants (refractive index n and absorption coefficient k) are determined by interrelation between the volumes of the two phases of the effective medium. By varying relief geometry, one can change the ratio between the above volumes and, correspondingly, the values of the optical constants of the effective medium. The results of straightforward calculations of the volume fraction f of the $Al_xGa_{1-x}As$ phase in the effective-medium layer for several

widespread reliefs used in the SC manufacturing technology are given in Table 4.1.

Table 4.1. Volume fraction of the $Al_xGa_{1-x}As$ phase in the effective-medium layer

Type of relief of illuminated surface	f
Regular V-grooves	0.5
Regular inverted pyramids	0.67
Regular pyramidal relief	0.33
Partial filling with pyramids	0.1…0.33
Truncated pyramids	0.33…0.9
Porous $Al_xGa_{1-x}As$ layer	0.2…0.9

From this Table one can see that, by varying the type of relief of illuminated $Al_xGa_{1-x}As$ surface, it is possible to obtain an effective-medium layer whose optical parameters can be changed from those of air to those of $Al_xGa_{1-x}As$. In this case we performed calculations and analyzed theoretical spectral curves for the transmission coefficient T and coefficient R of light reflection from surfaces of GaAs, $Al_xGa_{1-x}As$−GaAs system and SiO_2−relief $Al_xGa_{1-x}As$ layer−$Al_xGa_{1-x}As$−GaAs system, depending on thicknesses of $Al_xGa_{1-x}As$, SiO_2 and relief $Al_xGa_{1-x}As$ layers. From the obtained R(λ) curves we calculated the averaged over the solar spectrum under AM0 conditions and GaAs integral reflection coefficient R^*, as well as SC short-circuit current density J_{SC} (under the same conditions). The calculations were made at x = 0.8, i.e., we considered a wide-gap $Al_{0.8}Ga_{0.2}As$ “window” and varied f from 0.1 up to 0.9. The values of optical constants were taken from [13].

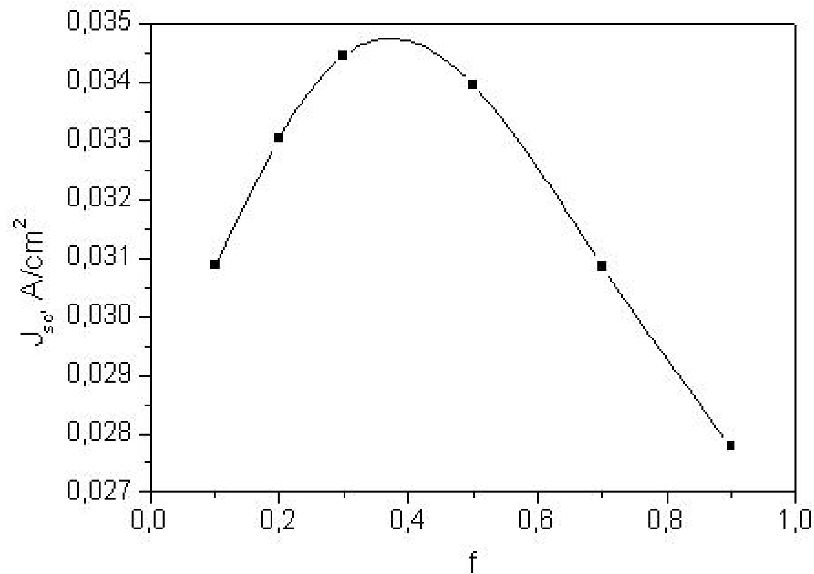

Fig. 4.7. Theoretical dependencies of the short-circuit current density J_{SC} for SC based on the "relief $Al_{0.8}Ga_{0.2}As$ layer–AlGaAs–GaAs" system on the fraction f of the $Al_{0.8}Ga_{0.2}As$ phase in the "relief AlGaAs layer–air" effective medium (Bruggeman model).

An analysis of the results obtained has shown that maximal reduction of the coefficient of light reflection occurs when the volume fraction f of the $Al_{0.8}Ga_{0.2}As$ phase in the "relief $Al_{0.8}Ga_{0.2}As$ layer–air" effective medium is 0.33 (see Fig.4.7). This value corresponds to pyramidal relief of the $Al_xGa_{1-x}As$ layer surface. In this case the coefficient of light reflection (averaged over the solar spectrum) is about 9%. The increase of photocurrent due to reduction of light reflection is comparable to that obtained for a flat interface using a SiO_2 antireflecting coating.

4.3. CALCULATION OF SHORT-CIRCUIT CURRENT IN $In_xGa_{1-x}As$-BASED *p-n* JUNCTIONS

From general considerations, short-circuit current in GaAs-based heterojunctions is below that in semiconductors with narrower gaps, even if the coefficient of light reflection is minimized. As semiconductor gap decreases, short-circuit current has to increase due to shift of the photoelectric threshold. Ternary compounds $In_xGa_{1-x}As$ have narrower gaps as compared with GaAs.

$In_xGa_{1-x}As$-based p-n junctions are prepared on GaAs substrates at low x and on Ge substrates at sufficiently high x. This is related to variation of the $In_xGa_{1-x}As$ lattice constant with x. We shall consider below the case when x = 0.02, and an $In_{0.02}Ga_{0.98}As$-based p-n junction is grown on GaAs substrate. The $In_{0.02}Ga_{0.98}As$ gap (determined using linear extrapolation) is 1.41 eV at a temperature of 300 K. When calculating spectral dependence of the absorption coefficient α for direct-gap semiconductor $In_{0.02}Ga_{0.98}As$ in the region near its fundamental absorption, we took into account change of its gap as compared to that of GaAs. At intermediate and high photon energies (when $\alpha > 10^4$ cm^{-1}) we used the α value for GaAs shifted by 0.02 eV toward lower energies. All the other parameters (both optical and photoelectric) were taken equal to the corresponding parameters for GaAs.

The dependence of short-circuit current in $In_{0.02}Ga_{0.98}As$-based p-n junction on the p-region thickness is presented in Fig. 4.8.

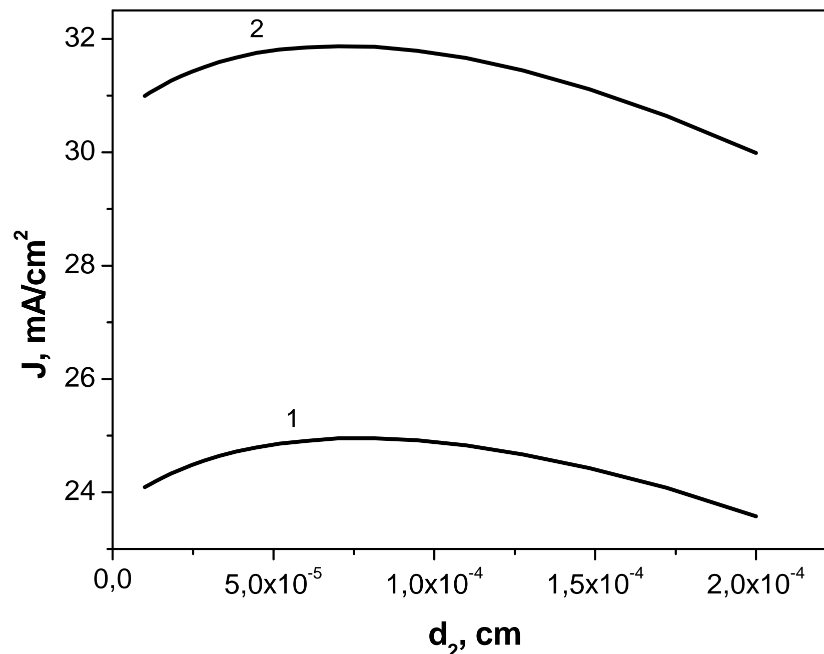

Fig. 4.8. Short-circuit current density for In0.02Ga0.98As-based p-n junction of optimal density without (1) and with antireflecting SiO2 layer (2) as function of the p-region thickness d2.

The n-region thickness was assumed to be over 5 μm. This enabled us to neglect absorption and current collection in GaAs substrate when calculating short-circuit current. One can see from Fig.4.8 that in this case (as for $Al_xGa_{1-x}As$/GaAs heterojunction) short-circuit current peaks at certain value of p-region thickness. This value is 0.7 μm, as in the case of $Al_xGa_{1-x}As$/GaAs heterojunction with flat surface. At the same time short-circuit current in an $In_{0.02}Ga_{0.98}As$-based p-n junction is about 5% over that for $Al_xGa_{1-x}As$/GaAs heterojunction. This is due to lower gap and higher coefficient of light absorption in the first case.

4.4. PHOTOCONVERSION EFFICIENCY IN TEXTURED $Al_xGa_{1-x}As$–p-GaAs–n-GaAs HETEROSYSTEM

When calculating the photoconversion power and efficiency, let us make the traditional assumption that a forward bias and illumination (in the presence of a load resistance) lead to equivalent results. Then:

$$I(V) = I_{SC} - I_d \exp\left(\frac{qV}{kT}\right) + I_r \exp\left(\frac{qV}{2kT}\right), \qquad (12)$$

where I_d (I_r) is the saturation value of the diffusion (recombination) component of total current. From here on we shall use the following interrelation between the total currents and current densities: I = AJ, where A is the SC area.

Two constructions of SC with $Al_xGa_{1-x}As$–GaAs heterojunction are known at present. In one of them has $Al_xGa_{1-x}As$ layer is continuous over the whole SC area, while in another such layer exists only between contacts (which are connected immediately to GaAs). For relief surfaces we have in the first case

$$I_d = \frac{A}{\cos\varphi_1}\left[\frac{qn_i^2}{p_p}\frac{D_n}{L_n}\frac{\sinh(d_2/L_n) + (S_n L_n/D_g)\cosh(d_2/L_n)}{(S_n L_n/D_n)\sinh(d_2/L_n) + \cosh(d_2/L_n)} + \frac{qn_i^2}{n_n}\frac{D_p}{L_p}\right] \qquad (13)$$

and in the second case

$$I_d = \frac{A}{\cos\varphi_1}\left[\frac{qn_i^2}{p_p}\frac{D_n}{L_n}\frac{\sinh(d_2/L_n)+(S_nL_n/D_n)\cosh(d_2/L_n)}{(S_nL_n/D_n)\sinh(d_2/L_n)+\cosh(d_2/L_n)}(1-m)\right]+$$

$$\frac{A}{\cos\varphi_1}\left[\frac{qn_i^2}{p_p}\frac{D_n}{L_n}\frac{\sinh(d_2/L_n)+((1/4)V_TL_n/D_n)\cosh(d_2/L_n)}{((1/4)V_TL_n/D_n)\sinh(d_2/L_n)+\cosh(d_2/L_n)}m+\frac{qn_i^2}{n_n}\frac{D_p}{L_p}\right] \quad (14)$$

.

Here n_i is the electron concentration in intrinsic GaAs; m is the relative metallization area at the illuminated SC surface; V_T is the electron mean-square thermal velocity InGaAs.

It should be noted that the second summand in expression (14) is related to electron recombination in a metal that occurs under contacts; in general, the effective recombination velocity under contacts and between them is heterogeneous in this case. However, in spite of very high ($\approx 4\cdot 10^7$ cm/s) V_T value, the effect of recombination under contacts is not disastrous. It is limited by electron supply rate and small m value. As a result, the effective electron recombination velocity in the metal (at m = 0.05, $d_2 = 5\cdot 10^{-5}$ cm and $D_n = 75$ cm^2/s) is about $5\cdot 10^4$ cm/s. This is of the same order as the bulk recombination rate in GaAs.

According to [4], for relief surfaces the saturation value of the recombination component of the total current I_r is

$$I_r \approx \frac{A}{\cos\varphi_1}\frac{qwn_i}{\tau_p}\frac{\pi}{2}\frac{kT}{q(V_b - V_{OC})}, \quad (15)$$

where qV_b is the barrier height in the p-n junction and V_{OC} is the open-circuit voltage.

Using the condition for maximal takeoff power (i.e., putting the derivative $d(I(V)V)/dV$ to zero), one can obtain a transcendental equation in V_m, and then determine the maximal takeoff photoconversion power, $P_m = I(V_{m)}V_m$. The efficiency for SC of unit area may be written down (ignoring the series resistance) as

$$\eta^* = \frac{I(V_m)\ V\ _m}{P_S}, \quad (16)$$

where P_S = 0.136 W/cm^2. Taking into account presence of a grid made as a comb with a thick bus (the relative metallization area m_1) and “fingers” (the relative metallization area m_2), so that $m_1 + m_2 = m$, and ignoring grid resistance, one gets

$$\eta = \eta^* \frac{2L}{l} \tanh\left(\frac{l}{2L}\right). \tag{17}$$

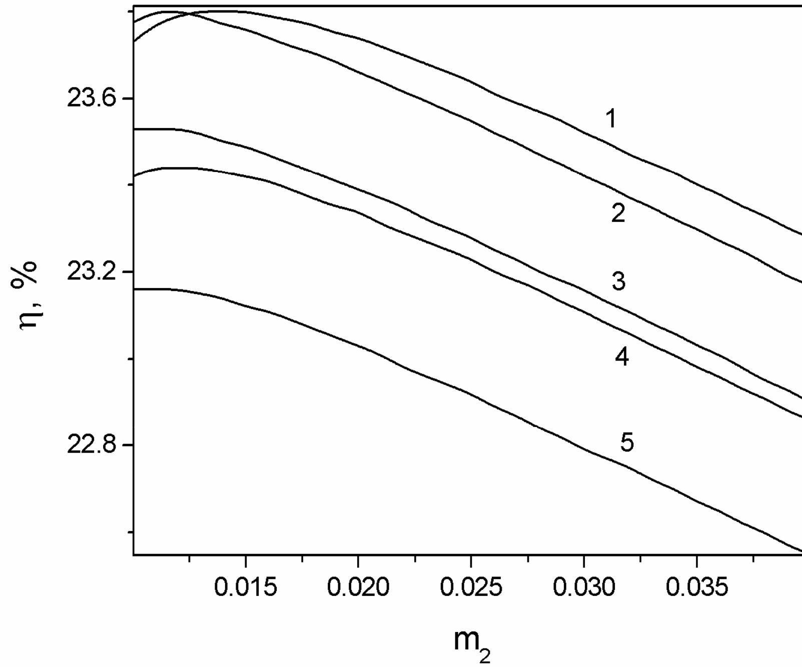

Fig. 4.9 Photoconversion efficiency of $Al_xGa_{1-x}As$–p-GaAs–n-GaAs heterostructure as function of the “finger” metallization relative area (m_1 = 0.03, p_p/n_n = 5). p_p (cm^{-3}): 1 - 2.5·10^{18}; 2 - 5·10^{18}; 3 - 10^{18}; 4 - 10^{19}; 1 - 5·10^{17}.

Here $L \cong \left(q\mu_p p_p d_2 V_{OC} / I_{SC}\right)^{1/2}$; $l = l_f(1-m_2)/m_2$ is the spacing between the grid “fingers”; μ_p is the hole mobility in heavily doped p-GaAs layer; l_f is the grid “tooth” width. It should be noted that expression (17) takes into account not the total series resistance but only its component related to the p-GaAs layer resistance.

Using expression (17) and those for I_d and I_r, one can minimize the effect of recombination on photovoltage and optimize relative contact-shaded area m_2, as is illustrated by Fig. 4.9. One can see that for the heterostructures studied the highest efficiency η

is achieved at doping levels p_p = (3–5) 10^{18} cm^{-3} and n_n = (5–7) 10^{17} cm^{-3}; the optimal m_2 value is (1–1.5)% at “tooth” width of 10 μm.

For coated textured structures with m = 0.045 and optimized parameters of $Al_xGa_{1-x}As$ film and p- and n-GaAs layers, the photoconversion efficiency η is somewhat over 24%. This is 9% higher than that for coated structures without texture.

4.5. THEORETICAL ANALYSIS OF PHOTORESPONSIVITY FOR THE HETEROJUNCTION PHOTOCONVERTERS WITH MICRORELIEF INTERFACES

Improvement of photoresponsivity of heterostructures with microrelief interfaces is related, first of all, to reduction of the coefficient of light reflection in the spectral region of photosensitivity [11]. Another factor is that, at microrelief interfaces, solar beams enter semiconductor at a nonzero angle of incidence. This leads to growth of their path in the absorber, as well as to increase of both light absorption in this region and photocurrent collection coefficient [14].

We studied theoretically the photoconversion efficiency in the AlGaAs–GaAs system with a regular relief as function of relative area of metallization by contact grid “fingers” at different levels of p-GaAs layer doping. It was shown that the corresponding curve has a peak from whose position one can determine the optimal degree of contact grid filling with “fingers”. Depending on the doping level of p-GaAs layer (that varied from $5\cdot10^{17}$ up to 10^{19} cm^{-3}), this peak is achieved when the degree of contact grid filling with “fingers” is from 4% to 1% the total solar cell (SC) area, the “finger” width being 30 μm. If this width is reduced to 10 μm, then the value of relative area of contact grid shadowing with “fingers” at which photoconversion efficiency has a peak becomes half as large as in the previous case.

On the basis of the results of our calculation of photoconversion efficiency in the AlGaAs–GaAs system with a

regular relief, we formulated the following recommendations for technologists concerning the parameter values:

- the AlGaAs layer width - 30 nm, doping level - $2\cdot10^{19}$ cm^{-3};
- the p-GaAs layer width - 0.5–0.7 μm, doping level - $2\cdot10^{18}$–$5\cdot10^{18}$ cm^{-3};
- the n-GaAs layer width - 5 μm, doping level - $5\cdot10^{17}$–10^{18} cm^{-3};
- the width of contact grid "fingers" - 30 μm, their spacing - 1.5–2 mm;
- two contact buses, each 150 μm wide.

We analyzed also the case when the contact grid is deposited immediately onto the p-GaAs layer. At that the surface recombination velocity of minority charge carriers (electrons) in the contact is 10^7 cm/s. Our calculations of diffusion saturation current showed that it increases by no more than three times as compared to the case when the contacts are deposited onto the AlGaAs layer. At the same time the surface recombination velocity grew by three orders of magnitude. This result may be explained in the following way. First, in this case the effective surface recombination velocity of electrons in contact is determined by the rate of electron supply to contact from the place of their generation. This rate is of the order of electron diffusion velocity, thus being much below 10^7 cm/s. Second, the contact grid area is much below the total SC area (≤5%), while in the regions between contacts the effective surface recombination velocity of electrons remains small due to the AlGaAs layer. Now the open-circuit voltage V_{OC} decreases insignificantly (no more than by 30 mV) as compared to the case when the contacts are deposited onto the AlGaAs layer; the same is true also for photoconversion efficiency.

We performed a theoretical analysis of the effect of p-n junction relief on the saturation currents (both diffusion and recombination). At that we considered the case when the Debye shielding length is much below the relief period, i.e., shielding is

one-dimensional, and presence of relief results in electric field increase by a factor K at the relief projections only. This effect can be calculated from the expression $K = 2\cos(\varphi/2)$ where φ is the relief vertex angle. To illustrate, as the angle φ varies from 90 to 60°, K increases from 1.41 up to 1.73.

It should be noted that the diffusion saturation current at any single relief area has not to depend directly on presence of relief, since it is related to recombination in quasi-neutral bulk. In our case presence of relief results only in increase of the effective diffusion saturation current by a factor of $1/\cos(\pi/2-\varphi/2)$ as compared to a flat surface (due to increase of the length of relief part). To illustrate, at relief vertex angles of 90 and 60° the corresponding factors are 1.41 and 2.

As a rule, the same considerations are valid for the recombination saturation current too, because it is proportional to the width of the depletion layer in the p-n junction region whose low doping level is determined by those of the p- and n-regions only. Thus our analysis enables us to conclude that (contrary to the case of Schottky contacts) relief affects the saturation currents in p-n junctions weakly, so the open-circuit voltage in photoelectric converters (PECs) on the basis of the AlGaAs–p-GaAs–n-GaAs system will decrease insufficiently, taking into account weak increase of saturation currents due to presence of relief.

The technology which is applied for obtaining SCs with microrelief surface on the basis of the AlGaAs–p-GaAs–n-GaAs system uses zinc diffusion from the zinc-doped AlGaAs layer for formation of a p-n junction in GaAs. In the case of microrelief interfaces one should take into account the specific features of diffusion (that were absent in the case of flat interfaces) and their effect on photosensitivity of the AlGaAs–p-GaAs–n-GaAs system. This effect has to manifest itself, first of all, in nonuniform distribution (in the interface plane) of hole concentration in the p-GaAs layer. This may result in appearance of nonuniform

distribution (in the interface plane) of both the effective recombination rate and electron diffusion length in the p-region. We have made a theoretical analysis of the effect of the above factors on short-circuit current J_{SC} in microrelief structures using the model of “spotty” structure in the plane parallel to that of interface.

The short-circuit current averaged over the total area A is calculated using the following expression:

$$\bar{J}_{SC} = \frac{1}{A}\sum_{i=1}^{n} A_i J_i \,. \tag{18}$$

Here A_i and J_i are the area and short-circuit current, respectively, in local structure areas with different hole concentrations in the p-GaAs layer, and n is the total number of such local areas.

When averaging open-circuit voltage V_{OC}, we used the condition of parallel connection of local voltages and capacitances: $C = Q/V$, where

$$C = C_1 + C_2 + \cdots C_n == Q/V_1 + Q/V_2 + \cdots Q/V_n \,. \tag{19}$$

Here $Q = Sq_s$ is the total charge; $C_i \sim A_i$, where A is the total area and A_i is the area of the i-th element with the i-th value of hole concentration in the p-GaAs layer. Thus one obtains for $\bar{V}_{OC}$:

$$\bar{\bar{V}}_{OC} = \left(\sum_{i=1}^{n} \frac{A_i}{A} \cdot \frac{1}{V_i} \right)^{-1} , \tag{20}$$

where V_i are the open-circuit voltages in the local structure areas with different hole concentrations in the p-GaAs layer. One can see from Eq. (20) that open-circuit voltage is determined by the areas with smaller local values; this reduction, however, depends on the ratio between the corresponding area of such (with lower voltages) regions and the total area.

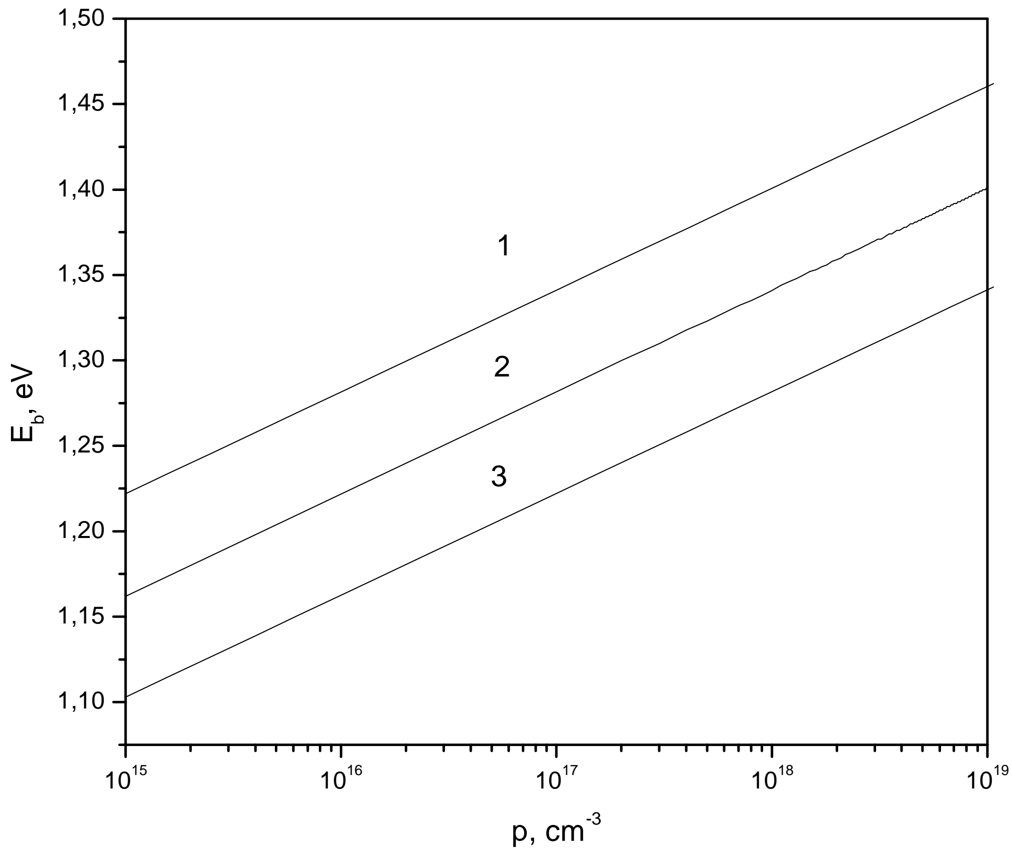

Fig. 4.10. Theoretical dependencies of the barrier height in the GaAs p-n junction on the hole concentration in the p-GaAs layer at T = 300 K. $n_n = 10^{18}$ cm^3, p_p, cm^{-3}: 1 – 10^{16}; 2 – 10^{17}; 3 – 10^{18}.

The potential barrier height E_B in the p-n junction is given by the following expression:

$$E_B = kT \ln\left(\frac{n_n p_p}{n_i^2}\right), \tag{21}$$

where n_n and p_p are the majority charge carrier concentrations (those of electrons in n-GaAs and holes in p-GaAs).

Shown in Fig. 4.10 are the E_B in GaAs p-n junction vs hole concentration in the p-GaAs curves at a temperature T = 300 K. The electron concentration in the n-GaAs layer serves as parameter. One can see that the lowest barrier height at room temperature (1.1 eV) is realized at $p_p = 10^{15}$ cm^{-3} and $n_n = 10^{16}$ cm^{-3}. Local values of open-circuit voltage which is realized at the corresponding electron and hole concentrations cannot exceed 1.1 eV; actually it is even lower (see below).

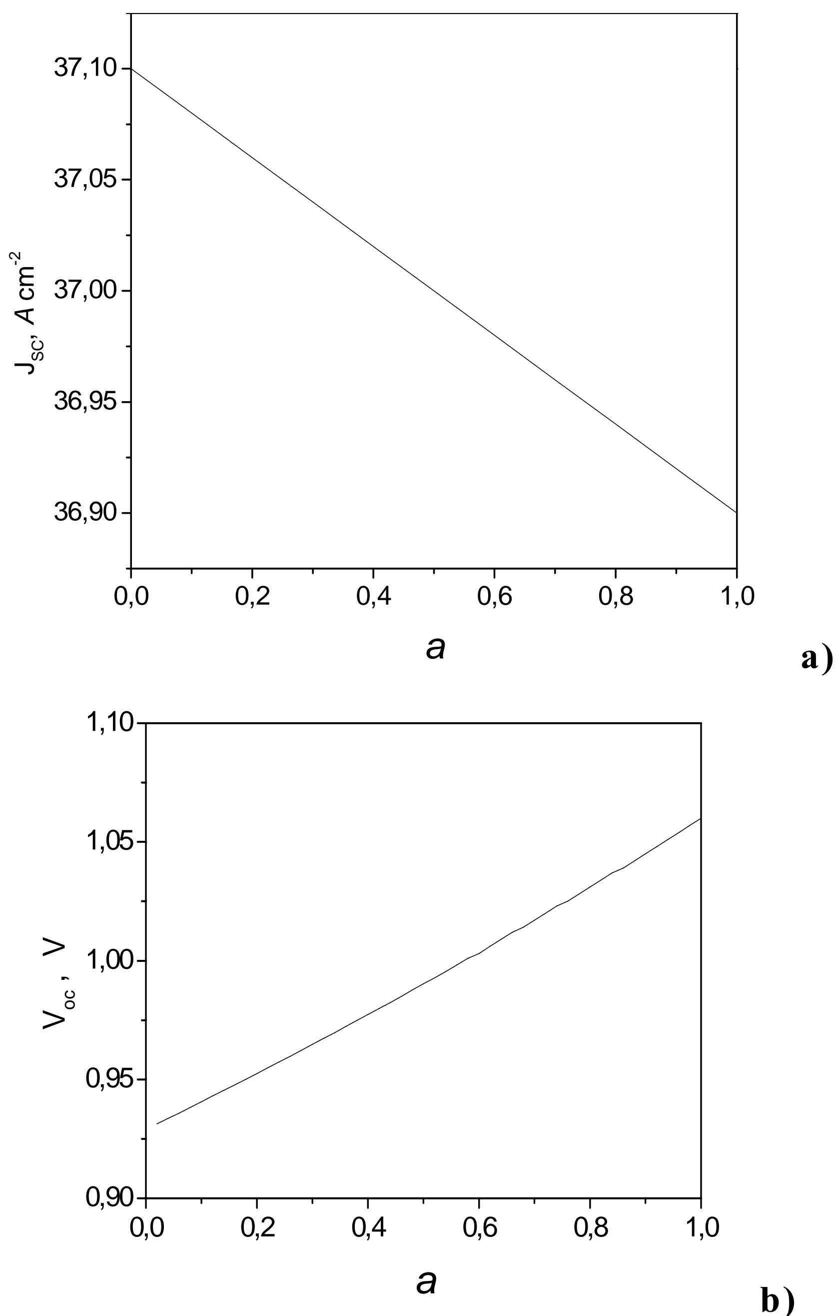

Fig. 4.11. a) The dependence of short-circuit current on the ratio between areas A_1 and A_2 with different hole concentrations in the p-GaAs layer. b) The dependence of open-circuit voltage on the ratio between areas A_1 and A_2. $n_n = 10^{18}$ cm^{-3}, p_p, cm^{-3}: 1 – 10^{16}; 2 – 10^{13}; 3 – 10^{10}; 4 – 10^{7}.

Figures 4.11a and 4.11b present, correspondingly, short-circuit current and open-circuit voltage vs the ratio A_1/A curves calculated in the ray optics approximation [5] for optimized thicknesses of the AlGaAs and p-GaAs layers. When calculating short-circuit current, it was assumed that hole concentration in the p-GaAs layer is

$5 \cdot 10^{18}$ cm^{-3} in the structure region whose area is A_1, while in another region it is $5 \cdot 10^{15}$ cm^{-3}. Open-circuit voltage V_{OC} was calculated for the cases when hole concentration in the p-GaAs layer is $5 \cdot 10^{18}$ cm^{-3} in the structure region whose area is A_1, while in the other region it is 10^{16}, 10^{13}, 10^{10} and 10^{7} cm^{-3}, respectively. In our calculations we used the parameter values given in [7] at which short-circuit current is close to the highest possible: the electron lifetime in the p-GaAs $\tau_n = 10^{-8}$ s, the hole lifetime in the n-GaAs $\tau_p = 2 \cdot 10^{-8}$ s, the charge carrier lifetime in AlGaAs $\tau_a = 10^{-9}$ s; the diffusion length in AlGaAs $L_a = 10^{-4}$ cm; the coefficient of electron diffusion in the n-GaAs layer $D_n = 64.5$ cm^2/s^{-1}, while that of hole diffusion in the p-GaAs $D_p = 6.45$ cm^2/s^{-1}.

One can see from Fig. 4.11a that big variations of hole concentration in the p-GaAs layer do not change considerably the averaged current J_{SC}. It can change by no more than 0.5% as compared to the case when hole concentration in the p-GaAs layer is $5 \cdot 10^{18}$ cm^{-3} over all the structure area.

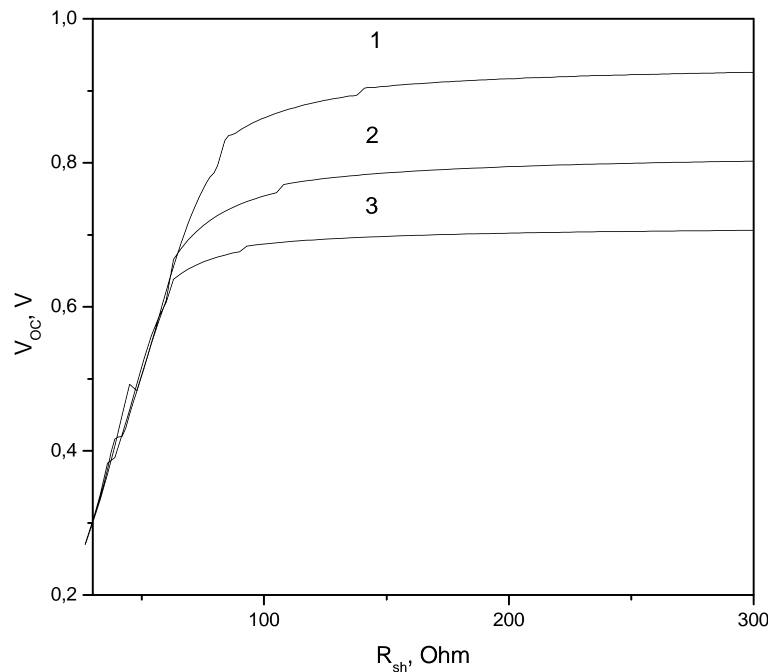

Fig. 4.12. The dependence of open-circuit voltage on the shunt resistance. $n_n = 10^{18}$ cm^{-3}, p_p, cm^{-3}: 1 – 10^{18}; 2 – 10^{15}; 3 – 10^{12}.

The averaged open-circuit voltage, as one can see from Fig. 4.11, may change essentially at big variations of hole concentration in the *p*-GaAs layer. To illustrate, if the hole concentration in another region of the structure is 10^{16}, 10^{13}, 10^{10} and 10^{7} cm^{-3}, then the V_{OC} values at $A_1/A_2 = 1$ are 0.99, 0.88, 0.74 and 0.58 V, respectively.

Thus nonuniformity of hole concentration in the *p*-GaAs layer in the heterojunction PECs on the basis of the AlGaAs–*p*-GaAs–*n*-GaAs system makes it possible, in principle, to explain spread of open-circuit voltage observed in the test samples with microrelief interface. It should be noted, however, that there is one more reason which makes it possible to explain abrupt drop of open-circuit voltage that has been observed experimentally at certain technologies of obtaining PECs in microrelief AlGaAs–*p*-GaAs–*n*-GaAs heterosystems.

We performed computer simulation of the open-circuit voltage dependence on the shunt resistance R_{SH} in the above SCs. Figure 4.12 presents the calculated $V_{OC}(R_{SH})$ curves for a number of PECs. The parameters of their light I–V curves were determined from comparison with experimental I–V curves using the three-exponential model. This model takes into account the following components of recombination current: (i) diffusion current, (ii) recombination current in the space-charge region, and (iii) excess-tunnel current related to dislocations. The $V_{OC}(R_{SH})$ value was determined by solving the following equation:

$$J_{SC} = J_{Sd} \exp\left(\frac{qV_{OC}}{kT}\right) + J_{Sr} \exp\left(\frac{qV_{OC}}{2kT}\right) + J_{ST} \exp\left(\frac{qV_{OC}}{\varepsilon_T}\right) + \frac{V_{OC}}{R_{SH}}, \quad (22)$$

where J_{Sd}, J_{Sr} and J_{ST} are, correspondingly, the diffusion, recombination and tunnel saturation currents; ε_T is the characteristic tunneling energy

One can see from Fig. 4.12 that, when the shunt resistance R_{SH} is over 10^2 Ω, open-circuit voltage V_{OC} is maximal and does not depend on R_{SH}. However, when $R_{SH} < 10^2$ Ω, then V_{OC} drops

abruptly as R_{SH} goes down. For instance, at R_{SH} = 10 Ω, V_{OC} ≈0.1 V.

One can separate the reason for abrupt decrease of open-circuit voltage from the form of experimental light I–V curves. If this decrease is due to variation of hole concentration in the p-GaAs layer, then the photocurrent vs. load resistance R_L curves should be "convex". But if this decrease is related to a small value of the shunt resistance R_{SH}, then one should expect that the above-mentioned curves are "concave".

* *

*

Our computer simulation has shown that for textured $Al_xGa_{1-x}As$–*p*-GaAs–*n*-GaAs heterosystem (with two antireflecting films) it is possible to make the reflection coefficient very small (< 1%). This fact, as well as increase of photon path in *p*-GaAs layer of a SC based on the above heterosystem, can provide short-circuit current density almost equal to the limiting value (0.04 A/cm^2 under the AM0 condition).

Starting from the requirement for obtaining maximal photoconversion efficiency, we got the conditions for optimization of (i) doping levels in *p*- and *n*-GaAs layers and (ii) grid area.

It was found that no considerable increase of the saturation value of the diffusion component of total current occurs if contacts immediately adjoin *p*-GaAs. This is due to a small relative grid area, as well as to the fact that the effective recombination velocity is restricted by the time needed to supply electrons to the contacts.

It was shown that allowance for both the "spotty" character of hole concentration distribution in the *p*-GaAs region of SCs made on the basis of textured $Al_xGa_{1-x}As$–*p*-GaAs–*n*-GaAs heterosystem and low values of the shunt resistance R_{SH} make it possible to explain a big spread of open-circuit voltage values observed for the experimental SC samples.

REFERENCES

[46] Koltun M.M. Selective Optical Surfaces for Solar Energy Converters. Allerton Press. Inc. New York. 1981.

[47] Dmitruk N.L., Borkovskaya O.Yu., Mamontova I.B., Mamykin S.V. Solar Energy Materials and Solar Cells 2000. v.60. p.379.

[48] Berning P.H. In:, Physics of Thin Films. G. Hass (Ed.). v.1. Academic Press. New York. 1963. p. 69.

[49] Howell H.J. In: Semiconductors and Semimetals. R.K. Willardson, A.C. Beer (Eds.). v.11. Academic Press. New York. 1975.

[50] Augustine G., Rohatgi A., Jokerst N.M. IEEE Trans. Electron. Dev. 1992. v ED39. N 10. p.2395.

[51] Fahrenbruch A.L., Bube R.H. Fundamentals of Solar Cells. Photovoltaic Solar Energy Conversion. New York. 1983.

[52] Andreev V.M.. In: Photovoltaic and Photoactive Materials–Properties, Technology and Application. Y.M. Marshall, D. Dimova-Malinovska (Eds.). vol.80. Kluwer Acad. Publ. London. 2002. p.131.

[53] Aspnes D.E. et al. J. Appl. Phys. 1986. v.60. N 2. p.754.

[54] Dabney B.T. J. Appl. Phys. 1979. v.50. N 11. p. 7210.

[55] Sze S.M. Physics of Semiconductor Devices. Second Edition. John Wiley & Sons. Inc. New York–Chichester–Brisbane–Toronto–Singapore. 1981.

[56] Dmitruk N.L., Borkovskaya O.Yu., Dmitruk I.N., Mamontova I.B. Solar Energy Materials and Solar Cells. 2003. v.76. p.625.

[57] Rowlands S.F., Livingstone J., Lund C.P. In: Proc. 17th EPVSEC. Munich. Germany. 2001. p. 3011.

[58] http://www.ioffe.ru/SVA/NSM/Semicond/GaAs/optic.html.

[59] Borkovskaya O.Yu., Dmitruk N.L., Lyapin V.G., Sachenko A.V., Thin Solid Films. 2004. v.451-452. p.402.

Chapter V

PHOTORESPONSIVITY OF THE PHOTOCONVERTERS

We studied light *I*–*V* curves and photosensitivity spectra of solar cells (SCs). The aim of these studies was choosing the most efficient technology of heteroepitaxy, as well as the best values of parameters of the active region of photoelectric converters (PECs). (Among these parameters were thicknesses and doping levels of the p^+-GaAs, p^+-$Al_xGa_{1-x}As$ and *n*-GaAs layers, as well as composition *x*.) SCs were produced at the Physical-Technical Institute of the Scientific Association "Physics–Sun" of the Academy of Sciences of Republic of Uzbekistan. They were made on flat and microtextured substrates, with variation of the LPE technique and temperature modes:

1.1 Capillary LPE – on the substrate front surface, with the distance between the substrates (capillar) being equal to 500 nm

a) samples #: 2, 61, 129, 238 – on the flat substrate.

1.2 LPE with previous vapor-phase diffusion of Zn from the quasi locked up volume – the layers are grown on both sides of the n^+-GaAs substrate; those on the substrate back surface are removed by polishing before contact formation;

a) samples #: 42, 43, 44, 45, 46, #3 RK, 25/127 – on the flat substrate;

b) #5-RKT, 75m/128, 96m/119 on the microtextured (quasi-grating) substrate.

1.3 LPE with forced cooling in the horizontal plant with a shifting container:

a) 71-XO, AK: N 144, 146, 148, 150 – on the flat substrate;

b) 70-XO, AK: 143, 145, 147, 149 – substrate-quasi-grating, #35-XO I – diffraction grating, II – quasi-grating, #64-XO - quasi-grating.

Besides, we studied also the VPE-grown p^+-GaAs/p^+-$Al_{0.6}Ga_{0.4}As$/p^+-n-n^+-GaAs structures on flat (MO4) and microtextured (MO1-MO3) substrates. According to our calculations, the layer parameters corresponded to those optimal at optimal morphology and statistical-geometric microrelief parameters. In the latter case we measured characteristics of the structures with a contact grid In:Zn or Au/Zn/Au on the p^+-GaAs layer and Au:Ge contact to n^+-GaAs, both with the upper p^+-GaAs layer (0.3 μm thick) and after etching it in citric acid:H_2O_2.

5.1. MEASUREMENTS AND MODELLING OF CHARACTERISTICS TO DETERMINE PHOTOCONVERSION PARAMETERS

We studied the spectral dependencies of photocurrent $I_{\mathrm{ph}}(\lambda)$ in solar cells (SCs) in the 400–1200 nm wavelength range. The samples were irradiated with monochromatic light modulated with frequency of 20 Hz; sample irradiance was not varied during measurements which were performed in the short-circuit mode at zero reverse bias ($V_r = 0$).

The studies of SC light I–V curves and determination of SC photoelectric parameters were made under AM0 conditions; the irradiance of sample surface was 136 mW/cm^2.

The SC $I_{sc}(V_{oc})$ curves were taken at different (from ~100 to ~0.1 mW/cm^2) illumination intensities. (Here I_{sc} is short-circuit current and V_{oc} is open-circuit voltage) The parameters of SC equivalent circuit (Fig. 5.1) were calculated from the experimentally obtained $I_{sc}(V_{oc})$ curves.

At that we used SC light I–V curve in the two-exponential model:

$$I = I_{\mathrm{ph}} - I_{01}\left[\exp\frac{q(V+IR_s)}{A_1kT} - 1\right] - I_{02}\left[\exp\frac{q(V+IR_s)}{A_2kT} - 1\right] - \frac{IR_s + V}{R_{sh}}\,. \quad (1)$$

Here I (V) is SC current (voltage); I_{ph} is the photogeneration current (it depends on the intensity and spectral composition of the incident light; for dark I–V curve $I_{ph} = 0$); A_1 and A_2 are the diode (ideality) factors of *p-n* junction; I_{01} and I_{02} are the saturation currents of reverse-biased *p-n* junction (they are determined by the predominant current flow mechanisms in SC – diffusion, generation-recombination); R_s is the series resistance composed of contact layer resistances, those of SC *p-n* regions and junction resistances of metal–semiconductor contacts connected in series; R_{sh} is the shunt resistance parallel to *p-n* junction (through it surface and volume currents flow).

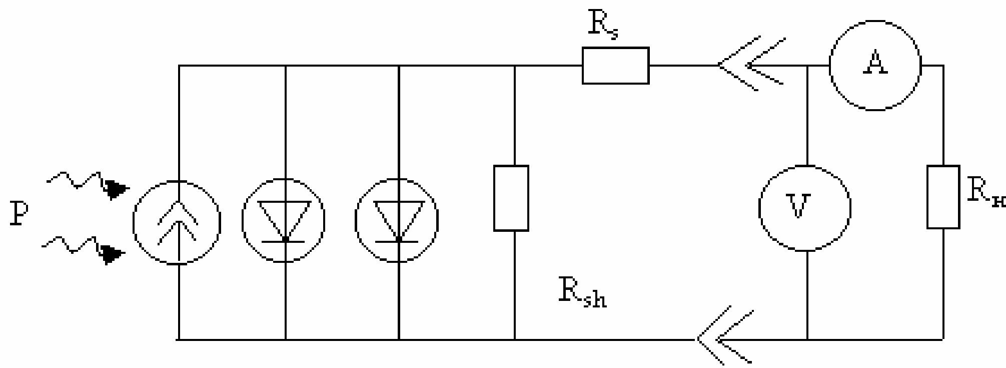

Fig. 5.1. SC equivalent circuit with an external load resistance.

In the open-circuit mode $I = 0$, $V = V_{oc}$, $I_{ph} = I_{sc}$, so one has from Eq. (1):

$$I_{sc} = I_{01}\left[\exp\frac{qV_{oc}}{A_1 kT} - 1\right] + I_{02}\left[\exp\frac{qV_{oc}}{A_2 kT} - 1\right] + \frac{V_{oc}}{R_{sh}}. \quad (2)$$

All the above parameters were determined by computer fitting of Eq. (2) to the experimental dependencies of short-circuit current on open-circuit voltage, $I_{sc}(V_{oc})$, taken at different intensities of illumination of SC surface.

To determine, from the experimental curves, the following five parameters A_1, A_2 I_{01}, I_{02} and R_{sh} of SC equivalent circuit, one should have at least five equations (written, say, for five points of

the $I_{sc}(V_{oc})$ curves (2)). Thus the above problem is reduced to solving a set of five transcendental equations (i.e., factually, to fitting the theoretical dependencies to the experimental ones).

Such inverse problem belongs to the class of ill-posed problems that may have several solutions. A complicating factor is that the experimental dependencies are measured with a certain error, and the set of equations may be inconsistent (has no exact solution at all). So one has to apply the regularization methods (e.g., that advanced by Tikhonov). Moreover, to improve accuracy of parameter determination, one should make the set overdetermined (i.e., the number of equations should exceed that of unknowns) and minimize deviation of the theoretical dependence from the experimental one. In addition, it is desirable to determine parameters (or, at least, their range) from independent measurements or physical considerations.

5.2. PHOTORESPONSIVITY OF THE PHOTOCONVERTERS FABRICATED BY VARIOUS MODIFICATION OF THE LPE TECHNIQUE

Figure 5.2 presents typical light I–V curves for several PECs, while Fig. 5.3 shows their photosensitivity spectra.

The study of the $J_{SC}(V_{oc})$ curves (Fig. 5.4 a, b) and their simulation together with the light I–V curve using the two-exponential model enables one to determine more accurately and unambiguously the equivalent circuit parameters (although fitting of the ln $J_{SC}(Voc)$ dependence only gives several versions of parameter sets.

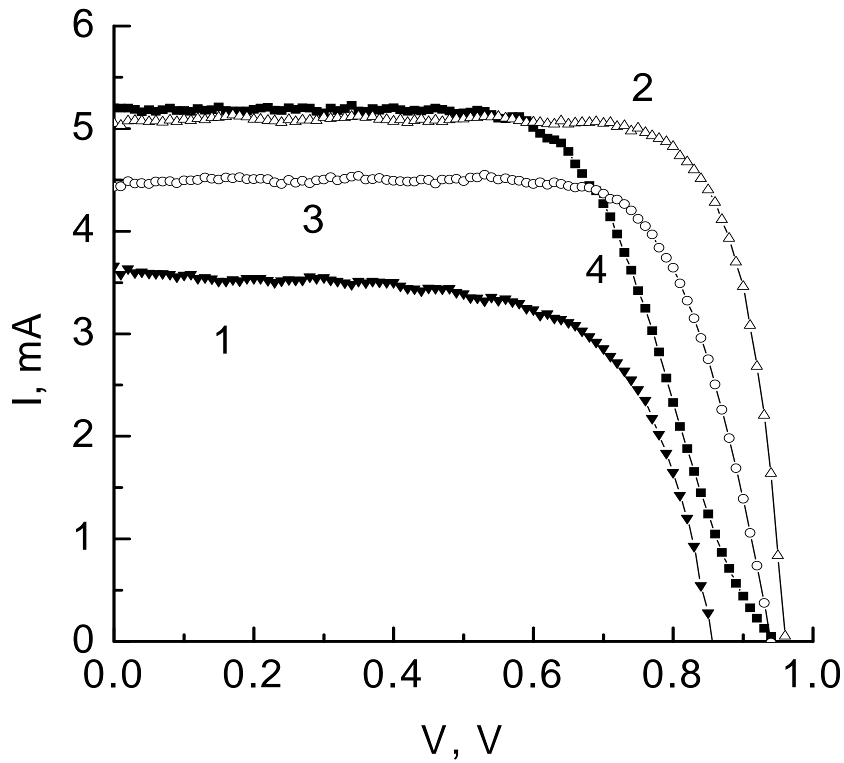

Fig. 5.2. Light *I–V* curves at AM0 conditions of irradiation of SC samples ##129 (1), 42(2), 44(3), 45(4).

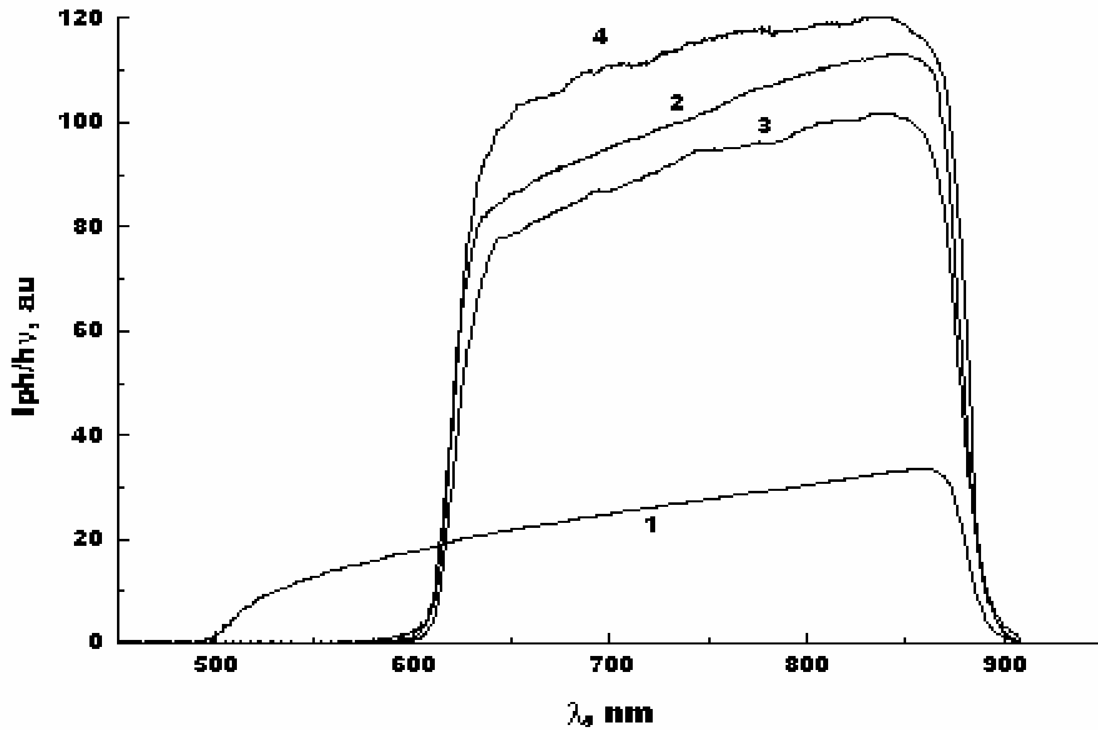

Fig. 5.3. Photocurrent spectral curves (normalized to a constant number of incident photons) for SC samples ##129(1)90, 42(2), 44(3), 45(4) made on the basis of $Al_xGa_{1-x}As$–GaAs heterostructure.

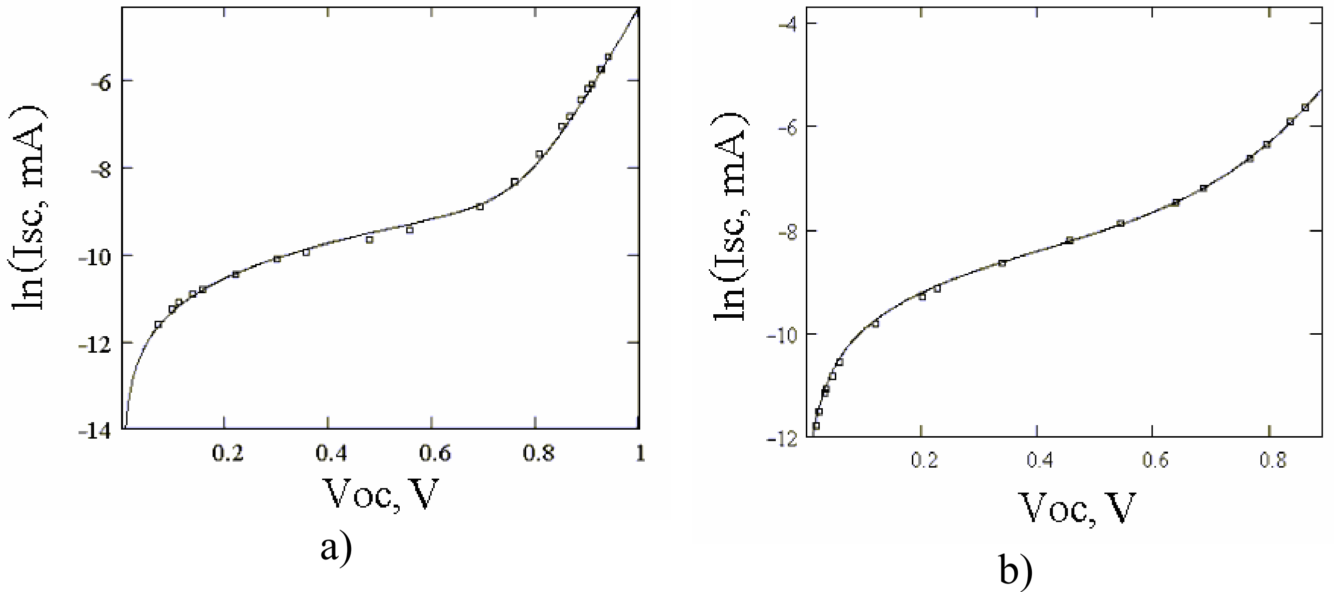

Fig. 5.4. The results of fitting the theoretical dependence ln $I_{sc}(V_{oc})$ (curve) to the experimental one (dots):

(a) for the SC sample #42p (parameters of the theoretical curve: A_1 = 1.682; A_2 = 3.333; I_{01} = 1.161·10^{-12} A; I_{02} = 1.824·10^{-8} A; R_{sh} =8263 Ω);

(b) for the SC sample #129 (A_1 = 2.145; A_2 = 4.3; I_{01} = 2.329··10^{-10} A; I_{02} = 6.895·10^{-7} A; R_{sh} = 2030 Ω).

The SC photoconversion parameters obtained from light $I–V$ curves under simulated AM0 conditions are given in Table 5.1 (FF – filling factor, η - photoconversion efficiency). By comparing the photoconversion parameters and J_{SC} spectra taken for different PECs, one can see that PECs from the group 1.1 have wider photosensitivity region (due to higher content x of Al in the $Al_xGa_{1-x}As$ layer). However, the filling factor value (which is restricted by the series and shunt resistance values) may become of more importance for photoconversion efficiency. To illustrate, for the structure #129 R_s = 24.4 Ω and R_{sh} = 1597 Ω, while for the structure #42 R_s = 1.8 Ω and R_{sh} = 11340 Ω; the above values determine those of FF and η.

Such situation is observed for both flat structures and those grown on textured substrates.

Table 5.1. The SC photoconversion parameters

Sample #	J_{SC}, mA/cm^2	V_{oc}, V	FF	η, %
61	16.33	0.893	0.675	8.22
2	17.47	0.932	0.682	9.09
238	13.44	0.681	0.498	3.34
129	12.20	0.857	0.648	4.97
42	16.84	0.961	0.795	9.43
43	15.02	0.945	0.732	7.61
44	14.78	0.940	0.747	7.60
45	17.35	0.945	0.632	7.59
46	16.70	0.945	0.781	9.04

The characteristics of structures grown with the capillary epitaxy technique are presented in Figs. 5.5 and 5.6 and in Table 5.2, while those for the structures with heteroepitaxial layers of different thicknesses grown in a horizontal plant (on both flat and textured substrates) are presented in Figs. 5.7 and 5.8 and in Table 5.3. In the latter case heteroepitaxy was realized directly onto the n^+-GaAs substrate (with $N_d \sim 10^{17}$ cm^{-3}), without previous growing of the n-GaAs buffer layer.

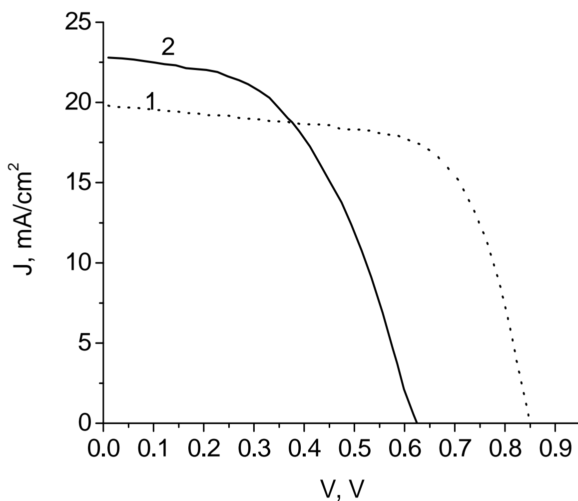

Fig. 5.5.

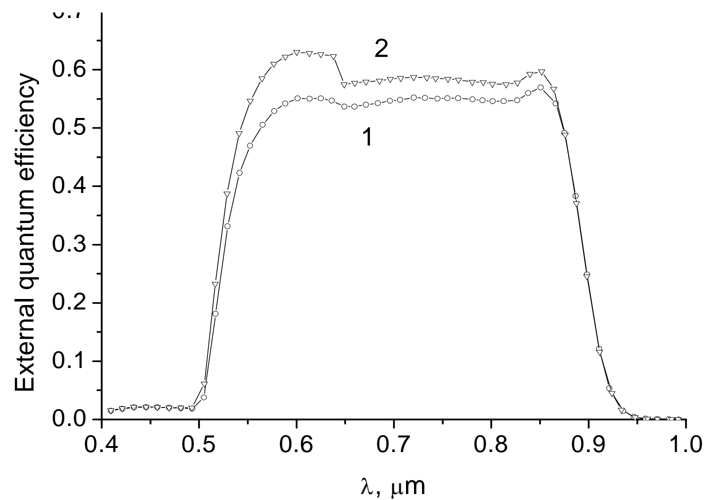

Fig. 5.6.

Fig. 5.5. Light *I–V* curves at AM0 conditions for SC samples RK 25 with flat substrate (1) and RKT 75 with microtextured substrate (2).

Fig. 5.6. External quantum efficiency spectra for structures with flat RK 25 (1) and microtextured RK 75 (2) substrates.

Table 5.2. Photoconversion parameters at AM0 condition for SC samples fabricated by LPE with previous vapor-phase diffusion of Zn

Sample #	J_{SC}, mA/cm^2	V_{oc}, V	FF	η, %
3-RK	12.3	0.813	0.619	4.54
5-RKT	12.2	0.822	0.615	4.55
RK-25	19.8	0.850	0.659	8.1
RK-75M	22.8	0.624	0.499	5.2

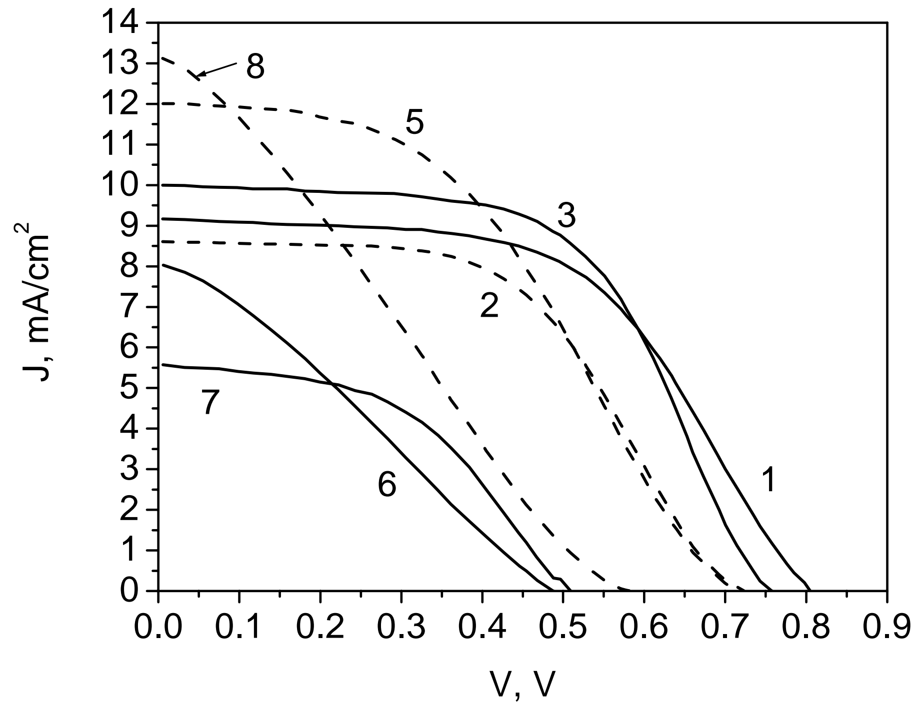

Fig. 5.7. Light I–V curves at AM0 conditions for SC samples with flat substrate: #150 (2), 146 (5), 144 (8) and substrate microrelief of quasigrating type: #149 (1), 145 (3), 143-1 (6), 143-2 (7).

From comparison the results obtained, one can draw the following conclusions:

The highest efficiency η has been obtained for the structures grown with the capillary epitaxy technique using Zn diffusion from the vapor phase. However, due to rather big (≥ 5 μm) thickness of the $Al_xGa_{1-x}As$ layer, the front surface relief is smoothed out, and the effect of interface microtexturing is reduced.

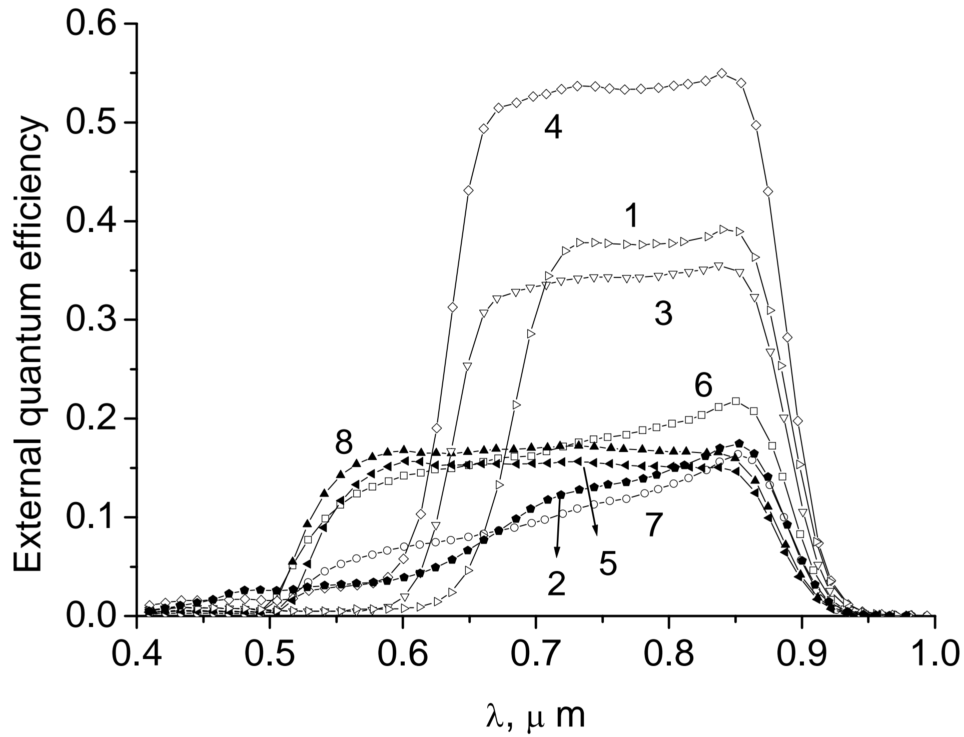

Fig. 5.8. External quantum efficiency spectra for SC samples with flat substrate: #150 (2), 146 (5), 144 (8) and substrate microrelief of quasigrating type: #149 (1), 145-1 (3), 142-2 (4), 143-1 (6), 143-2 (7).

Table 5.3. Photoconversion parameters at AM0 condition for SC samples fabricated by LPE in the horizontal plant with a shifting container

Sample #	J_{SC}, mA/cm^2	V_{oc}, V	FF	η, %
149-AK	9.17	0.805	0.553	3.0
150-AK	8.606	0.723	0.532	2.4
145-AK1	9.996	0.758	0.575	3.2
145-AK2	10.834	0.611	0.273	1.3
146-AK	12.01	0.717	0.438	2.8
143-AK1	8.025	0.488	0.282	0.8
143-AK2	5.571	0.509	0.477	1.0
144-AK	13.124	0.585	0.259	1.5

When heteroepitaxy is realized in a horizontal plant, the most effective growth mode is that with forced cooling by ΔT ~ 7 °C (d ~ 3 μm, the structures #145 and 146).

The effect of microtexturing is enhanced as the heteroepitaxial layer thickness goes down. For the structures #149 and 150 we

obtained growth of η by a factor of 1.25 due to substrate microtexturing.

The main factor that reduces photoconversion efficiency is nonuniformity of thin LPE-grown heteroepitaxial layers and presence of defects (especially pores) in them. This leads to shunting of the *p*-*n* junction and reduction of both the filling factor FF and open-circuit voltage V_{oc}. Our investigation showed that heteroepitaxial growth of $Al_xGa_{1-x}As$ on a microtextured substrate is more uniform than that of GaAs. (This fact manifested itself, in particular, in more pronounced effect of microtexturing for the structures AK-143–150 as compared to the structures RK-RKT.) Therefore, when fabricating SCs, microtexturing of the *n*-GaAs buffer layer will be more effective than substrate microtexturing.

5.3. PHOTORESPONSIVITY OF THE PHOTOCONVERTERS FABRICATED BY GPE

Shown in Fig. 5.9 are the spectra of short-circuit photocurrent taken for the VPE-grown p^+-GaAs/p^+-$Al_xGa_{1-x}As$/p^+-n-n^+–GaAs (MO1-MO4) structures before (a) and after (b) etching off the p^+-GaAs “cap”-layer, that demonstrate their dependence on the character and degree of the substrate microrelief development: MO4 - flat, MO1 and MO2 - quasi-gratings (the structure MO1 has a more developed relief), MO3 - dendrite-like.

The degree of microrelief development increases in the following sequence of structures: MO4, MO2, MO1 and MO3. Before etching-off the GaAs layer, the flat (MO2) structure had the lowest (highest) photosensitivity. No complete correlation exists with the spectra of total reflection R_{tot}. The R_{tot} spectra for the MO4, MO1 and MO2 samples are almost the same, while for the MO3 sample R_{tot} is the lowest. After etching-off the absorbing GaAs layer, the R_{tot} spectrum for the structure MO2 remained almost the same as before. But for the other structures R_{tot} dropped considerably, thus making an additional contribution into

photosensitivity increase. One can see from the photosensitivity spectrum for the structure MO3 that light absorption in the $Al_xGa_{1-x}As$ layer affects it to a lesser extent.

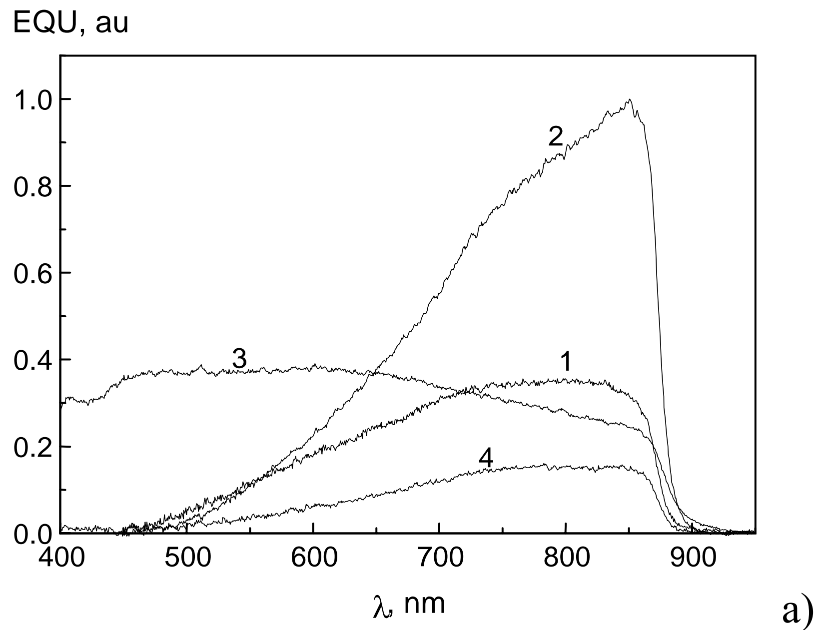

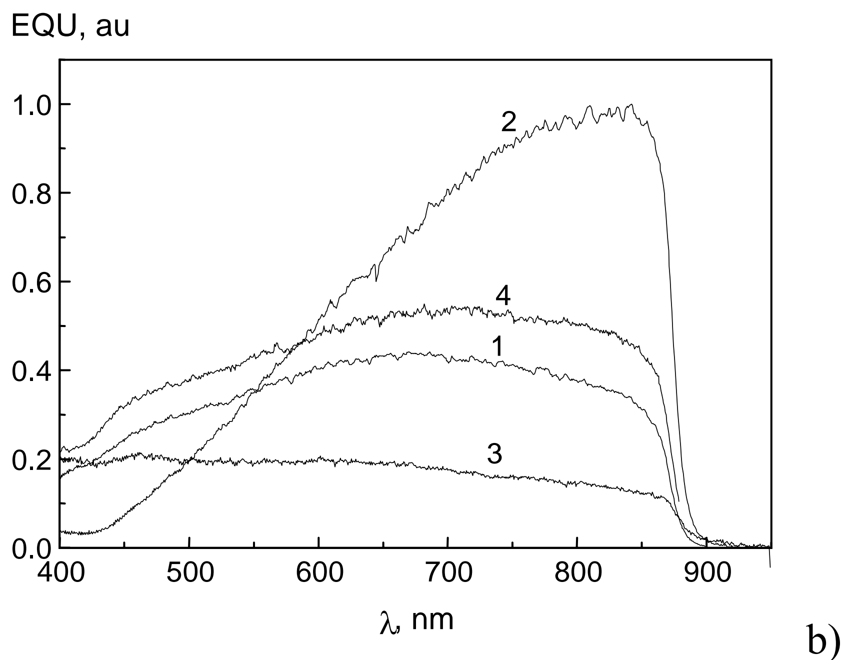

Fig. 5.9. a – Spectral dependencies of the external quantum efficiency per unit active area for the SC samples M01-C2.1 (1), M02-C2 (2), M03-C2 (3) and M04-C1.1 (4) on the basis of the $Al_xGa_{1-x}As$–GaAs heterostructure.

b – Same as a, but after etching-off the upper layer. (The scale for the sample M03-C2 (3) is enlarged by a factor of 20.)

This indicates at incomplete continuousness of the $Al_xGa_{1-x}As$ layer at a given interrelation between its thickness and microrelief height. Another evidence of this is that the character of photocurrent spectrum did not change after etching. The more developed quasi-grating-like microrelief (structure MO1) is also less efficient for photosensitivity increase. Thus, for the applied epitaxial growth technology and at preset geometric parameters of the active area, the highest efficiency was demonstrated by the quasi-grating-like microrelief obtained after anisotropic etching in $2HF:2H_2SO_4:1H_2O_2$ (T = 24 °C, 30 s.).

The following Table 5.4 gives a comparison between photoelectric parameters of the structures MO1–MO4 under AM0 conditions before (b) and after (a) etching-off the GaAs layer.

Table 5.4. The photoelectric parameters under AM0 conditions (at irradiance P = 136 mW/cm^2; T = 25 °C) for SC samples fabricated by the gas phase epitaxy

SC #	Isc, mA	Jsc, mA/cm2	Voc, V	Im, mA	Vm, V	FF	η, %
M01-C2.1 (b)	2.3	6.71	0.641	1.65	0.412	0.462	1.46
M01-C2.1 (a)	3.44	10.1	0.77	2.02	0.435	0.35	1.89
M02-C2 (b)	4.95	6.28	0.758	4.03	0.597	0.641	2.24
M02-C2 (a)	7.26	9.21	0.789	6.1	0.614	0.664	3.55
M03-C2 (b)	1.39	1.63	0.298	0.89	0.209	0.461	0.16
M03-C2 (a)	0.11	0.128	0.2	0.05	0.045	0.001	0.01
M04-C1.1 (b)	1.87	7.12	0.439	1.53	0.313	0.585	1.34
M04-C1.1 (a)	3.44	13.1	0.406	2.89	1.313	0.647	2.53

Thus our physico-technological studies have demonstrated that a quasi-grating-like microrelief and the diffusion technique of heteroepitaxy are the most efficient ones.

5.4. EFFECT OF GAMMA IRRADIATION ON PHOTOCONVERSION CHARACTERISTICS OF GALLIUM ARSENIDE BARRIER STRUCTURES WITH TEXTURED INTERFACE

GaAs-based Schottky-barrier solar cells are promising for space application because they may offer a high efficiency-to-weight ratio and have a higher resistance to hard radiation (fast protons and neutrons) than Si cells [1-4]. Moreover, in a certain dose range, irradiation by fast electrons and ^{60}Co gamma quanta causes radiation-induced ordering or gettering of active recombination centers (the so-called low-dose effect).

This effect shows up as an increase in the diffusion length of charge carriers and a decrease in the recombination rate at the interface [5,6]. The interface here serves the function of a sink for intrinsic and radiation-induced defects. Therefore, both the amount of the low-dose effect and the dose range of its existence depend on the degree of structure perfection at the interface and on the presence of mechanical stress fields in the interface region [7]. One of the most promising ways of increasing the efficiency of the cells is the use of a textured active interface. In deciding on a particular microrelief morphology and a technique for its formation, one usually takes into consideration the effect of the microrelief on the optical and recombination parameters, i.e., on the photoconversion efficiency. However, for space application, the effect of the microrelief morphology on the radiation resistance of the structures should also be taken into account.

We studied the effect of ^{60}Co γ radiation on the photoconversion efficiency of metal Au/GaAs and heterostructure barrier structures with various morphologies of the interface microrelief obtained by chemical anisotropy etching of the GaAs surface [8].

Au/GaAs barrier structures were fabricated with the planar technology by thermally evaporating a semitransparent gold film

onto n-GaAs wafers (N_d = 1-3×10^{16} cm^{-3}). Two types of the GaAs (100) surface microrelief promising for use in photodetectors and solar cells [9] were investigated: the dendrite microrelief and the quasi-grating one. The parameters of the semiconductor and the interface were determined from dark I-V characteristics and high-frequency (1 MHz) C-V characteristics.

We also recorded the spectral dependence's of the short-circuit current and I-V characteristics under illumination using a solar simulator based on an incandescent lamp with a tungsten filament. The simulator was calibrated with a reference silicon solar cells. The ^{60}Co gamma irradiation was performed with an MPX-γ-25M setup in the 10^3– 2×10^5 Gy dose range.

The forward branches of the I-V characteristics are presented in Fig. 5.10 for the structures with a different interface microrelief.

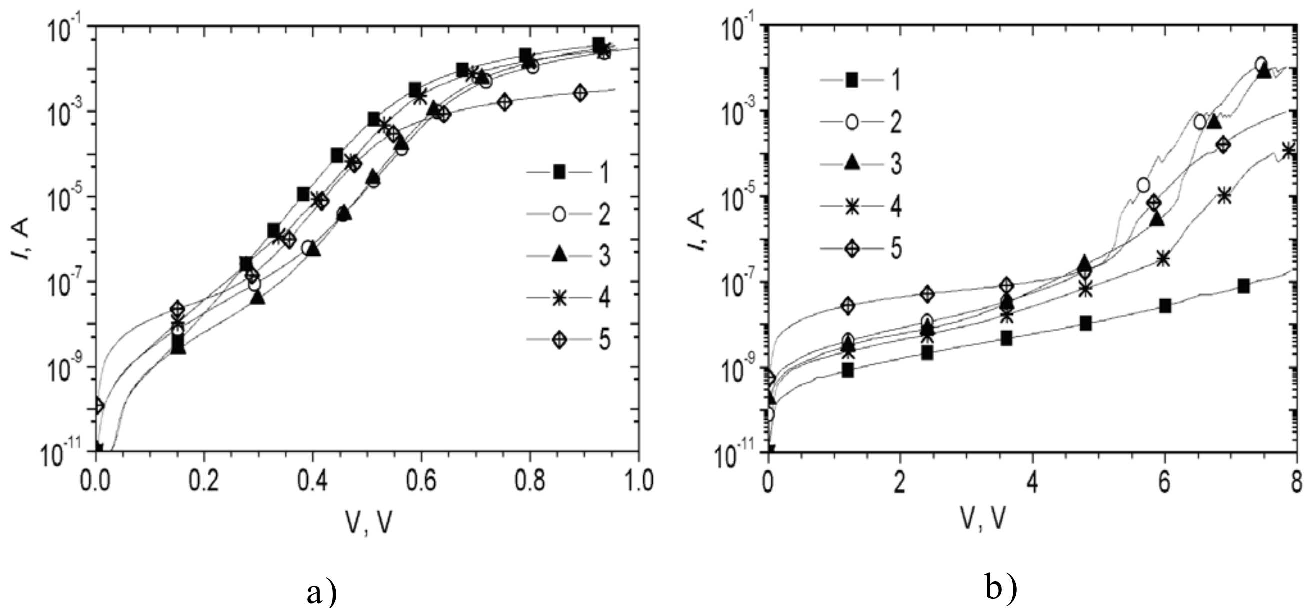

Fig.5.10. Forward (a) and reverse (b) dark I-V characteristics of Au/GaAs diodes with flat (1) and textured (2-5) interfaces. Quasi-grating microreief (2, 3) and dendritic microrelief (4, 5) (3 and 5 correspond to the developed microrelief).

Along with the thermions and recombination mechanisms of carrier transport [10], the thermal-field component should also be taken into account. The effect of this component shows up as an apparent decrease in the barrier height in certain surface regions.

The inclusion of the barrier height distribution over the diode surface [11], which is broader in the case of the dendritic morphology, enables us to explain both the current rise in the initial region of the I-V characteristics and the smaller ideality factor *n* (in the range of high biases) for the structures with the developed microrelief. However, the latter can also be related to a thinner transition layer at the interface and/or to a higher density of interface states, which are filled through the exchange with the metal.

Figure 5.11 shows the I-V characteristics under illumination (a) and demonstrates the spectra of the short-circuit photocurrent (b) in the surface-barrier structures.

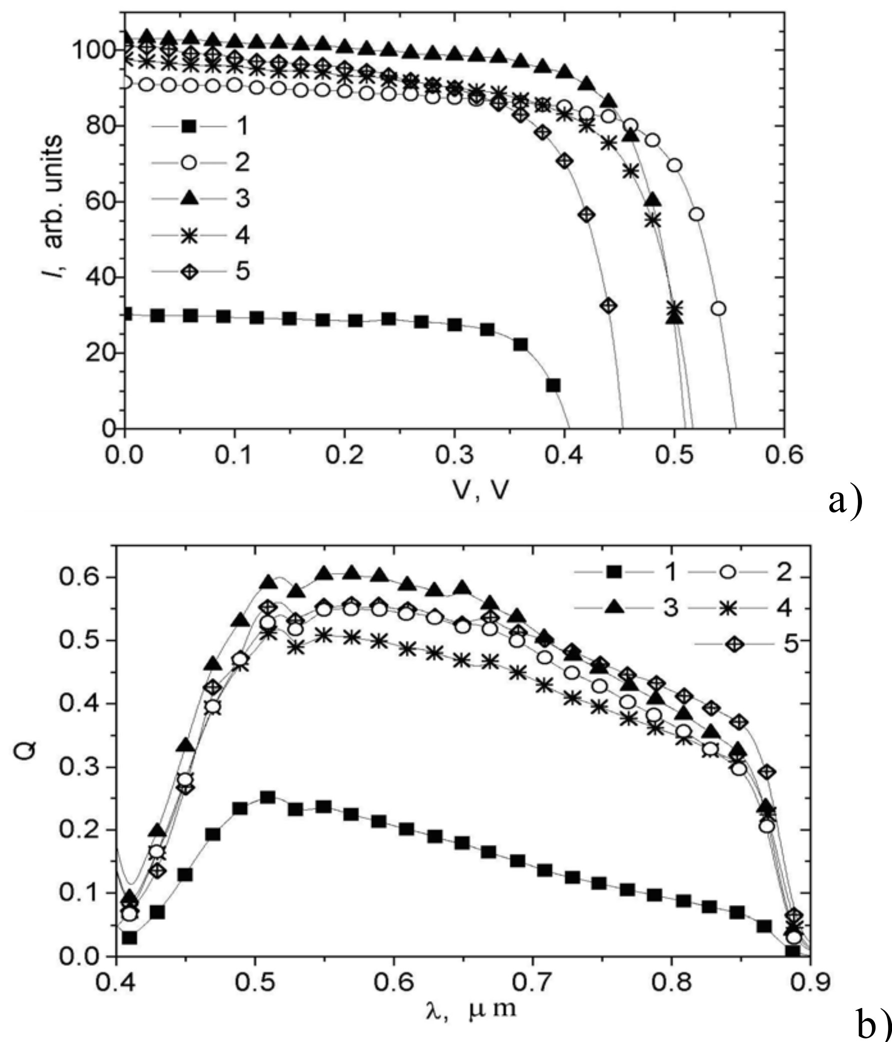

Fig. 5.11. I-V characteristics under illumination (a) and spectral dependences of the short-circuit photocurrent (external quantum efficiency) (b) of Au/GaAs photoconverters with flat (1) and textured (2-5) interfaces. Figures mean the same as in Fig.5.10.

As is seen, the short-circuit current I_{sc} grows in comparison with that for the flat structure as the microrelief develops (approximately three times and 3.2 times for the quasi-grating and developed dendritic microreliefs, respectively). However, the open-circuit voltage V_{oc} increases to a lesser extent: by a factor of $\approx$ 1.3 for the quasi-grating microrelief and by factors of $\approx$ 1.25 and $\approx$ 1.16 for the incipient and developed dendritic microreliefs, respectively. The structures with the dendritic microrelief exhibit a lower fill factor *FF* of the I-V characteristics under illumination than the flat structures and those with the quasi-grating microrelief. Accordingly, the quasi-grating structures have the highest efficiency.

It turned out that the effect of gamma irradiation is more pronounced in the structures with the developed microrelief. The low-dose effect (which decreases the recombination rate at the interface and the ideality factor n, as well as increases the minority carrier diffusion length L_P and contact barrier height φ_b) is observed in the structures with the dendritic relief and developed quasi-grating microrelief at doses lower than 10^4 Gy (Fig. 5.12).

Among the parameters of the I-V characteristics under illumination, the short-circuit current I_{sc} is the most sensitive to the irradiation. Figure 5.13 depicts the spectral dependence's of the relative photocurrent when the diodes with the developed interface microreliefs were irradiated by improving ($\approx 10^3$ Gy) and degrading ($\approx 2\times10^5$ Gy) doses.

It is evident that the basic effect of the gamma irradiation, which is virtually wavelength-independent, is on the interface recombination rate [12]. The I-V characteristics under illumination start to degrade from the irradiation dose 10^5 Gy.

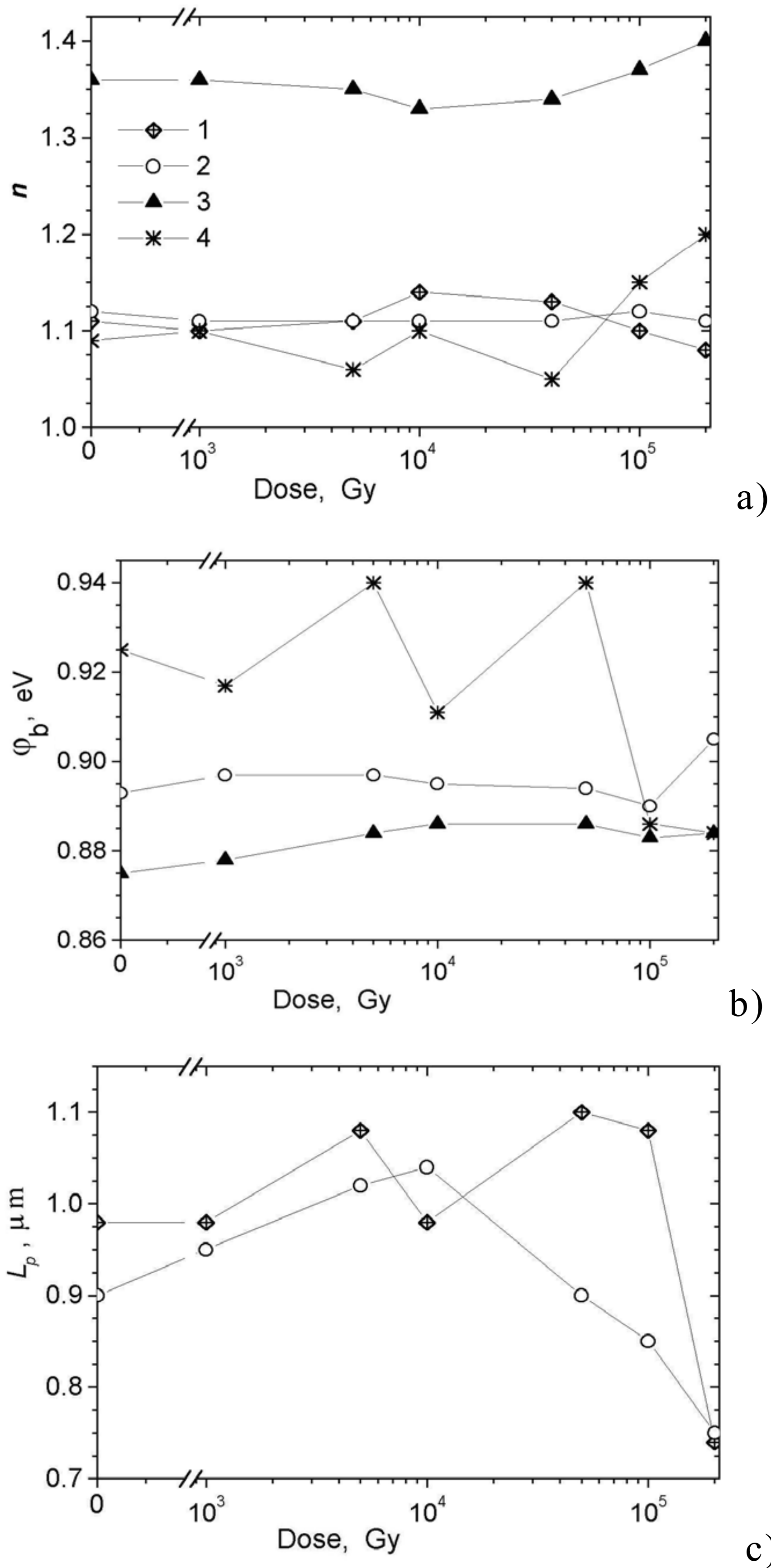

Fig. 5.12. Dose dependences of ideality factor n (a), barrier height φ_b (b) and minority carrier diffusion length for diodes with the textured interfaces. Quasi-grating microreief (1, 2) and dendritic microrelief (3, 4) (2 and 4 correspond to the developed microrelief).

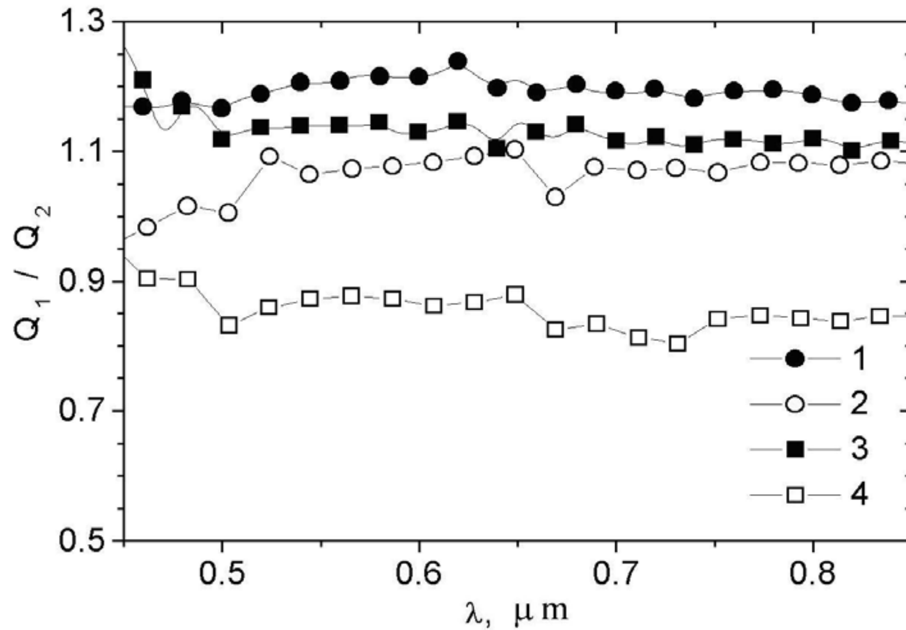

Fig. 5.13. Spectral dependences of the ratio between the photocurrents in the irradiated and nonirradiated structures with the developed quasi-grating (1, 2) and dendritic (3, 4) interface microreliefs. Dose equals 10^3 (1, 3) and 2×10^5 (2, 4) Gy.

The structures with the developed dendritic microrelief are the least resistant. Here, the efficiency drops by about 5% from the initial value at a dose of 2×10^5 Gy. The quasi-grating microrelief imparts to the structures the highest resistance: the efficiency drops by no more than 2% from the initial value.

The radiation effects similar to the above ones were observed in the AlGaAs–GaAs heterostructures that were prototypes of heterophotoconverters. At low γ-irradiation doses, radiation-induced gettering was observed. It manifested itself in decrease of the dark current on the reverse branch of *I*–*V* curve, as well as decrease of the leakage current and saturation current on the forward branch of *I*–*V* curve.

Thus our experimental data enable us to conclude that it is possible to exert efficient control over the recombination properties of the microrelief surface-barrier structures made on the basis of GaAs and $Al_xGa_{1-x}As$–GaAs heterojunctions and, as a result,

improve their parameters. The range of low doses of irradiation resulting in improvement of the barrier structure parameters was found to be narrower (down to ≤ 10^3 Gy), as compared to the case of flat structures.

The results of studies of the effect of γ-irradiation on the SC photoelectric parameters are presented in Table 5.5.

Table 5.5. Effect of γ-irradiation on the SC photoelectric parameters under AM0 conditions (irradiance of 117 mW/cm^2, T = 25 °C).

SC #	Dose	I_{sc}, mA	J_{sc}, mA/cm^2	V_{oc}, V	I_m, mA	V_m, V	FF	η, %
463	0	3.24	13	0.885	2.69	0.693	0.634	6.35
	D1	3.25	13	0.885	2.69	0.701	0.657	6.45
465	0	3.9	15.6	0.79	3.13	0.528	0.533	5.62
	D1	3.86	15.6	0.81	3.05	0.581	0.567	6.1
141	0	3.95	15.8	0.881	3.46	0.693	0.69	8.2
	D1	3.93	15.7	0.864	3.22	0.676	0.641	7.45
AK-2	0			0.397			0.575	4.9
	D1			0.385			0.587	4.9
AK-4	0							3.0
	D1							3.14
45p	0	4.7	18.8	0.916			0.63	7.9
	D1	4.7	18.8	0.872			0.565	6.74

They indicate that this effect is various, namely:

1) At low doses ($D_1 = 1 \cdot 10^3$ Gy) short-circuit current I_{sc} practically did not change.

2) Some photoelectric parameters degrade, while other parameters improve. To illustrate, for the sample # 141 open-circuit voltage V_{oc}, filling factor of I–V curve FF and efficiency η are considerably impaired. For the microrelief sample # AK-2, V_{oc} decreases slightly. However, the highest power point remains the same. As a result, FF grows and η does not change. At the same

time the flat samples # 463 and (especially) # 465 demonstrate improvement of their principal photoelectric parameters.

3) The results of our studies of spectral dependencies of the photocurrent, $I_{ph}(\lambda)$, made for the above samples evidence that the minority charge carrier diffusion length in SC base does not change. This fact correlates with practical invariance of I_{sc}. High-energy sensitivity, however, somewhat increases. This fact, along with increase of open-circuit voltage, enables one to conclude that γ-irradiation improves the parameters of *p*-*n* junction or reduces surface recombination velocity (the low-dose effect).

References

1. Wysocki J. // J. Appl. Phys. 1963. v.34. p.2915.
2. Gebert H., Edmund J. // J. Electrochem. Soc. 1978. v.125. p.678.
3. Grigor’eva G.M., Grilikhes V.A., Zvyagina K.N., et al. // Geliotekhnika. 1989. No.1. p.8.
4. Bakirov M.Ya.. // Geliotekhnika. 1991. No.6. p. 32.
5. Borkovskaya O.Yu., Dmitruk N.L., Konakova R.V., et al. // Radiat. Eff. 1979. v.42. p.249.
6. Borkovskaya O.Yu., Dmitruk N.L., Konakova R.V., et al. // Fiz. Tekh. Poluprovodn. (Leningrad). 1986. v.20. p.1640 [Sov. Phys. Semicond. 1986. v.20. p.1028)].
7. Borkovskaya O.Yu., Dmitruk N.L., Litovchenko V.G., and Mishchuk O.N. // Fiz. Tekh. Poluprovodn. (Leningrad). 1989. v.23. p.207 [Sov. Phys. Semicond. 1989. v.23. p.129].
8. Dmitruk N.L., Borkovskaya O.Yu., Konakova R.V., et al. // Technical Physics. 2002. v.47. No.6. p.698.
9. Dmitruk N.L., Borkovskaya O.Yu., Mamontova I.B., Mamykin S.V. // Sol. Energy Mater. Sol. Cells 2000. v.60. p.379.
10. Borkovskaya O.Yu., Dmitruk N.L., Voitsikhovskiy D.I., et al. // Poverkhnost. 1999. No.8. p.87.
11. Dmitruk N.L., Borkovskaya O.Yu., Dmitruk I.N., et al. // Appl. Surf. Sci. 2001. v.190. p.455.
12. Dmitruk N.L., Borkovskaya O.Yu., Mamontova I.B. // Geliotekhnika. 1989. No.5. p.3.

Conclusion

We have considered but several aspects of the problem of development of highly efficient photoconverters made on the basis of AlGaAs/GaAs heterojunctions LPE-grown on textured GaAs substrates. These aspects are as follows:

- the techniques for microrelief formation on the growth surfaces of substrates;
- the optical characteristics of the textured semiconductor surfaces;
- the features of growth of AlGaAs and GaAs epitaxial layers on microrelief surfaces;
- the formation mechanisms and properties of ohmic contacts to textured GaAs surface;
- the photoelectric characteristics of hetero-photoconverters on microrelief surfaces.

It turned out that, despite the considerable progress in technology of GaAs and AlGaAs epitaxy, the mechanisms for epitaxial layers growth on textured (soft) GaAs surface, as well as mass transfer at interfaces between phases with such surfaces, still remain not adequately understood. The mechanisms for relaxation of intrinsic stresses in heterostructures grown on microrelief GaAs substrates are practically not studied. And it is just these phenomena that determine the hetero-photoconverter parameters.

One should note also that the theoretical and experimental investigations made by now did not solve the problem of increasing the hetero-photoconverter efficiency. However, intense development of the technology of materials and devices on porous and purposely formed textured surfaces of III–V semiconductors offer hopes that the photoconverters made on their basis will become competitive with the existing energy sources in conversion of concentrated solar radiation and space applications.